UNIVERSITY OF Hull

Faculty of Science

Synthesis and Characterisation of Liquid Crystal Gold Nanoparticles

being a Thesis submitted for the Degree of Doctor of Philosophy

in the University of Hull

by

BaiJia Tang MChem (Hons) MRSC

December 2013

“Science is a difficult field that demands great effort and dedication, but if you are willing to make the effort, there is much to gain.”

George William Gray

Publications

The following publications have included work which is contained within this thesis.

- T.Scharf, J. Dintinger, B. J. Tang, G. H. Mehl, X. Zeng, G. Ungar, S. Muhlig, T. Kienzler, C. Rockstuhl, in *Emerging Liquid Crystal Technologies VIII*, Spie-Int Soc Optical Engineering, Bellingham, 2013, vol. **8642**.

- J. Dintinger, B. J. Tang, X. B. Zeng, F. Liu, T. Kienzler, G. H. Mehl, G. Ungar, C. Rockstuhl, and T. Scharf, *Adv. Mater.*, 2013, **25**, 1999.

- J. Dintinger, B. J. Tang, X. B. Zeng, T. Kienzler, G. H. Mehl, G. Ungar, C. Rockstuhl, and T. Scharf, in *Quantum Dots and Nanostructures: Synthesis, Charaterization, and Modeling IX*, Spie-Int Soc Optical Engineering, Bellingham, 2012, vol. **8271**.

- X. B. Mang, X. B. Zeng, B. J. Tang, F. Liu, G. Ungar, R. B. Zhang, L. Cseh, and G. H. Mehl, *J. Mater. Chem.*, 2012, **22**, 11101.

- C. H. Yu, C. P. J. Schubert, C. Welch, B. J. Tang, M. G. Tamba, and G. H. Mehl, *J. Am. Chem. Soc.*, 2012, **134**, 5076.

Conference presentations and activities

The following Oral Presentations and Posters have included work which is contained within this thesis.

Oral Presentations (presenting author in **bold**)

- **B.J. Tang** and G.H. Mehl, "Synthesis and Characterisation of Liquid Crystals Gold Nanoparticles", *Oral Presentation at 26th Annual Conference of the British Liquid Crystal Society*, **2012**. University of Strathclyde, Glasgow, UK (best oral presentation prize).
- **B.J. Tang** and G.H. Mehl, "Synthesis and Characterisation of Liquid Crystals Gold Nanoparticles", *Oral Presentation at Departmental Research Colloquia*, **2012**. University of Hull, Hull, UK.

Oral Presentations as co-author

- **G. H. Mehl (invited- plenary)**, B. J. Tang, L. Cseh, C. Schubert. C. H. Yu, X. B. Zeng, X. Mang, F. Liu, G. Ungar, J. Dintinger, T. Scharf, T. Kienzler, C. Rockstuhl, "The design of self-organized nanocomposites for the construction of metamaterials", *12th European Conference on Liquid Crystals*, **22-27. 09. 2013**. Rhodes, Greece.
- **T. Scharf (invited),** J. Dintinger, B.J. Tang, G. H. Mehl, X. Zeng, G. Ungar, S. Mühlig, T. Kienzler and C. Rockstuhl, "Liquid crystal based plasmonic metamaterials", *12th European Conference on Liquid Crystals*, **22-27. 09. 2013**, Rhodes, Greece.
- **G. Ungar (invited),** X.B. Zeng, G.H. Mehl, X. Mang, L. Cseh, F. Liu, B.-J.Tang, "Anisotropic, Isotropic and Helically Ordered Nanoparticle Arrays and Supercrystals by LC and induced LC Ligands", *12th European Conference on Liquid Crystals*, **22-27. 09. 2013**, Rhodes, Greece.
- C. H. Yu, B. J. Tang, C. Schubert, M. G. Tamba, C. Welch, X. B. Zeng, X. Mang, F. Liu, G. Ungar, J. Dintinger, T. Scharf, T. Kienzler, C. Rockstuhl, **G. H. Mehl**; **(invited**). "Design and control of liquid crystal superlattice forming gold nanoparticles – a route to plasmonic metamaterials", *27th Annual Conference of the British Liquid Crystal Society Conference*, **25-27.03. 2013**, Cambridge, UK.

- J. Dintinger, B. J. Tang, X. Zeng, F. Liu, T. Kienzler, G. H. Mehl, G. Ungar, C. Rockstuh**l, T. Scharf**, "Liquid crystal based plasmonic metamaterials", *META '13, 4th International Conference on Metamaterials*, **18-22. 03. 2013**, Sharjah, UEA
- C. H. Yu, B. J. Tang, C. Schubert, M. G. Tamba, C. Welch, X. B. Zeng, X. Mang, F. Liu, G. Ungar, **G. H. Mehl, (invited), "**Designing liquid crystal superlattice forming gold nanoparticles and controlling the self-assembly behaviour**",** *24th Int. Liq. Cryst. Conf*. **19-24. 08. 2012**, Mainz, Germany.
- C.H. Yu, B.J. Tang, C. Schubert, C. Welch, M. G. Tamba X. B. Mang, X. B. Zeng, G. Ungar, **G. H. Mehl (invited)**, "The design and the control of the self-assembly behaviour of liquid crystal gold nanoparticles with plasmonic properties and controlled 1D, 2D and 3D self assembly behaviour", *International Conference on Metamaterials*, **3-4. 06. 2012**, Jena, Germany.
- **H.C. Yu**, B. J. Tang, C. Welch, C. J. Schubert, M.G. Tamba, G. H. Mehl, "Synthesis and investigations of mesogen encapsulated gold nanoparticles", *American Physical Society Meeting*, **27.02-02.03.2012**, Boston, USA.
- **R. Caputo**, B.J. Tang, L. De Sio, G.H. Mehl, C. "Self-organisation of Nematic Gold Nanoparticles in Periodic Polymeric Structures", *Umeton1; 8th Meeting of Diffractive Optics (DO12)*, **27. 02. 2012 -01. 03. 2012**. Delft, Holland.
- R. Caputo, B.J. Tang, L. De Sio, G. H. Mehl, C. Umeton, "Polymeric Platform Assisted Self-organisation of Nematic Gold Nanoparticles mixed with other Liquid Crystalline Phases", *14th Topical Optics of Liquid Crystals*, **25.09. - 01. 10. 2011**, Yerevan, Armenia.
- B. J. Tang, L. Cseh, C.-H. Yu, X. Mang, X. B. Zeng. F. Liu, G. Ungar, J. Dintinger, T. Scharf, **G. H. Mehl (invited)**, "The chemistry of self organized nanocomposites for negative refractive index materials", *18th Course, Liquid Crystal Nanostructures and Self-Assembling: from Organic Electronics to Metamaterials*, **3-10. 07. 2011**. Erice, Italy.
- B. J. Tang, L. Cseh, C.-H. Yu, X. Mang, X. B. Zeng. F. Liu, G. Ungar, **G. H. Mehl (invited), "**The self assembly behaviour of LC gold nanoparticles forming superstructures**",** *10th Mediteranean Workshop and Topical Meeting - Novel Optical Materials and Applications, Cetraro*, **05-11. 06, 2011**, Cetraro, Italy

- **C. H. Yu**, C. Welch, B. J. Tang, G.H. Mehl, "Synthesis and characterisation of nematic gold nanopartciles", *25th British Liquid Crystal Society Conference*, **18-20. 04. 2011**, Nottingham, UK.
- L.Cseh, B. J. Tang, X. B. Zeng, G. Ungar, **G. H. Mehl** (**invited**), "The design and control of the self-assembly behaviour of liquid crystal superlattice forming gold nanoparticles", *Pacifichem 2010*,**15- 20. 12. 2010**, Honolulu, Hawaii, USA

Posters (presenting author in **bold**)

- **B.J. Tang**, L. Cseh, C.H. Yu, Ungar, X.B. Mang, X.B. Zeng, R.B. Zhang, G.H. Mehl, "Synthesis and Characterization of the self-assembly of mesogen coated gold nanoparticles", *24th Int. Liq. Cryst. Conf.* **19-24. 08. 2012**, Mainz, Germany.
- **B.J. Tang** L. Cseh, C.H. Yu, Ungar, X.B. Mang, X.B. Zeng, R.B. Zhang, G.H. Mehl, "Synthesis and Characterisation of Liquid Crystals Gold Nanoparticles", *Poster Presentation at International Conference on Metamaterials and Dissemination Workshop*, **2012**. University of Jena, Jena, Germany.
- **C.H. Yu**, C. Welch, B.J. Tang, C. J. Schubert, G. H. Mehl, "Design, synthesis and investigation of mesogen encapsulated gold nanoaprticles", *Tech Connect World*, **18-21. 06. 2012**, Santa Clara, CA, USA.
- C.H. Yu, C. Welch, B.J. Tang, L.Cseh, G. H. Mehl, "Synthesis and characterisation of nematic gold nanoparticles", *Tech Connect World*, **18-21. 06. 2012**, Santa Clara, CA, USA.
- C.H. Yu, C. Welch, B.J. Tang, C. J. Schubert, G. H. Mehl, "Size effect on properties in hybrid gold nanoparticles and calamitic mesogens", *Tech Connect World*, **18-21. 06. 2012**, Santa Clara, CA, USA.
- M.G. Tamba, A. Kohlmeier, C. H. Yu, B.J. Tang, G. H. Mehl, "Nematic-Nematic phase transtions in binary mixtures containing gold nanoparticles and symmetric dimeric molecules", *British Lqiuid Crystal Soc. Conference*, **02- 04. 04. 2012**, Glasgow, UK.
- H.C. Yu, B.J. Tang, C. Welch, C. J. Schubert, L. Cseh, "Size effect of properties in a hybrid of Au NPs and a clamitic mesogen", *American Physical Society Meeting*, **27.02-02.03.2012**, Boston, USA.

- **B.J. Tang** and G.H. Mehl, "Synthesis and Characterisation of Liquid Crystals Gold Nanoparticles", *Poster Presentation at Departmental Research Colloquia* (University of Hull, Hull, UK) **2011**
- **B.J. Tang** and G.H. Mehl, "Synthesis and Characterisation of Liquid Crystals Gold Nanoparticles", *Poster Presentation at 10th Mediterranean Workshop and Topical Conference of the Novel Optical Materials and Applications* (University of Calabria, Cetraro Italy) **2011**
- B.J. Tang, L. Cseh, C. H. Yu, G. H. Mehl, "Synthesis and and investigation of self-assembling mesogne coated gold nanoprticles"' *10th Mediteranean Workshop and Topical Meeting - Novel Optical Materials and Applications*, **05-11. 06, 2011**, Cetraro, Italy.
- J. Dintinger, H. Sellame, T. Scharf, B.J. Tang, G. H. Mehl, "Towards the bottom-up fabrication of nanoparticle based metamaterials"' *10th Mediteranean Workshop and Topical Meeting - Novel Optical Materials and Applications*, **05-11. 06, 2011**, Cetraro, Italy.
- B. J. Tang, L. Cseh, C. H. Yu, G. H. Mehl, "Nematic-nematic phase transiton in dimmers with a negative dielectric anisotropy", *25th British Liquid Crystal Socety Conference*, **18-20. 04. 2011**, Nottingham, UK.
- **B.J. Tang**, L. Cseh, C. H. Yu, G. H. Mehl, "Synthesis and and investigation of self-assembling mesogne coated gold nanoprticles"' *25th British Liquid Crystal Socety Conference*, **18-20. 04. 2011**, Nottingham, UK.

Acknowledgment

First and foremost, I would like to deeply thank my supervisor and mentor Prof. Georg H. Mehl for this precious PhD research opportunity, it has been a life changing experience. There has always been constant support with inspirational guidance and encouragement, especially understanding from him, which have helped me through the most difficult times during my research programme and I will never forget. I am extremely grateful for the many insightful discussions that we have had on various aspects of chemical synthesis, gold nanoparticles research and his advice concerning the preparation of various posters, presentations and the completion of this thesis. All of them could not be complete without the support and effort he devoted in. I would also like to thank Dr. Liliana Cesh who inspired me to start this project and to be able to help me solve any problems and enquiries throughout my research. Finally, I would like to thank Dr. Mike Hird and Dr Robert A Lewis for their enthusiasm, help and guidance over the years.

This programme of research would not have been possible without the financial support of the "NANOGOLD" project under EU Commission, and carried out at the University of Hull at the Chemistry Department in the group of Prof. Georg H. Mehl. I would like to sincerely thanks to Dr XiaoBing Zeng, Prof. Goran Ungar, Dr XiaoBing Mang and Dr RuiBin Zhang from the University of Sheffield UK who carried out all XRD, GISAX and Synchrotron measurements for the physical properties of my samples, which has been included in this thesis. Sincerely thanks to Dr Jose Dintinger and Dr Toralf Scharf from the EPFL Switzerland, who helped determining the optical properties of my samples, which forms a part of this thesis. The driving force of this project is from Dr Carsten Rockstuhl, Dr Stefan Mühlig and Mr Tobias Kienzler at the University of Jena Germany, who conducted all simulations and calculations providing us with directions. I thank Dr Roberto Caputo and Prof. Cesare Umeton from the University of Calabria, who prepared liquid crystals mixtures with my liquid crystal gold nanoparticles and obtained some promising results. I thank Prof. Thomas Bürgi and Dr Alastair Cunningham from the University of Geneva, who supplied me the sample (Au38), which the details of all analysis are not included in this thesis. Many thanks to all participants from the EU research project NANOGOLD, it was my privilege to work with this many experts from different scientific fields, this has been an eye opening experience. I will never forget all

the interesting discussion and laughs we had. I really feel sad that this project has come to the end and I wish you all the best.

I am also grateful to be a part of The Liquid Crystal Group at the Department of Chemistry, University of Hull, for their help, support and useful discussions over the years. I would like to say a special thank you to Anne Lowry, Mr Ian Dobson, Mrs Carol Kennedy and all other technical staff for their help and expertise in the analytical services. My thanks to all the people I have shared a laboratory with over my PhD period, for all the interesting discussions and laughs along the way, to establish such a good working environment. Thank you to all members of our research group for all the motivation, encouragement and help to make me a better person and always being there for me.

Finally I would like to express my eternal gratitude to my family, whom I have always had unconditioned support from. In particular, I would like to purvey my extreme gratitude to my Mother and Father who have selflessly provided many years of unconditional help and advice, both academically and financially. None of this would have been possible without them. I would like to dedicate this work to my family who would be very proud.

致谢

博士期间时光一晃而过，回首走过的岁月，心中倍感充实，博士即将完成之日，感慨良多。首先诚挚的感谢我的指导导师 Georg H Mehl 教授给予我这个难得和珍贵的博士研究机会，这对我来说是一段特殊的经历，改变和丰富了我的人生。在这段就读博士的学习生涯中，我永远都不会忘记先生一直持续地给予我的支持，热情关怀，激励和鼓舞人心的悉心指导，师恩难忘！特别是先生的宽厚仁慈的胸怀，耐心和体谅，这些都为我能够渡过我的研究计划中最艰难的时刻起到了非常大的帮助，使我得以顺利地完成博士研究生阶段的学习。我非常感激先生无时无刻的给与我在化学合成和纳米金粒子等各个方面的研究，所提供的许多有见地的建议和讨论，使我取得了长足进步，而且这些对于我在其他各种海报，演讲和论文的准备上起到了不可忽视的显著作用，使我从中受益匪浅并取得了在全英国液晶 2012 年度会议上获取演讲第一和一系列文章的发表。先生渊博的学识、严谨的治学态度、科学求实的作风和忘我的敬业精神给我留下了深刻的印象，并将激励我在今后的科学道路上不懈攀登！先生的敬业精神，对工作的努力，脚踏实地的作风和积极乐观的生活态度都为我树立了良好的榜样，这些潜移默化的作用将对我今后的工作、学习起着不可估量的影响。我博士期间的实验和本文能得以顺利完成，也必然少不了先生倾注的大量的心血和汗水，可以说如果不是先生，这些所有的一切都不可能会如此顺利，在此谨让我再次向先生导师 Georg H Mehl 教授致以崇高的敬意和衷心的感谢！我还需要感谢 Liliana Cesh 教授，是她激励和启发了我在这方面的研究，并能够提供无私的咨询和帮助我解决了许多研究方面的问题。我还需要感谢 Mike Hird 教授和 Robert A Lewis 教授在这几年里给予了我热情的帮助和悉心指导，在此一并向他们表示衷心的感谢。

我要以最诚挚的心意感谢欧盟委员会 NANOGOLD 项目和赫尔大学化学系的财政支持，感谢他们对我的博士研究所给予的全力支持，为我提供了所有实验所需的必备条件，从实验的思路、经费、员到实验仪器，可以说没有他们，就没有我今天的这些成果。我要衷心感谢来自英国谢菲尔德大学的 XiaoBing Zeng 博士，Goran Ungar 教授，XiaoBing Mang 博士及 RuiBin Zhang 博士为我样品的物理性质测量进行的所有 X 射线衍射，掠入射小角 X 射线衍射和其他同步测验，现已概括

在本论文中。衷心感谢来自瑞士洛桑联邦理工学院的博士 Jose Dintinger 及教授 Toralf Scharf 为我样品的光学性质所做的分析, 同样也会在这篇论文中所提起。该项目的推动力来自德国耶拿大学的教授 Carsten Rockstuhl，博士 Stefan Mühlig 及 Tobias Kienzler 先生，感谢他们进行的所有模拟和计算，为我们提供了探索方向。我感谢来自意大利卡拉布里亚大学的博士 Roberto Caputo 及教授 Cesare Umeton 用我的样品配备的液晶混合物所取得了一些可喜的成果。我感谢来自瑞士日内瓦大学的教授 Thomas Bürgi 及在读博士 Alasair Cunningham 给我提供的样品（Au38），以及获取的一些有趣的成果，因考虑到此项目涉及到其他在读博士所研究的课题，所以相关的分析结果就不再在本论文中作详细说明。非常感谢来自欧盟的纳米金研究项目的所有参与者，很荣幸能与多个来自不同的科学领域的专家们一起合作，这所有一切经历都让我大开眼界，我永远不会忘记我们之间所有有趣的讨论。时光一晃而过，这个项目已经完成了，我祝你们的未来一切顺利。

我也很高兴能够成为 Georg H Mehl 组和赫尔大学化学系液晶团队的一员，感谢团队全体同仁们多年来的帮助和支持。再次特别感谢 Anne Lowry, Mr Ian Dobson, Mrs Carol Kennedy 以及其他技术人员对我所有样品的分析所提供的专业帮助。在此，我还要郑重感谢所有与我一起共享过实验室和奋战的博士朋友们，也是我的“酒友”和“饭团”同志们，难忘我们在一起时的欢乐有趣的讨论。一起，我们建立了这样一个良好的工作环境。与你们在一起的日子开心而充实，你们给我单调枯燥的科研生活增添了绚丽的色彩，你们将是我记忆里最美的风景。在我心情低落时为我分忧，在我信心不足时给我打气，从生活的点点滴滴中给我帮助和鼓励，使我成为一个奋发上进的人。

最后，我想表达我对我家人永恒的感激之情。我要特别感谢我的父母，是他们启发了我攀登知识高峰。为了学业，我多年没有在他们身边尽儿孝，他们没有任何怨言，令我深感愧疚。为了支持我完成学业，他们多年来一直对我的学习和生活默默的支持、鼓励和关爱，使我得以顺利完成了博士学业。本文凝结了他们的教诲、关爱和温暖，没有他们的支持，就没有我今天的成就。在此，谨让我表达对父母及家人永恒的感激，我想将我的所有研究成果奉献给为我感到骄傲的亲人们，祝愿他们身体健康、心情愉快、美梦成真。

To my parents

BaiZhi Qing and SheCheng Tang,

who made everything possible.

感谢我的父母

唐社成和柏芝青，让这一切

成为了可能。

Abstract

This thesis is focused on the design and synthesis of liquid crystal gold nanoparticles and all of the relevant molecular sub-structures.

In particular it is focused on the optimisation of the synthesis of nematic mesogens with thiolated functional groups. The synthesis of gold nanoparticles in the size regime of 2.0 – 3.5 nm, either functionalised with hydrocarbon or deuterated hydrocarbon groups was achieved. The attachment of the thiolated functionalised mesogens to the gold particles was explored and a series of materials characterised in detail by using transmission electron microscopy (TEM) and gel permeation chromatography (GPC). A particular focus was on the purification methods in order to obtain pure and very well characterised gold nanoparticles (AuNPs) systems. Clear protocols for the preparation of high quality liquid crystal gold nanoparticles (LC AuNPs) were developed. Methods were explored to obtain liquid crystal optical polarised microscopy textures and the liquid crystal behaviour was determined by using DSC studies.

In a collaborative effort, the 2D and 3D structures of these materials were determined and the plasmonic properties characterised, showing that this novel class of materials exhibit synergistic optical properties based on the interaction of both the hydrocarbon groups and the AuNPs.

Overall, significant new knowledge has been added to the field of LC gold nanocomposites.

摘要

本论文的叙述的重点是液晶金纳米粒子超材料和所有与其相关子结构的设计和合成。特别着重于向列介晶与硫醇功能团搭配合成的优化。

本论文所叙述的金纳米粒子直径大小是在 2 纳米和 3.5 纳米之间，其中功能化包括与烃链或氘代烃链的搭配合成。本文同时也介绍了对功能化与巯基化液晶材料的结合的探索并通过使用透射电子显微镜和凝胶渗透色谱法等一系列技术对此材料的特征与属性进行了周密和详细的分析和表征。为了能得以获得高品质和具有完美表征的金纳米粒子系统，整个过程中特别要指出的重点是高品质样品的纯化方法。本课题研究的过程中研发了高品质液晶金纳米粒子的制备所必需的一系列方法与步骤，同时也研发了为获得液晶光学偏光显微镜层纹理质地所需要的方法。本论文也叙述了怎样用差示扫描量热法来探测和确定样品的液晶特征。

在与本科研项目的其他组成员的协作努力下，使得这些超材料的的二维和三维结构能够得到测定和表征，同时也确认了此超材料的等离激元属性特征，并表明该材料所含有光学特性基于烃链和介晶的相互作用。

List of Abbreviations

DCM	Dichloromethane
EtOH	Ethanol
MeOH	Methanol
NaSMe	Sodium thiomethoxide
DMF	Dimethylformamide
THF	Tetrahydrofuran
TFA	Trifluoroacetic acid
HCl	Hydrochloric acid
DNA	Deoxyribonucleic acid
DCC	*N,N'*-Dicyclohexylcarbodiimide
DMAP	4-(*N,N'*-Dimethylaminopyridine)
DEAD	Diethyl azodicarboxylate
DIAD	Diisopropyl azodicarboxylate
PPh_3	Triphenylphosphine
DT	1-dodecanethiol
LC	Liquid crystal
LCD	Liquid crystal display
Col	Columnar phase
Cr	Crystalline phase
Iso	Isotropic liquid

N	Nematic phase
N_D	Discotic nematic phase
N_{Col}	Columnar nematic phase
Sm	Smectic phase
GISAXS	Grazing-incidence small-angle scattering
TEM	Transmission electron microscopy
HRTEM	High resolution transmission electron microscopy
GPC	Gel-permeation chromatography
GC	Gas chromatography
HPLC	High performance liquid chromatography
TGA	Thermogravimetric analysis
ICP	Inductively coupled plasma
MS	Mass spectrometry
TLC	Thin layer chromatography
Prep-TLC	Preparative thin layer chromatography
SEC	Size exclusion chromatography
GFC	Gel filtration chromatography
n-BuLi	*n*-Butyllithium
EtOAc	Ethyl acetate
Et_2O	Diethyl ether
AIBN	Azobisisobutyronitrile

TOAB	Tetraoctylammonium bromide
DMSO	Dimethylsulphoxide
nm	Nanometre
µm	Micrometre
mm	Millimetre
ml	Millilitre
L	Litre
Au	Gold
NP	Nanoparticle
NC	Nanocluster
AuNP	Gold nanoparticle
LC AuNP	Liquid crystal gold nanoparticle
SPR	Surface Plasmon resonance
LSPR	Localised surface Plasmon resonance
FCC	Face centred cubic
RI	Refractive index
UV-Vis	Ultraviolet-Visible
RT	Room temperature
Me	Methyl group
Et	Ethyl group
CNT	Carbon nano tubes

Table of Contents

Aims and Objectives

The overall scientific objectives of the research in this thesis are the synthesis and characterisation of liquid crystal gold nanoparticles with non-conventional electromagnetic properties by using bottom-up fabrication technique. In a bottom-up approach, the gold nanoparticles are organised via self-organisation on the molecular scale. This is a unique approach that overcomes the limitation of conventional planar fabrication technology, which is, at present, nearly exclusively used for the fabrication of metamaterials. This research will help closing the technological gap between a bottom-up nanostructure fabrication and real world applications.

The objective of this thesis is to methodically clarify, optimise and understand all synthetic and purification aspects leading towards liquid crystal gold nanoparticles. This includes an improvement in the synthetic materials leading towards suitably functionalised liquid crystal groups as well as the synthesis and characterisation of gold nanoparticles.

Additionally, a set of novel liquid crystal gold nanoparticles with particle sizes of 2 – 3.5 nm diameter were designed, synthesised and characterised in order to be further investigated by collaborative researchers in the EU project “NANOGOLD” for surface plasmonic properties. These materials were studied with the metamaterial behaviour, due to the aim of seeing optical interactions of the liquid crystals groups and the gold nanoparticles.

Layout of this Thesis

The research carried out in this thesis was part of the work proposal in the EU funded project "NANOGOLD", focused on the design and characterisation of novel optical metamaterials based on self-assembling liquid crystal nano-composites. The thesis covers two topics with quite distinct focus: (i) liquid crystal design, and (ii) investigation and research into gold nanoparticles. This thesis is thus presented into two chapters, and each chapter consists of an individual specific introduction to the subject.

Chapter One

Chapter One addresses the discussion of the synthesis and characterisation of liquid crystalline compounds with a thiolated functional group, this also includes all intermediates involved. The synthetic methodology of the target mesogenic materials have been investigated in detail to increase the sample yield and simplify purification procedures. This Chapter One consists of six main sections.

First of all, the history and general background of liquid crystals (LC) are introduced. This includes their optical properties, the fundamentals of liquid crystal (LC) birefringence and specifically a discussion of the nematic phase of thermotropic calamitic liquid crystals, typical mesogenic structures and their self-organisation. This is followed by a brief description of the identification of liquid crystals and characterisation techniques, such as optical polarising microscopy (OPM) and differential scanning calorimetry (DSC). Finally, a simple introduction of modern applications of liquid crystals (LC) technologies in our daily life is added.

After the aims and objectives are defined, the synthetic results and methodology approaches are discussed in the following section. This section discusses the synthesis of the main mesogenic groups and important synthetic optimisations of some crucial intermediates. This part is then followed by the synthesis description of the thiolated mesogenic compounds, where a series of different synthetic routes are compared and discussed. The synthesis of a set of compounds using an optimised route is described as well as that of a series of intermediates and the characterisation of these materials. In the following sections, the synthetic procedures and instrumentation details are presented. Finally this chapter is summarised with a conclusion.

Chapter Two

In Chapter Two, the synthesis and characterisation of monodisperse gold nanoparticles (AuNPs) and liquid crystal functionalised gold nanoparticles (LC AuNPs) with well-defined size is discussed.

The first section consists of an introduction to nanotechnology, to the general history and background of gold nanoparticles (AuNPs), plus a short review of typical ligand exchange reactions on gold nanoparticles (AuNPs). Surface plasmonic resonance (SPR) effects in metal nanoparticles are briefly introduced. This is followed by an overview of self-assembly superstructures. The final part is mainly focused on the introductions of important characterisation techniques used for nanoparticles in this research project, such as transmission electron microscopy (TEM), gel-permeation chromatography (GPC) and thermogravimetric analysis (TGA).

After defining the aims and objectives of this part of the research, the following section illustrates the results of the synthesis of monolayer protected AuNPs via direct reaction, and possible optimisations steps which can be taken to modify the size, and to improve the monodispersity, of nanoparticles. This AuNPs synthesis part is then followed by a discussion of the results of characterisation experiments on LC AuNPs obtained via ligand exchange reactions. Here it is clearly shown that liquid crystal phase behaviour is a property of the liquid crystalline gold nanohybrid and not simply a result of a mixture of AuNPs and LCs. Purification methods applied to improve the yield of monodisperse nanoparticles are also discussed thoroughly in the same part of this section, as well as the content of materials and the mesomorphic behaviour of the LC AuNPs. The final part of this section shows results of the research efforts obtained for AuNPs protected by a deuterated hydrocarbon monolayer and of such a system functionalised with liquid crystal ligands. Finally, conclusions are drawn and instrumentation details are summarised.

Chapter One

Liquid Crystals

1. 1 Introduction

1. 1.1 History of Liquid Crystals

Liquid crystals are well known today to a wide scientific community. Liquid crystals are partially ordered, anisotropic fluids, thermodynamically located between the three dimensionally ordered solid state crystals and the isotropic liquid state. The liquid crystalline state was detected more than 100 years ago. During the 19th century researchers began reporting unusual "double melting" and "double refracting" phenomena.[1] One such early discovery was by Virchow in 1855 whilst working with nerve fibre Myeline,[2] which was later reported by Mettenheimer to be double refracting[1] and another discovery was by Heintz in 1855, who noticed that stearin melted to a cloudy fluid at 52 ^{o}C, which became opaque at 58 ^{o}C, and a clear liquid at 62.5 ^{o}C.[1, 3, 4] These observations probably marked the discovery of liquid crystalline substances, but they were not recognised as such. In 1888, an Austrian botanist and chemist Friedrich Reinitzer[5-8] at the University of Graz synthesised several esters of the natural product cholesterol occurring in plants and animals, noticed that cholesteryl benzoate (Figure 1.1), melted to a "turbid but absolutely fluid liquid" at 145.5 ^{o}C which "suddenly became clear" at 178.8 ^{o}C.[1, 4-6]

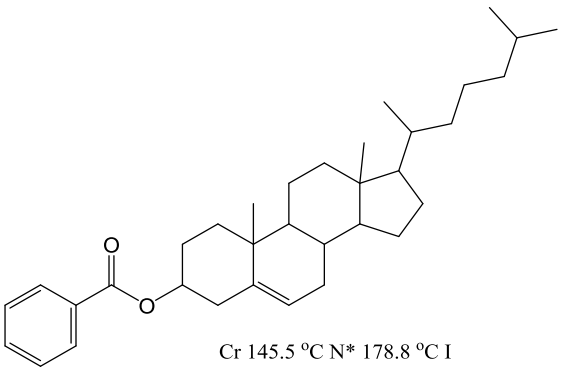

Figure 1. 1. Natural cholesterol compound of cholesteryl benzoate.

Reinitzer found the phenomenon of "double melting" behaviour for cholesteryl benzoate, and these phase changes were reproducible with increasing and decreasing temperature in several compounds. Looking to the literature before Reinitzer, some indication can be found that several scientists indeed dealt with liquid crystals, but did not notice the unique phenomena and therefore did not become aware of this new state.

Reinitzer himself was not able to explain this apparently strange phenomenon of "double melting" and the existence of the opaque liquid. Therefore, he contacted a physicist, Otto Lehmann, who was an experienced crystallographer of the time in Germany, and he is credited with the development of the polarisation microscope, which has played an important role in the discovery and development of liquid crystals.[1, 7] After studying the opaque liquid phases of cholesteryl benzoate by Reinitzer, he quickly found the optical anisotropy of the sample and concluded that the 'cloudy appearance' exhibited double refraction, characteristic of a crystal but behaved like a uniform phase of matter, eliminating the possibility of solid and liquid phases occurring simultaneously.[7, 9] Therefore, Lehmann described it as "*Über Fliessende Kristalle*" (On Flowing Crystals), which inspired the use of the term "liquid crystal".[8, 10-12] Today, it is clear that, in principle, this explanation was valid. Lehmann created the designation "fluid crystals" and "liquid crystals".[8]

From this point on there was an interest in liquid crystals, albeit mostly academic in nature. Some research was carried out, and the most prolific researcher of the time was Vorländer, who undertook a vast programme of research (more than 2000 compounds were investigated) which was aimed at determining basic structure-property relationships in liquid crystals.[13, 14] Vorländer's research led to many interesting new discoveries *e.g.* the understanding that molecular shape was important to liquid crystal phase generation and room temperature liquid crystalline materials, Vorländer reported that "the crystalline-liquid state results from a molecular structure which is as linear as possible".[15, 16]

Friedel, who believed the term "liquid crystal" to be misleading, introduced the term "mesomorphic" and a new classification system of liquid crystals in 1922.[17] Optical microscopy had revealed that there was more than one type of mesomorphism and hence Friedel proposed the terms: nematic, smectic, and cholesteric, which have since been refined, however they are still widely used today.[17-19]

Between 1920 and 1940 the first X-ray experiments were conducted upon mesomorphic materials which provided a definitive model of mesophase structure.[20] By the end of World War II, however, liquid crystal research had virtually disappeared, in part due to the lack of perceived applications and reductions in funding.[13, 18] During the 1960's and 1970's, however, there was a resurgence of liquid crystal research due to the lure of new applications. This research period was pioneered by Gray who made many discoveries,

e.g. the first stable room temperature nematic liquid crystal that could be used in a display device as shown in Figure 1.2, and has contributed greatly together with others to the current classification of smectics.[13-15, 21, 22]

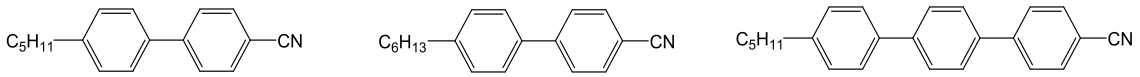

Cr 24.5 ^{o}C N 35.5 ^{o}C I Cr 13.5 ^{o}C N 28.0 ^{o}C I Cr 131.0 ^{o}C N 240.0 ^{o}C I

Figure 1. 2. First generation of stable room temperature nematic liquid crystals.

After this, many compounds with other molecular shapes have also been shown to exhibit a variety of liquid crystalline phases, such as disc-like, wedge-shaped, T-shaped and banana-shaped.[23-25]

1. 1.2 Introduction to Liquid Crystals

Prior to the discovery of the liquid crystalline phase by Reinitzer, it was a common perception that only three states of matter ever existed: solid, liquid, and gas, as shown in Figure 1. 3. The solid state is the most ordered of the states of matter, with long range positional and orientational ordering of the constituent molecules in three dimensions. When thermal energy is introduced to a fully ordered molecular crystalline solid, the molecules' thermal motions within the lattice increase until eventually they break the forces of attraction which hold the regular arrangement of molecules together, and the solid melts into a disorganised liquid phase. Molecules in the liquid phase are free to rotate, vibrate and flow randomly. The constituent molecules are completely disordered with respect to each other, however they do not possess enough thermal energy to break into the gas phase. They are described as isotropic ("*iso*" is a Greek word meaning equal, as liquid phase has the same physical properties when measured from any direction), since they no longer possess any positional and orientational ordering. Further heating the liquid phase increases the vibrations and motions of the molecules increase until it reaches its boiling point, turning into the gaseous phase. There are fewer constituent molecules in a given volume than any of the other states of matter and this is the most disordered of the states of matter.

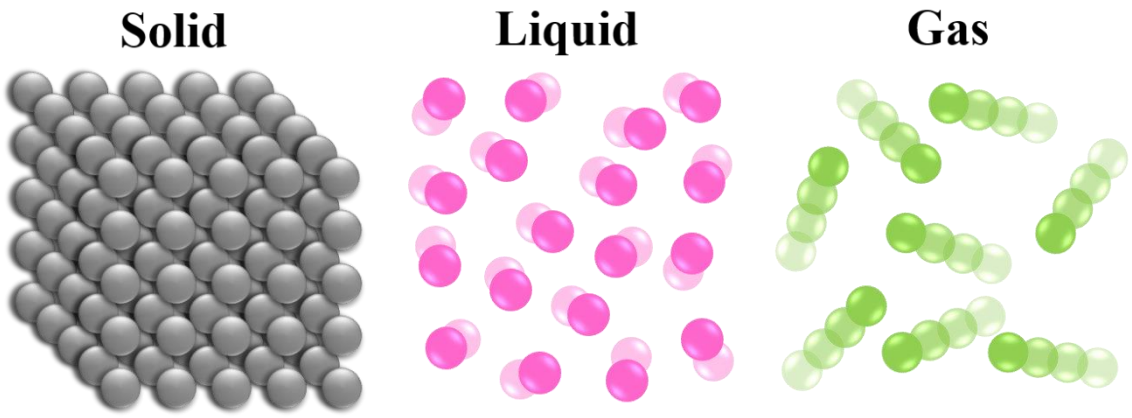

Figure 1. 3. Molecule arrangements within the three common states of matter.

However, such a simplistic view is not universal. There are many other physical properties of materials that do not follow this simplistic pattern, *e.g.* deoxyribonucleic acid (DNA) and cell membranes.[26] DNA is capable of self-organisation during the process of replication, which is possible either in the crystalline solid or isotropic liquid states. Cell membranes are another example. They consist of a lipid bilayer, which is not in the

crystalline state, as movement of molecules would be impossible. Membranes could not be in the isotropic liquid state either, as there would be no cohesive force holding a biological body together, and an individual human being would exist as a puddle of liquid. Those behaviours are very different in comparison with cholesteryl benzoate, which shows the phenomenon of "double melting" between the solid and liquid phases upon heating. This is due to the wide ranging nature of the materials termed as "liquid crystals".[18]

The liquid crystal state is the fourth state of matter, one or more intermediate phases exist between the disordered isotropic liquid phase and the regular molecular arrangement of a crystalline solid. Liquid crystals are called mesophases and can flow like fluids despite having retained some of the anisotropic properties of crystals. Liquid crystalline phases have physical properties between those of the fully ordered crystalline solid and the isotropic liquid. Those properties can be characterised by their molecular positional, orientational order and their anisotropic properties. As established by Friedel in 1922, the name "liquid crystals" is misleading and liquid crystals should be termed "mesomorphic" phases ("*mesos*" and "*morph*" are Greek words meaning "middle" and "form") composed of molecules, which exhibits mesomorphism (consist of mesophases). Physical properties of liquid crystals can be widely influenced by the nature of the core and the side chains, allowing molecules to be designed for a specific purpose. Hence, numerous variations to these general molecular structures may be implemented, leading to the large variety of mesogenic compounds known today.[10]

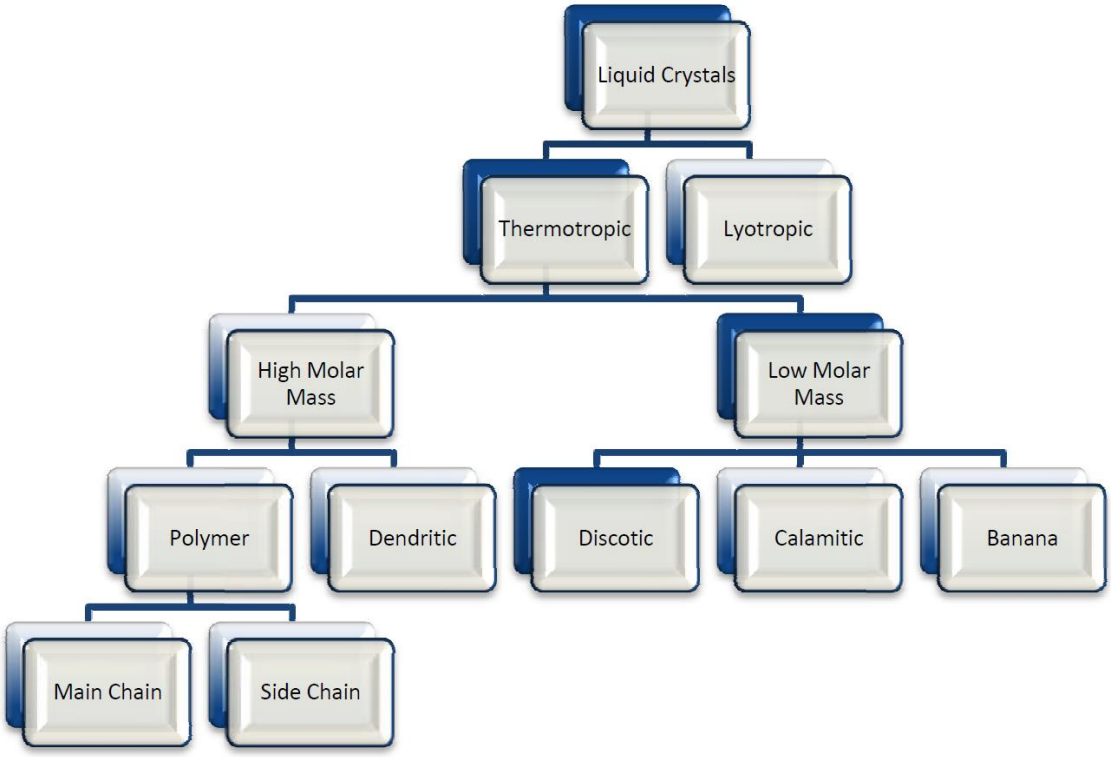

Figure 1. 4. Classification of liquid crystals.[4]

Liquid crystals are classified based on the stimulus of how the mesomorphism is generated. The breakdown of liquid crystals is shown in Figure 1. 4 below. The main two types of liquid crystals are lyotropic and thermotropic. The mesomorphic behaviour of lyotropic liquid crystals is controlled by its concentration in a solvent. Molecules exhibiting such phases are mainly amphiphilic, such as soap. In thermotropic liquid crystals, the mesomorphic behaviours are controlled by temperature and can arise from various different types of molecules, which possess a molecular structure that contains two segments which are different in chemical or structural character. As was noted by Vorländer, in particular, the molecular shape is extremely important, such as rod-like[15] (calamitic), disc-like[16] (discotic) and banana-like[7] (calamitic with a bent core), which are usually anisotropic fluids. This is mainly because the molecules themselves are anisotropic. As represented in Figure 1. 5, a calamitic liquid crystal and discotic liquid crystal molecule showing the significant difference in the length and width of the compounds.

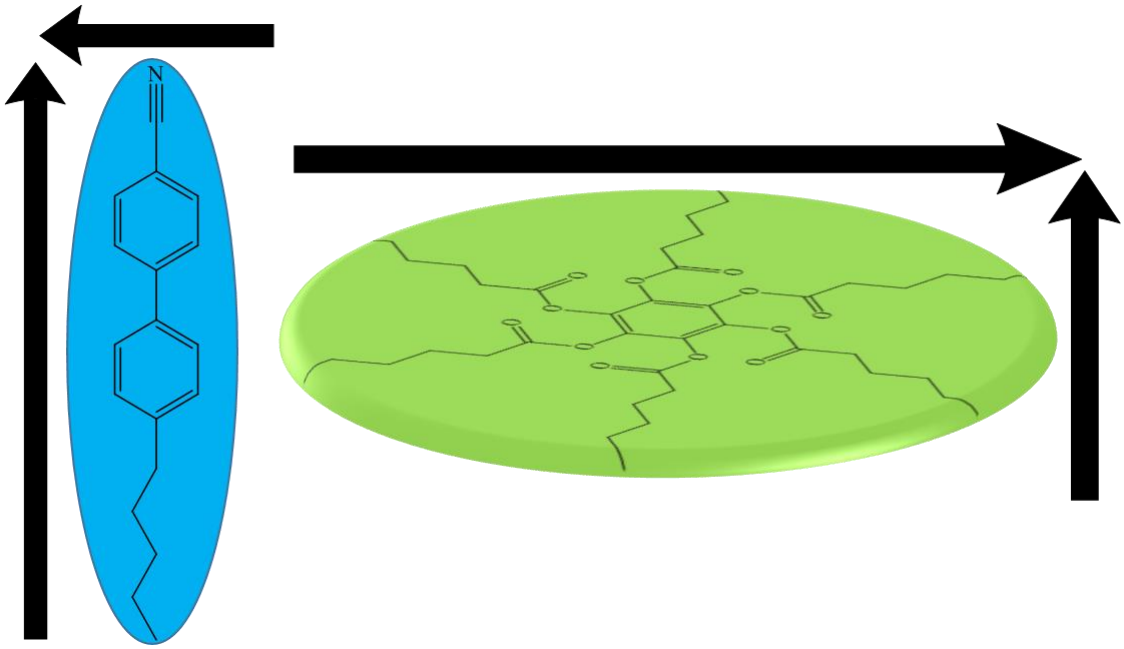

Figure 1. 5. Molecule anisotropy in a calamic and a discotic mesogen showing the difference in length and width of two different types of molecules.[4]

The thermotropic liquid crystals can be further subdivided into high molar mass and low molar mass materials. Only low molar mass thermotropic liquid crystals are being discussed from this point on, in particular the subdivision in this class – calamitic mesophorphic will be presented in more detail.

Thermotropic liquid crystal compounds generally consist of long, narrow, lath-like and fairly rigid molecular systems. Those segments are functioinalised by flexible alkyl or perfluorinated end-chains to make the necessary mobility.[27, 28] Unlike a fully ordered crystalline solid, those calamitic mesophorphic molecules organise themselves into one or more intermediate mesophases upon heating from a crystalline solid or on cooling from the isotropic liquid,[29] which are more complex than simple solid, liquid and gas one step transitions. All possible phase transitions of materials are presented in Figure 1. 6. A fully ordered crystalline solid will undergo a one-step transition T1 to an isotropic liquid and reaches its melting point on heating. From the isotropic liquid, it is able to fall back to the crystalline state, if steady cooling is allowed. By fast cooling, such as supercooling, molecules will “freeze” before they fall into crystalline state. In the calamitic liquid crystal state (C), the rod-like molecules are anisotropic and held together by strong intermolecular forces of attraction. It is described that the smectic phase arises if the terminal forces are destroyed before lateral intermolecular forces of attraction as temperature increases (T2), in-plane translational order is lost and a layered structure

forms, which still possess orientational order with molecules aligning themselves statistically pointing in a preferred direction.[4, 18] This preferred direction is known as the "director" (*n*).[19] The lateral attraction forces within the smectic mesophases can be broken upon heating, and the layered structure breaks down, but the orientational order still remains (T4), which produces the nematic phase, or clear directly into the isotropic liquid phase with further heating to a point when the orientational ordering is lost (T6). T3 represents liquid crystal transition straight from the crystalline solid to the nematic phase, as not every mesophorphic compound exhibits all possible mesophase types but many compounds do exhibit two or three different types of liquid crystalline phases.[18] T5 depicts the loss of orientational ordering of the smectic phase to give the isotropic liquid. Generally, rod-like molecules organise themselves into lamellar structures (smectic phases) or a nematic phase, while disc-like molecules order themselves into columnar phases.

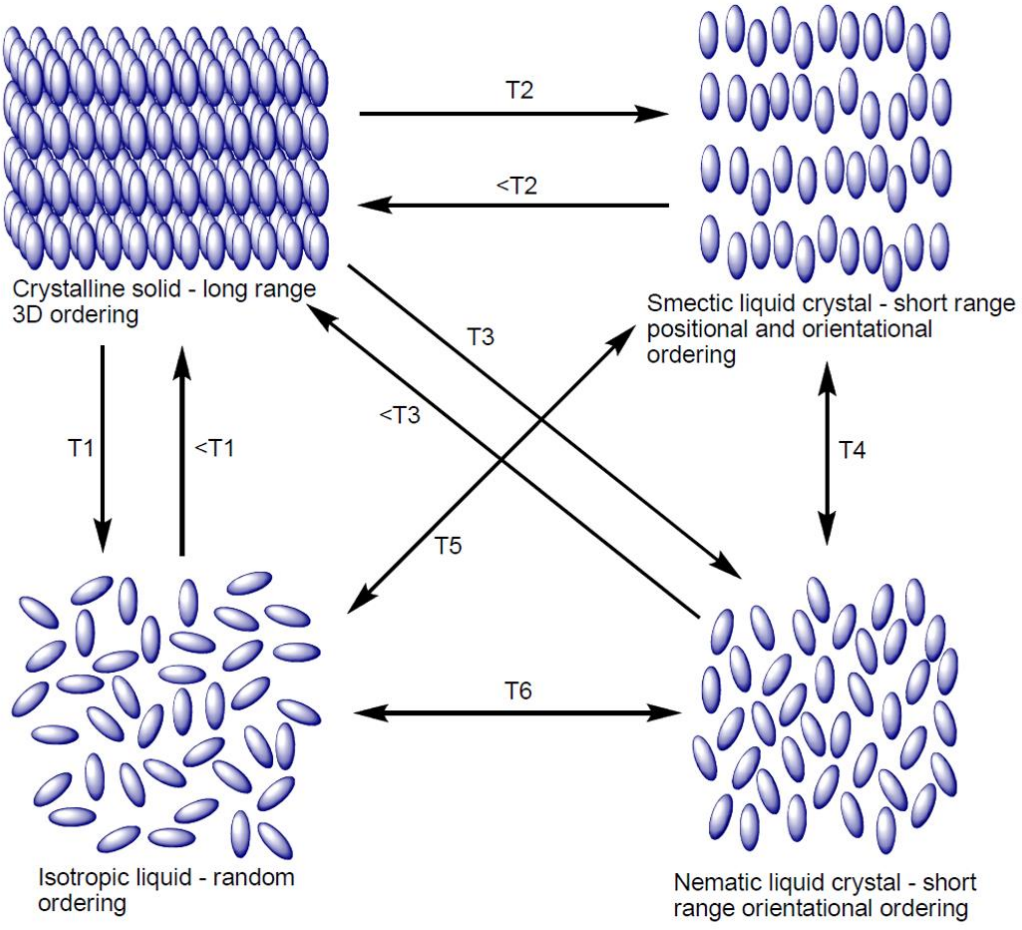

Figure 1. 6. Possible transitions of thermotropic liquid crystals.[4, 18]

1. 1.2.1 Optical Properties of Liquid Crystals

Knowledge of the optical properties of liquid crystals with polarised light is required to understand their principal technological applications. Polarised light is generally used to investigate the liquid crystals property as it can be altered by liquid crystals when passing through them. Polarised light is an electromagnetic wave propagating through space, except oscillating with only one orientation. Electromagnetic waves, such as visible light, consist of both electric and magnetic field components, which oscillate in more than one orientation, but perpendicular to the direction of energy and wave travel, as well as perpendicular to each other in a fixed relationship. In order to generate polarised light with electric and magnetic field with only one orientation, a polarising filter is needed to absorb all components of incoming unpolarised visible light electromagnetic waves apart from a single component of polarised light electromagnetic wave selected to pass through. Light waves with different orientation are unable to pass through the second polarising filter with the polarisation axis placed 90° above the first, because the polarisation passed by the first filter is precisely the polarisation blocked by the second filter. However light may get through if optically active materials such as liquid crystals are placed between the crossed polarising filters, because the intervening material changes the polarisation of the light. If the liquid crystals molecular director is not aligned with either of the polarising filters, polarised light then becomes partially polarised along the liquid crystal molecular director after passing through the first filter. As a result, the electric and magnetic field orientation becomes aligned with the top polarising filter and passes through the entire assembly. The amount of light passing through is the largest when the liquid crystal molecular director is positioned at a 45° angle from both filters. The light is fully blocked when the director lies parallel to one filter or the other.

The liquid crystal molecular director alignment may be induced artificially. For example, the surfaces of a glass container can be rubbed in an appropriate direction, forcing the director to lie perpendicular or parallel to the wall adjacent to the liquid crystal. It is not necessary to force the director in one wall to be consistent with other walls. However this will vary the director orientation between the walls.

1. 1.2.2 Principles of Birefringence

Liquid crystalline materials are doubly refractive or birefringent due to their molecular anisotropy. Birefringence is the optical behaviour, which is well known for solid materials

and the process is essentially the same in liquid crystals. It occurs when light is decomposed into ordinary and extraordinary rays, the ordinary rays will travel parallel to the director and the extraordinary rays will travel perpendicular to the director. This is because the electric and magnetic fields of light (transverse wave of electromagnetic energy) are fluctuating. The two constituent components of the light travelling through the material will travel at different velocities (the ordinary ray travels faster than the extraordinary ray). This arises due to optical anisotropy associated with the liquid crystal phase. The two waves are recombined out of phase with one another after exiting the material, a change in the polarisation state occurs. The refractive indices of the ordinary ray and extraordinary ray can be calculated as equations shown below:

$$n_e = \frac{c}{v_{\parallel}} \qquad\qquad n_o = \frac{c}{v_{\perp}}$$

Equation 1. 1

$n_e = refractive\ index\ parallel\ to\ the\ director$;

$n_o = refractive\ index\ perpendicular\ to\ the\ director$

$c\ = the\ speed\ of\ light\ through\ a\ vacuum$;

$v_{\perp} =\ light\ travelling\ velocity\ perpendicular\ to\ the\ \ molecules\ orientation$;

$v_{\parallel} = velocity\ of\ light\ travelling\ parallel\ to\ the\ orientation\ of\ the\ molecules$;

Hence, the magnitude of birefringence can be summarised by Equation 1. 2.

$$\Delta\, \boldsymbol{n} = \boldsymbol{n_e} - \boldsymbol{n_o}$$

Equation 1. 2

$\Delta\, n = magnitude\ of\ birefringence$;

$n_e and\ n_o\ are\ the\ same\ as\ above$

Light polarised parallel to the director has a different refractive index compared to light polarised perpendicular to the director. As presented in Figure 1. 7, showing how the different waves travel through the birefringent material.[24]

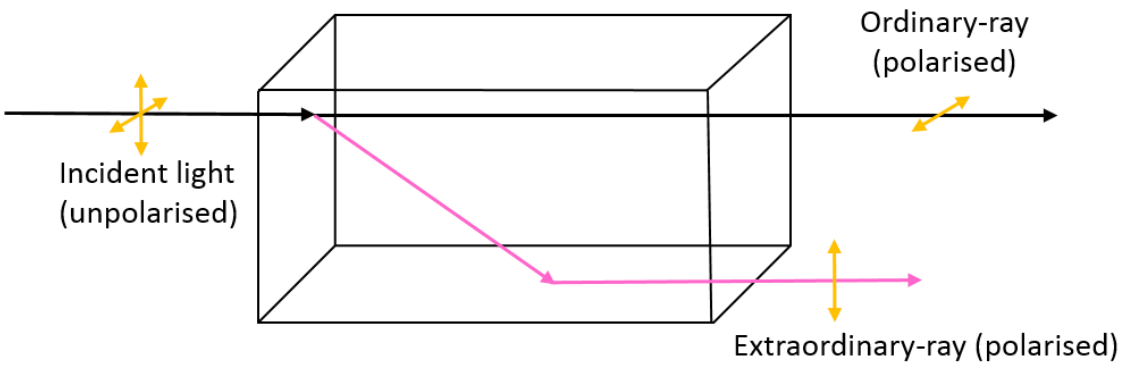

Figure 1. 7. passage of linearly polarized light through a birefringent medium.

The birefringence is crucially affected by the shape of liquid crystals molecules and dielectric permittivity (ε) of liquid crystals. The birefringence is typically positive for calamitic compounds, whereas for discotic materials, it is usually negative, due to the molecules' arrangement being perpendicular to calamitic molecules (Figure 1. 5). The dielectric permittivity is a measurement of electrical dipole of a compound either permanent or induced with an electrical field. Compounds with induced strong dipoles usually contain groups such as cyano or fluoro substituents, which will interact strongly with an applied electric field.[18] The anisotropic nature of liquid crystalline compounds is the difference of permittivity measured either perpendicular or parallel to the director *n*. The result of both birefringence and dielectric permittivity have important implications for liquid crystals applications, and is important in optoelectronic devices and the design of fast switching molecules for display devices.

In an optical polarised microscope (OPM), light travelling through the material will be affected by the birefringence of the media.[18] Consequently when no birefringent medium or a non-birefringent medium (*e.g.* an isotropic liquid) is present the light will not be affected and hence the light will be blocked by the crossed polarisers and thus appear dark.[18] When passing through a birefringent material, however, the light is affected to different degrees based upon several factors *e.g.* the thickness of the sample, the magnitude of the birefringence, the orientation of the director and defects in the structure of the material. Since the molecular organisation of each phase is unique, each mesophase has a characteristic texture (or textures) associated with it and an experienced researcher can distinguish between the various subtleties of these textures to positively determine mesophase morphology. Therefore, OPM is one of the most powerful techniques available for swift and definitive identification of mesophase morphology. Indeed, OPM

can be viewed as the first-line in the identification and characterisation of a mesophase. When liquid crystalline materials are viewed through crossed polarisers, some areas appear lighter and some areas are darker, this is the result of birefringence. The difference in the intensity of light passing through the second polariser is dependent on director orientation, birefringence and sample thickness. Areas of darkness occur where the director is parallel to the polarisation of the incident light. The birefringence shows significant temperature dependence, as the liquid crystal anisotropy is strongly dependent on temperature and the birefringence of a material is determined by the phase anisotropy, which vanishes at the nematic to isotropic phase transition.

1. 1.2.3 Thermotropic Calamitic Liquid Crystals

Thermotropic liquid crystals are the most widely researched liquid crystals and many reported thermotropic liquid crystals are single compounds.[7, 10] A common structural feature of calamitic liquid crystals is a relatively rigid core, often incorporating aromatic phenyl or biphenyl groups ensuring the anisotropic character, together with flexible polar end groups, often alkyl or alkoxy chains, which provide stabilizing effects within the mesophases.

The orientational order of thermotropic liquid crystals is well defined and the molecular axes are oriented on average in the same direction. Liquid crystals can exhibit short-range or long-range positional order, but are less organised in comparison to a crystalline solid. Thermotropic liquid crystals are the most widely used liquid crystals and are extensively studied for their linear as well as nonlinear optical properties. They exhibit various liquid crystalline phases as a function of temperature. Although their molecular structures are quite complicated, they are often represented as "rigid rods". These rigid rods interact with one another and form distinctive ordered structures.

Calamitic liquid crystals were the first thermotropic liquid crystal compounds to be discovered. This class of materials exhibit a rich range of mesophases between crystalline and liquid phases. There are two principal liquid crystalline phases for calamitic (rod-shaped) liquid crystal. The most observed of these mesophases are the nematic and various smectic phases, as illustrated in Figure 1. 8 below.[30]

Smectic mesophases are formed mainly by calamitic mesogens, organised into layers while exhibiting both the orientational and positional order.[19] They are more ordered than

the nematic phase and the smectic mesophases layers are not rigid and are able to slide over one another. They were named in the order of discovery, hence the first smectic discovered was named smectic A, the second smectic B, *etc*.[18] As represented in Figure 1.8, there is only one nematic mesophase structure existing, whereas there are many different types of smectic phases, as there are many ways in which positional order can be achieved in a layered structure. There are two main types of smectic phases: orthogonal or tilted, they can be further divided according to the extent of the positional order within the layers, such as smectic A (short-range) or smectic C (long range) where positional order occurs. Some other true smectics (B, I, F) are also mesophases with layered structures (diffusion between the layers occurs). The mesophases are fluid but more viscous and considerably more ordered with inter-layer correlations appearing. Another subdivision of smectic phases are some ordered crystal smectics (B, E, G, J, K), where the molecules possess long-range positional order in three dimensions. They are soft crystal mesophases (less order than a crystalline solid) but not liquid crystal mesophases, even though there is considerable disorder of molecular orientation.[13, 19] An overview of smectic mesophases can be find in the Figure 1.8. It is noted that this thesis is focused only on the nematic mesophase.

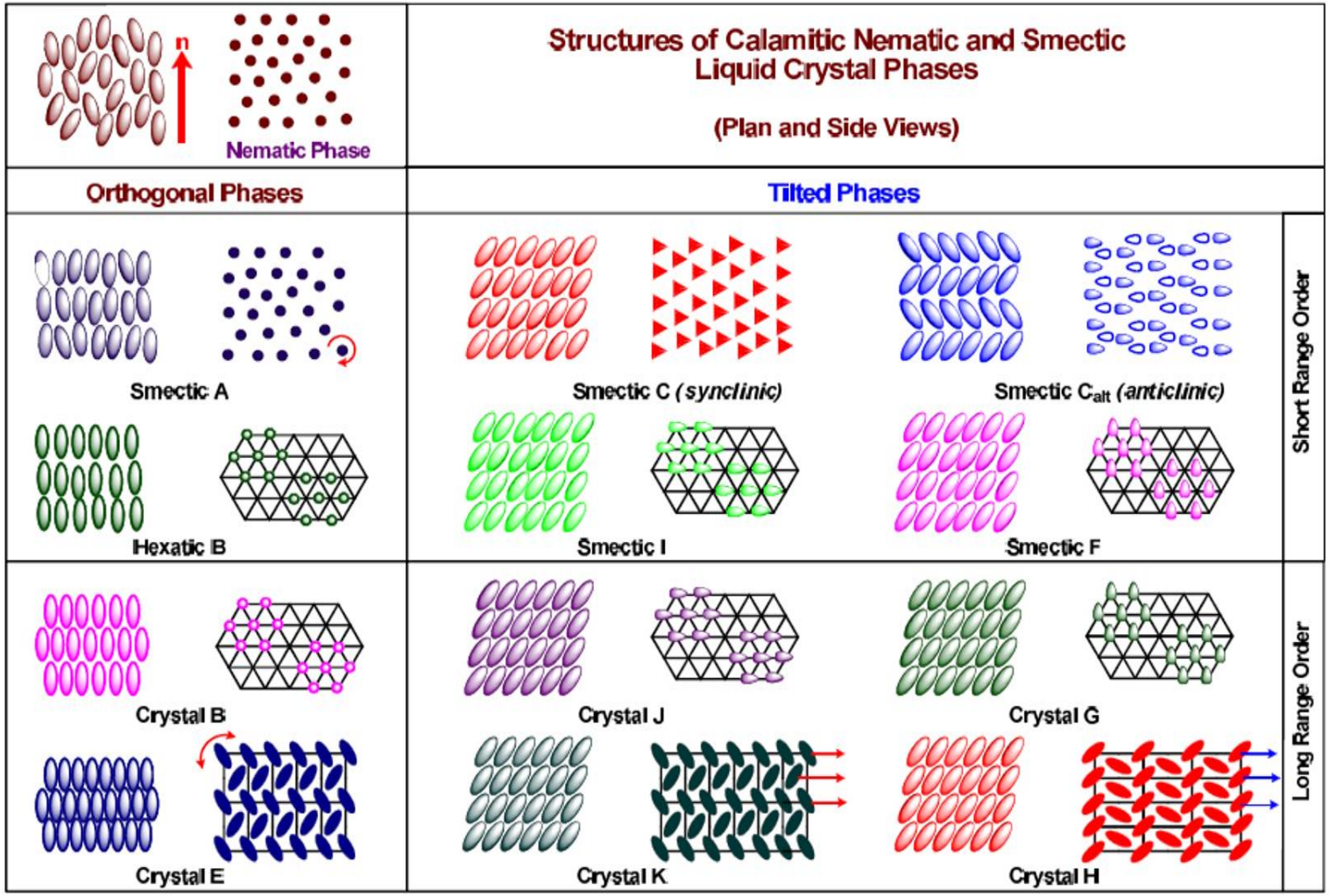

Figure 1. 8. Schematic representation of nematic and smectic liquid crystal phases.[4]

1. 1.2.3.1 Nematic Phase (N)

As observed by Friedel in 1922, liquid crystal molecules in the nematic (Greek, meaning thread-like, since thread-like textures are observed during optical microscopy investigation) phase are not completely disordered with respect to each other, but the molecules statistically self-align to point in a preferred direction to have long-range directional order with their long axes roughly parallel along the director *n*. [31] As only short-range positional order exists in the nematic mesophase, this puts it close to an ordinary isotropic liquid (Figure 1. 9). Due to the uniaxial nature of the ordering with locally preferred direction varies throughout the medium, there is only one nematic phase. This mesophase is the least ordered with a high degree of fluidity and the simplest mesophases of all. A nematic liquid crystal phase can be generated by both calamitic rod-like molecules and discotic molecules. Although both variations exhibit the same optical texture, these two nematic phases are not miscible and hence they are different systems. The nematic (N) liquid crystal phase is technologically the most important of the many different types of liquid crystal phases, because in this type of materials, molecular orientation could be chemically designed to be easily switched by an electric field. In combining the property of this low viscosity with the anisotropic nature of this type of molecules, make them the perfect basis for the operation of a liquid crystal display.[4, 18, 32, 33] The world market for liquid crystal displays continues to expand strongly and is currently worth more than $130 billion per year, which accounts for a large proportion of all displays with hundreds of million of units being shipped every year. Nematic liquid crystal displays are currently used in high-definition and large-sized displays (up to 82 inches), also expected to satisfy future demand for 3D displays.[27]

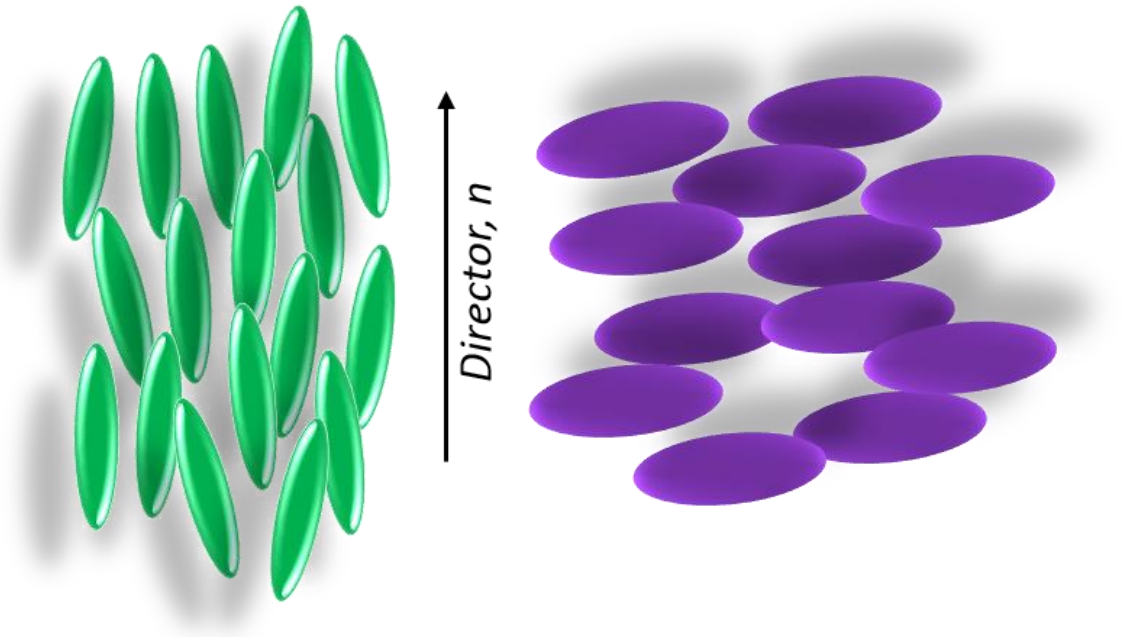

Figure 1. 9. Schematic representation of the nematic phase (left) and discotic nematic phase (right).[34]

The degree of order between the molecules is defined by the order parameter *S*, which can be represented by the equation shown below: [35]

$$S = \left\langle \frac{1}{2}\left(3\overline{\cos\theta^2} - 1\right)\right\rangle$$

Equation 1. 3

Here θ is the angle between the director *n* and the long axis of the individual molecule long axis (Figure 1. 10).[18, 35]

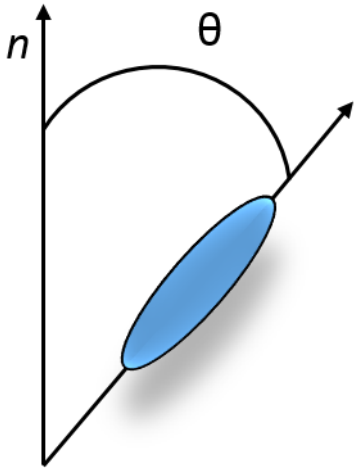

Figure 1. 10. Definition of the angel θ between the director n and a LC molecule.

In a perfectly oriented crystalline solid system $S = 1$ when all molecules are parallel to *n* which denotes the highest possible order. In an isotropic liquid state with no orientational

order at all $S = 0$, hence the material is isotropic. For the nematic phase this value is comprised between $0.4 – 0.9$.[18, 19]

The nematic phase typically for discotic liquid crystals is similar to the one for calamitic smectic mesophases. The discotic nematic phase has an orientationally ordered arrangement of the disc-like molecules with the aligned cores, which are surrounded by the side chains without any long-range translational order (Figure 1. 5 right). Like the calamitic nematic molecules, the discotic nematic phase (N_D) is the least ordered and least viscous of all mesophases. Unlike the classical nematic phase of rod-like molecules, this phase is less common as discotic molecules have a great tendency of assembling to columns, forming columnar phases.[23]

Additionally, there is also a chiral variation of the nematic phases, commonly called the cholesteric phase. Since it was observed in cholesterol derivatives, such as cholesteryl benzoate, and was therefore originally designated as the cholesteric phase.[1, 5, 36] It is often called the chiral nematic liquid crystal phase with molecules statistically arranged in a helix and aligned to a local director *n* as shown in Figure 1. 11. This phase is only encountered when the mesogens contain chiral groups. Some materials such as cholesterol esters are naturally chiral. Due to the lack of relevance of this type of molecules towards this thesis, discotic and chiral nematic mesophases are not discussed further.

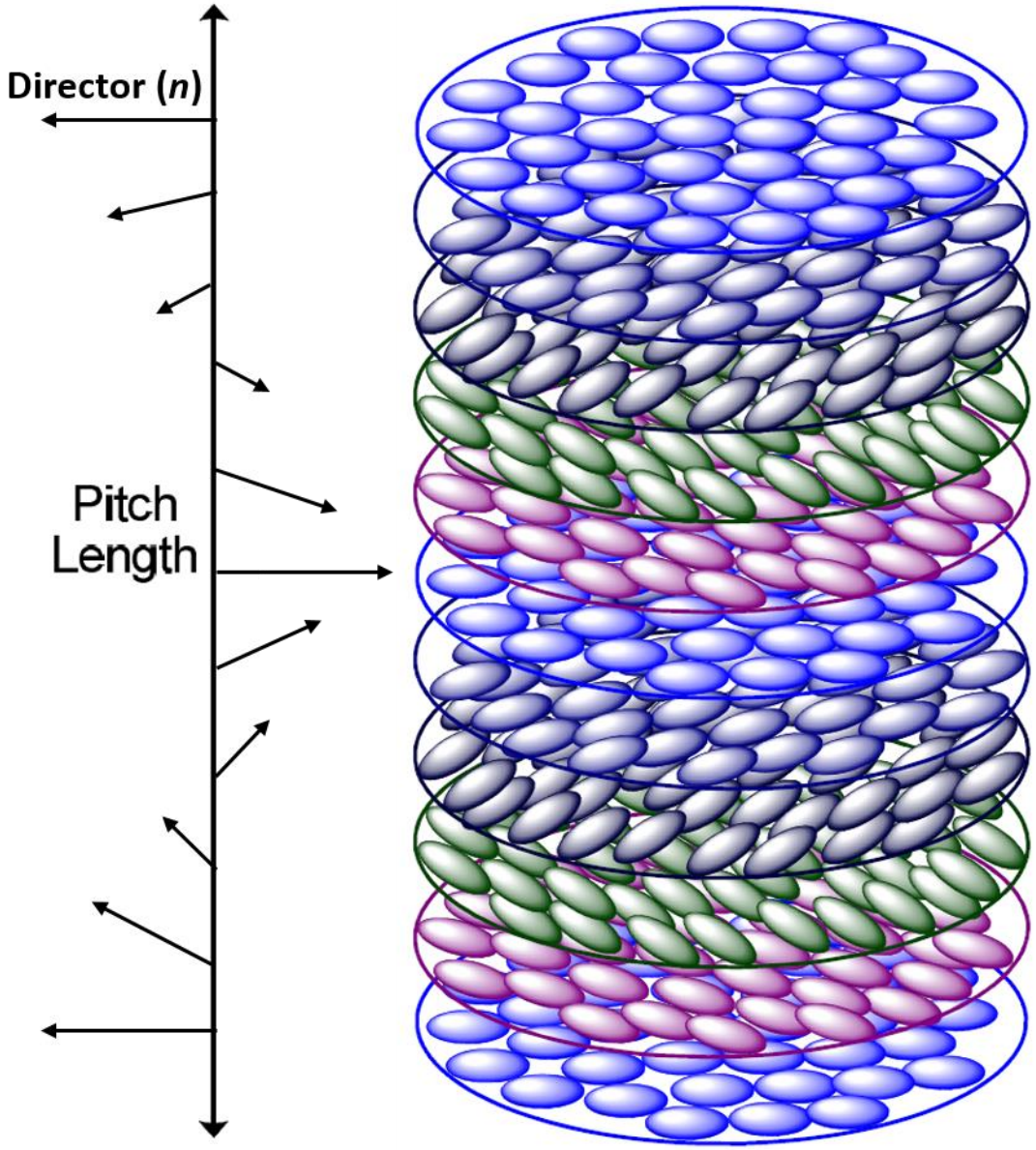

Figure 1. 11. The liquid crystal arrangement in a cholesteric phase.[4, 18, 37]

There is another rarely observed nematic mesophase, called columnar nematic (N_{Col}). It is comprises of short columns possessing orientational order but no positional order relative to one another. Similar to the single molecules in the nematic or nematic discotic mesophase, the columns act as a singular "building-block" of the nematic phase. This type of mesophase exhibit the same symmetry as the N_D and N mesophases. It can also be characterised by Schlieren optical microscopy textures.

1. 1.3 Identification and Characterisation of Mesophase Morphology

The aim of this section is to consider the techniques used for mesophase characterisation and identification. There are many different types of liquid crystalline mesophases with subtle differences in the short range and long range order. Each mesophases are different in structure, and a precise classification of liquid crystal mesophases requires the use of several analytical techniques to be more certain of mesophase type.

Optical Polarising Microscopy (OPM) is the most widely used technique of liquid crystal mesophase identification. It reveals that each different liquid crystal phase has a distinct optical texture. However, it is often very difficult to distinguish the identification of liquid crystal phases through OPM, as this requires a lot of experience. Therefore, Differential Scanning Calorimetry (DSC) is always employed as a great complementary tool to OPM. DSC is able to reveal the presence of mesophases by detecting the enthalpy change during a phase transition. Although this technique cannot identify the type of liquid crystal mesophases, the magnitude of the enthalpy change does give some information about the degree of molecular ordering within a mesophase. The ultimate technique for the identification and classification of mesophases is X-Ray Diffraction (XRD). Aligned samples are often required to maximise information from this technique. As this technique can determine the phase structure by mapping the positions of the molecules within the phase. There are other techniques used to identify the structure of liquid crystalline mesophases, such as neutron scattering studies and nuclear magnetic resonance (NMR) studies. However only OPM and DSC of those most commonly used liquid crystalline mesophases identification techniques will be described in this section.

1. 1.3.1 Optical Polarised Microscopy (OPM)

Optical polarised microscopy is one of the most powerful techniques designed to observe and aid the identification of liquid crystalline mesophase with optically anisotropic character. It is basically a contrast-enhancing technique that improves the quality of the image obtained with birefringent materials, in this case of liquid crystalline materials. Primarily, OPM enables the identification of the type of liquid crystal and other mesophases from the optical texture. As mentioned in previous sections, liquid crystals are birefringent and have a double refraction, which can be observed under polarised light,

primarily due to their optically anisotropic nature. Valuable information on isotropic optical properties can be identified and diagnosed.[38] It is also extremely useful to determine the different structures and evaluate the physical properties of the liquid crystal phases. Indeed, OPM has always been used as the initial identification and characterisation of a mesophase.[18]

Light from an ordinary light source (*e.g.* natural light) transmitted in random directions is called non-polarised light. In contrast, light with transverse wave vibrations that possess direction is called polarised light. The principle of such microscope technique is reliant on the polarisation of light. In order to achieve this, the microscope must be equipped with both an analyser and a polariser. The analyser is placed in between the objective rear aperture and the observation tubes or camera port of the optical pathway. The polariser is positioned in the light path somewhere before the specimen and behaves as a filter that only permits the light with its electric field oriented in a specific direction to pass through. These two polarisers are oriented at right angles to each other as (crossed polariser as shown in Figure 1. 12 left). As mentioned in the previous section, when polarised light enters a birefringent material, it is refracted into slow extraordinary and fast ordinary rays, each polarised in mutually perpendicular planes. Both rays are recombined out of phase after exiting the material and an image contrast will be created after passing through the analyser with constructive and destructive interference. The fundamental of crossed polariser is illustrated in Figure 1. 12 left, only the vertical component of the electric field of light wave with the same direction as the polariser can pass through. This is because the polarising direction of the first polariser is oriented vertically to the incident beam. The passed wave is subsequently blocked by the second polariser, since this polariser is oriented horizontally to the incident wave.[39] The wave front field generated by a hypothetical birefringent specimen are outlined in Figure 1. 12 right. Additionally, the critical optical and mechanical components of a modern polarised light microscope are also demonstrated.

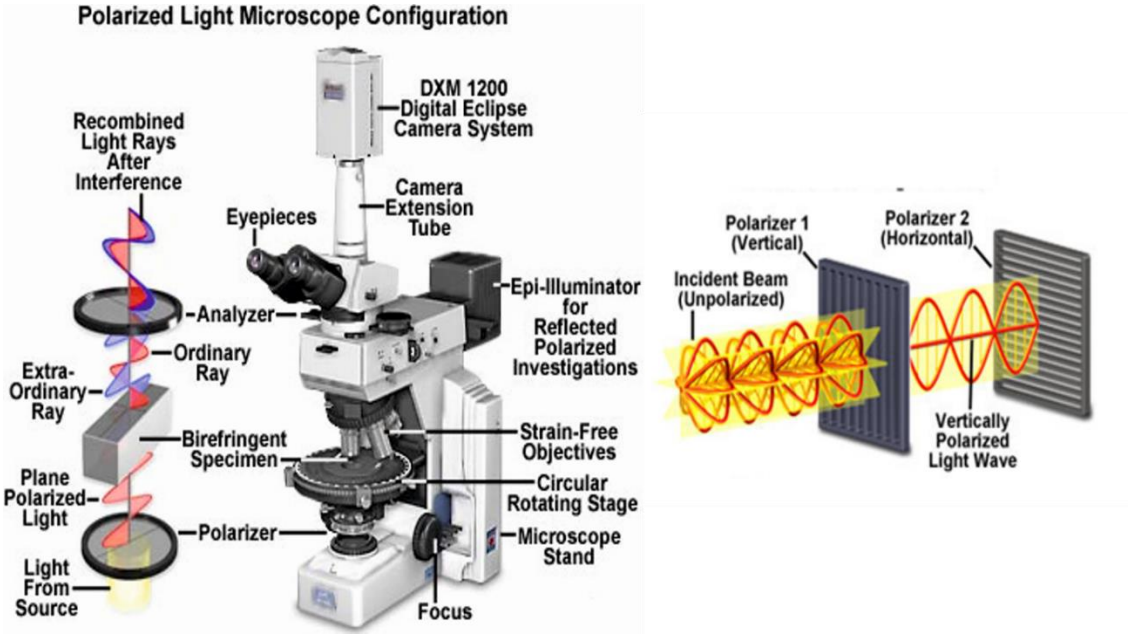

Figure 1. 12. The basic configuration of a polarised optical microscope.[38]

The identification of liquid crystalline mesophases under OPM usually requires the magnified view of a thin film of mesogenic sample on a microscope slide between crossed polariser at 90^{o} to each other. This mesogenic sample is usually placed on an accurately temperature controlled stage. The incoming linearly polarised light is not extinguished and an optical texture appears, as the light travelling through is affected by the birefringence of liquid crystals. It gives information relating to the arrangement of the molecules within the medium. The region becomes bright as the component can pass through after the ray reaches the second polariser (analyser). Consequently, the light will remain unaffected when non-birefringent material (*e.g.* isotropic liquid) is present, hence the light will be blocked by the second polariser (analyser) and thus appear dark. However, the light is affected to varying degrees based upon several factors, *e.g.* the thickness of the sample, the magnitude of the birefringence, the sample alignment and defects in the structure of the material. If the sample is very thin, the ordinary and extraordinary components do not get very far out of phase. Likewise, if the sample is thick, the phase difference can be large. The size of the phase shift determines the intensity of the transmitted light. The light does not break up into components and the polarisation state still remains unchanged, if the transmission axis of the first polariser is parallel to either the ordinary or extraordinary directions. In this case, dark region appears as there is not a transmitted component. If the phase difference equals 360 degrees, the wave returns to its original polarisation state and is blocked by the second polariser. On the other hand, the

birefringence and sample thickness are usually inhomogeneous over the entire sample in a typical liquid crystal. Hence some areas of the sample under OPM appear to be lighter than others, as shown in the OPM picture of a nematic liquid crystal taken between crossed polarisers (Figure 1. 13). The light and dark areas represent different regions of different director orientation, birefringence and length. Additionally, the molecular organisation of each phase is unique, each mesophase is associated with a characteristic texture or textures. Therefore, the detail of the various mesophases of these textures will require a lot of experience to positively identify and determine.

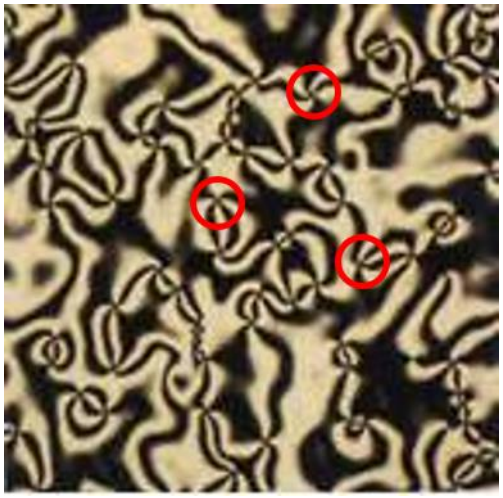

Figure 1. 13. A OPM picture of a typical nematic liquid crystal.[40]

Birefringence can lead to multi-coloured images in the examination of liquid crystals under polarised white light. The only light source used to investigate the optical properties of materials so far is monochromatic light. The result will not just show intensity differences, and different colours that are observed in liquid crystals placed between crossed linear polarisers under microscope. They are very useful in the study of liquid crystals in many situations, such as the identification of textures of liquid crystal phases and phase transitions. Additionally, these colours are mainly due to the local defects that create intensity differences and the layer thickness cause shifts in wavelengths as the changes in angle accumulate as the light passes through, hence the light is "broken" when it arrives, resulting colour patterns in the final picture.[30, 33]

The nematic phase is usually very easy to identify by OPM. It is the least viscous and most fluid of all mesophases. The unaligned nematic mesophases usually have directors pointing in the different directions in all regions of this sample. The director abruptly changes direction without any director can be defined and a defect is generated. This

results in the Schlieren brushes (Figure 1.13), appearing black because of optical extinction caused by the crossed polariser. Additionally, the nematic mesophase exhibits a Schlieren texture and often appears as spherical birefringent droplets against the black background of the optically extinct isotropic liquid as indicated with the red circle in Figure 1.13.[18]

1. 1.3.2 Differential Scanning Calorimetry (DSC)

Differential Scanning Calorimetry (DSC) is an important technique in the identification of liquid crystalline mesophases. DSC measures thermal transition of materials and monitors the detailed energy absorbed (endothermic) or released (exothermic) by a sample to passing from an ordered to another less ordered state (*e.g.* solid to liquid), as a function of time and temperature in a controlled atmosphere.[18, 50, 54-56] It is applied to monitor the subtle structural changes involved in phase transitions of liquid crystal of materials.[41-43] It is capable of revealing the presence of phase transitions in liquid crystals by detecting detailed and relatively small transition enthalpy changes between phases, especially if those mesophases have been missed by OPM. It confirms the number of transitions, the enthalpy of the transition and the temperature ranges of the transitions between the phases, which occur in a sample within a regulated increase or decrease in temperature. Although it cannot be used to precisely identify liquid crystalline mesophases, the level of enthalpy change involved at the phase transition does provide some indication of the types of phases involved. Therefore, DSC is usually used as a complimentary technique with OPM observation to determine and confirm the type of mesophase of liquid crystalline materials.[18, 44] In order for a material to pass from a crystal to a mesomorphic state, energy is absorbed due to loss of positional and orientational order (break the intermolecular forces of attraction), hence this process is endothermic. On the other hand, energy is released for the formation of intermolecular forces (more positional or orientational order), as material passes from a less ordered mesomorphic state to a more ordered crystal state.

There are usually two furnaces in a typical DSC spectrometer as shown in Figure 1. 14, one is for the sample under investigation and the other is for an inert reference material (either gold or aluminium). Both are constructed of platinum to allow high temperature operation. Under each holder are a resistance heater and a temperature sensor. Both furnaces are heated separately, but connected by two control loops at the same time to

control the currents applied to change temperature at the same selected rate. This is to ensure that the temperature and temperature changing rate of both remains constantly identical through a heating or cooling cycle. In a DSC experiment, energy is introduced simultaneously into a reference cell and sample cell which contains mesogenic compound of interest. The sample is sealed into a small aluminium pan which holds up to about 10 mg of material depending on the type of DSC instrument.[45] A nitrogen atmosphere also eliminates air oxidation of the samples at high temperatures. Temperatures of both cells are raised at the same rate. The difference in the input energy is required to match the temperature of the sample and reference. This would be the amount of excess energy absorbed or released by the molecule in the sample during an endothermic or exothermic process, respectively.[41, 46-50]

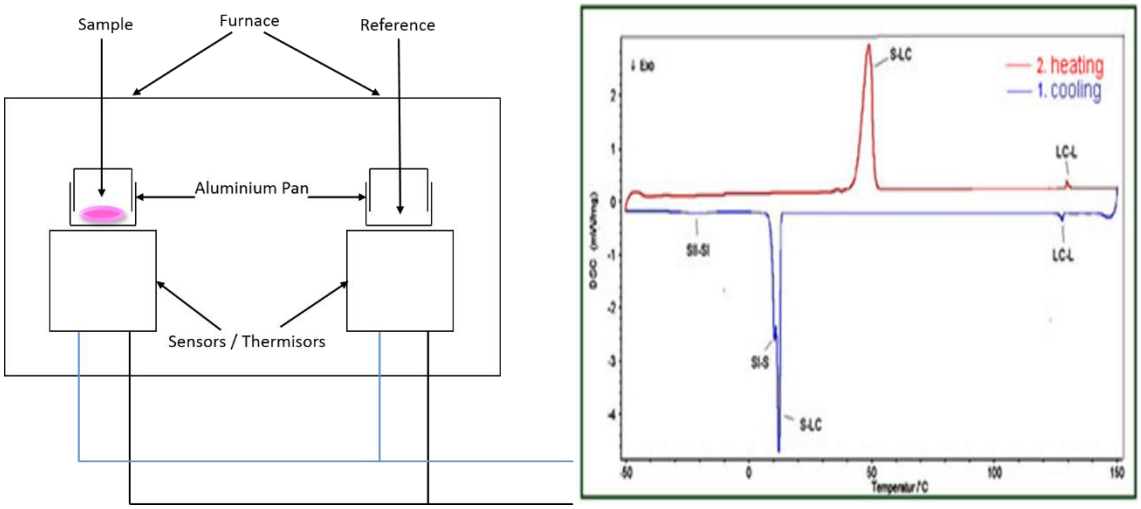

Figure 1. 14. Schematic representation of the operation of a DSC and a sample thermogram.[4, 51]

DSC studies the thermal transition of a material by measuring the amount of enthalpy change (*ΔH*) associated with phase transitions as a function of temperature T. The transition is expressed below as:

$$\Delta \frac{dH}{dT} = \left(\frac{dH}{dT}\right)_{sample} - \left(\frac{dH}{dT}\right)_{reference}$$

Equation 1. 4

Here $\frac{dH}{dT}$ is proportional to the heat flow measured in millicalories per second. The difference in the power to the two holders necessary to maintain the holders at the same temperature is used to calculate $\Delta \frac{dH}{dT}$. This difference can be either positive or negative. In an endothermic process, such as most phase transitions, heat is absorbed and therefore

heat flow to the sample is higher than that to the reference, hence $\Delta \frac{dH}{dT}$ is positive. In an exothermic process, such as crystallisation, some cross-linking process and some decomposition reactions, the opposite is true and $\Delta \frac{dH}{dT}$ is negative.[18, 41, 45]

As phase transitions occur in the sample, the sample furnace must be supplied with more or less heat flow to maintain the same temperature as the reference sample. This energy is measured and recorded by plotting enthalpy changes (*ΔH*) from the instrument as a peak on a baseline to form a DSC thermogram (Figure 1. 14). The larger peaks usually represent high energy transition regarding on molecular ordering. The first peak is normally the largest, and this process is associated with the melting of a compound from the crystalline phase into either a mesomorphic state or the isotropic liquid. The area beneath the peak is proportional to the amount of enthalpy change of the transition which corresponds to the energy required for this phase transition. A typical enthalpy change of a crystal – mesophase or isotropic liquid transitions is about 30-50 kJ/mol. This is a good indication that a considerable structural ordering is developing. A much smaller enthalpy change is involved within a mesophase – mesophase and mesophase – isotropic liquid transitions, usually those have values of less than 10 kJ/mol. Although the types of phase transitions cannot be identified by the enthalpy changes, the magnitude of the enthalpy change can provide an indication of the level of phase order involved before and after the transition, *e.g.* extremely small enthalpies of transition for a mesophase-isotropic liquid transition indicates a very small change in the level of ordering, indicating a mesophase with a low level of order, *e.g.* nematic phase. As a powerful analytical tool, a DSC thermogram is useful to give an indication as to the approximate change in the level of order between phases; it gives an excellent indication of the number of mesophases that a compound exhibits and a precise measure of their respective transition temperatures. It certainly cannot be used to identify the mesophase morphology on its own.[4, 18, 52]

1. 1.4 Application of Liquid Crystals

When considering the practical applications that have been developed as a result of the discovery of liquid crystals and their fascinating properties, it is easy to declare that their usage only began in 1970's with the advent of liquid crystal display (LCD) technology.[53] LCDs are, perhaps, the most visible use of liquid crystals, with more LCDs in the world than people and an industry worth in excess of more than $130 billion per year, it is perhaps an understandable misconception that applications of liquid crystals start and end with LCDs. However, nature has been successfully using liquid crystals for untold millennia for many purposes (*e.g.* cell membranes and DNA). Indeed, human technological use of liquid crystals also predates the LCD, and the use of lyotropic liquid crystals as soaps and detergents dates back nearly five thousand years,[7] although, the concept of 'liquid crystals' was obviously not considered at the time.[18] Whilst the action of soaps and detergents have become more and more advanced as the understanding of these liquid crystalline systems has been established, new and exciting uses of liquid crystals are being explored, not only in detergents and display devices, but also in artificial skin and muscle tissues, electrical conductivity, photovoltaic and holographic data storage (Figure 1. 15)![53]

Figure 1. 15. Applications of Liquid Crystals

As shown in Figure 1. 15, chiral nematic materials are widely seen in cosmetic applications, and for the fabrication of small flexible thermometers used on aquariums and as cheap disposable forehead thermometers. Products such as lipsticks and liquid crystal thermometers are some examples of commercially available daily products in the market made from chiral nematic. The colour changing nature of chiral nematic liquid crystals has also found a use in medical imaging. It is often used as a cheap and effective indicator of breast cancer in women, particularly in remote areas where access to large medical instruments is impossible. The increased vascular activity associated with

neoplastic disease is identified when a chiral nematic paint is applied to the skin. A difference in colour is observed around the area of tumour growth that identifies the disease.

1. 2 Aims and Objectives of Chapter One

Interest in metallic nanoparticles (AuNPs) research is now more than a few decades old, due to a wide range of possible applications,[54] which rely on their plasmonic resonances,[55] ranging from molecular biosensing [56] to solar energy conversion [57] or cancer phototherapy.[58] Forming dense arrangements of such resonant structures allows the creation of artificial composites, termed metamaterials.[59, 60] They are appealing as they promise to provide material properties inaccessible by their constituents. Most current realisations of metamaterials rely on top-down techniques which offer a great flexibility in the design of the metamaterial building blocks, but the accessible materials are essentially planar, being based on 2D assemblies.

Bottom-up approaches based on the self-assembly of metal colloids are currently considered as one of the most promising options to achieve metamaterial properties.[61-65] Fostered by these prospects, various techniques have been developed to direct the aggregation of spherical metal nanoparticles into prescribed 3D superlattices to stipulate material properties of interest. It was recently demonstrated that mesogenic ligands could be induced in the packing geometry of spherical NPs.[66-73] In particular, using laterally grafted rod-like nematogens onto the nanoparticles surface is a promising strategy. They have shown the formation of a columnar phase made of gold nanoparticles strings surrounded by axially aligned mesogens.[66, 71, 72, 74] In addition to provide a new degree of control of nanoparticles organisation, this approach offering the possibility of designing highly anisotropic self-assembled metamaterials. Critical for that is to obtain suitably functionalised mesogenic groups, in sufficient amounts so that LC AuNPs systems can be prepared for investigations.

Therefore, the ultimate aim of the work described in Chapter One is to synthesise targeted thiolate mesogens of the structure show in Figure 1. 16 using optimised reaction conditions.

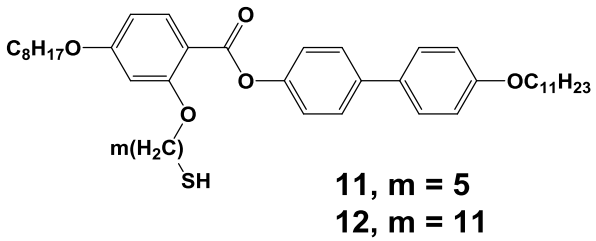

Figure 1. 16. Targeted thiolate mesogens.

In order to obtain this thiolated mesogens, mesogenic precursor containing an olefin group positioned at the end of a lateral chain of a mesogenic group, known to promote nematic phase behaviour needed to be synthesised. The materials were prepared according to the Scheme 1.1 shown in the next section. This first part of objective involved optimisation of the synthetic conditions for the synthesis of some intermediates to obtain these compounds in higher yields.

Following the synthesis of the liquid crystal precursors **9** and **10** are obtained (Scheme 1.1), the targeted thiolated mesogens **11** and **12** were synthesised by using a conventional free radical addition reaction method. However, due to the low yields, time consuming purification process and the limited scale up options, it was a target to improve the reaction conditions and yields significantly.

Other similar thiolated mesogenic compounds and some sub-structures were also synthesised by using a newly established and optimised synthetic method.

Overall, the aims outlined in this Chapter One are:

- Main mesogens frame synthesis, obtaining compounds **9** and **10** through a multi-step scheme 1.1;
- Intermediate compound **8** synthesis optimisations for higher yield and simple purification procedures;
- Thiolated mesogenic compound **11** and **12** direct synthesis by using a free radical addition reaction;
- Optimisation of free radical reaction procedures for high yield reactions for compound **11** and **12**;
- New synthetic route development for the synthesis of compound **11** and **12** including reaction optimisations for higher yield and simple purification procedures;

- Synthesis of further structurally related thiolated mesogenic compounds (**26** and **27**) and intermediates **42**;

1. 3 Results and Discussion

The synthesis of thiolated mesogens is discussed in this section. It is divided into three major sections, where the results of synthesis of the unsaturated mesogens main frame is discussed first, followed by some optimisations for those intermediates that were difficult to synthesise or obtain from purification. Finally, the thiolated mesogen synthesis from the unsaturated mesogens is explored. Due to the low yield and a time consuming purification step of the initial thiolated mesogens synthesis, a large amount of time was spent to develop a new synthetic route. Therefore, this thiolated mesogen synthesis is further divided, to compare the new synthetic route with the initial methodology.

1. 3.1 Synthesis of the Main Mesogenic Group

The synthesis of thiolate mesogens with pentyl (**11**) and undecyl (**12**) thiol lateral functional groups, followed the same method, the same reaction conditions, as well as the purification methodology reported by Diez *et al* and Cseh *et al*[70, 75, 76] (Scheme 1.1).

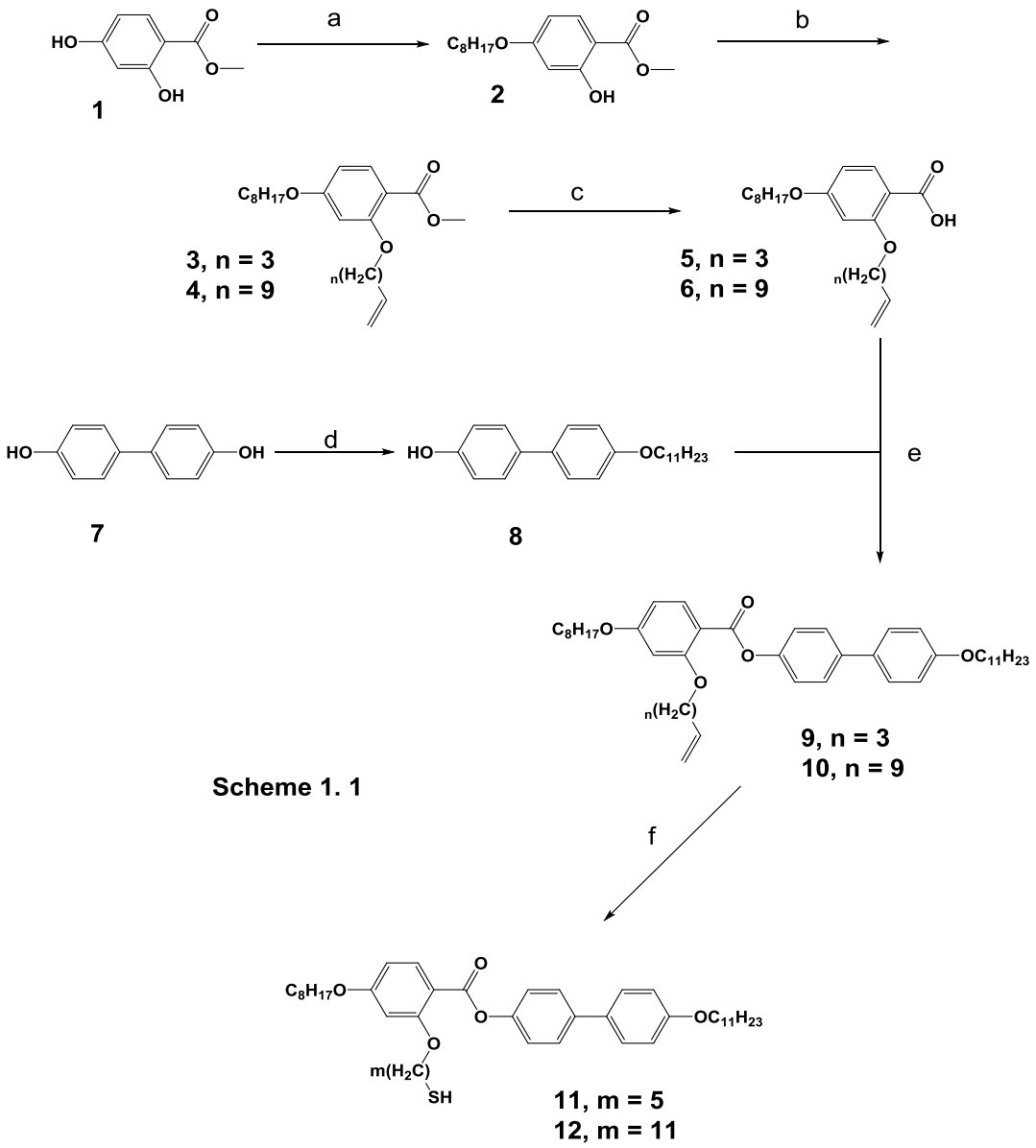

Scheme 1. 1

a... K_2CO_3, KI, 4Å molecular sieves, butanone, 1-bromo-octane, reflux, 79%;
b... K_2CO_3, KI, 4Å molecular sieves, butanone, 5-bromo-1-pentene, reflux, 94%;
c... (i) NaOH, H_2O, MeOH, THF, (ii) HCl, H_2O, 89%;
d... metal Na, 1-bromoundecane, KI and methanol;
e... (i) $SOCl_2$, toluene, reflux, (ii) pyridine, toluene, reflux, 85%;
f... (i)Ph_3SiSH, AIBN, benzene, reflux, (ii) TFA, room temperature.

Scheme 1. 1. Synthetic Scheme for the mesogenic precursors.

The synthesis of thiolate mesogens started from the alkylation of methyl 2,4-dihydroxybenzoate (**1**) in the *p*-position. This was achieved by reacting compound **1** with 1-bromooctane under reflux in dry butanone to obtain methyl 2-hydroxy-4-octyloxybenzoate (**2**). Followed by a Williamson etherification in the *o*-position, with either bromopent-4-ene or bromo-1-undecene under reflux in dry butanone, for approximately 8 days. This reaction was also used to obtain methyl 4-octyloxy-2-(pent-

4-en-1-yloxy) benzoate (**3**) and methyl 4-octyloxy-2-(undec-10-en-1-yloxy) benzoate (**4**). The reaction time to synthesise compound **3** and **4** were far greater than that of compound (**2**), due to the steric hindrance effect of the etherification position. 4-octyloxy-2-(pent-4-en-1-yloxy) benzoic acid (**5**) and 4-octyloxy-2-(undec-10-en-1-yloxy) benzoic acid (**6**) were synthesised, by removal of the methyl protecting group the carboxylic acid of (**3**) and (**4**). This was carried out in THF and methanol with excess of KOH mixed at room temperature. The intermediate 4-hydroxy-4'-undecyloxybiphenyl (**8**) was synthesised by nucleophilic substitution of a hydroxyl group of 4, 4'-dihydroxy biphenyl (**7**) with 1-bromoundecane in dry methanol, with presence of sodium methoxide (prepared by dissolving metallic sodium in methanol). The precursor 4'-undecyloxybiphenyl-4-yl-4-octyloxy-2-(pent-4-en-1-yloxy) benzoate (**9**) and 4'-undecyloxy-1, 1'-biphenyl-4-yl 4-octyloxy-2-(undec-10-en-1-yloxy) benzoate (**10**), were synthesised via esterification of either (**5**) or (**6**) with 4-hydroxy-4'-undecyloxybiphenyl (**8**). Intermediate (**5**) or (**6**) were heated at 80 ^{o}C for 3 h with dry toluene and thionyl chloride under nitrogen, followed by removal of thionyl chloride under nitrogen, before the reaction mixture was heated in the presence of 4-hydroxy-4'-undecyloxybiphenyl (**8**) in pyridine and toluene for 18 hours, and finally refluxing for 1 hour to obtain compound (**9**) and (**10**).

1. 3.2 Intermediates Synthesis Optimisation

The original synthetic method of 4-hydroxy-4'-undecyloxybiphenyl (**8**) was by using nucleophilic substitution of 4, 4'-dihydroxy biphenyl (**7**) with excess bromoundecane in dry methanol, and only achieved a yield of ~ 45%. It was recognised that the original method will always produce the disubstituted biphenyl by-products, which were found to be difficult to separate by recrystallisation and silica gel chromatography, even with a good separation shown on a TLC plate. This was a time-consuming, repetitive and relatively low yield step for this essential intermediate synthesis. The sufficient amount of olefins were often not able to be obtained due to the lack of compound (**8**). It was decided that such useful essential compound (**8**) would be very convenient to stock up on, for future mesogen synthesis. As a result, an extensive investigation was carried out to improve the yield of 4-hydroxy-4'-undecyloxybiphenyl (**8**) synthesis (Scheme 1.2). (4'-(undecyloxy)-[1,1'-biphenyl]-4-yl)boronic acid (**15**) was initially obtained from 4-bromo-4'-(undecyloxy)-1,1'-biphenyl (**14**) via alkylation of 4,4-bromobiphenyl-ol (**13**) with bromoundecane in dry butanone, followed by an oxidation process with n-butyllithium in dry THF, and then trimethyl borate to obtain compound (**8**) as shown in Scheme 1.2. The synthesis of compound (**14**) included many straight forward alkylation procedures, with a high yield. Nevertheless, a low yield of boronic acid (**15**) was obtained due to the solubility of starting material (**14**) in the reaction step at low temperature – 78 ^{o}C, resulting in an overall low yield for the desired product (**8**). Poor solubility at low temperature was believed to be the common drawback for these biphenyl compounds. Therefore, this synthetic approach was only tried once. However, it should be noted that the key to success in this reaction is to keep all glassware dry, with the reaction carry out in an inert environment.

Scheme 1. 2

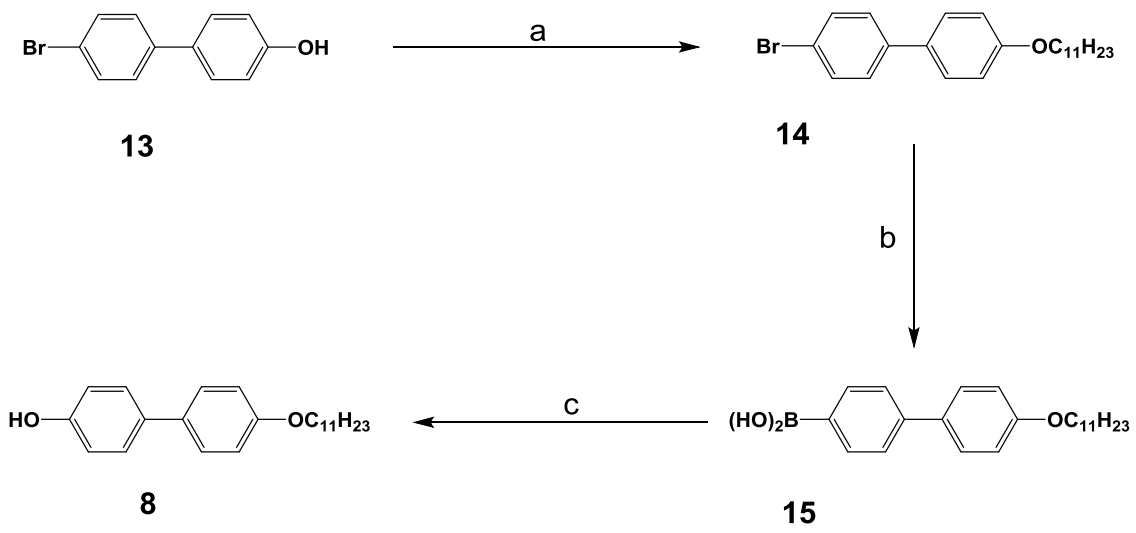

a... (i) K_2CO_3, 4A powdered molecule sieves, dry butanone; (ii) 1-bromoundecane;
b... (i) n-butyllithium, dry THF; (ii) trimethyl borate; (iii) 10% HCl;
c... H_2O_2, Et_2O.

Scheme 1. 1. Alternative synthetic Scheme for the compound 8.

A different approach was taken, which involved the addition of the alkyl chain to 1-iodo-4-(undecyloxy) benzene (**16**) via alkylation with bromoundecane in dry butanone. This was followed by (4-(undecyloxy) phenyl) boronic acid (**18**, available in the laboratory) synthesis with trimethyl borate. The final product was obtained by using a Suzuki coupling with the same starting material (**16**) in dry THF, with $Pd(Ph_3)_4$ under reflux for 24 hours as shown in Scheme 1.3. The final yield was still low when compared to literature reported values, possibly due to the low quality of boronic acid. It could also be the reaction conditions required for the catalyst to work were not met. Due to the lack of experience of this method, this scheme was only tried once with no further actions taken.

Scheme 1. 3

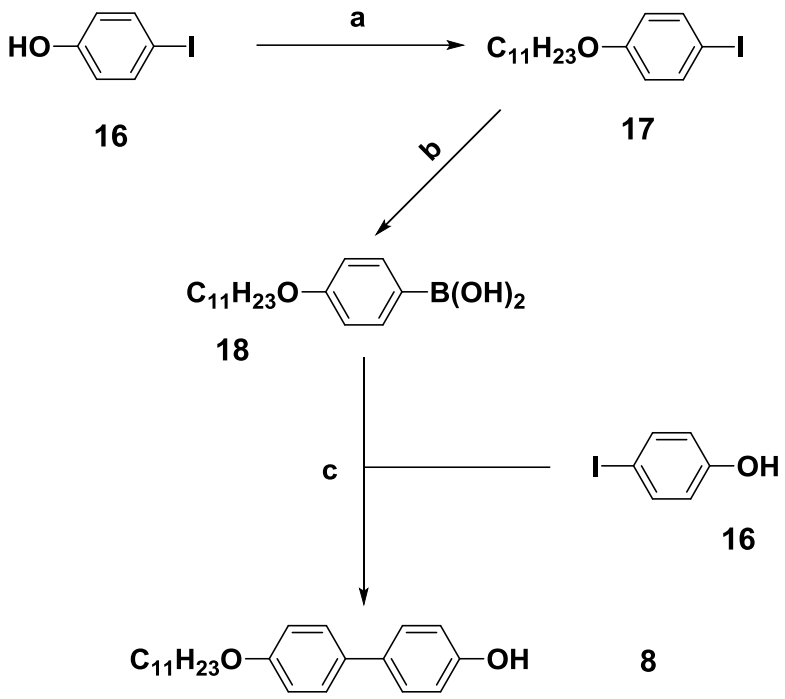

a... (i) K_2CO_3, 4A powdered molecule sieves, dry butanone; (ii) 1-bromoundecane;
b... (i) n-butyllithium, dry THF; (ii) trimethyl borate; (iii) 10% HCl;
c... (i) 4-iodophenol, KF, dry THF;
(ii) (4-(undecyloxy)phenyl)boronic acid, dry THF, $Pd(PPh_3)_4$, reflux 24 h.

Scheme 1. 2. Another synthetic Scheme for compound 8.

1. 3.3 Thiolated Mesogens Synthetic Route 1

The initial synthesis of final compounds, thiolate mesogens 4'-(undecyloxy)-[1,1'-biphenyl]-4-yl-2-((5-mercaptopentyl)oxy)-4-(octyloxy)benzoate (**11**) and 4'-(undecyloxy)-[1,1'-biphenyl]-4-yl-2-((11-mercaptoundecyl)oxy)-4-(octyloxy)benzoate (**12**) were obtained following the reported protocol.[77] A free-radical addition to either (**9**) or (**10**) in the presence of triphenylsilanethiol, then AIBN and trifluoroacetic acid (TFA) mixed in benzene was employed. The thiolate mesogen compound was formed after deprotection by trifluoroacetic acid (TFA), which tends to hydrolyse the ester group of the olefin at the same time, resulting in by-products. TLC analysis showed the reaction progressed quite slowly and the reaction mixture contained significant amounts of starting materials and impurities. Moreover, it was found that the desired thiolate compound was very difficult to isolate by silica gel chromatographic separation, due to the similarity in molecular structure and polarity between the final thiolate compound and its precursor. Additionally, the final thiolate mesogen is more polar when compared to the olefin starting material, hence it will always elute after the starting material under conventional silica chromatography separation. As a result, a large amount of thiolate mesogen would always be obtained in a mixture with the starting material, even with a very slow eluting rate. Thus this silica column chromatography purification process had to be repeated in order to obtain pure product. Although ~ 20% of these thiolate mesogens were able to be isolated after repeatedly purification, it was rather time-consuming for each reaction carried out. This reaction was scaled up to attempt producing sufficient thiolate mesogens material for further steps. However, this resulted in an even worse yield when compared to the literature reported yield value and it was found that the optimal reaction conditions for this free-radical addition reaction is to use only a small scale, below 1 g. Although some of the starting material was able to be recovered, it was impractical, uneconomical and again very time-consuming. Several reaction conditions were optimised to try to improve the reaction yield of this protocol, as shown in the Experimental section, such as amount of reagents used, quality of reagents, radical generation source and reaction temperatures. However the improvement in yields was minimal and the isolation of the final product was still found to be problematic.

It was assumed the low yield of this step was the result of steric hindrance. Therefore this free radical addition method was repeated with a simple molecule 3-butenylbenzene (**19**) (Scheme 1.4). This molecule (**19**) has an unsaturated bonding similar to compound (**9**)

and (**10**), more importantly this was one of the compounds used to synthesise thiolated product as described by Gareau *et al*,[77] using the method of free radical addition as described above. However there was not any obvious improvement in the yield of final thiolated compound 4-phenylbutane-1-thiol (**20**) in this case, even when the procedures were followed as delineated as in the publication. Although the thiolate compound (**20**) was formed after deprotection by TFA, the process was still slow, with low yields, and the final thiolate product isolation problem still remaining.

Scheme 1. 4

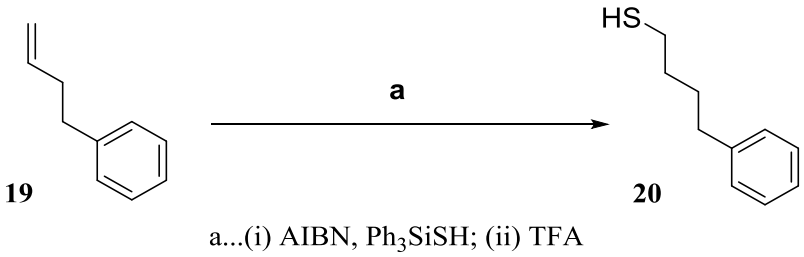

a...(i) AIBN, Ph_3SiSH; (ii) TFA

Scheme 1. 3. Synthetic Scheme for the compound 20.

There are a total of six steps in Scheme 1.1, five direct steps towards the final compound with one separated step to synthesise compound (**8**). All previous four direct steps worked, with a ~ 85% yield for each step and a ~ 50% yield overall. Nevertheless, this final step of Scheme 1.1 was a major drawback, with a poor yield of ~ 20%, brought down the overall yield to less than 10%. Not only did this lead to a potential higher cost in producing the desired compound, it also demanded a large amount of effort and time to only achieve a negligible amount of product. This was indeed a bottleneck problem for the research. It was simply not possible to gain enough final thiolated mesogens in a reasonable amount of time for the next steps.

It was eventually realised that some yields of thiolate products, reported by Gareau *et al*,[77] were only determined by NMR using an internal standard (dichloroethane or dibenzylether), without any product isolation. This has shown that such a free-radical addition method reported by Gareau *et al*[77] is unsuitable for my compounds, although it works with some other similar olefins. In the end, it was decided that such a method is not suitable and impractical to synthesise my compound. Consequently, there was an urgent need for an alternative synthetic route to resolve this situation, improve reaction yields and reduce the purification time required, in order to carry on my research work.

1. 3.4 Thiolated Mesogens Synthetic Route 2

After a thorough literature research, few potential methods attracted my attention. Some required a different functional group instead of the unsaturated double bond, such as introducing an alcohol group or halogen group. Some required a different technique, such as using a microwave reactor and reaction under UV.[78, 79] Others required the introduction of an extra step to synthesise another intermediate compound before the final product. A completely new reaction plan would be required, if the final thiolated mesogenic compound was prepared from starting materials containing a different functional group. It was judged that it would be very time consuming to start all over again and wasting all previous work, especially at this stage. Another possible option was to functionalise this existing starting material with an unsaturated double bond, into either an alcohol or a halogen group. This would require different reaction conditions, which was potentially problematic as the ester group within olefin (**9**) and (**10**) would not be able to survive, therefore this was not viable. Although a microwave reactor was available to use in the laboratory, the relatively small scale of reaction was the reason not to proceed, however this powerful technique was taken into consideration for future experiments. The introduction of another intermediate compound seemed to be more ideal, as this method does not require a new scheme, further reagents required are widely available and the mild reaction condition are suitable to preserve the ester groups of the olefin mesogens. For those purposes, the synthesis method of introducing an addition intermediate step was decided to be a more viable approach.

This new adopted protocol is shown in Scheme 1.5. The final thioester mesogens 4'-(undecyloxy)-[1,1'-biphenyl]-4-yl 2-((5-(acetylthio)pentyl)oxy)-4-(octyloxy) benzoate (**21**) and 4'-(undecyloxy)-[1,1'-biphenyl]-4-yl 2-((11-(acetylthio)undecyl)oxy)-4-(octyloxy)benzoate (**22**) were synthesised by treating the olefins (**9**) or (**10**) with thioacetic acid and AIBN in dry THF under thermal or photolytic conditions.[79, 80] Finally the desired thiol mesogens (**11**) and (**12**) were achieved by hydrolysis.

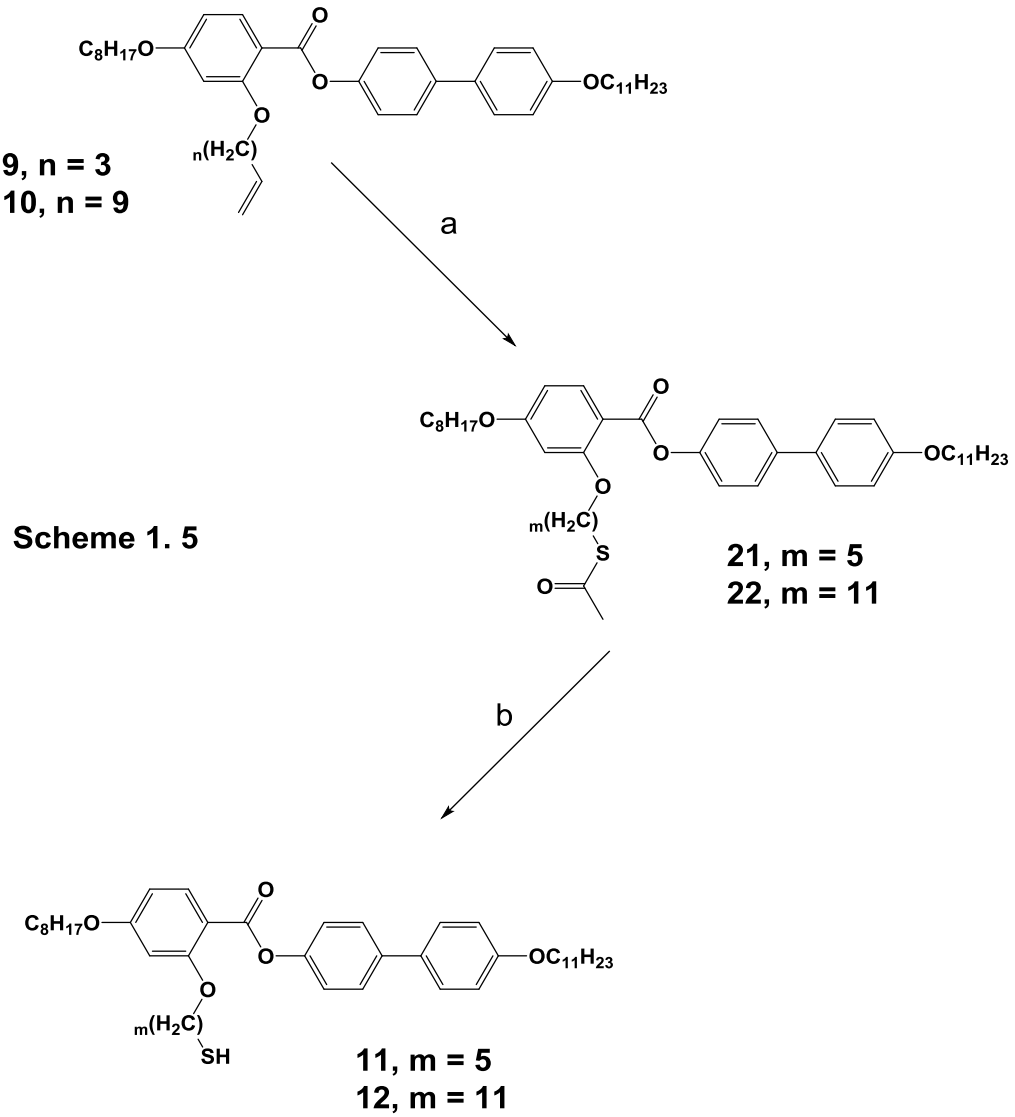

Scheme 1. 5

a... AIBN, CH_3COSH, methanol, dry THF;
b... (i) NaSMe, MeOH, THF under N_2; (ii) HCl (0.1 M).

Scheme 1. 4. Alternative synthetic Scheme for the compound 11 and 12.

A conventional hydrolysis method was carried out to synthesise the final thiolate mesogens, thioester mesogens (**21**) or (**22**) was mixed with acid or base under reflux. However protecting the ester group of thioester mesogens has proven to be rather challenging, as the ester group tends to be hydrolysed under strong acidic or basic conditions. This could be improved by carefully controlling the amount of acid or base added, but this was considered to be time consuming too, hence this method was only carried out once. Another approach was to hydrolyse the thioester by using $TiCl_4$ with

Zinc powder at low temperature. $TiCl_4$ is highly volatile, it forms spectacular opaque clouds of titanium oxide (TiO_2) and hydrogen chloride (HCl), when coming to contact with moisture from air. Consequently $TiCl_4$ had to be stored and collected in a nitrogen box with thoroughly dried glassware. This reaction was much easier in terms of purification process, but a low reaction yield (~ 23 %) was observed. This was possibly due the reaction conditions required for such a sensitive starting material and demanded more practical experience, made this approach not suitable in this case. The final approach was to use NaSMe as a mild reagent that selectively hydrolyses the thioester only. This approach dramatically improved the reaction yields (~ 75 % after the method was optimised compared to ~ 20% in the initial approach), and the purification process was found to be less time consuming. This synthetic method was modified and repeated several times to ensure its reliability. A different amount of azobisisoburyronitrile (AIBN) was introduced at different stages of this reaction, and different reaction temperatures were tested to find out the most suitable range for AIBN to perform well. No significant improvements in yield were observed until a better quality of AIBN was used. It was noted throughout the literature, AIBN is considered as an explosive compound, which decomposes under strong light, above 65 ^{o}C and in the presence of moisture in air. Thus all AIBN was carefully recrystallised from methanol at 60 ^{o}C, and any excess recrystallised AIBN was stored under dry nitrogen in a dark environment at 5 ^{o}C. This better quality of AIBN increased the yield significantly, especially when this reaction was operated at temperatures around 60 ^{o}C. Another key factor to ensure a high yield was the reaction solvents. All reactions were initially carried out in dry tetrahydrofuran (THF), nevertheless chloroform was found to be the much better co-solvent to reduce the formation of disulfides during thioesters deprotection reaction, as suggested by Holmes *et al*.[81] One possibility was due to the fact that THF absorbs moisture from air much easier when compared to chloroform.

The advantage of this method is a much simpler, convenient and less time-consuming isolation process, as the addition of thioacetic group of intermediate (**21**) or (**22**) is much less polar compared to the olefins. This enabled intermediate (**21**) or (**22**) to be collected first when using silica chromatography purification technique, a reversed order when compared to the method described previously. In comparison with the final thiolate mesogen, the much bigger polarity difference allowed a much better separation, hence a much more user-friendly isolation process when compared to the original method.

Furthermore, a good yield with ~ 75% for each step was able to be achieved after this method has been perfected with some modifications. Although this method introduced an extra step, an overall ~ 30% yield of the final product was still obtained, which is also a huge improvement when compared with the previous method where an overall yield of less than 10% was found. This was a major improvement and my research was able to progress to the next step, as the required thiolate mesogens were able to be produced whenever needed, by this much more convenient and reliable method.

1. 3.5 Thiolated Mesogens Synthetic Route 3

One way to avoid the ester group hydrolysis problem was to introduce this thioester group to compound (**6**) first, followed by hydrolysis of the thioester compound (**23**) to synthesise compound (**24**) with the thiol functional group. Finally using esterification to add the biphenyl part, to achieve the final thiolate mesogens. However this Scheme 1.6 was never investigated further after compound **23**, due to the chance of the thiol functional group reacting under the esterification reaction conditions of the final step, leading to multiple reaction side products.

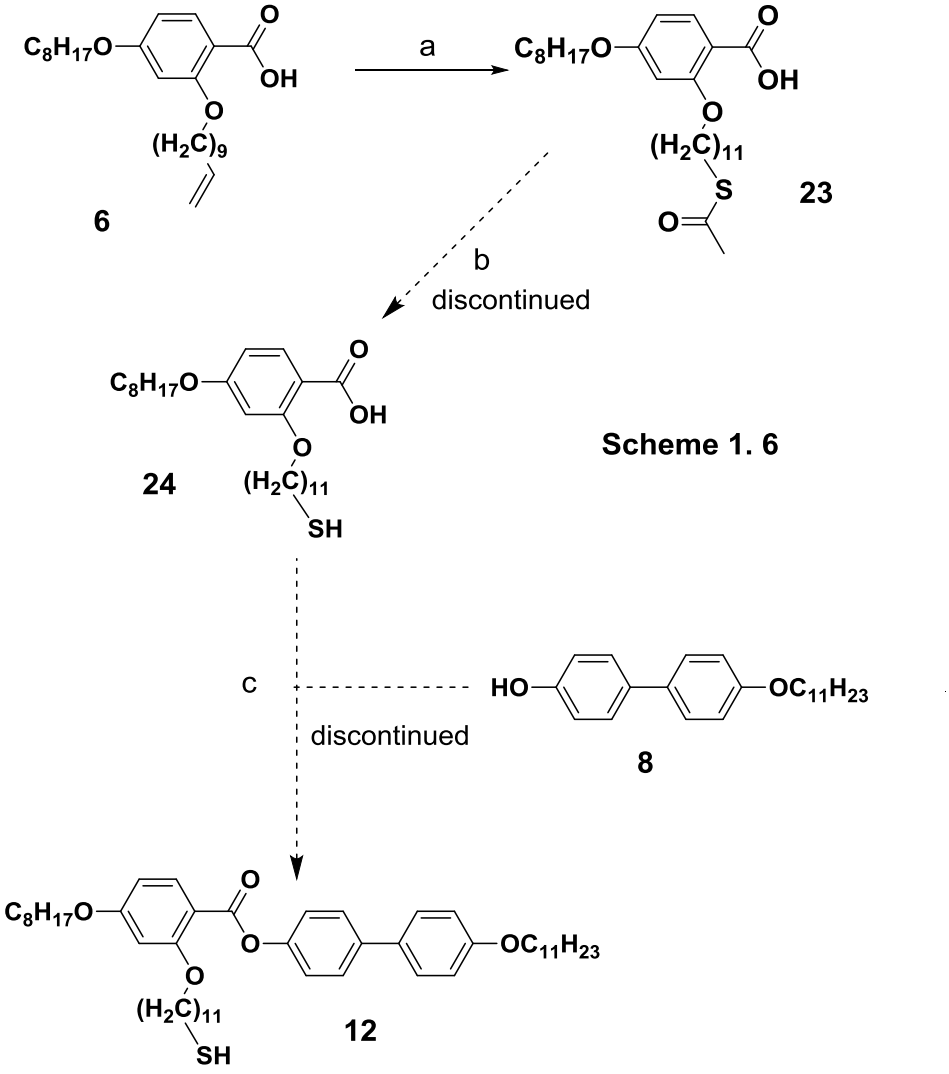

Scheme 1. 5. Another synthetic Scheme for the compound 12.

1. 3.6 Synthesis of Other Thiolated Mesogens

The thiolate mesogens 4'-(4-octyloxyphenylcarbonyloxy)biphen-4-yl 4-octyloxy-2-(11-mercaptoundecyloxy)benzoate (**27**) was required for LC AuNPs synthesis, in order to compare the LC AuNPs systems generated from thiolate mesogens (**11**) and (**12**). Accordingly, a similar synthetic procedure for the synthesis of thiolate mesogens (**11**) and (**12**) using thioacetic acid via a mild hydrolysis with NaSMe was adopted, to synthesise 4'-(4-octyloxyphenylcarbonyloxy) biphen-4-yl 4-octyloxy-2-(11-mercaptoundecyloxy) benzoate (**27**) as shown in Scheme 1.7. The overall yield was found to be lower when compared to those obtained for the thiolate mesogens (**11**) and (**12**). It was suspected that the added benzene ring in the system introduced more steric hindrance; the additional ester linking group may have a lack of stability, as possible hydrolysis might occur. Following this consideration, another mild hydrolysis reagent $NaSC(Me)_3$ was also used to optimise the reaction yield. It was anticipated that the larger tri-methyl group would make it more difficult to hydrolyse the linking ester groups between aromatic rings of the mesogen. It was hoped that this would push the hydrolysis equilibrium towards the thioester group, resulting in a better yield in the thiolate formation reaction. However no product was obtained. This is possibly due to that all other reaction conditions were not suitable for the reagent $NaSC(Me)_3$, and this reaction was only tried once and this was not able to be explored further.

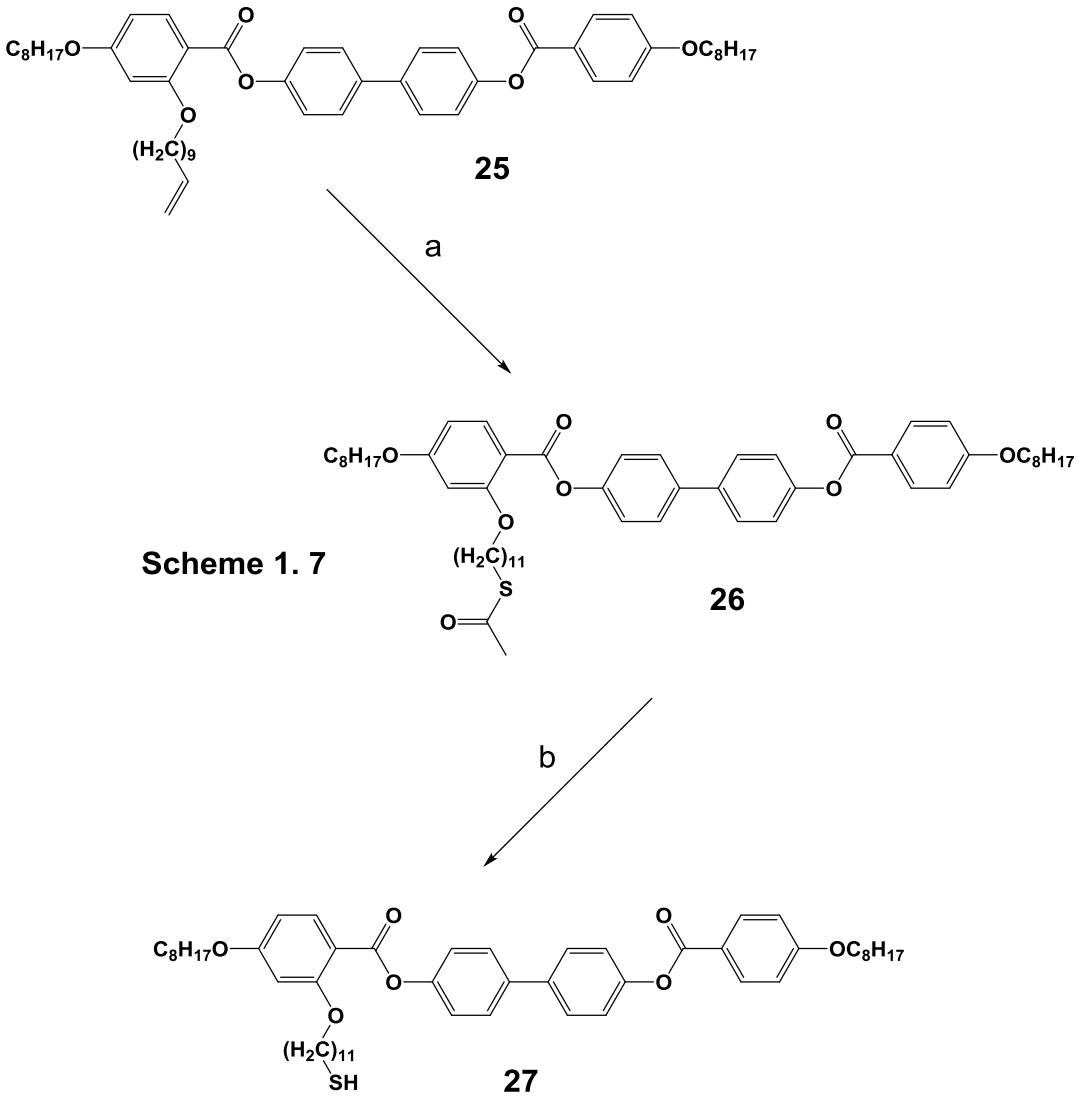

Scheme 1. 7

a... AIBN, CH_3COSH, methanol, dry THF;
b... (i) $NaSCMe_3$, MeOH, THF under N_2; (ii) HCl (0.1 M).

Scheme 1. 6. Synthetic Scheme for the compound 27.

1. 3.7 Characterisation

All organic intermediate compounds were prepared using reported procedures.[70, 75, 82] The purification of all intermediates were monitored by thin layer chromatography (TLC) before being analysed further with other instruments. All intermediates were initially checked by TLC before structures were determined by Nuclear Magnetic Resonance (NMR) spectroscopy. Subsequently, elemental analysis (EA) of carbon, hydrogen and sulphur were characterised. Mass spectroscopy (MS) were used to provide further evidence of all intermediates. The mass spectroscopy analysis were carried out by technicians and the types of MS and method used are described in the Experimental section. Some of compounds were analysed by the EPSRC National Mass Spectrometry Service Centre Swansea.

The compound **9-12**, **21**, **22** and **25** were investigated extensively by differential scanning calorimetry (DSC) and optical polarising microscopy (OPM). High performance liquid chromatography (HPLC) and gel-permeation chromatography (GPC) were also used to investigate the purity of some compounds, due to their relatively large mass. All obtained data were compared with published results in the literature by Diez *et al*[75] and Cseh *et al*[70, 71] for full compound characterisation and comparison.

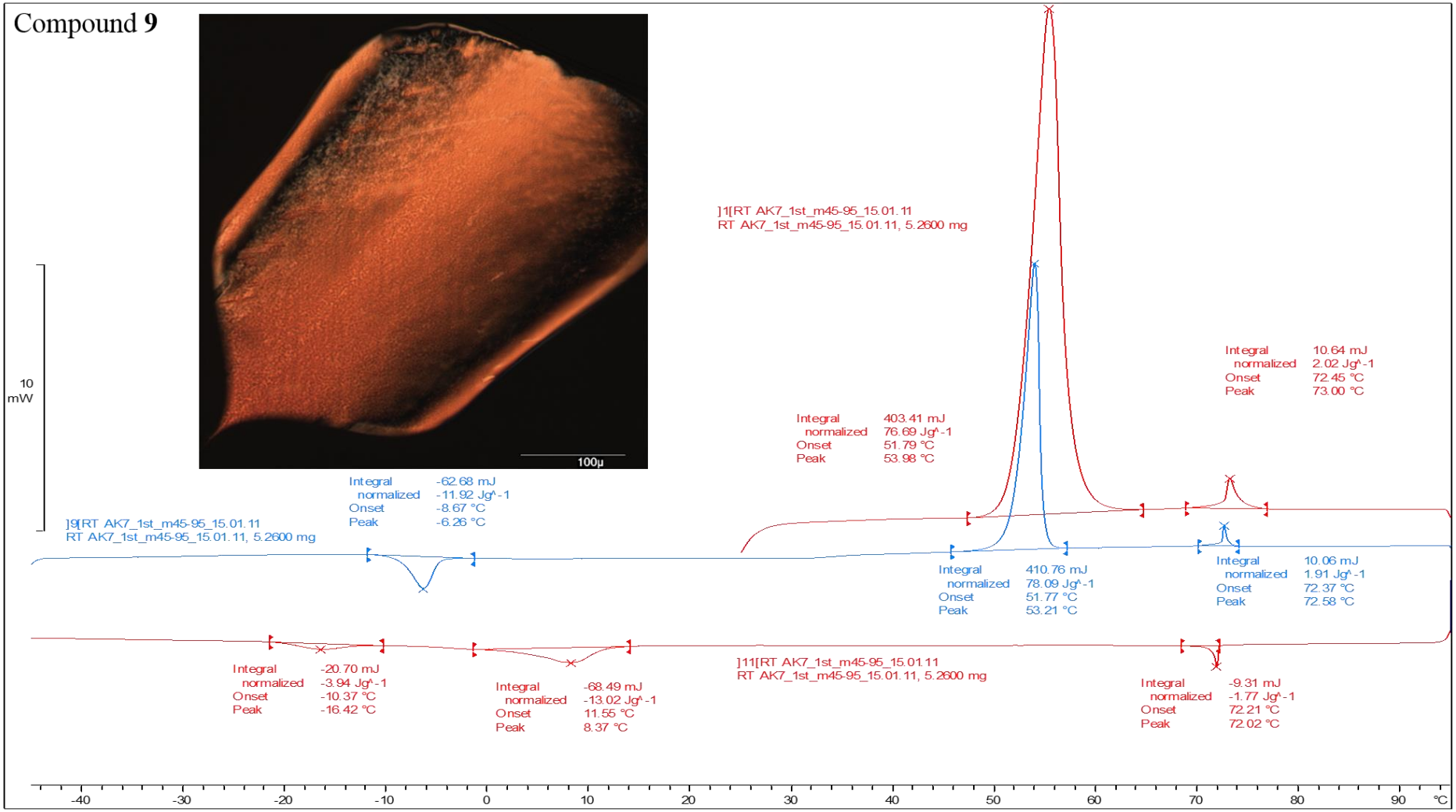

Figure 1. 17. DSC spectrum of compound 9 and OPM at 71.8 ºC.

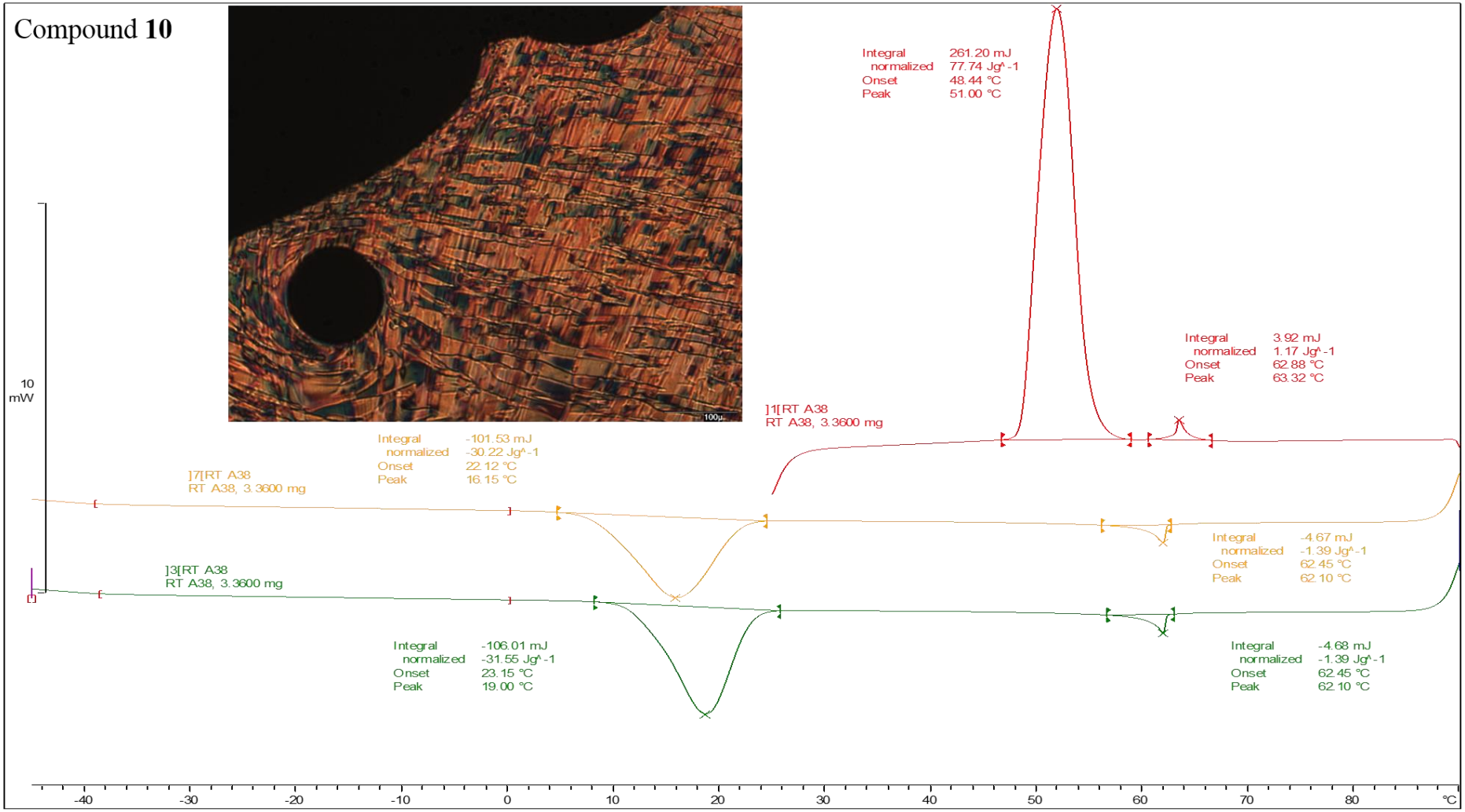

Figure 1. 18. DSC spectrum of compound 10 and OPM at 61.5 ºC, HPLC 98.9% purity.

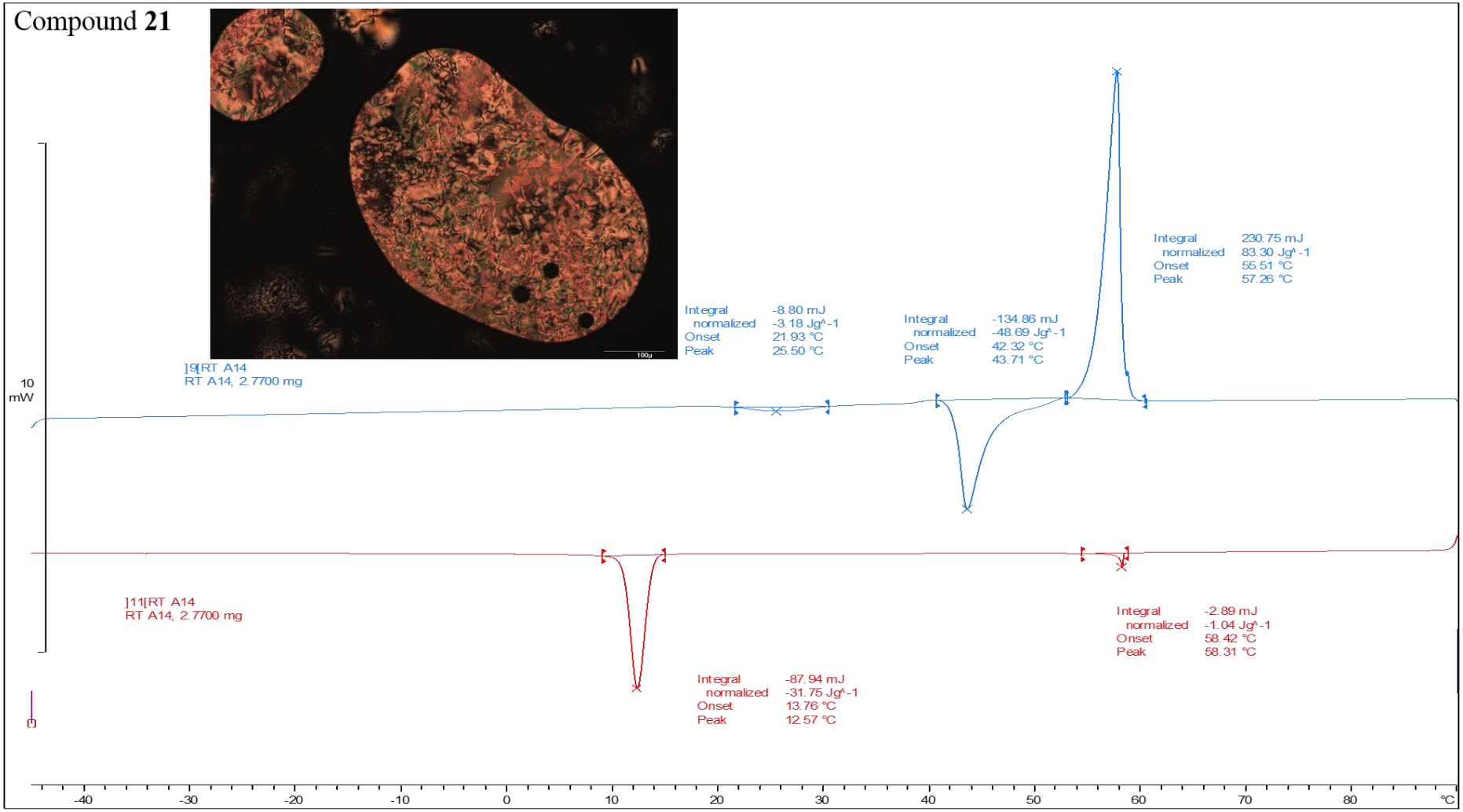

Figure 1. 19. DSC spectrum of compound 21 and OPM at 57.8 ºC, HPLC 99.74% purity.

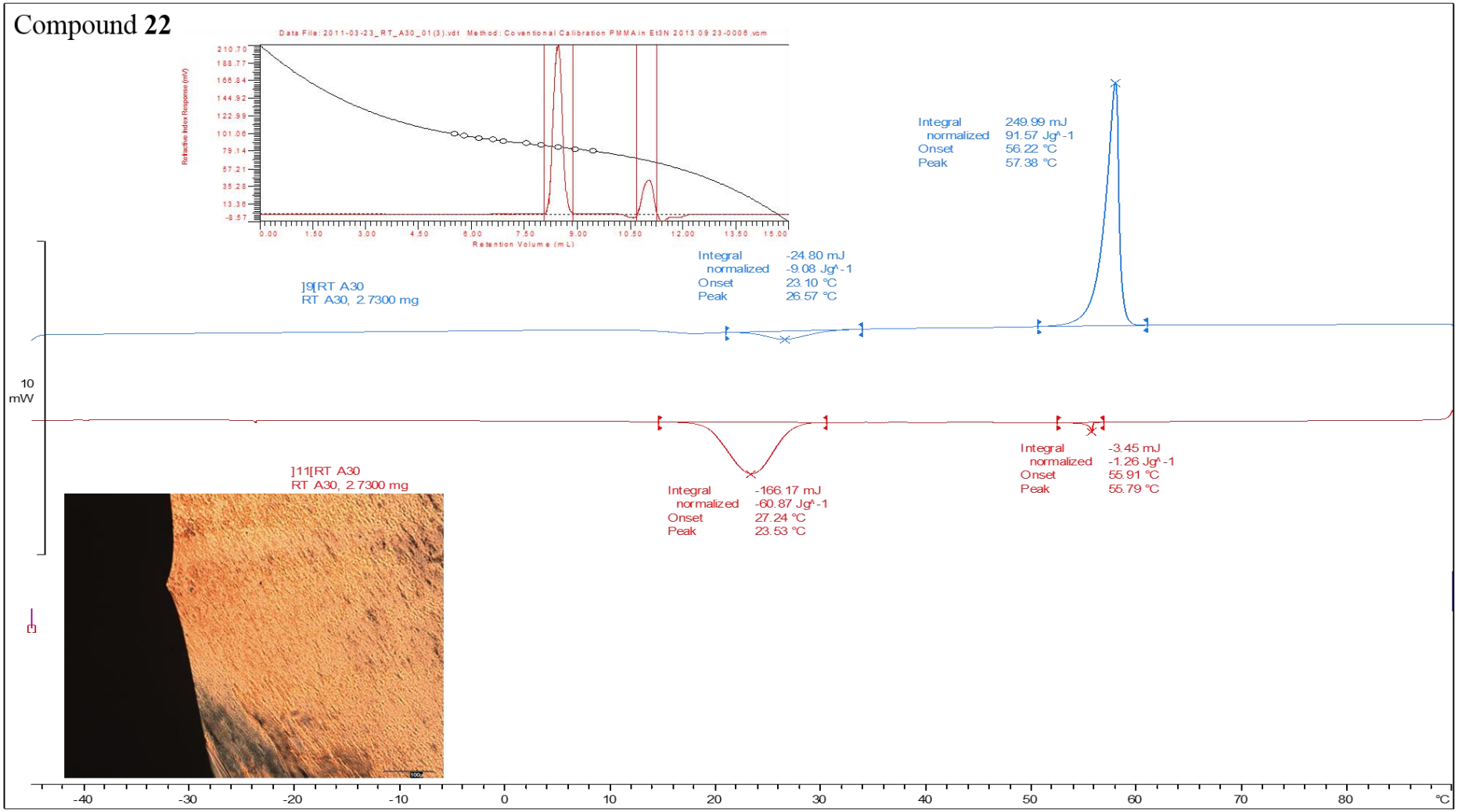

Figure 1. 20. DSC spectrum of compound 22, OPM at 55.4 ºC, HPLC 99% purity and GPC showing that one majority compound exists.

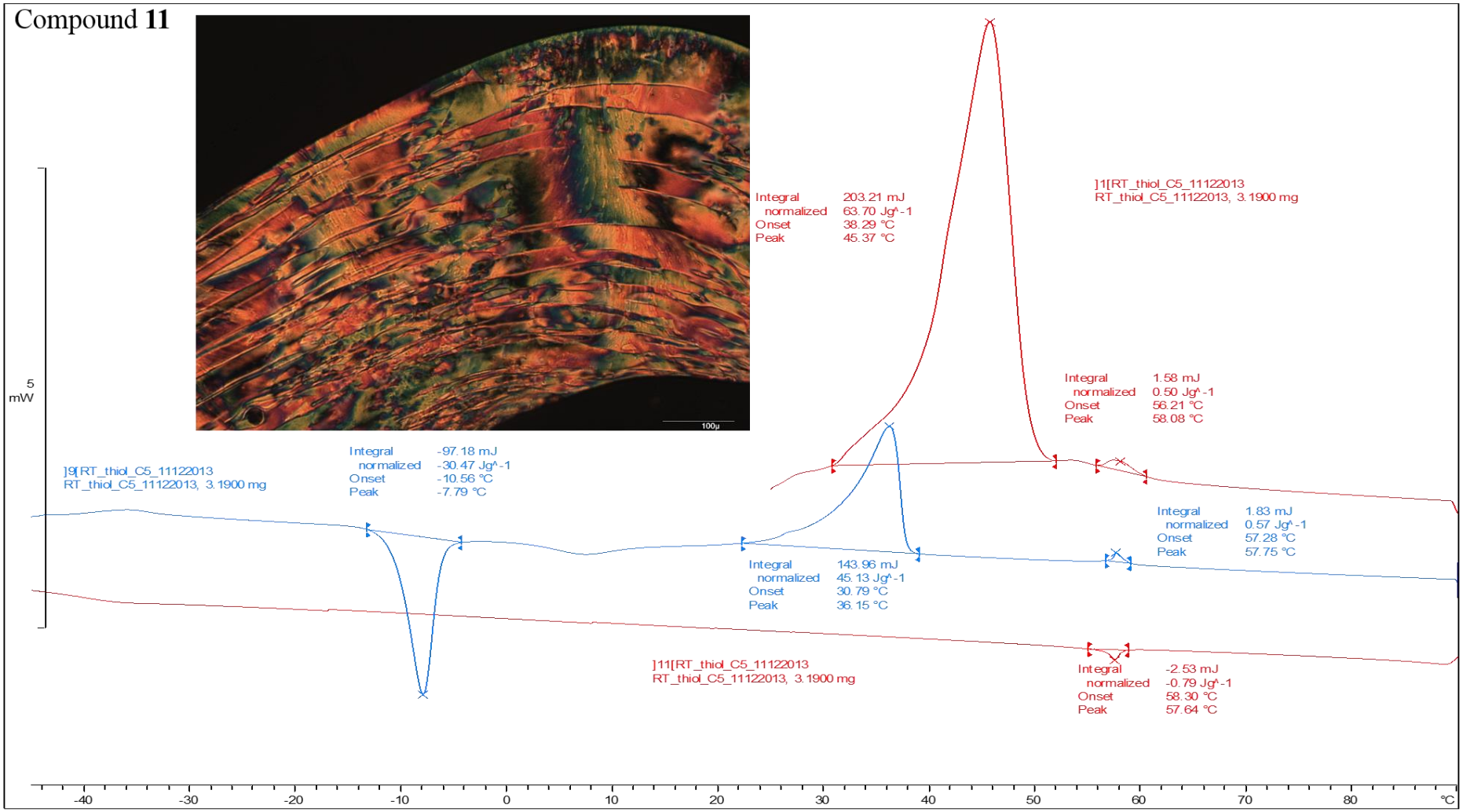

Figure 1. 21. DSC spectrum of compound 11 and OPM at 54.2 ºC.

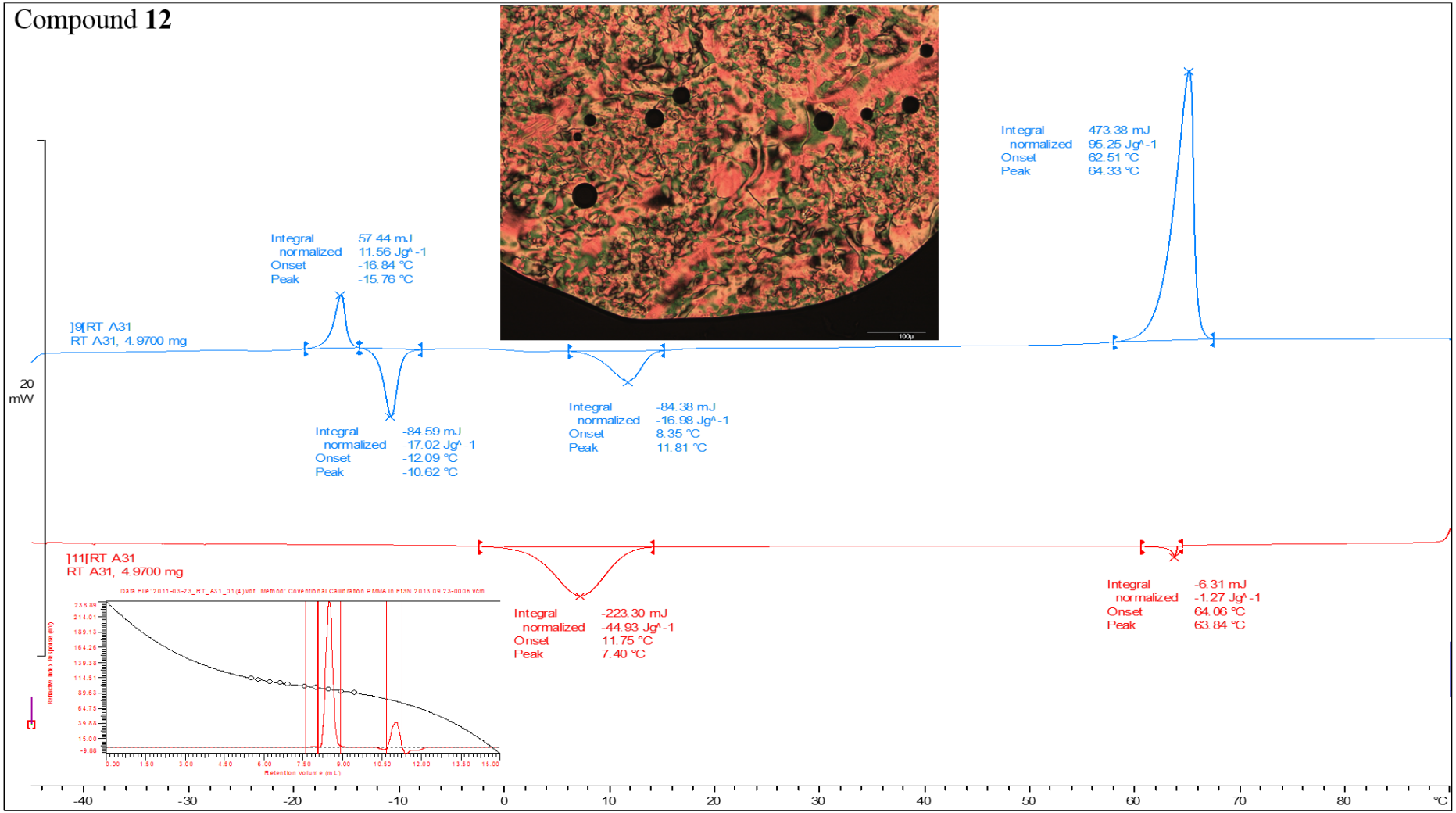

Figure 1. 22. DSC spectrum of compound 12, OPM at 63.6 ºC, HPLC 99.96% purity and GPC showing that one majority compound exists.

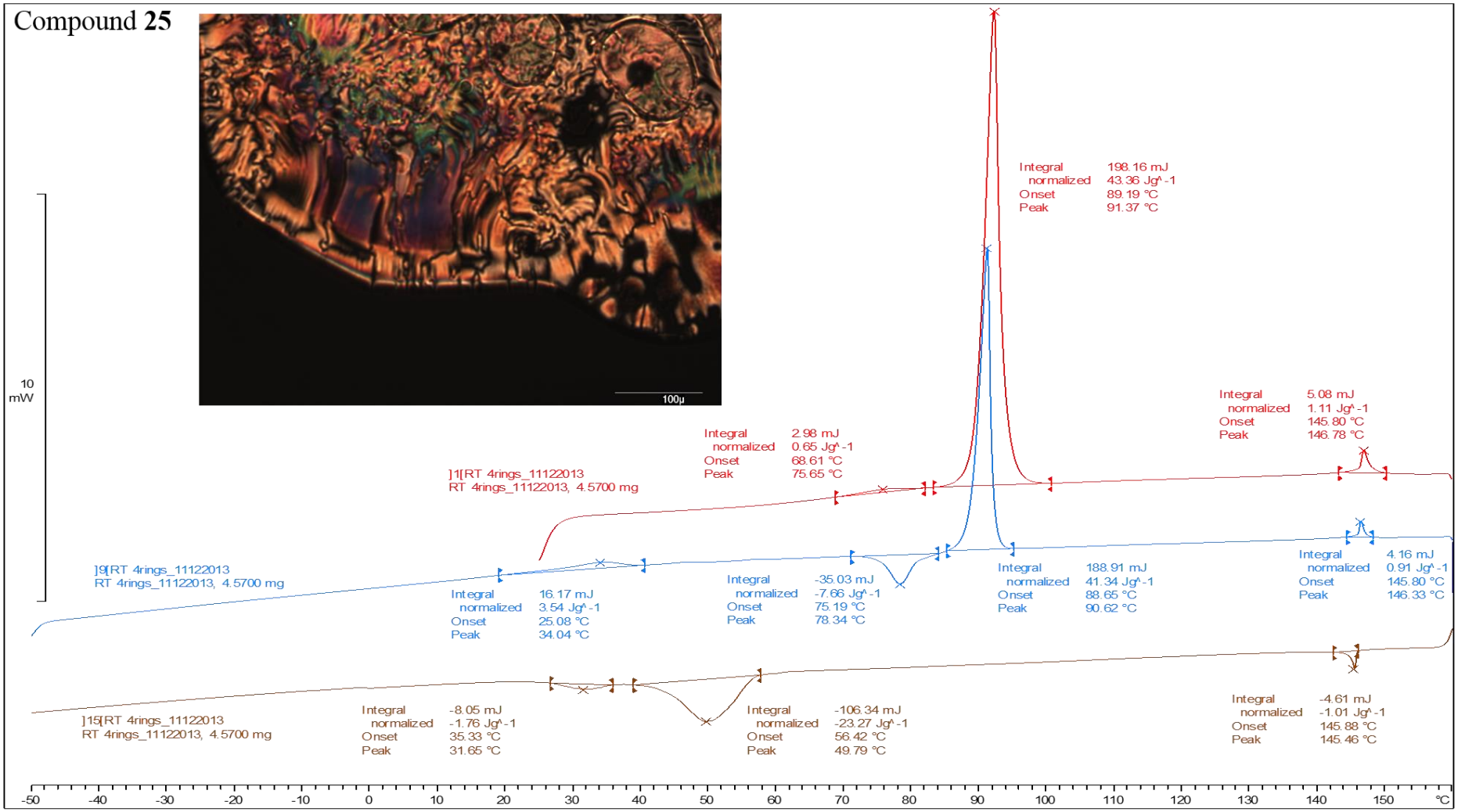

Figure 1. 23. DSC of compound 25 and OPM at 145.5 ºC.

1. 4 Conclusions

In summary, a considerable part of this work was focused on the synthetic yields and purification procedures to obtain suitable amounts of mesogenic compounds containing thiol groups. Optimisation were carried out for both intermediates and thiolated mesogenic compounds.

The overall conclusions are:

- Typical calamitic mesogens precursors, such as 4'-Undecyloxybiphenyl-4-yl-4-octyloxy-2-(pent-4-en-1-yloxy) benzoate (**9**) and 4'-Undecyloxy-1, 1'-biphenyl-4-yl 4-octyloxy-2-(undec-10-en-1-yloxy) benzoate (**10**) were obtained as the main starting mesogenic groups;
- The optimisation of intermediates synthesis were carried out by using Suzuki coupling reaction conditions with low outcomes, due to the new problem with solubility of biphenyl compounds in the reaction solvents;
- The thiol functional groups were introduced to the unsaturated mesogens precursors by using the free radical addition method. However low yields and purification difficulties were constant problems, due to the harsh reaction conditions;
- The reasons why this free radical addition method are not viable were investigated. It was found that yield percentages of compounds reported in literature were estimated from the ^{1}H NMR spectra and the final products were not isolated;
- A new thiolated mesogens synthetic route leading to the thiol group containing mesogens, with an overall reaction yield of the thiol introduction reaction of 70% was developed and optimised. This was achieved by the introduction of additional intermediates **21** or **22**, which were much more robust when compared with the reaction intermediates of the free radical addition reaction.
- Other similar thiolated mesogens were also synthesised by using this newly established thiolated mesogens synthetic route with thioacetic acid. This development allowed the research work to progress further and also solved a major challenge in the early part of this research. A much better synthetic route for the target mesogens was designed and this enables the routine preparation of the final liquid crystals gold nanoparticles (LC AuNPs) in much larger quantities.

1. 5 Instrumentations and Techniques

All compounds synthesised were purified and subjected to a range of analytical techniques by using the following instruments, as required, in order to assess both structure and purity. Intermediate compounds were subjected to ^{1}H Nuclear Magnetic Resonance (NMR) spectroscopy in most cases.

1. 5.1 ^{1}H and ^{13}C Nuclear Magnetic Resonance (NMR) Spectrometry

The structures of all intermediates and final products were confirmed by ^{1}H NMR spectroscopy using a JEOL Lambda JNM ECP400 spectrometer with TMS δ_H = 0 ppm as the internal standard or residual protic solvent deuterated chloroform ($CDCl_3$) δ_H = 7.26 ppm, deuterated dimethylsulfoxide ($(CD_3)_2SO$, DMSO-D6) δ_H = 2.50 ppm, deuterated dichloromethane (CD_2Cl_2) δ_H = 5.32 ppm. ^{1}H NMR was recorded at 400 MHz; an internal standard of tetramethylsilane (TMS) was used. All carbon (^{13}C) NMR spectra were recorded at 100.5 MHz, with the central peak of deuterated chloroform ($CDCl_3$) δ_C = 77.00 ppm, deuterated dimethylsulfoxide ($(CD_3)_2SO$, DMSO-D6) δ_C = 30.8 ppm used as the internal reference.

Splitting patterns of proton signals are described by the following abbreviations:

s - singlet	d – doublet
t - triplet	quart - quartet
quint - quintet	sext - sextet
dd – double doublet	dt - double triplet
tt – triple triplet	m - multiplet

1. 5.2 Elemental Analysis (EA)

Elemental analysis was performed on products to determine the relative ratios of carbon, hydrogen and sulphur in the sample and compared to expected values for the materials.

All results obtained were within ± 0.30% of the expected value, and the analysis was performed using a Fisons EA 1108 CHNS analyser.

1. 5.3 Mass Spectrometry (MS)

A mass spectrum was recorded to confirm the molecular mass of the material. All masses reported are the relative molecular masses (rounded to the nearest integer) and all mass spectra were recorded using either: solid probe electronic ionisation (EI) or matrix assisted laser desorption ionisation (MALDI) techniques.

a) Solid Probe Electron Impact (EI) mass spectra were recorded using a Simadzu GCMS-QP5050A quadropole GC/MS instrument at 70eV, with the probe heated to 350 ^{o}C to vapourise the sample. For each compound only the most important peaks are reported and the mass ion is indicated with M^{+}. Data was processed on a PC running Shimadzu Class-5000 processing software.
b) MALDI spectra were recorded using a Bruker Reflex IV MALDI-TOF mass spectrometer operating in reflection mode with accelerating viltage in the range of 20-25 kV, using a nitrogen laser providing photons at 337 nm and typically 100-150 laser shots were accumulated and averaged. MALDI mass spectra were processed using Bruker Compass software comprising FlexControl and FlexAnalysis packages.

Some of compounds were also analysed by the EPSRC National Mass Spectrometry Service Centre Swansea.

1. 5.4 Gas Chromatography (GC)

GC was used to monitor the progress of several reactions, and to determine the purity of several commercially available starting materials before use. The system used comprised a Varian CP 3380 gas chromatograph with a Chrompack capillary column with a 10m long CP-Sil 5 CB stationary phase column with an internal diameter of 0.25 mm and a film thickness of 0.12 μm, a flame ionisation detector (FID – constantly held in an oven at 300 ^{o}C) and in onjunction with Varian Star GC workstation software version 5.52.

1. 5.5 High Performance Liquid Chromatography (HPLC)

Final products and several intermediate products were subjected to analysis by HPLC on one of two systems, and to purifiy several final products:

a) Gilson HPLC system comprising of 233XL autosampler/fraction collector, 321 binary solvent pump, Valvemate column changer, Hewlett Packard 1100 series Diode Array Detector, Unipoint ver. 3.3 software, and Phenomenex Luna 5 µm C18(2) 250 x 4.6 mm analytical column, utilising (typically) 20 % dichloromethane (DCM) / 80 % acetonitrile as eluent.
b) The preparatory HPLC system comprised a Gilson 233XL auto sampler/fraction collector, 321 binary solvent pump, 151 UV/VIS detector, and a Phenomenex Luna 5 µm C18 250 x 25 mm column.

1. 5.6 Gel-Permeation Chromatography (GPC)

GPC was used to quantitatively determine the size of gold nanoparticles distribution and to check if possible dimers have formed during the reaction of synthesizing this thiol mesogen for the final Liquid Crystal Gold Nanoparticles. The GPC data was obtained by a generic system using RI detector with Polymer Labs Calibre Software (set of two columns plus guard PLgel). The columns used in the system were 5 um mixed-D columns (300 x 7.5 mm). pLgel is a highly cross-linked porous polystyrene/divinylbenzene matrix. The system was calibrated for conventional calibration with 10 polystyrene narrow standards to give polystyrene equivalent molecular weight.

1. 5.7 Optical Polarising Microscopy (OPM)

Identification and determination of melting points, all liquid crystal compounds transitions and mesophases were undertaken using an Olympus BX51 Polarizing Microscope with a Mettler FP52 hot-stage and Mettler FP5 Central Processor. Photomicrographs of the mesophases were taken using an Infinity *lite* Colour Video Camera, in conjunction with Mettler Studio Capture Software and the polarised microscopy setup. Liquid crystal phase nomenclature is used according to the following abbreviations:

Cr – Crystalline State Iso – Isotropic Liquid

N – Nematic Phase SmA – Smectic A Phase

SmC – Smectic C Phase

1. 5.8 Differential Scanning Calorimetry (DSC)

Transitions, isotropisation temperatures and melting points of all liquid crystal products observed via OPM were confirmed by DSC on one of two instruments:

a) Perkin Elmer DSC7 calibrated using indium (melting point onset 156.6 ^{o}C, enthalpy 28.45 J/g) and lead (melting point onset 327.47 ^{o}C). the calibration of the DSC was checked daily using the indium standard allowing ± 0.3 ^{o}C and ± 0.3 J/g experimental error, and using an gold reference pan. Data was collected via a PC running Pyris software.
b) Mettler DSC822e with STAR^{e} software, which was calibrated using indium (melting point onset 156.6 ^{o}C, 28.45 J/g). The calibration of the DSC was checked daily using the indium standard allowing ± 0.3 ^{o}C and ± 0.3 J/g experimental errors, and using an aluminium reference pan.

The following phase identification terms are used:

Mp = melting point Tg = glass transition Tm = melting point transition

The rest are the same as above

1. 5.9 Evaluation of Starting Materials and Solvents

All starting materials and dry-solvents were obtained from Aldrich, Avocado, Fluorochem, Strem Chem. Inc., Acros, Fisher scientific or Lancaster Synthesis without further purification, with the following exceptions:

- The **AIBN** as received from the laboratory cupboard was used in most of early stage experiments;
- At late stage experiments, purified **AIBN** by recrystallization from Methanol was used;

- The **AIBN** used in experiments **6a** – **b** was provided by Mark Ward;
- **RTG3** (compound **11**) previously obtained from the first 8 months research was used to synthesise LC AuNPs in experiments **12a** – **c**.
- Starting material **(4-(undecyloxy) phenyl) boronic acid** used in experiment **4a** – **b** was present in the laboratory.

All solvents used for column chromatography were used without further purification unless otherwise stated. All other solvents were used as purchased, except tetrahydrofuran which was dried over sodium, chloroform was dried by pass through a basic alumina (grade I, 10g per 14 ml) and methanol dried over magnesium turnings and iodine.

1. 6 Experimental

The Experimental section started with main mesogens frame development, followed by some intermediates optimisation procedures. The initial thiolated mesogens synthesis method is described and compared with other new synthetic routes. The newly developed method was then used to synthesize other desired thiolated mesogens.

1. 6.1 Main Mesogens Frame Synthesis

1. 6.1.1 Methyl 2-hydroxy-4-octyloxybenzoate (2)

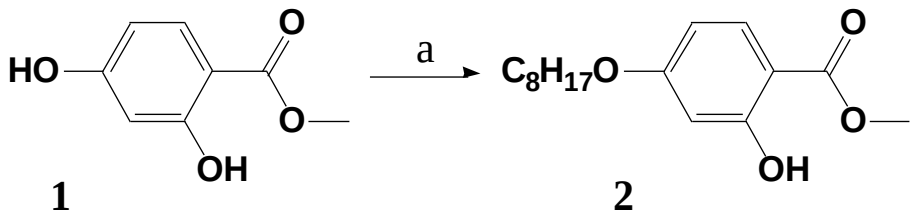

1 2

a... $C_8H_{17}Br$, K_2CO_3, powdered 4Å molecular sieves, dry butanone
heat 7h, then reflux further 18h.

A solution of bromo-octane (31.5 ml, 0.18 mol) in dry butanone (100 ml) was added under reflux to a suspension of methyl 2,4-dihydroxybenzoate (**1**, 25.5 g, 0.15 mol), K_2CO_3 (103.5 g, 0.75 mol) and powdered 4 Å molecular sieves (30 g) in dry butanone (500 ml) over a 7 h period. The reaction mixture was heated under reflux for an additional 18 h until the reaction was complete (TLC). After filtration of the reaction mixture, butanone solvent was distilled off and the residue recrystallised three times from methanol (50 ml) to yield white crystals (33.21 g, 0.12 mol, 79%). R_f (CH_2Cl_2) = 0.63. ^{1}H NMR 400 MHz ($CDCl_3$): δ [ppm] = 0.87 (t, 3H, CH_3), 1.38 (m, 10H, CH_2), 1.72 (m, 2H, OCH_2-$\underline{CH_2}$), 3.90 (s, 3H, CH_3), 3.95 (t, 2H, OCH_2), 6.42 (m, 2H, CH_{arom}), 7.72 (m, 1H, CH_{arom}), 10.96 (s, 1H, OH). Elemental analysis: calculated (%) for $C_{16}H_{24}O_4$ requires C 68.54 %, H 8.63 %; Found C 68.35 %, H 8.83 %.[75]

1. 6.1.2 Methyl 4-octyloxy-2-(pent-4-en-1-yloxy) benzoate (3)

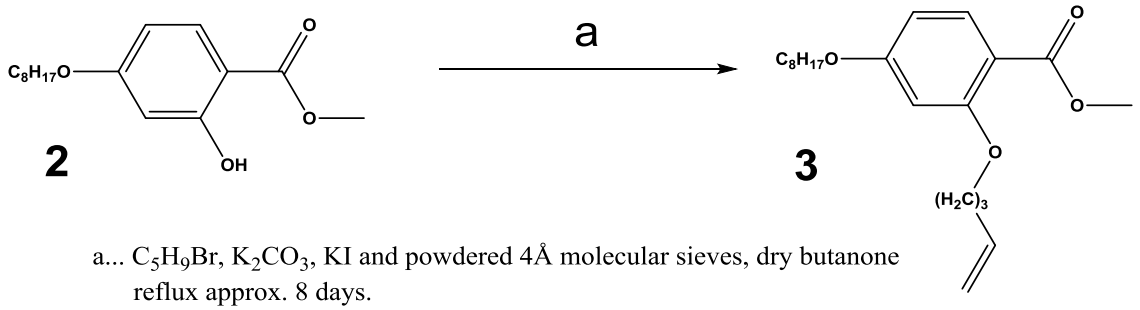

a... C_5H_9Br, K_2CO_3, KI and powdered 4Å molecular sieves, dry butanone reflux approx. 8 days.

Bromopent-4-ene (15.35 g, 0.103 mol) was added to a suspension of compound **2** (22.7 g, 0.0803 mol), K_2CO_3 (71.1 g, 0.515 mol), KI (1.72 g, 0.0103 mol) and powdered 4 Å molecular sieves (17.2 g) in dry butanone (240 ml), and the mixture was heated under reflux until the reaction was complete (approx. 8 days). The reaction mixture was filtered and the butanone distilled off. After drying the residue in vacuum, slightly yellow oil (26.29 g, 0.0746 mol, 94%) was obtained, which could be used in the next reaction without further purification. R_f (CH_2Cl_2) = 0.51. ^{1}H NMR 400 MHz ($CDCl_3$): δ [ppm] = 0.87 (m, 3H, CH_3), 1.35 (m, 10H, CH_2), 1.77 (m, 2H, OCH_2-$\underline{CH_2}$), 1.94 (m, 2H, OCH_2-$\underline{CH_2}$), 2.28 (m, 2H, $\underline{CH_2}$-$CH{=}CH_2$), 3.85 (s, 3H, OCH_3), 3.99 (m, 4H, OCH_2), 5.03 (m, 2H, $CH{=}\underline{CH_2}$), 5.82-5.91 (m, 1H, $\underline{CH}{=}CH_2$), 6.44-6.48 (m, 2H, CH_{arom}), 7.83 (m, 1H, CH_{arom}). Elemental analysis was not required as the resulting compound was used straight away for the next step without any further purification.[75]

1. 6.1.3 Methyl 4-octyloxy-2-(undec-10-en-1-yloxy) benzoate (4)

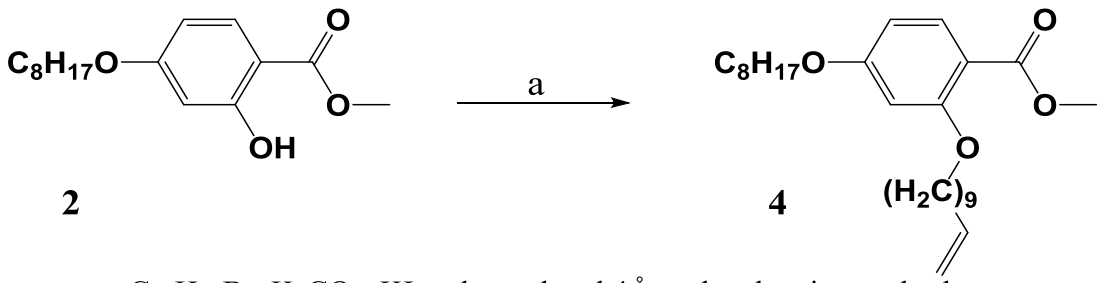

2 4

a... $C_{11}H_{23}Br$, K_2CO_3, KI and powdered 4Å molecular sieves, dry butanone reflux approx. 8 days.

The same procedure was carried out as for compound 3 using the following quantities: 11-Bromo-1-undecene (7.29 g, 0.03 mol), compound **2** (6.61 g, 0.0234 mol), K_2CO_3 (20.7 g, 0.15 mol), KI (0.5 g, 0.003 mol) and powdered 4 Å molecular sieves (5 g) in dry butanone (70 ml). The procedure yielded a slightly yellow oil (13.77 g, 0.318 mol, 136%), which could be used in the next reaction without further purification. ^{1}H NMR 400 MHz ($CDCl_3$): δ [ppm] = 0.89 (m, 3H, CH_3), 1.30 (m, 18H, CH_2), 1.45 (m, 4H, OCH_2-$\underline{CH_2}\underline{CH_2}$), 1.94 (m, 2H, OCH_2-$\underline{CH_2}$), 2.04 (m, 2H, $\underline{CH_2}$-CH=CH_2), 3.84 (s, 3H, OCH_3), 3.99 (m, 4H, OCH_2), 5.03 (m, 2H, CH=$\underline{CH_2}$), 5.86 (m, 1H, $\underline{CH}$=CH_2), 6.46 (m, 2H, CH_{arom}), 7.82 (m, 1H, CH_{arom}). Elemental analysis was not required as the resulting compound was used straight away for the next step without any further purification.[75]

1. 6.1.4 4-Octyloxy-2-(pent-4-en-1-yloxy) benzoic acid (5)

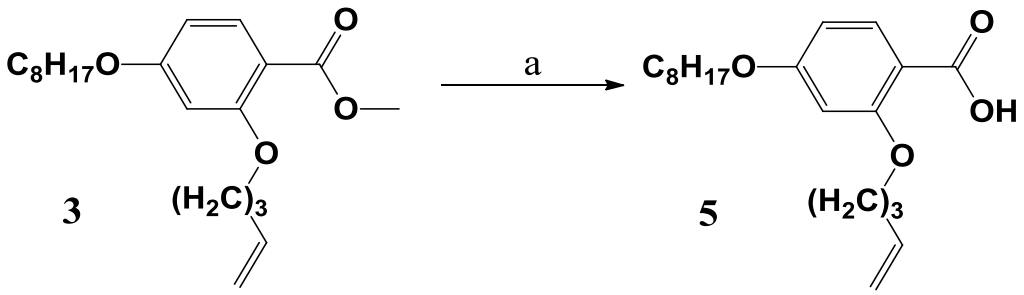

a...KOH, THF, methanol, stirring 2 days at r.t. then reflux 2h

Compound **3** (26.29 g, 0.0746 mol) was dissolved in THF (85 ml) and methanol (475 ml). A solution of KOH (22.59 g, 0.404 mol) in water (69 ml) was added. After stirring for 2 days at r.t. the reaction was completed by heating at reflux for 2 h. The solvents were distilled off and ice/water (306 ml) added. After acidification with conc. HCl (37 ml) the mixture was extracted with CH_2Cl_2 (6 x 85 ml). After drying the CH_2Cl_2 phase with $MgSO_4$ the solvent was distilled off. Recrystallization from hexane yielded off-white crystals (22.21 g, 0.066 mol, 89%). R_f (CH_2Cl_2) = 0.60. ^{1}H NMR 400 MHz ($CDCl_3$): δ [ppm] = 0.89 (t, 3H, CH_3), 1.38 (m, 10H, CH_2), 1.80 (m, 2H, OCH_2-$\underline{CH_2}$), 2.02 (m, 2H, OCH_2-$\underline{CH_2}$), 2.30 (m, 2H, $\underline{CH_2}$-$CH{=}CH_2$), 4.01 (t, 2H, OCH_2), 4.22 (t, 2H, OCH_2), 5.09 (m, 2H, $CH{=}\underline{CH_2}$), 5.82 (m, 1H, $\underline{CH}{=}CH_2$), 6.51 (d, 1 H, CH_{arom}), 6.62 (dd, 1 H, CH_{arom}), 8.12 (d, 1 H, CH_{arom}), 10.69 (br, 1 H, COOH). Elemental analysis: calculated (%) for $C_{20}H_{30}O_4$ requires C 71.82 %, H 9.04 %; Found C 71.68 %, H 9.08 %.[75]

1. 6.1.5 4-Octyloxy-2-(undec-10-en-1-yloxy)benzoic acid (6)

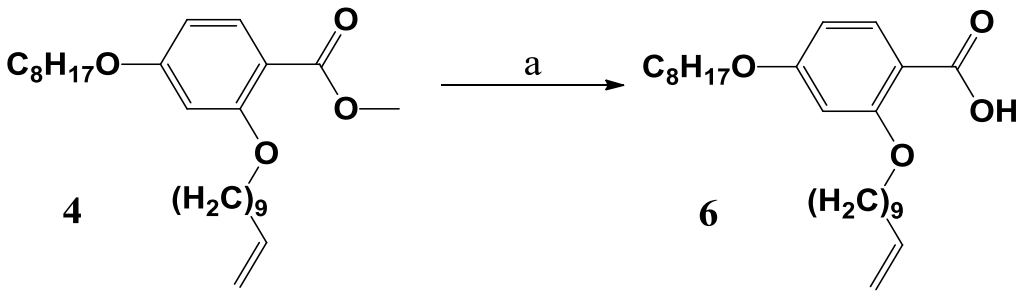

a...KOH, THF, methanol, stirring 2 days at r.t. then reflux 2h

The same procedure was carried out as for compound **5** using the following quantities: Compound **4** (13.77 g, 0.318 mol), THF (37.5 ml), methanol (210 ml) and a solution of KOH (9.64 g, 0.1722 mol) in water (30 ml). After recrystallisation from hexane, this procedure yielded off-white crystals (8.49 g, 0.0203 mol, 63.8%). ^{1}H NMR 400 MHz ($CDCl_3$): δ [ppm] = 0.89 (t, 3H, CH_3), 1.42 (m, 22H, CH_2), 1.78 (m, 2H, OCH_2-$\underline{CH_2}$), 1.89 (m, 2H, OCH_2-$\underline{CH_2}$), 2.04 (m, 2 H, $\underline{CH_2}$-$CH{=}CH_2$), 4.01 (t, 2 H, OCH_2), 4.19 (t, 2H, OCH_2), 5.01 (m, 2H, $CH{=}\underline{CH_2}$), 5.81 (m, 1H, $\underline{CH}{=}CH_2$), 6.50-6.63 (d, 1H, CH_{arom}), 6.61 (dd, 1H, CH_{arom}), 8.12 (d, 1H, CH_{arom}), 10.75 (br, 1H, COOH). Elemental analysis: calculated (%) for $C_{26}H_{42}O_4$ requires C 74.60 %, H 10.11 %; Found C 74.68 %, H 10.01 %.[75]

1. 6.1.6 4-Hydroxy-4’-undecyloxybiphenyl (8)

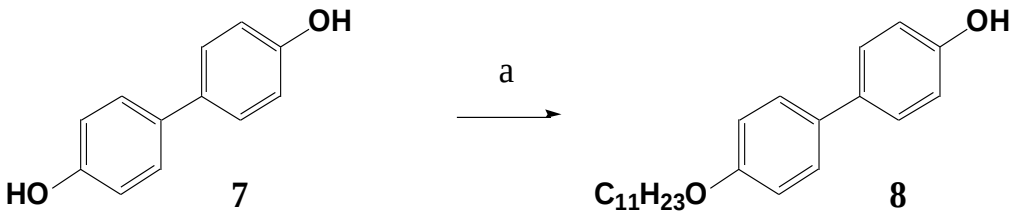

a...metal Na, $C_{11}H_{23}Br$, KI and methanol.

Sodium metal (8.6 g, 0.36 mol) was dissolved in dry methanol (300 ml) with exclusion of moisture and followed by 4, 4’-dihydroxy biphenyl (**7**, 25.3 g, 0.36 mol) added immediately. Bromo-undecane (29 ml) was added drop wise to this solution and after adding KI (2.3 g) the reaction mixture was heated at reflux for 20 h. After cooling to RT a solution of NH_4Cl (10 g) in water (250 ml) was added. The product was filtered off, washed with water (50 ml) and methanol (50 ml). Repeated Recrystallisation from butanone (400 ml) yielded a beige powder (18.9 g, 0.0556 mol, 39%). ^{1}H NMR 400 MHz ($CDCl_3$): δ [ppm] = 0.89 (t, 3H, CH_3), 1.42 (m, 16H, CH_2), 1.78 (m, 2H, OCH_2-$\underline{CH_2}$), 3.99 (t, 2 H, OCH_2), 6.86 (m, 2H, CH_{arom}), 6.90 (m, 2H, CH_{arom}), 7.35 (m, 2H, CH_{arom}), 7.42 (m, 2H, CH_{arom}), 9.00 (s, 1H, OH). Elemental analysis: calculated (%) for $C_{23}H_{32}O_2$ requires C 81.13 %, H 9.47 %; Found C 82.04 %, H 9.71 %.[75]

1. 6.1.7 4'-Undecyloxybiphenyl-4-yl-4-octyloxy-2-(pent-4-en-1-yloxy) benzoate (9)

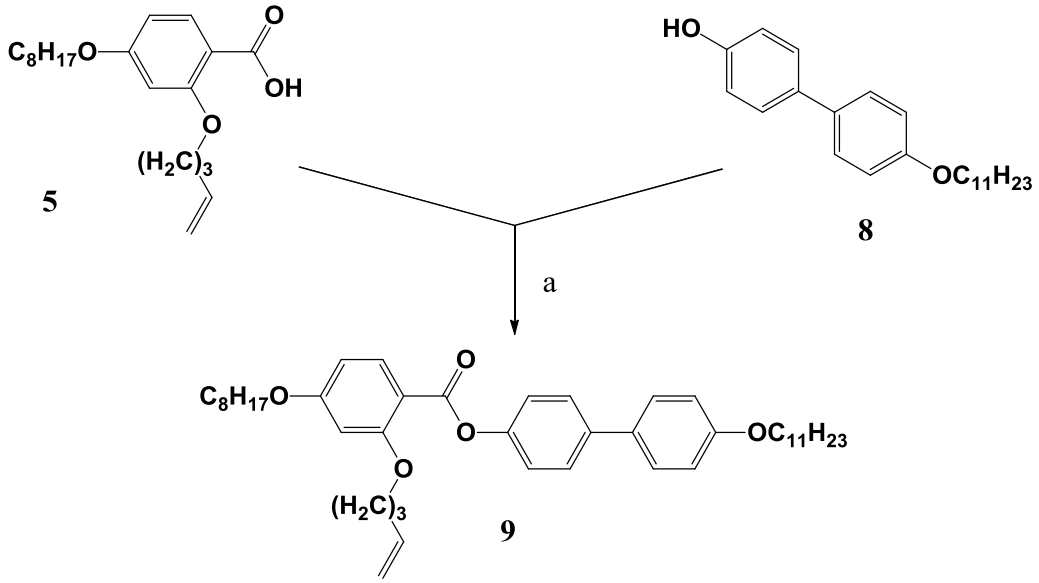

a...(i) compound 5, thionyl chloride, dry toluene heat at 80 ^{o}C 3h, then reflux 45 mins under N_2;
(ii) compound 8, pyridine, toluene heat at 80 ^{o}C 18h and reflux 1h.

Compound **5** (10.6 g, 31.7 mmol) was dissolved in dry toluene (130 ml) under nitrogen; thionyl chloride (50ml, 0.68 mol) was added and the solution heated to 80 ^{o}C for 3 h, the reaction being completed after heating for 45 min at reflux. The thionyl chloride was distilled off under nitrogen. A solution of compound **8** (10.8 g, 31.7 mmol) and pyridine (50 ml, 0.62 mol) in toluene (50 ml) was added to the residue. This reaction mixture was heated at 80 ^{o}C for 18 h and the reaction completed after reflux for 1 h. Ice-water (400 ml) and 1/1 ether/hexane (400 ml) was then added; the phases were separated and the aqueous layer was washed with $CHCl_3$ (2 x 250 ml). The combined organic layers were dried with $MgSO_4$ and the solvents distilled off. The residue was purified by column chromatography (silica gel, CH_2Cl_2/hexane = 4/1). Recrystallisation from hexane yielded a white product (17.67 g, 26.9 mmol, 85%). ^{1}H NMR 400 MHz ($CDCl_3$): δ [ppm] = 0.89 (m, 6H, CH_3), 1.38 (m, 26H, CH_2), 1.79 (m, 4H, O$\underline{CH_2}\underline{CH_2}$), 1.95 (m, 2H, OCH_2-$\underline{CH_2}$), 2.29 (m, 2H, $\underline{CH_2}$-CH=CH_2), 4.02 (m, 6H, OCH_2), 5.00 (m, 2H, CH=$\underline{CH_2}$), 5.88 (m, 1H, $\underline{CH}$=CH_2), 6.53 (m, 2H, CH_{arom}), 6.97 (m, 2H, CH_{arom}), 7.23 (m, 2H, CH_{arom}), 7.52 (m, 4H, CH_{arom}), 8.05 (d, 1H, CH_{arom}). Elemental analysis: calculated (%) for $C_{43}H_{60}O_5$ requires C 78.62 %, H 9.21 %; Found C 78.61 %, H 9.46 %.[75]

1. 6.1.8 4'-Undecyloxy-1, 1'-biphenyl-4-yl 4-octyloxy-2-(undec-10-en-1-yloxy) benzoate (10)

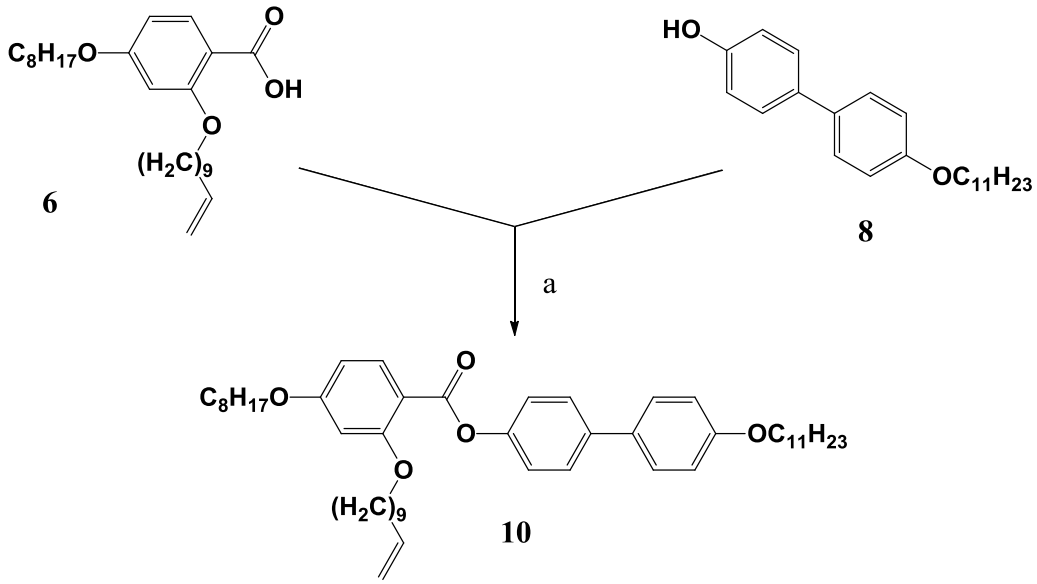

a...(i) compound 6, thionyl chloride, dry toluene heat at 80 ^{o}C 3h, then reflux 45 mins under N_2;
(ii) compound 8, pyridine, toluene heat at 80 ^{o}C 18h and reflux 1h.

The same procedure was carried out as for compound 5 using the following quantities: Compound **6** (3.317 g, 7.925 mmol) and dry toluene (32.5 ml) and (12.5 ml, 0.17 mol). Compound **8** (2.698 g, 7.925 mmol), pyridine (12.5 ml, 0.155 mol) and toluene (12.5 ml). After recrystallisation from hexane, this procedure yielded off-white crystals (4.29 g, 5.793 mmol, 73.1%). ^{1}H NMR 400 MHz ($CDCl_3$): δ [ppm] = 0.89 (m, 6H, CH_3), 1.37 (m, 38H, CH_2), 1.82 (m, 4 H, O$\underline{CH_2}\underline{CH_2}$), 2.00 (m, 2H, OCH_2-$\underline{CH_2}$), 4.02 (m, 6H, 3xOCH_2), 5.10 (m, 2H, CH=$\underline{CH_2}$), 5.78 (m, 1H, $\underline{CH}$=CH_2), 6.52 (m, 2H, CH_{arom}), 6.96 (m, 2H, CH_{arom}), 7.24 (m, 2H, CH_{arom}), 7.52 (m, 4H, CH_{arom}), 8.03 (d, 1H, CH_{arom}). Elemental analysis: calculated (%) for $C_{49}H_{72}O_5$ requires C 79.41 %, H 9.79 %; Found C 79.60 %, H 9.97 %. Transition temperature: Cr: 45.7 ^{o}C, N: 62.3 ^{o}C, Iso on heating.[75]

1. 6.2 Intermediates Synthesis Optimisation

1. 6.2.1 4-bromo-4'-(undecyloxy)-1,1'-biphenyl (14)

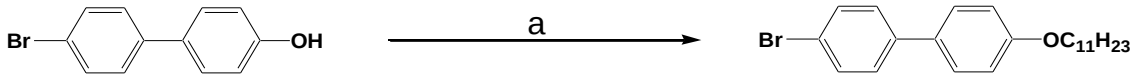

13 **14**

a... (i) K_2CO_3, 4A powdered molecule sieves, dry butanone; (ii) Bromoundecane.

Several methods were employed in preparing this compound.[75]

Method 1

A solution of bromoundecane (2.822 g, 12 mmol, and 2.68 ml) in dry butanone (7 ml) was added under reflux to a suspension of 4,4-bromobiphenyl-ol (**13**, 2.49 g, 10 mmol), K_2CO_3 (6.91 g, 50 mmol) and powdered 4Å molecular sieves (2 g) in dry butanone (34 ml) over 1 h. The reaction mixture was heated under reflux in a N_2 environment for an additional of 18 h until the reaction mixture was complete (TLC and GC). After filtration of the reaction mixture, the solvent was distilled off under reduced pressure before column chromatograph (silica gel, CH_2Cl_2/hexane = 3/7). Recrystallization from butanone yielded a white crystal (1.98 g, 49.1%). ^{1}H-NMR 400 MHz ($CDCl_3$): δ [ppm] = 0.89 (m, 3H, CH_3), 1.30 (m, 16H, CH_2), 1.79 (m, 2 H, OCH_2-$\underline{CH_2}$), 4.02 (m, 2 H, OCH_2), 6.96 (m, 2H, CH_{arom}), 7.53 (m, 6H, CH_{arom}). Elemental analysis: calculated (%) for $C_{23}H_{31}BrO$: C 68.48 %, H 7.75 %; Found C 68.69 %, H 7.97 %.

Method 2

The same procedures were followed as method 1, except a longer addition time of bromoundecane and extra portions of bromoundecane were also added to enhance the yield. The final compound **14** was recrystallised from butanone to yield a white crystalline solid (31.85 g, 79%). ^{1}H-NMR 400 MHz ($CDCl_3$): δ [ppm] = 0.88 (m, 3H), 1.30 (m, 16H, CH_2), 1.79 (m, 2H, OCH_2-$\underline{CH_2}$), 4.02 (m, 2H, OCH_2), 6.96 (m, 2H, CH_{arom}), 7.53 (m, 6H, CH_{arom}). Elemental analysis: calculated (%) for $C_{23}H_{31}BrO$: C 68.48 %, H 7.75 %; Found C 68.74 %, H 7.85 %.

1. 6.2.2 (4'-(undecyloxy)-[1,1'-biphenyl]-4-yl)boronic acid (15)

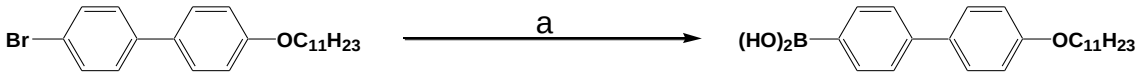

14 **15**

a... (i) n-Butyllithium, dry THF; (ii) trimethyl borate; (iii) 10% HCl.

n-Butyllithium in hexane (1.5 ml, 3.72 mmol) was added to a stirred solution of compound **14** (1 g, 2.48 mmol) in dry THF (70 ml) at – 78 ^{o}C under a dry nitrogen atmosphere. Another portion of dry THF (230 ml) was introduced to help dissolving compound **14** at this low temperature. The mixture was stirred for 45 mins and then trimethyl borate (0.46g, 3.72 mmol) was added drop-wise slowly. The reaction mixture was allowed to warm to RT overnight and then stirred for 1 h with 10 % HCl (50 ml). The product was extracted into ether (2 x 20 ml), followed by washing with water (2 x 20), and dried with $MgSO_4$. Solvent was removed in *vaccuo* and the crude product was stirred with hexane and a small amount of purified water to yield a white pale yellow impure solid (0.1 g, 11%), and no product was collected after washing with hexane and purified water again.[4, 7, 85]

1. 6.2.3 4-hydroxy-4’-undecyloxybiphenyl (8)

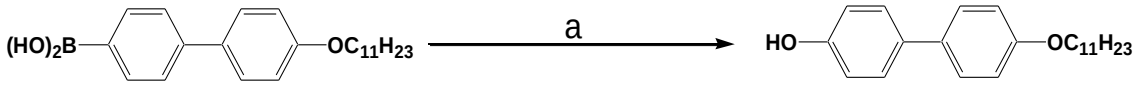

15 **8**

a... H_2O_2, Et_2O.

H_2O_2 (1 ml) was added into a solution of compound **15** (available in the laboratory, 0.1 g, 0.33 mmol) dissolved in diethyl ether (1.5 ml) under reflux, then it was heated under reflux for a further 18 h. After the reaction cooled, DCM (2 ml) and water (1 ml) was added. The layers were separated and the aqueous layer was washed with DCM (2 x 1 ml). The combined organic layers were washed with saturated aqueous solution of iron (II) sulphate until all excess H_2O_2 was destroyed [colour changed from green → brown (Fe^{2+} → Fe^{3+}), when all the H_2O_2 was destroyed, iron (II) sulphate remained green after washing]. The organic layers was washed with water and dried over $MgSO_4$. The solvent was removed under *vacco*. However both TLC and crude sample ^1H NMR showed very a small amount of targeted product.[4, 7]

1. 6.2.4 1-iodo-4-(undecyloxy) benzene (17)

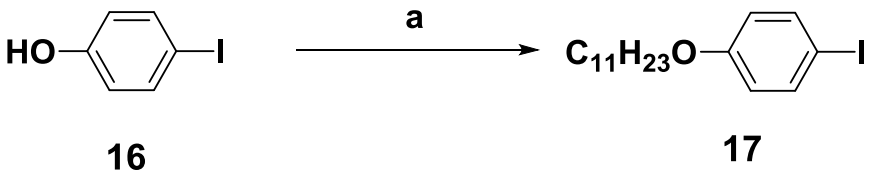

16 17

a... (i) K_2CO_3, 4Å powdered molecular sieves, dry butanone; (ii) Bromoundecane.

A solution of bromoundecane (14.34 g, 60.69 mmol, and 13.6 ml) in dry butanone (35 ml) was added under reflux to a suspension of 4-iodophenol (**16**, 12 g, 50.8 mmol), K_2CO_3 (35.05 g, 0.254 mol), KI (0.85 g, 5.12 mmol) and powdered 4Å molecular sieves (10.5 g) in dry butanone (170 ml) over 6 h. The reaction mixture was refluxed under N_2 for an additional of 24 h until the reaction mixture was complete (TLC and GC). After filtration of the reaction mixture, the solvent was distilled off before column chromatography (silica gel, CH_2Cl_2/hexane = 3/7). Recrystallization from hexane with a minimum of ethyl acetate yielded pale pinkish crystal (14.48 g, 76.2%). ^{1}H NMR 400 MHz ($CDCl_3$): δ [ppm] = 0.88 (t, 3H, CH_3), 1.34 (m, 16H, CH_2), 1.75 (m, 2H, OCH_2-$\underline{CH_2}$), 3.90 (t, 2H, OCH_2), 6.65 (m, 2H, CH_{arom}), 6.90 (m, 2H, CH_{arom}), 7.52 (m, 2H). Elemental analysis: calculated (%) for $C_{17}H_{27}OI$: C 54.55 %, H 7.27 %; Found C 54.67 %, H 7.47 %.[75]

1. 6.2.5 4-hydroxy-4'-undecyloxybiphenyl (8)

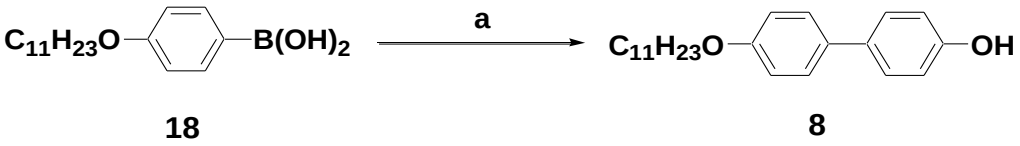

18 **8**

a... (i) 4-iodophenol, KF, dry THF;
(ii) (4-(undecyloxy)phenyl)boronic acid, dry THF, $Pd(PPh_3)_4$, reflux 24 h.

Several methods were employed in preparing this compound.[4, 7, 83]

Method 1

$Pd(PPh_3)_4$ (0.115 g, 0.1 mmol) and (4-(undecyloxy)phenyl)boronic acid (**18**, 1.19 g, 5.405 mmol) were added sequentially to a stirred mixture of 4-iodophenol (**16**, 1.41 g, 5.974 mmol), KF (1.74 g, 0.03 mol) and dry THF (100 ml) under N_2. The mixture was heated under reflux for 20 hrs. GC was used to monitor the reaction and no significant progress. After cooling the mixture, it was extracted into ether (2 x 75 ml), and the combined organic phase was washed with water (2 x 50 ml), brine (30 ml) and dried over $MgSO_4$ and solvents distilled off before column chromatography (silica gel, CH_2Cl_2/hexane = 4/6), ^1H NMR checking showed that no product was present.

Method 2

The same procedures were followed as for method 1, except careful solvents degassing and glassware drying processes were applied in this case. GC was used to monitor the reaction and no significant progress was observed. Organic materials were obtained by column chromatography (silica gel, CH_2Cl_2/hexane = 4/6), ^1H NMR spectroscopy showed that no product had been formed.

1. 6.3 Thiolated Mesogens Synthesis Route 1

1. 6.3.1 4'-(undecyloxy)-[1,1'-biphenyl]-4-yl-2-((5-mercaptopentyl)oxy)-4-(octyloxy)benzoate (11)

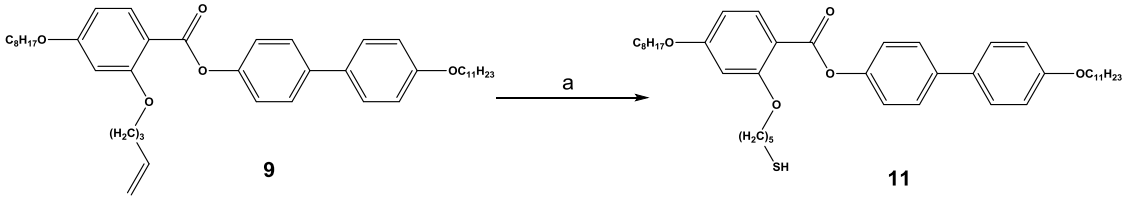

a...(i) Ph_3SiSH in benzene and UV, 48h;
(ii) TFA, 30mins

Several methods were employed in preparing this compound.[77]

Method 1

Compound **9** (3.285 g, 5 mmol), Ph_3SiSH (1.671 g, 50714 mmol) and AIBN (0.2346 g, 1.429 mmol in benzene (5 ml) was heated under reflux for 48 h. It was cooled to room temperature and treated with 5 eq. of TFA (6 g, 28.57 mmol, and 4 ml) stirred for 30 min. The solvent was removed under reduced pressure and column chromatography (silica gel, CH_2Cl_2/hexane = 3/7) was used for thiol mesogen isolation. However this isolation process was also time consuming and the compounds were inseparable, hence there was no yield and the final mixture residue was stored for further purification and future analysis.

Method 2

A mixture of compound **9** (0.9197 g) and Ph_3SiSH (98%, 0.4775 g) in benzene (99.7%, 2 ml) was irradiated under this strong light source (250 Watts, Professional MULTILITE from Johnson) 1 cm away in a foil wrapped seal environment for 48 h until disappearance of starting material, and a bright yellow mixture before adding TFA (1.14 ml) dropwise. It became yellow after adding TFA (99+%, 1.14 ml) to this cooled mixture and stirred for a further 30 min. TLC was used to monitor this reaction. Solvents were evaporated before column chromatography (DCM/hexane, 1/9), however this isolation process was very time consuming and the desired compound was also difficult to separate from the mixture, hence no yield was recorded and the final mixture residue was stored for further purification and analysis.

Several reaction conditions were optimised as shown in the Table 1. 1 below:

Exp.	Reaction condition	Yield %
11 a	UV (250 watt light bulb) replace thermal initiation and better quality AIBN;	< 25 % product inseparable
11 b	UV (TLC UV lamp 365 nm) replace thermal initiation and better quality AIBN;	< 25 % product inseparable

Table 1. 1. Optimised reaction condition for compound 11 synthesis.

GC indicated only a trace of the desired product and were difficult to separate from the residue mixture by silica gel chromatography and degradation occurred over period of time.

1. 6.3.2 4'-(undecyloxy)-[1,1'-biphenyl]-4-yl-2-((11-mercaptoundecyl)oxy)-4-(octyloxy)benzoate (12)

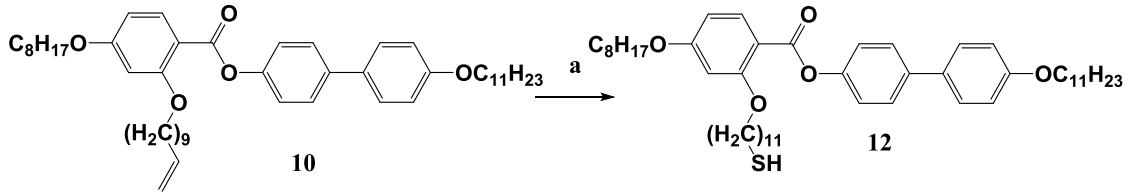

a...(i) Ph_3SiSH in benzene and UV, 48h;
(ii) TFA, 30min

Several methods were employed in preparing this compound.[77]

Method 1

The same procedure was carried out as for compound **11** *method 1* using the following quantities: Compound **10** (1.038 g, 1.4 mmol), Ph_3SiSH (0.4680 g, 1.6 mmol) and AIBN (0.06568 g, 0.4 mmol) in benzene (1.4 ml) was heated under reflux for 48 h. It was then cooled to room temperature and treated with 5 eq. of TFA (1.687 g, 8 mmol, 1.4 ml) for c.a. 30 min. The solvent was removed and column chromatography (silica gel, CH_2Cl_2/hexane = 3/7) was used for thiol mesogen isolation. However this isolation process was also time consuming and compounds inseparable, hence no yield was recorded and the mixture was stored for further purification and future analysis.

Method 2

The same procedure was carried out as for compound **11** *method 2* using a strong light source (preferably a strong UV source) with the following quantities: compound **10** (1.038 g), Ph_3SiSH (98%, 0.4775 g) and AIBN (65.68 mg, 0.4 mmol) in benzene (99.7%, 2 ml), then TFA (99+%, 1.14 ml) was added to this cooled mixture and stirred for a further 30 min. TLC was used to monitor this reaction. Solvents were evaporated before column chromatography (DCM/hexane, 1/9). This isolation process was very time consuming, hence no yield was recorded and the mixture was stored for further purification and future analysis.

Several reaction conditions were optimised as shown in the Table 1. 2 below:

Exp.	Reaction condition	Yield %
12a	TFA was not added;	< 25 % product inseparable
12b	Extra portion of AIBN was added;	< 25 % product inseparable
12c	Double the amount of starting material;	< 25 % product inseparable
12d	Higher purity of AIBN used;	< 25 % product inseparable
12e	UV (strong light bulb) instead of thermal initiation;	< 25 % product inseparable
12f	UV (TLC UV lamp 365 nm) to replace thermal initiation;	< 25 % product inseparable
12g	UV (strong light bulb) replace thermal initiation and better quality AIBN;	< 25 % product inseparable
12h	UV (TLC UV lamp 365 nm) to replace thermal initiation and better quality AIBN;	< 25 % product inseparable
12i	UV (TLC UV lamp 365 nm) to replace thermal initiation, better quality AIBN and without adding TFA;	< 25 % product inseparable

Table 1. 2. Optimised reaction condition for compound 12 synthesis.

The same results were found that only trace levels of product were present and inseparable.

1. 6.3.3 4-phenylbutane-1-thiol (20)

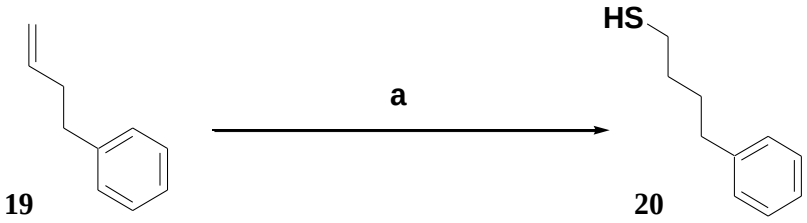

a...(i) AIBN, Ph_3SiSH; (ii) TFA

A mixture of but-3-en-1-ylbenzene (**19**, 0.1851 g, 0.21 ml), Ph_3SiSH (98%, 0.4775 g) and AIBN (Fisher laboratory reagent grade) (65.68 mg) in benzene (99.7%, 2 ml) was heated under reflux for 48 h until complete disappearance of starting material, which was monitored by TLC. TFA (99+%, 1.141 ml) was added to this cooled mixture and stirred for a further 30 min. TLC was used to monitor this reaction. Solvents were evaporated before column chromatography (DCM/hexane, 1/9), however this isolation process was also very time consuming, hence yielded no product and the final mixture residue was stored for further purification and future analysis. Reaction conditions were also optimised as for compound **11** and **12**, and the same issues were present here.[77]

1. 6.4 Thiolated Mesogens Synthesis Route 2

1. 6.4.1 4'-(undecyloxy)-[1,1'-biphenyl]-4-yl-2-((11-(acetylthio)undecyl)oxy)-4-(octyloxy)benzoate (22)

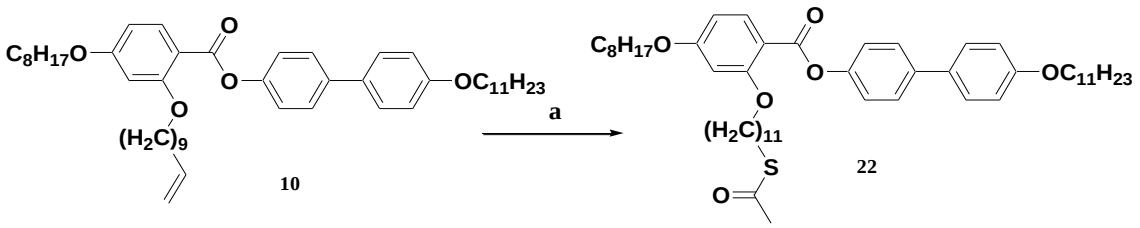

a...AIBN, CH_3COSH, methanol, dry THF

Thioacetic acid (97%, 0.11 ml, 0.5889 mmol) was introduced to a stirred mixture of compound **10** (0.3706 g, 0.5 mmol) and AIBN (9.766 mg, 0.058 mmol) in dry THF (7.5 ml) under nitrogen. This mixture was heated at 80 ^oC for 6 h, then heated at 65 ^oC for a further 24 h. Finally a small portion of AIBN (~ 5 mg) was added to this mixture and heated for another 4 hrs with the reaction monitored by TLC until disappearance of starting material, then this mixture was heated at 85 ^oC for another further 18 h and this reaction was completed by heating under reflux for another 4 h. Solvents were evaporated before column chromatography (DCM / hexane, 4 / 6) yielded light yellow solid (0.139 g, 34 %). ^1H NMR 400 MHz ($CDCl_3$): δ [ppm] = 0.89 (m, 6H, CH_3), 1.45 (m, 30H, CH_2), 1.84 (m, 6H, 3xOCH_2-$\underline{CH_2}$), 2.20 (m, 2H, $\underline{CH_2}$-CH_2S), 2.31 (s, 3H, SCO-$\underline{CH_3}$), 2.83 (t, 2H, CH_2S), 4.03 (m, 6H, OCH_2), 6.53 (m, 2H, CH_{arom}), 6.95 (d, 2H, CH_{arom}), 7.23 (d, 2H, CH_{arom}), 7.52 (dd, 4H, CH_{arom}), 8.03 (dd, 1H, CH_{arom}). Elemental analysis: calculated (%) for $C_{51}H_{76}O_6S$ requires C 74.96 %, H 9.37 %, S 3.92 %; Found C 74.83 %, H 9.5 %, S 4.02 %. [81, 83, 84]

Reaction conditions were optimised to achieve a high yield as shown in Table 1. 3 below:

Exp.	**Reaction Conditions**	**Yield %**	**EA expected**: **C** 74.96 %, **H** 9.37 %, **S** 3.92 %
22a	60 ^{o}C, 12h;	93.1 %	**C** 75.1 %, **H** 9.52 %, **S** 4.05 %
22b	Recrystallized AIBN, 60 ^{o}C and 12h;	85.8 %	**C** 74.71 %, **H** 9.42 %, **S** 3.81 %
22c	Same as **22b**;	78.4 %	**C** 74.9 %, **H** 9.52 %, **S** 3.95 %
22d	3 x SM, 60 ^{o}C and 3h;	91.5 %	**C** 75.1 %, **H** 9.22 %
22e	2 x SM, 60 ^{o}C and 3h;	71.6 %	**C** 74.82 %, **H** 9.56 %
22f	6 x SM, 60 ^{o}C and 3h;	74.4 %	**C** 74.95 %, **H** 9.38 %
22g	dry chloroform, 60 ^{o}C and 6h;	83.3 %	**C** 74.68 %, **H** 9.49 %, **S** 3.7 %

Table 1. 3. Optimised reaction condition for compound 22 synthesis.

1. 6.4.2 4'-(undecyloxy)-[1,1'-biphenyl]-4-yl-2-((5-(acetylthio)pentyl)oxy)-4-(octyloxy) benzoate (21)

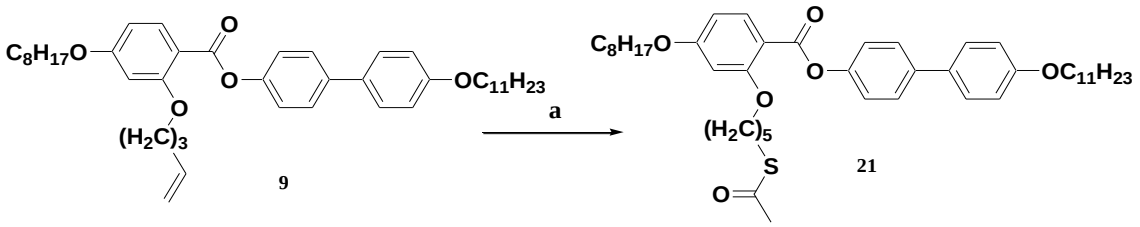

a...AIBN, CH_3COSH, methanol, dry THF

The optimised procedure was carried out as for compound **22** using the following quantities: Thioacetic acid (97%, 0.22 ml, 1 mmol) compound **9** (0.3285 g, 0.5 mmol) and purified AIBN (Fisher laboratory reagent grade) (82.1 mg, 0.5mmol) in dry THF (7.5 ml) under nitrogen. This final mixture was heated at 60 ^oC for 3 hrs. The reaction was monitored by TLC until disappearance of starting material. Solvents were evaporated before column chromatography (DCM / hexane, 3.5 / 6.5). Recrystallization from 1-propanol yielded a light yellow solid (0.31 g, 84.6 %). ^1H NMR 400 MHz ($CDCl_3$): δ [ppm] = 0.89 (m, 6H, CH_3), 1.45 (m, 28H, CH_2), 1.84 (m, 6H, 3xOCH_2-$\underline{CH_2}$), 2.20 (m, 2H, $\underline{CH_2}$-CH_2S), 2.31 (s, 3H, $SCO\underline{CH_3}$), 2.83 (t, 2H, CH_2S), 4.03 (m, 6H, 3xOCH_2), 6.54 (m, 2H, CH_{arom}), 6.95 (d, 2H, CH_{arom}), 7.23 (d, 2H, CH_{arom}), 7.52 (dd, 4H, CH_{arom}), 8.03 (dd, 1H, CH_{arom}). Elemental analysis: calculated (%) for $C_{45}H_{64}O_6S$ requires C 73.73 %, 8 H.80 %, S 4.37 %; Found C 73.82 %, H 9.08 %, S 4.20 %. HPLC: 99.74%. Transition temperature (^oC): N 52.88 ^oC Iso.[79, 81, 82]

1. 6.4.3 4'–(undecyloxy)–[1,1'–biphenyl]–4–yl–2–((11–mercaptoundecyl) oxy)–4–(octyloxy)benzoate (12)

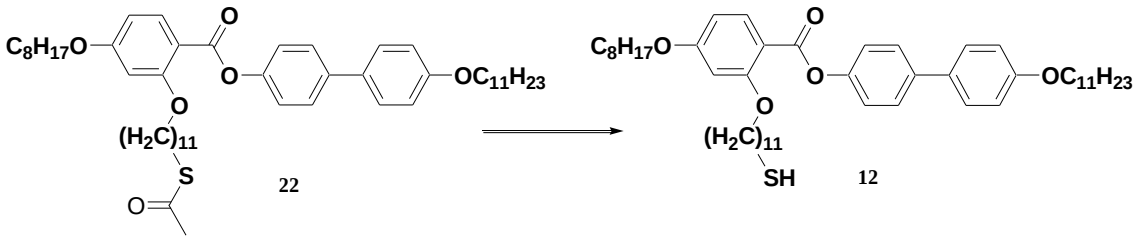

a...AIBN, CH_3COSH, methanol, dry THF

Several methods were employed in preparing this compound.[75, 82, 84]

Method 1

Compound **22** (0.32 g, 0.392 mmol) was dissolved in methanol (90 ml), and 30 drops of HCl (12 N) was added. After stirring for 2 days at r.t. the reaction was completed by heating at reflux under nitrogen for 2 h. The solvents were distilled off and followed by flash column chromatography (DCM/hexane, 3.5/6.5). However the targeted product was unable to obtain and only by products were present within the final reaction residue which was consistent with the results monitored by TLC.

Method 2

Zinc powder (14.5 mg, 0.222 mmol) was added into an ice cold sealed solution of $TiCl_4$ (21.1 mg, 0.122 ml, 0.111 mmol) under argon and stirred for 30 min in an ice-water bath. A solution of compound **22** (60.4 mg, 0.074 mmol) in DCM (2.5 ml) was introduced and this mixture was stirred at r.t. for a further 15 min. The reaction was monitored by TLC. Ice water (4 ml) and ethyl acetate (4 ml) was added, and the organic layer was washed with water (2 x 2 ml) and brine (2 x 2 ml). The organic layer was dried over $MgSO_4$ and the solvents were distilled off. A light yellow solid (0.0132 g, 23%) was isolated by a prep-TLC. ^1H NMR 400 MHz ($CDCl_3$): δ [ppm] = 0.89 (m, 6H, CH_3), 1.49 (m, 43H, CH_2), 1.82 (m, 6H, 3xOCH_2-$\underline{CH_2}$), 2.48 (q, 2H, CH_2S), 4.01 (m, 6H, 3xOCH_2), 6.52 (m, 2H, CH_{arom}), 6.96 (d, 2H, CH_{arom}), 7.22 (m, 2H, CH_{arom}), 7.52 (dd, 4H, CH_{arom}), 8.03 (d, 1H, CH_{arom}). Elemental analysis: calculated (%) for $C_{49}H_{74}O_5S$ requires 75.92 % C, 9.62 % H, 4.14 % S; Found 75.70 % C, 9.82 % H, 3.95 % S.

Method 3

NaSMe (74 mg, 1.056 mmol) was dissolved in a minimum of MeOH, and this solution was added drop-wise into a mixture of compound **22** (72.3 mg, 0.089 mmol) dissolved in methanol (3 ml) and THF (1 ml) under nitrogen at 45 ^{o}C. The reaction mixture was heated to 45 ^{o}C for 30 mins, and the reaction was completed by stirring at r.t. for 18 hrs. The whole reaction was monitored by TLC. HCl (0.1 M, 2 ml) and DCM (4 ml) was added, the organic layer was washed by water (2 x 4 ml) and brine (2 x 4 ml). The organic layer was dried over $MgSO_4$ and solvents were distilled off. A light yellow solid (0.0233 mg, 34%) was isolated by a prep-TLC. ^{1}H NMR 400 MHz ($CDCl_3$): δ [ppm] = 0.89 (m, 6H, CH_3), 1.49 (m, 43H, CH_2), 1.82 (m, 6H, 3xOCH_2-$\underline{CH_2}$), 2.48 (q, 2H, CH_2S), 4.01 (m, 6H, OCH_2), 6.52 (m, 2H, CH_{arom}), 6.96 (d, 2H, CH_{arom}), 7.22 (m, 2H, CH_{arom}), 7.52 (dd, 4H, CH_{arom}), 8.03 (d, 1H, CH_{arom}). Elemental analysis: calculated (%) for $C_{49}H_{74}O_5S$ requires 76.00 % C, 9.70 % H, 4.06 % S; Found 76 % C, 9.70 % H, 4.06 % S.

Reaction conditions were optimised to achieve high yield as shown in Table 1. 4 below:

Sample	**Reaction Conditions**	**Yield %**	**EA expected**: **C** 74.96 %, **H** 9.37 %, **S** 3.92 %
12a	50 ^{o}C, methanol: THF (2: 3);	55 %	N/ A
12b	2 x SM, RT, methanol: THF (1: 2);	81.8 %	N/ A
12c	4 x SM, RT, methanol: THF (1: 2);	62.5 %	**C** 76.00 %, **H** 9.70 %, **S** 4.06 %
12d	8 x SM, RT, methanol: chloroform (1: 2);	71 %	**C** 76.09 %, **H** 9.43 %, **S** 3.82 %
12e	6 x SM, RT, methanol: chloroform (3: 4);	73.5 %	**C** 76.09 %, **H** 9.43 %, **S** 3.82 %
12f	20 x SM, RT, methanol: chloroform (3: 2);	82.3 %	**C** 75.93 %, **H** 9.59 %, **S** 3.89 %

Table 1. 4. Optimised reaction condition for compound 17 synthesis.

All reaction yields are between 55 - 85 % with elemental analysis determined within the error range and ^{1}H NMR was compared. Due to lack of product in the reaction leading to **12a** and **12b**, elemental analysis was not performed. Compound **12d** showed a transition temperature (^{o}C): N 64.9 ^{o}C Iso. Compound **12e** was characterised by MS *m/z*: 775 (M^{+}), 776 (M^{+}+1) and transition temperatures (^{o}C): N 63.8 ^{o}C Iso. Compound **12f** was characterised by MS *m/z*: 797 (M^{+}+Na^{+}), purity (HPLC): > 95 %, purity (GPC): > 95 %, and transition temperatures (^{o}C): N 63 ^{o}C Iso.

1. 6.5 Thiolated Mesogens Synthesis Route 3

1. 6.5.1 2-((11-(acetylthio)undecyl)oxy)-4-(octyloxy) benzoic acid (23)

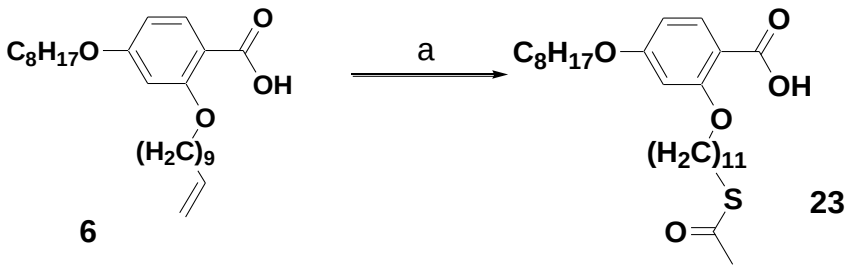

a...(i) AIBN, CH_3COSH and dry THF

In experiment **23**, the method used in experiments **22** to synthesise thioester was used to explore whether it could be extended to molecules with other functional group such as –COOH functions with another molecule. On the other hand, this is also part of an on-going scheme 1.6 to synthesis the final thiol mesogen *via* a different direction.

Thioactic acid (97%, 0.44 ml, 0.5 mmol) was introduced to a stirred mixture of compound **6** (0.1047 g, 0.25 mmol) and purified AIBN (Fisher laboratory reagent grade, 42 mg, 0.25mmol) in dry THF (4 ml) under nitrogen. This final mixture was heated at 60 ^oC for 3 hrs. The reaction was monitored by TLC until disappearance of starting material, and the final reaction mixture solvents were evaporated before preparative TLC (DCM / hexane, 3.5 / 6.5). However due to insufficient amount of sample, only NMR analysis was carried out. ^1H NMR 400 MHz ($CDCl_3$): δ [ppm] = 0.88 (t, 3H, CH_3), 1.42 (m, 22H, CH_2), 1.50 (m, 4H, 2xOCH_2-$\underline{CH_2}$), 1.82 (s, 2H, CH_2-$\underline{CH_2}S$), 2.83 (s, 3H, $\underline{CH_3}COS$), 4.04 (m, 4H, 2xOCH_2), 6.81 (m, 2H, CH_{arom}), 8.15 (d, 1H, CH_{arom}), 10.99 (broad, 1H).[79]

1. 6.6 Synthesis of Other Compounds

1. 6.6.1 4’-(4-octyloxyphenylcarbonyloxy)biphen-4-yl 4-octyloxy-2-((11-(acetylthio)undecyl)oxy)benzoate (26)

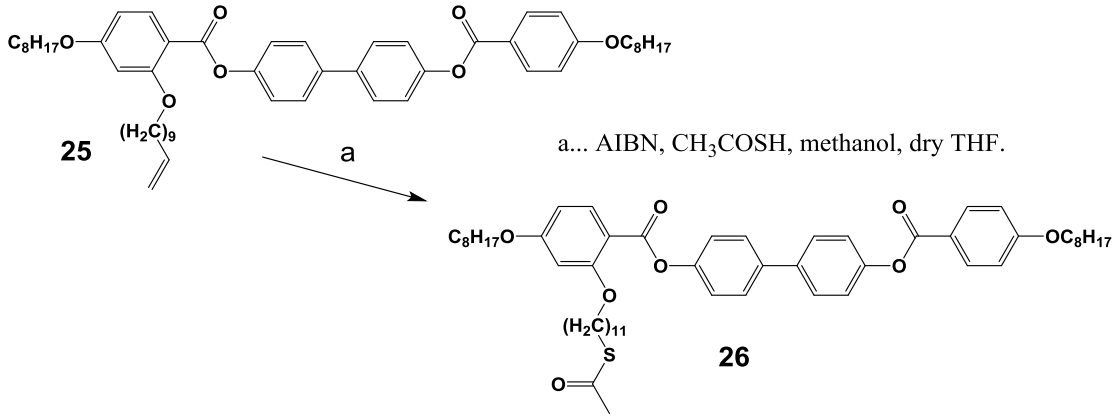

Thioacetic acid (97%, 0.17 ml, 2 mmol) was introduced to a stirred mixture of 4’-(4-octyloxybenzoyloxy)biphenyl-4-yl 4-octyloxy-2-(undec-10-en-1-yloxy) benzoate (**25**, available in the laboratory, 0.8192 g, 1 mmol) and AIBN (197 mg, 1 mmol) in dry chloroform (20 ml) under nitrogen. This mixture was heated at 60 ^{o}C for 6 h. Finally a small portion of AIBN (~ 5 mg) was added to this mixture and heated for another 4 h. The reaction was monitored by TLC until disappearance of the starting material. Solvents were evaporated under reduced pressure before column chromatography (DCM / hexane, 4 / 6), yielded a light yellow solid (0.358 g, 40 %). ^{1}H NMR 400 MHz ($CDCl_3$): δ [ppm] = 0.88 (t, 6H, CH_3), 1.30 (m, 28H, CH_2), 1.40 (m, 6H, 3xOCH_2CH_2-$\underline{CH_2}$), 1.82 (m, 8H, 3xOCH_2-$\underline{CH_2}$ and $\underline{CH_2}$-CH_2S), 2.29 (s, 3H, $SCOCH_3$), 4.03 (m, 6H, 3xOCH_2), 6.54 (m, 2H, CH_{arom}), 6.98 (d, 2H, CH_{arom}), 7.26 (d, 4H, CH_{arom}), 7.61 (d, 4H, CH_{arom}), 8.05 (d, 1H, CH_{arom}), 8.16 (d, 2H, CH_{arom}).

1. 6.6.2 4’-(4-octyloxyphenylcarbonyloxy)biphen-4-yl 4-octyloxy-2-(11-mercaptoundecyloxy)benzoate (27)

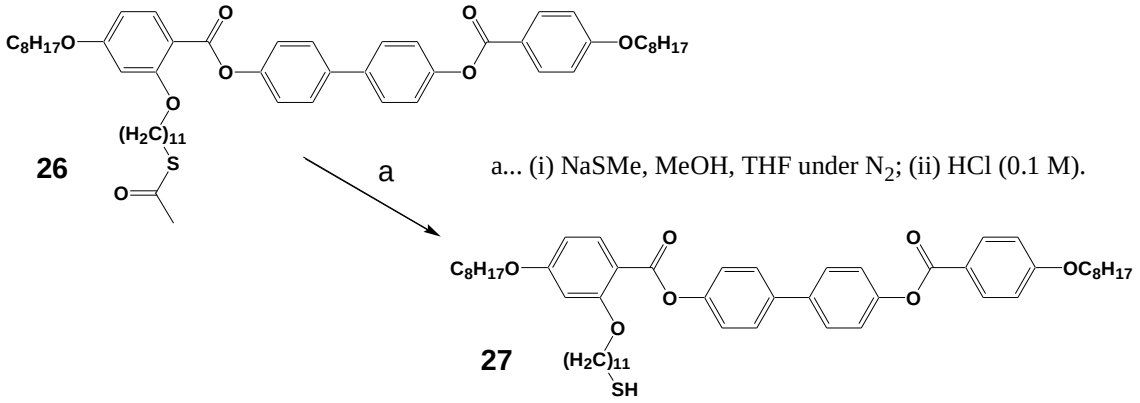

Method 1

NaSMe (74 mg, 1.06 mmol) was dissolved in a minimum amount of MeOH, and this solution was added drop-wise into a mixture of compound **26** (72.3 mg, 0.089 mmol) dissolved in methanol (3 ml) and THF (1 ml) under nitrogen at 45 ^{o}C. The final reaction mixture was heated at 45 ^{o}C for 30 min, and it was completed by stirring at r.t. for 18 h. The reaction was monitored by TLC. HCl (0.1 M, 2 ml) and DCM (4 ml) was added, the organic layer was washed with water (2 x 4 ml) and brine (2 x 4 ml). The organic layer was dried over $MgSO_4$ and solvents were distilled off. A light yellow solid (0.0233 mg, 34%) was isolated by a prep-TLC. ^{1}H NMR 400 MHz ($CDCl_3$): δ [ppm] = 0.89 (t, 6H, CH_3), 1.30 (m, 37H, CH_2 and SH), 1.87 (m, 6 H, 3xOCH_2-$\underline{CH_2}$), 2.48 (quart, 2H, $\underline{CH_2}$-SH), 4.03 (m, 6H, 3xOCH_2), 6.54 (m, 2H, CH_{arom}), 6.98 (d, 2H, CH_{arom}), 7.26 (d, 4H, CH_{arom}), 7.61 (d, 4H, CH_{arom}), 8.05 (d, 1H, CH_{arom}), 8.16 (d, 2H, CH_{arom}).

Method 2

$NaSC(Me)_3$ (74 mg, 1.056 mmol) was dissolved in a minimum of MeOH, and this solution was added drop-wise to a mixture of compound **26** (72.3 mg, 0.089 mmol) dissolved in methanol (3 ml) and THF (1 ml) under nitrogen at 45 ^{o}C. The reaction mixture was heated at 45 ^{o}C for 30 min, and the reaction was completed by stirring at RT for 18 h. The reaction was monitored by TLC. HCl (0.1 M, 2 ml) and DCM (4 ml) was added, the organic layer was washed by water (2 x 4 ml) and brine (2 x 4 ml). The organic layer was dried over $MgSO_4$ and solvents were distilled off under reduced pressure. However the final product was unable to obtain via column chromatography.

1. 6.6.3 4’-Hydroxy-biphenyl-4-yl 4-octyloxybenzoate (42)

a... (i) *N,N*-dimethylaminopyridine, *N,N'*-cyclohexylcarbodiimide and dry THF, 18h;
(ii) hot ethanol under reflux.

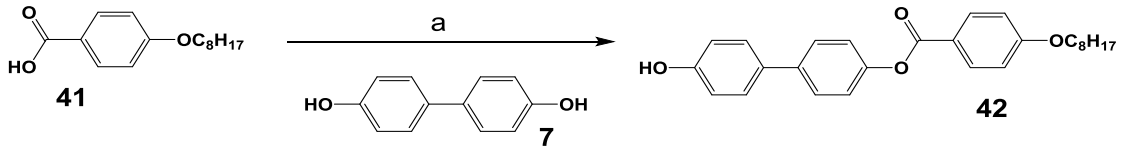

4-octyloxybenzoic acid (**41**, 5 g, 0.02 mol), 4,4’-dihydroxybiphenyl (**7**, 8 g, 0.043 mol) and *N,N*-dimethylaminopyridine (DMAP, 0.6 g, 4.92 mmol) were dissolved in dry THF (112 ml) and was stirred for up to 2 h until the all reagents dissolved, followed by adding *N,N’*-cyclohexylcarbodiimide (DCC, 5 g, 0.0239 mol). After stirring 18 h at r.t, the reaction mixture was filtered, the filtrate was washed with DCM and the solvent was distilled off under reduced pressure. The final residue was dissolved in hot ethanol under reflux and after cooling to r.t, the suspension was filtered. The residue was dissolved in a hot solution of hexane/DCM/THF (2/2/1) and after cooling to RT, the residue was filtered off, followed by repeated recrystallization to yield a pure white product (3.60 g, 43.1%). ^{1}H NMR 400 MHz ($CDCl_3$): δ [ppm] = 0.89 (t, 3H, CH_3), 1.33 (m, 8H, CH_2), 1.47 (m, 2H, $\underline{CH_2}$-CH_2CH_2O), 1.84 (quint, 2H, $\underline{CH_2}$-CH_2O), 4.05 (t, 2H, CH_3), 6.87 (d, 2H, CH_{arom}), 6.99 (d, 2H, CH_{arom}), 7.25 (d, 2H, CH_{arom}), 7.50 (dd, 4H, CH_{arom}), 8.11 (d, 2H, CH_{arom}). Elemental analysis: calculated (%) for $C_{27}H_{30}O_4$ requires C 77.48 %, H 7.23 %; Found C 77.21 %, H 7.45 %.

1. 7 References

1. H. Kelker and P. M. Knoll, *Liq. Cryst.*, 1989, 5, 19-42.
2. H. Virchow, *Virchows Arch. path. Anat. Physiol*, 1853, 571.
3. R. Heintz, *J. Prakt. Chem.*, 1855, 66, 1.
4. P. J. Stackhouse, PhD thesis, PhD thesis "The Design, Synthesis and Mesomorphic Properties of Discotic Liquid Crystals", Hull, 2008.
5. F. Reinitzer, *Liq. Cryst.*, 1989, 5, 7-18.
6. F. Reinitzer, *Monatsch*, 1888, 9, 421-441.
7. K. M. Fergusson, PhD thesis, PhD thesis "The Synthesis and Properties of Achiral and Chiral Bent-core Liquid Crystals", Hull, 2008.
8. H. Stegemeyer, *Liquid Crystals*, Darmstadt: Steinkopff; New York: Springer, Darmstadt and New York, 1994.
9. H. Kawamoto, *Proc. IEEE*, 2002, 90, 460-500.
10. I. Dierking, *Textures of Liquid Crystals*, Wiley-VCH Verlag GmbH & Co. KGaA, 2003.
11. O. Lehmann, *Zeitschrift für Physikalische Chemie*, 1889, 4, 462-467.
12. D. Demus, Goodby, J. W., Gray, G. W., Spiess, H. W., and Vill, V., *Gray, G. W. in Physical Properties of Liquid Crystals*, Wiley-VCH, Weinheim, 1999.
13. T. J. Sluckin, Dunmur, D. A. and Stegemeyer, H., ed., *Crystals that Flow*, Taylor and Francis, London & New York, 2004.
14. V. Vill, *Liq. Cryst.*, 1988, 24, 21-24.
15. J. Billard, *Liq. Cryst.*, 1998, 24, 99-103.
16. S. Laschat, A. Baro, N. Steinke, F. Giesselmann, C. Hagele, G. Scalia, R. Judele, E. Kapatsina, S. Sauer, A. Schreivogel and M. Tosoni, *Angew. Chem.-Int. Edit.*, 2007, 46, 4832-4887.
17. G. Friedel, *Annales de Physique*, 1922, 18, 273-474.
18. P. J. Collings and M. Hird, *Introduction to Liquid Crystals*, Taylor & Francis Ltd, UK Taylor & Francis Ltd, 1 Gunpowder Square, London EA4A 3DE, USA Taylor & Francis Inc., 325 Chestnut Street, 8th Floor, Philadelphia, PA 19106, 1997.
19. M. Baron, *Pure Appl. Chem.*, 2001, 73, 845-895.
20. M. a. F. de Broglie, E., *Comptes rendus de l'Académie des Sciences*, 1923, 176, 738-740.
21. G. W. Gray, K. J. Harrison and J. A. Nash, *Electron. Lett.*, 1973, 9, 130-131.
22. G. W. Gray and D. G. McDonnell, *Electron. Lett.*, 1975, 11, 556-557.
23. S. Chandrasekhar, *Liquid Crystals*, Cambridge University Press, 1992.
24. J. W. Lee, X. L. Piao, Y. K. Yun, J. I. Jin, Y. S. Kang and W. C. Zin, *Liq. Cryst.*, 1999, 26, 1671-1685.
25. X. B. Zeng, G. Ungar, Y. S. Liu, V. Percec, S. E. Dulcey and J. K. Hobbs, *Nature*, 2004, 428, 157-160.
26. J. W. Goodby, *Liq. Cryst.*, 1998, 24, 25-38.
27. D. Demus, J. W. Goodby, G. W. Gray, H. W. Spiess and V. Vill, Wiley-VCH, 1998, vol. 1.
28. C. Tschierske, *Nature*, 2002, 419, 681-+.
29. R. S. Werbowyj and D. G. Gray, *Molecular Crystals and Liquid Crystals*, 1976, 34, 97-103.
30. A. A. Collyer, *Liquid Crystal Polymers: From Structures to Applications*, Elsevier Science Publisheers Ltd, 1992.
31. J. A. Rego, J. A. A. Harvey, A. L. MacKinnon and E. Gatdula, *Liq. Cryst.*, 2010, 37, 37-43.

32. J. A. Castellano, *Liquid Gold: The Story of Liquid Crystal Displays and the Creation of an Industry*, World Scientific Publishing, London, 2005.
33. W. Gordon, in *Introduction to Liquid Crystals*, Case Western Reserve University Cleveland, USA., 2004, ch. 2004.
34. K. D. Dorkenoo, E. Sungur, H. Bulou, G. Taupier and A. Boeglin, in *Advanced Elastomers - Technology, Properties and Applications*, ed. A. Boczkowska, InTech, 2012, DOI: 10.5772/2784, ch. 2.
35. P. Yeh and C. Gu, *Optics of Liquid Crystal Displays*, John Wiley & Sons, Inc., Wiley, 1999.
36. F. Reinitzer, *Monatshefte für Chemie*, 1988, 9, 421-441.
37. J. W. Goodby, *J. Mater. Chem.*, 1991, 1, 307-318.
38. P. C. D. Robinson, M. W., Nikon, Florida, USA., 2000 - 2013.
39. C. S. B. Xiang, A. R., Connexions, Rice, USA., 2011, ch. 17/05/2011.
40. C. W. R. University, Case Western Reserve University, read in 2013.
41. V. A. Bershtein and V. M. Egorov, *Differential Scanning Calorimetry of Polymers - Physics, Chemistry, Analysis, Technology*, Ellis Horwood Limited, Warwick, 1994.
42. K. E. Van Holde, W. C. Johnson and H. P. S, *Principles of Physical Biochemistry: Thermodynamics and biochemistry*, USA: Pearson Prentice Hall, Upper Saddle River, NJ, 2nd edn., 2006.
43. A. Cooper, Nutley, M.A., Walood, A., in *Protein-Ligand Interactions: Hydrodynamics and Calorimetry*, ed. S. E. Harding, Chowdhry, B.Z, UK: Oxford University Press, Oxford, 2000, pp. 287-318.
44. P. M. Gill, T. T. Ranjbar, B., *Journal of Biomolecular Techniques*, 2010, 21, 167 - 193.
45. Colby-College-Staff, Chemistry Department, Colby College . Colby College, 5750 Mayflower Hill, Waterville, ME 04901, 30/03/2007 edn., 2007.
46. A. Cooper, *Biophys. Chem.*, 2000, 85, 25-39.
47. A. B. Travers, M., *DNA-Protein Interactions*, Oxford University Press, Oxford, UK., 2000.
48. A. Cooper, C. M. Johnson, J. H. Lakey and M. Nollmann, *Biophys. Chem.*, 2001, 93, 215-230.
49. A. Cooper, *Biophysical Chemistry*, Royal Society of Chemistry, London, UK., 2004.
50. D. W. Bruce, British Liquid Crystal Society Winter Workshop, University of Hull, 2012.
51. C. Tschierske, *J. Mater. Chem.*, 2001, 11, 2647-2671.
52. *Handbook of Liquid Crystals*, Wiley-VCH: New York, New York, 1998.
53. J. W. Goodby, *Chem. Soc. Rev.*, 2007, 36, 1855-1856.
54. M. I. Stockman, *Phys. Today*, 2011, 64, 39-44.
55. U. Kreibig and M. Vollmer, *Optical Properties of Metal Clusters*, Springer, 1995.
56. J. N. Anker, W. P. Hall, O. Lyandres, N. C. Shah, J. Zhao and R. P. Van Duyne, *Nat. Mater.*, 2008, 7, 442-453.
57. H. A. Atwater and A. Polman, *Nat. Mater.*, 2010, 9, 205-213.
58. S. Lal, S. E. Clare and N. J. Halas, *Accounts Chem. Res.*, 2008, 41, 1842-1851.
59. Y. M. Liu and X. Zhang, *Chem. Soc. Rev.*, 2011, 40, 2494-2507.
60. W. Cai and V. Shalaev, *Optical Metamaterials: Fundamentals and Applications Introduction*, Springer, 2010.
61. C. M. Soukoulis and M. Wegener, *Nat. Photonics*, 2011, 5, 523-530.

62. J. A. Fan, C. H. Wu, K. Bao, J. M. Bao, R. Bardhan, N. J. Halas, V. N. Manoharan, P. Nordlander, G. Shvets and F. Capasso, *Science*, 2010, 328, 1135-1138.
63. S. C. Glotzer and M. J. Solomon, *Nat. Mater.*, 2007, 6, 557-562.
64. A. Guerrero-Martinez, M. Grzelczak and L. M. Liz-Marzan, *ACS Nano*, 2012, 6, 3655-3662.
65. Z. H. Nie, A. Petukhova and E. Kumacheva, *Nat. Nanotechnol.*, 2010, 5, 15-25.
66. K. Kanie, M. Matsubara, X. B. Zeng, F. Liu, G. Ungar, H. Nakamura and A. Muramatsu, *J. Am. Chem. Soc.*, 2012, 134, 808-811.
67. M. Wojcik, W. Lewandowski, J. Matraszek, J. Mieczkowski, J. Borysiuk, D. Pociecha and E. Gorecka, *Angew. Chem.-Int. Edit.*, 2009, 48, 5167-5169.
68. M. Wojcik, M. Kolpaczynska, D. Pociecha, J. Mieczkowski and E. Gorecka, *Soft Matter*, 2010, 6, 5397-5400.
69. M. Draper, I. M. Saez, S. J. Cowling, P. Gai, B. Heinrich, B. Donnio, D. Guillon and J. W. Goodby, *Adv. Funct. Mater.*, 2011, 21, 1260-1278.
70. L. Cseh and G. H. Mehl, *J. Am. Chem. Soc.*, 2006, 128, 13376-13377.
71. L. Cseh and G. H. Mehl, *J. Mater. Chem.*, 2007, 17, 311-315.
72. X. B. Zeng, F. Liu, A. G. Fowler, G. Ungar, L. Cseh, G. H. Mehl and J. E. Macdonald, *Adv. Mater.*, 2009, 21, 1746-+.
73. C. H. Yu, C. P. J. Schubert, C. Welch, B. J. Tang, M. G. Tamba and G. H. Mehl, *J. Am. Chem. Soc.*, 2012, 134, 5076-5079.
74. X. B. Mang, X. B. Zeng, B. J. Tang, F. Liu, G. Ungar, R. B. Zhang, L. Cseh and G. H. Mehl, *J. Mater. Chem.*, 2012, 22, 11101-11106.
75. S. Diez, D. A. Dunmur, M. R. De la Fuente, P. K. Karahaliou, G. Mehl, T. Meyer, M. A. P. Jubindo and D. J. Photinos, *Liq. Cryst.*, 2003, 30, 1021-1030.
76. L. Cseh and G. H. Mehl, *J. Am. Chem. Soc.*, 2006, 128, 13376-13377. Supporting information.
77. B. Hache and Y. Gareau, *Tetrahedron Lett.*, 1994, 35, 1837-1840.
78. P. Kumar and K. C. Gupta, *Chem. Lett.*, 1996, 635-636.
79. Y. Y. Luk, N. L. Abbott, J. N. Crain and F. J. Himpsel, *J. Chem. Phys.*, 2004, 120, 10792-10798.
80. C. Palegrosdemange, E. S. Simon, K. L. Prime and G. M. Whitesides, *J. Am. Chem. Soc.*, 1991, 113, 12-20.
81. B. T. Holmes and A. W. Snow, *Tetrahedron*, 2005, 61, 12339-12342.
82. O. B. Wallace and D. M. Springer, *Tetrahedron Lett.*, 1998, 39, 2693-2694.
83. N. Miyaura and A. Suzuki, *Chem. Rev.*, 1995, 95, 2457-2483.
84. C. K. Jin, H. J. Jeong, M. K. Kim, J. Y. Kim, Y. J. Yoon and S. G. Lee, *Synlett*, 2001, 1956-1958.

Chapter Two

Liquid Crystal Gold Nanoparticles

2. 1 Introduction

2. 1.1 Nanotechnology

Nanotechnology is the field of study related to micromanipulation of nanostructure properties at dimensions between 1 and 100 nm. How small is one nanometre? The typical width of a human hair is 50 µm. One nanometre is 100,000th of a hair width. The preparation and characterisation of materials consisting of building blocks have dimensions in the order of only a few nanometres have the potential for many interesting and unique properties in miniaturising technologies. One logical way to condense enhanced functionalities into smaller spaces would of course be to use nanostructured materials. Over the last two decades, a considerable amount of effort has been spent in a number of different research areas, such as engineering, physics, chemistry, materials science and molecular biology. Nano-science has excited and concerned many scientists because it is on the verge of many innovative advances, such as a multitude of applications in areas of technology, manufacturing and medicine.

In materials research, development work is driven by the desire to create novel materials with improved strength, electrical or mechanical properties. Materials exhibit novel properties that are significantly improved by architecting structures with functional materials at atomic or molecular scale to construct nanomaterial. It gives rise to perform highly complex and more efficient tasks. Nanoscale objects often display physical attributes substantially different from those displayed by either atoms or bulk materials. This makes them excellent candidates for a large number of potential applications, for example, sensors, fuel cells, emulsion stabilisers, electronic optical displays, efficient energy storage materials, strong – lightweight building materials and biological bones or tissues. Many people may have understood nanotechnology as a process of ultra-miniaturization and in theory changes in quantity result in changes in quality. However device size shrinkage may lead to a change in operation principle due to quantum effects, which is the basic principle of physics for motion and interaction of electrons in atoms. Phenomena at the nanometre scale are likely to form a completely new world and nanotechnology can provide an unprecedented understanding of materials and devices and is likely to impact many fields. Many new properties of matter at the nanoscale are different to those observed at larger scales. Behaviour changes are caused not only by

continuous modification of characteristics with diminishing size, but also by the emergence of totally new phenomena such as quantum confinement, a typical example of which is that the colour of light emitted from semiconductor nanoparticles depends on their sizes. Nanomaterials also give a higher degree of miniaturization for circuits, storage media and transistors, which is highly sought after in computer technology in the electronics industry. Self-assembled linear molecule monolayers in an ordered array on a substrate surface can function as a new generation of chemical and biological sensors. Computer storage and operation capacity can be improved by a factor of a million by switching devices and functional units at nanoscale. Entirely new biological sensors facilitate early diagnostics and disease prevention of cancers. Nanostructured ceramics and metals have greatly improved mechanical properties, both in ductility and strength. Nanodevices which are capable of mimicking the complex mechanisms of nature could also be produced. For example, mechanical robot body parts that function the same as human body parts, or liposomes for efficient and selective drug delivery. The performance of existing chemicals and materials can be greatly expanded by using structure at nanoscale as a tuneable physical variable. All natural materials and systems establish their foundation at the nanoscale; the fundamental properties, phenomena and processes of matter can be tailored by controlling matter at atomic or molecular levels where basic properties are initiated. Nanotechnology could impact all production of human-made objects – from electronics to advanced diagnostics, surgery, advanced medicines and tissue and bone replacements. However, the challenges are to understand the interaction among atoms and molecules, how to keep them stable, how to examine them, how to produce nanomaterials that possess uniform and precisely determined properties in a large and financially viable scale.

Perhaps an acceptable definition of a nanoparticle can be given as follows. Nanoparticles are discrete particles with at least one characteristic dimension in the size of nanometres (nm). More than 200,000 nanoparticles (2 – 5 nm size) would fit onto a head of a pin. As small as one nanometre is, it is one-billionth of a meter and a hundred-thousandth the width of a human hair, and it is still larger when compared at atomic scale. A typical gold atom has a diameter of about 0.3 nm and they are assembled into nanoparticles, typically in the range of ~ 1 – 100 nanometres.[1] At this scale, they show electronic, physical and chemical properties that are often substantially and sometimes radically different from their constituents or bulk counterparts. In addition to the material composition, the size

and shape are two other important factors that determine properties of a nanoparticle. For instance, some materials display unique and interesting properties when they are scaled down which are not apparent in the bulk or even on the micron scale, such as catalysis. It is well-established that the activity of a metal nanoparticle can be most sensitive to the packing of atoms on the surface or the exposed facets of a nanoparticle,[2-5] the high ratio of surface to volume of the nanoparticles influences the physical and chemical properties, which are particularly sensitive to the surface structure of the material; the actual size of the nanoparticles is smaller than the Bohr radius[6] of the bulk-exciton (hole-electron pair),[7] giving rise to a blue shift of the absorption edge and the band gap due to quantum confinement as the particle size decreases,[6, 8] hence the wavelength of the emitted light produced by recombination of electrons and holes across the band gap can be tuned according to the physical size of the nanoparticles. Physicists predicted that nanoparticles in the diameter range 1 – 10 nm (intermediate between the size of small molecules and that of bulk metal) would display electronic structures, reflecting the electronic band structure of the nanoparticles, owing to quantum-mechanical rules.[7] The resulting physical properties are neither those of bulk metal nor those of molecular compounds, but they strongly depend on the particle size, inter-particle distance, nature of the protecting organic shell, and shape of the nanoparticles.[9-11] Furthermore, recent theoretical studies suggest that such systems could provide the materials base for metamaterials, with interesting properties including a negative refractive index.[12-16] This is in contrast to earlier work on metamaterials which focused more on top-down approaches.[17-19] Critically, theoretical studies have shown that in order to obtain negative dielectric permittivity the self-assembling particles can be much smaller than the wavelength of visible light. However, careful control of spatial assembly and distance, *i.e.* the long range ordering of particles forming bulk lattices is required. Within these parameters metallic nanoparticles, specifically gold nanoparticles are prime candidates due to their high stability and plasmonic resonance effects. In this part of thesis, how to determine these nanoparticles with other additional phenomenal properties, such as mesogenic groups and hydrocarbon chains involvement will be discussed, especially focus on the synthesis of 2 – 5 nm gold nanoparticles and aiming to obtain the final organic-inorganic composite materials – liquid crystal gold nanoparticles via exchange reaction and self-assembly methods.

2. 1.2 Gold Nanoparticles

Although gold nanoparticles are generally considered an invention of modern science, the investigation of gold is also the subject of one of the most ancient themes of investigation in science, and the renaissance of improved technology for the facile synthesis of thermally and air-stable gold nanoparticles of reduced dispersity and controlled size has led to an exponentially increasing number of publications. Gold nanoparticles are the most stable metal nanoparticles, and they present fascinating aspects such as their assembly of multiple types involving materials science, the behaviour of the individual particles, size-related electronic, magnetic and optical properties (quantum size effect), and their applications to catalysis and biology. Their promise is in these fields as well as in the bottom-up approach of nanotechnology, and they will be key materials and building block in the 21st century.

Dating back to the ancient time, the extraction of gold started in the 5th BC near Varna (Bulgaria) and reached 10 tons per year in Egypt around 1200 – 1300 BC when the marvellous mask of Tutankhamun was constructed. It is probable that "soluble" gold appeared around the 5th or 4th century BC in Egypt and China. In antiquity, materials were used for both aesthetic and curative purposes. Gold nanoparticles were used to generate ruby glass for colouring ceramics and resist oxidation, these applications are even still continuing now. Perhaps the most famous example is the Lycurgus Cup manufactured in the 4th century AD: it exhibits an outstanding green-red dichroism in reflected and transmitted light (Figure 2. 1).

Figure 2. 1. The Lycurgus Cup in reflected a) and transmitted b) light.[20]

During Roman time, gold and silver were added when the glass was molten to give colour, which was caused by the fine dispersion of silver-gold nanoparticles that were reduced during heat-treatment of the glass. In the last two centuries, various methods for the preparation of gold nanoparticles were reported and reviewed. Colloidal gold has fascinated people for centuries. It provided colour for medieval cathedral windows and until the eighteenth century was believed to have life prolonging and rejuvenating benefits if taken internally as *aurum potabilis*.[21] Faraday[22] reported that reduction of gold chloride with phosphorus resulted in the formation of deep red colloidal solutions of gold in 1857, he proposed that microscopic particles of gold are responsible for the beautiful coloration of the famed ruby-gold decorative glasses. In our times, there has been an exponential growth in the exploitation of colloidal gold for biological labels, markers and stains for various microscopies.[23] More recently, metallic nanoparticles and nanostructures have been fruitfully employed as molecular-recognition elements and amplifiers in sensors and biosensors, in addition to serving as components in nanoscale optical devices.[11] The inspiration of these recent and significant developments dates back to 1908, when Gustav Mie explained the phenomenon quantitatively as arising from a collective oscillation of the conduction electrons confined in these particles.[24] This collective oscillation is widely known as the surface-plasmon resonance, and it is one of the most fundamental optical excitations for metals. Metallic nanoparticles, especially the gold metals, have mainly been studied because of their strong optical absorption in the visible region.

Since Faraday's work, several methodologies have been developed for the synthesis of gold nanoparticles. The syntheses are usually based on stabilisation of previously reduced gold from a soluble gold salt ($HAuCl_4 \cdot 3H_2O$) with a suitable capping agent. Turkevich reported the way to obtain gold nanoparticles (AuNPs) in the size range of 10-150 nanometres by stabilising them in water by citrate in 1951,[25] but further increasing the particle size resulted a broad polydispersity. In 1994, Brust and co-worker published the first biphasic method using 1-dodecanethiol as a strong binding agent. This allowed one to obtain 2 nanometres size particles. The gold salts are transferred to the organic phase by tetraoctylammonium bromide (TOAB) and are then reduced by a sodium borohydride in the presence of thiols, as illustrated in the reaction equations below.

$$AuCl_4^-(aq) + N(C_8H_{17})_4^+(C_6H_5Me) \rightarrow N(C_8H_{17})_4^+AuCl_4^-(C_6H_5Me)$$

$$mAuCl_4^-(C_6H_5Me) + nC_{12}H_{25}SH + 3me^- \rightarrow 4mCl^-(aq) + [Au_m(C_{12}H_{25}SH)_n](C_6H_5Me)$$

Brust also extended this synthesis in 1995 to *p*-mercaptophenol AuNPs in a single phase. After the breakthrough for the facile synthesis of thermally- and air-stable AuNPs with reduced dispersity and controlled size by Brust. The fabrication of nano-devices with novel structures and functionalities[26-29] were able to be explored by scientists. Astruc [11] published a general review on AuNPs and their applications few years ago, which was followed with many other general publications,[10, 30-32] reviews[9, 33, 34] and a book[35] on NPs and their applications.[36-42]

A wide majority of other sulphur ligands have been used to stabilize AuNPs, such as xanthates[43] and disulphides,[44-46] di-[47] and trithiols,[48] and resorcinarene tetrathiols.[49-51] However, when compared with thiols, other stabilising agents such as disulfides are not good stabilisers[47-49] and thioethers do not bind AuNPs strongly.[52] Non-sulfur ligands such as phosphine,[53] phosphine oxide,[54] amine,[55] isocyanide,[56] acetone[57] and iodine[58] have also been reported to stabilize AuNPs.

In this work, efforts are mainly focused on the synthesis and characterisation of thiol ligand stabilised gold nanoparticles. The particles of interest are typically in the size range 1 – 5 nm. Chemical and physical properties of colloidal systems containing AuNPs have been intensively investigated in recent years. Fluorescence of molecules, for instance, can be strongly influenced by the presence of AuNPs. In fact they can enhance or quench molecular luminescent emission, depending on the particles' Plasmon resonance and on the molecule-nanoparticles separation.[59] AuNPs can also modify the linear and nonlinear absorption of a material, due to the electromagnetic interaction between the nanoparticles and the molecules in their vicinity. By exploiting these interactions it is possible to develop biological sensors and optical limiting devices.[60, 61] The spectroscopic properties of colloids containing AuNPs conjugated to monoclonal anti-epidermal growth factor receptor (anti-EGFR) were also employed for cancer diagnosis.[62] Similar electromagnetic interactions are responsible for the large enhancement in nonlinear refractive index observed for nanocomposite materials containing AuNPs.[63, 64]

One of the reasons for the popularity of gold is that it is one of the most stable materials, used as contrast agents in electron microscopy due to its high electron-dense metal presence. Gold nanoparticles also show fascinating aspects, such as their multiple types of assembly involved in materials science. The behaviour of the individual particles is size-related electronic, magnetic and optical properties (quantum size effect), and their

applications to catalysis and biology. AuNPs also exhibit a strong absorption band in the visible region which is indeed a particle effect since it is absent in the individual atom as well as in the bulk. This absorption is due a resonance of the electromagnetic field with the collective oscillation of the conduction band electrons and is known as the surface Plasmon resonance (SPR).[25] In addition, the resulting physical properties are neither those of bulk metal nor those of molecular compounds, but they strongly depend on the particle size, inter-particle distance, nature of the protecting organic shell, and shape of the nanoparticles. Finally when particles are large, the energy levels merge into the quasi-continuous band structure as for the bulk solid.[25] The optical and other properties become size-dependant for small AuNPs and can be modulated by controlled synthesis conditions. Their promises are in these fields as well as in the bottom-up approach to nanotechnology, and it is this size dependence that makes nanoparticles-based materials so attractive to be the key materials and building block in the 21st century.[10, 11]

2. 1.2.1 Ligand Exchange and Gold Nanoparticles

Monolayer protected gold nanoparticles can be further reacted in ligand-exchange reactions providing the opportunity to vary the ligands and adjust the properties according to experimental need. The advantages of ligand exchange reaction are that they allow one to preserve the average size and size dispersion of the initial particles while adding new features. When compared to direct synthesis, some ligands are often incompatible with the reaction conditions and the core size strongly depends on the applied ligands, limiting the structure and size of the nanoparticles. Additionally, ligand exchange reactions often require a smaller quantity of ligand, which tend to be difficult to synthesise. Nevertheless, some recent work related to direct synthesis with desired functional groups providing 100% of coverage to stabilise gold nanoparticles.[65, 66] This is particularly interesting, as such bi-functional groups enable stable nanoparticles and provided the capability of introducing other properties at the same time. Furthermore, AuNPs with ligand are organic-inorganic hybrids (inorganic gold core and organic thiol ligand shell) that can be easily dispersed in an organic medium which makes them a colloidal suspension, whereas nanoparticles are only soluble in a given solvent.

In ligand-exchange reactions, the size and structure of the nanoparticles remain the same or can be controlled independently of the ligand used. In the exchange step, different agents can be used to replace the original ligands used to stabilise nanoparticles.[66-68]

However, only thiols are considered in this thesis. Mechanistic studies were described extensively by Murray and Hutchison *et al*.[68, 69] Further investigations are also carried out by many other groups exchanging thiols for thiols,[70-72] phosphines for thiols[67, 68, 73] or even dimethylaminopyridine for thiols.[74, 75] One of the important aspects of ligand exchange is the morphology of NPs: they present different sites (terraces, edges and vertices),[69] the reactivity and speed of exchange is different depending on the initial ligand. It takes place more quickly on the edges and vertices, more slowly at the near-edge and interior terrace sites. Although the gold nanoparticles are considered to be spherical in this report. It was also found that the rate of place exchange decreases with the increase of the size of the original ligand in the protecting monolayer or the size of the entering ligand. A complete replacement of the original thiol ligands become impossible, but near 100% replacement can be obtained by increasing the ratio of the incoming ligands.[71] In the case of liquid crystals ligand exchange, it was firstly explored to synthesise monolayer protected gold nanoparticles according to the Brust two phase method, followed by the partial exchange of the original ligands with thiolated mesogens. Slightly larger monolayer protected gold nanoparticles were also prepared by the modified Brust two phase method, followed the same ligand exchange procedures with thiolated mesogens. All liquid crystal properties of those gold nanoparticles were characterised and investigated as shown in the results section.

2. 1.2.2 Surface Plasmonic Resonance

In 1902, an unexplained narrow dark band in the diffracted spectrum of metallic gratings illuminated with polychromatic light was reported by RW Wood.[76] This anomalous phenomenon, referred to as Wood's anomaly was the first documented observation of surface plasmons. These surface-plasmon resonances are actually a small particle effect, since they are absent in the individual atom as well as in their bulk[77] and it was then explained in terms of surface plasmon resonance (SPR) in 1968.[78] Optical excitation of surface plasmons by attenuated total reflection was introduced by Otto,[79] Kretschmann and Raether[80] in the same year. The application of surface plasmon resonance for gas detection and biosensing was later demonstrated in 1983.[81] Since then, surface plasmons have attracted the attention of physicists, chemists, biologists and material scientists for widespread applications in areas such as electronics, optical sensing, biomedicine, data storage and light generation. Remarkable research and development activities were carried out aiming at the realisation of those application during the last three decades. The

significant growth interests in this research field are mainly due to recent developments in nanotechnology, which have generated new insights about control of various properties of nanomaterials that can support surface plasmons for specific applications.[82]

Surface plasmonic resonance (SPR) are coherent oscillations of free electrons at the boundaries between metal and dielectric. In another words, the electric field of incident light can be deposited to collectively excite electrons of a conduction band, with the result being coherent localised plasmon oscillations with a resonant frequency. They are often being categorised into two classes: surface plasmon resonance (SPR) and localised surface plasmon resonance (LSPR). Surface plasmon resonance (SPR) is generally referring to the coherent oscillation of the surface conduction electrons, which is induced by incident electromagnetic field.[83] SPR can be excited on the metallic films, whereas LSPR is excited on metallic nanoparticles.

The oscillating electric field induces coherent charge density oscillation of the surface conduction electrons locally confined to the conductive nanoparticles, when the spherical particle size is much smaller than the wavelength of the incident electromagnetic field. As presented in Figure 2. 2, when the electron cloud is displaced relative to the nuclei, a restoring force arises from Coulomb attraction between electrons and nuclei that results in oscillation of the electron cloud relative to the nuclear framework. Like any driven oscillator system, in the nanoparticle case, a resonance can arise leading to the field amplification both inside and outside the particle. Excitation of LSPR by the electric field of light at an incident wavelength where resonance occurs results in strong light scattering, in the appearance of intense SPR absorption bands and an enhancement of the local electromagnetic fields. Such optical phenomena of frequency generated by light interacts with nanoparticles is known as the localised surface plasmon resonance (LSPR). It can also be understood that LSPR is an optical phenomena generated by a light wave trapped within conductive nanoparticles smaller than the wavelength of light. The phenomenon is a result of the interactions between the incident light and surface electrons in a conduction band.[84] A good example of such phenomenon is the intense red colour of aqueous dispersions of colloidal gold particles, which is a manifestation of LSPR. The frequency of both SPR and LSPR depend on the dielectric constant of the medium,[85] ε_m, resulting in changes in the colour of colloidal gold with the dielectric constant of the solvent or surrounding medium.[86, 87]

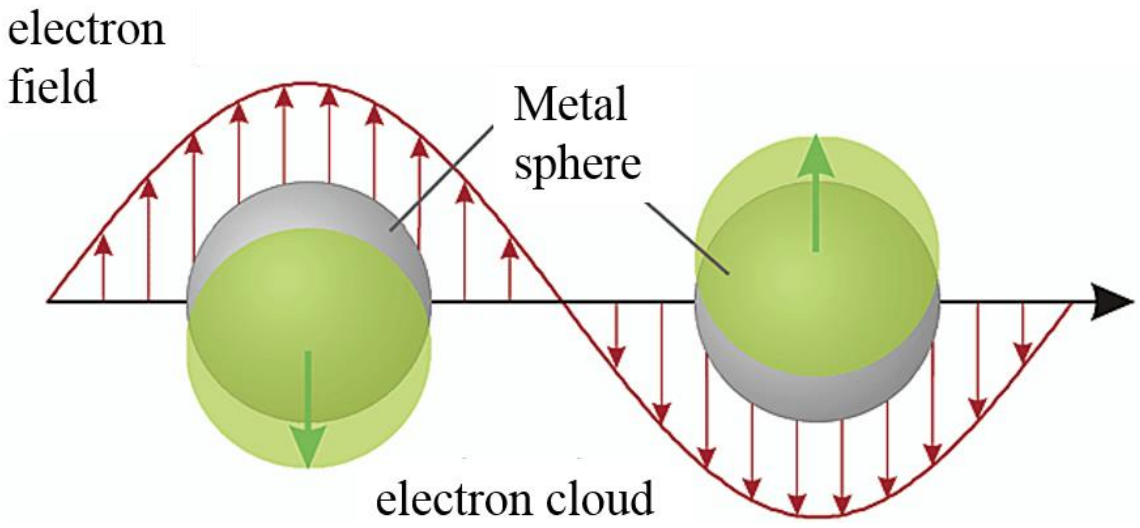

Figure 2. 2. Schematic presentation of Plasmon oscillation for a sphere, showing the displacement of the conduction electron charge cloud relative to the nuclei.[83]

Optical properties of the nanoparticles including the intensity and energy of its surface plasmon bands are strongly correlated to the properties of the nanoparticle.[87] This is mainly because of the LSPR interactions producing coherent localised plasmon oscillations with a resonant frequency that strongly depends on the composition, size, geometry, dielectric environment surrounded and particle-particle separation distance of nanoparticles.[82, 88-94] The frequency and intensity of the LSPR absorption bands are characteristic of the type of material, typically gold, silver or platinum, due to their energy levels of *d-d* transitions exhibit LSPR in the visible range of the spectrum, they are most common noble metal materials used for nanoparticle production.[95] Although, Ag exhibits the sharpest and strongest bands among all metals, Au is preferred for biological applications due to its inert nature and biocompatibility,[96] and thiol-gold association for immobilisation of biomolecules. The extremely intense and highly localised electromagnetic fields induced by LSPR make nanoparticles highly sensitive transducters of small changes in the local refractive index. These changes are exhibited in spectral shifts of extinction (absorption plus elastic light-scattering) and scattering spectra. Many organic molecules binding to nanoparticles would certainly result in a redshift, even they have a relatively high refractive index compared to solvent or air. Both types can induce a strong enhancement of electromagnetic field in the near-field region (resonance amplification), leading to an extensive application in surface-enhanced Raman scattering, fluorescence enhancement, refractive index (RI) measurement, biomolecular interaction detection, metal enhanced fluorescence, plasmon resonance energy transfer and nanoplasmonic molecular rulers.[97-101]

Additionally, LSPR spectra can easily be tuned from the near-UV through the visible spectrum[102] and even into the mid-IR by changing the size or shape of the nanoparticles.[97]

Metal nanoparticles exhibit a strong absorption band in the UV-visible region, which can be assigned to the surface plasmon band of the metal clusters. This allows the estimation of the diameter size of nanoparticle above 2 nm.[103] Increasing the particle size results in redshift of the maximum of the absorption spectra and changes in the plasmon band shape. At particles size of ~ 2 nm almost no plasmon resonance is observed, a weak plasmon band arises and the maxima can be distinguished at ~ 3 nm and a strong absorption band is observed at ~ 6 nm. As there is a clear relationship between extinction coefficient (ε*) and mean particle size.[104] The optical properties of metal nanoparticles all due to the effect of localized surface plasmons. These phenomena occur when light absorption by metallic nanoparticles is the coherent oscillation of the conduction band electrons induced by the interacting electromagnetic field, in this case light.[105] As a result, a strong absorption band appears in some regions of the electromagnetic spectrum, depending on the size of the particle. This plasmon absorption is a small particle effect, which is absent in the individual atoms as well as in the bulk. Even for thin films, at the interface between a metal and a dielectric, the electromagnetic field can couple to the oscillations of conduction electron plasma creating surface plasmon polaritons.[106] When small spherical metallic nanoparticles are placed in an oscillating field of incoming radiation, the electron cloud is driven into oscillations as shown in Figure 2. 2.

2. 1.3 Self-assembly Superstructures

Over the past decade or so, man-made self-assembly of nano-scale metamaterials into superstructure is an area of tremendous interest. There are many approaches developed to fabricate various superstructures. Most of them are organic-nanoparticle superstructures, they have been created to have unique desirable properties not found in natural materials. These include nanoparticle superlattices, which can shape into architectures which mimic the unique structures of natural biomolecules. The coverage of nanoparticles with organic groups not only enhances the processability of such systems, but suitable functional groups are included. They can self-assemble into 1-dimensional (1D), 2-dimensional (2D) and 3-dimensional (3D) well-defined morphologies, regular arrays of nanometre-sized structures that show promise for a range of technology applications, rely on their plasmonic resonance,[105] ranging from optics, catalysis to biomedical research, photovoltaics, memory storage, solar energy conversion, cancer phototherapy, chemical sensing and thermoelectrics aspects.[107-110] The assembly of nanoparticles into periodically ordered superlattices yields a new class of functional materials that not only possess or enhance size related effects, but also manifest collective properties. It has been found that the presence of nanoparticles can alter the dielectric behaviour dramatically and this could potentially result in devices with significantly enhanced switching speeds compared to current systems.[111-113] Assembly of nanoparticles in a controlled fashion also provides a link between "top-down"[114] and "bottom-up"[115] strategies for the construction of functional devices as well as flexible scaffolds for the introduction of chemical functionality. The 'top-down' approach is concerned with the formation of features on the bulk material in a serial parallel manner. However, fabrication of ordered structures with relatively stability are a great challenge, as the 'top-down' approach is rather limited, thus will not be detailed here. The 'bottom-up' approach as the "next technological revolution", such as Brust's two phase method[116] and *Turkevich* method,[117, 118] they are well known common metal nanoparticles synthetic methods used in this field of research, and open a route to nanostructures that is currently inaccessible by conventional lithographic techniques.

The main concern in this field of research is how to correctly place nanocomponents in proximity with one another. As inspired by nature, structures of NPs joining together with astonishing precision towards a wide variety of complex nanostructures, which can be achieved by self-assembly interactions, such as 2D and 3D architecture. In addition, the

"bottom up" approach benefits from having thermodynamic minima in its resulting nanostructures due to the reversible nature of secondary interactions. The focus of nanoscience and nanotechnology is gradually shifting from the synthesis of individual components to their integration into nanostructured materials and solid state devices.[107, 119] Obviously, the challenge is to synthetically create nanostructures with such precision as controlled architectures and specificity as seen in biological systems, which have undergone a million years of evolution, by cleverly incorporating complementary recognition sites in the components at molecular or even atomic level for secondary interactions. This is mainly due to the intrinsic properties of metals, unlike aqueous or organic liquids, metals/alloys normally have high melting temperatures and greatly diminish the effect of electrostatic interactions, making nanoparticles dispersion and assembly in liquid metals an extremely difficult task. This challenge could be solved by using building blocks with well-defined structures, which do not go through significant changes during the build-up of the hybrid systems, and has the possibility for better structure property prediction. Self-assembly is arguably one of the most promising techniques to fulfil this task and evolve large numbers of individual particles of appropriately chosen properties into higher order structures.[120] On the other hand, once the nanoparticles are fabricated the most important and challenging part left is the organisation of nanoparticles at the nanoscale level in an ordered manner for the desired applications. Metal nanoparticles derivatised with alkane thiols, acids or amines could be made to form bulk lattices with long-range order if they were highly monodispersed.[121, 122] The ligand present as a stabiliser on the nanoparticles provides the opportunity for the nanocomponents to interact with each other or target other moieties for the self-assembly process.[123] Since the first report of the three-dimensional (3D) self-assembly of a NC superlattice (also known as super-crystal) by Benton *et al*. in 1989, such a study has been advanced rapidly.[119, 120, 124-127]

The lattices were those expected from packing of spheres into body-centred cubic (bcc) or face-centred cubic (fcc). However, to achieve such unique properties, nanoparticles of narrow or ideally uniform size distribution have to be functionalised with suitable organic groups, and these materials have to be organised and oriented. A prominent strategy involves coating the nanoparticles surface with specifically designed ligands, such as DNA,[128-130] polymers,[131] dendrons[132-134] or small molecular linkers,[135] so as to control their self-assembly. For such systems the soft organic corona surrounding the

nanoparticles helps compensate for variations in size and shape, thus promoting order even when the particles are not highly monodispersed. Furthermore, by tailoring the radial density profile of the corona, *e.g.* by attaching dendrons of a selected profile, one can obtain unconventional superlattices.[136] In a recent work, the attachment of mesogenic dendrons to gold nanoparticles resulted in loss of liquid crystal behaviour, though interestingly, when deposited on surfaces, organisation in layer like structures was detected.[133] Several studies have dealt with the influence of the birefringence of nematic liquid crystals on plasmonic resonances and demonstrated the splitting of the plasmon resonance of isotropic nanoparticles.[137-143]

Synthesis of dendrimer gold nanoparticles can be carried out by stabilising or encapsulating the gold nanoparticles in new "clicked" dendrimers of generation zero to two (G0 – G2) containing tri- and tetra-ethyleneglycol tether (as presented in Figure 2. 3).[144, 145] In first case, the gold nanoparticles are bigger than the Dendron, ~ 4.1 nm and cannot be encapsulated. In the second case, the gold nanoparticles are smaller ~ 1.9 nm, than the higher generation dendrimer, which are able to encapsulate them.

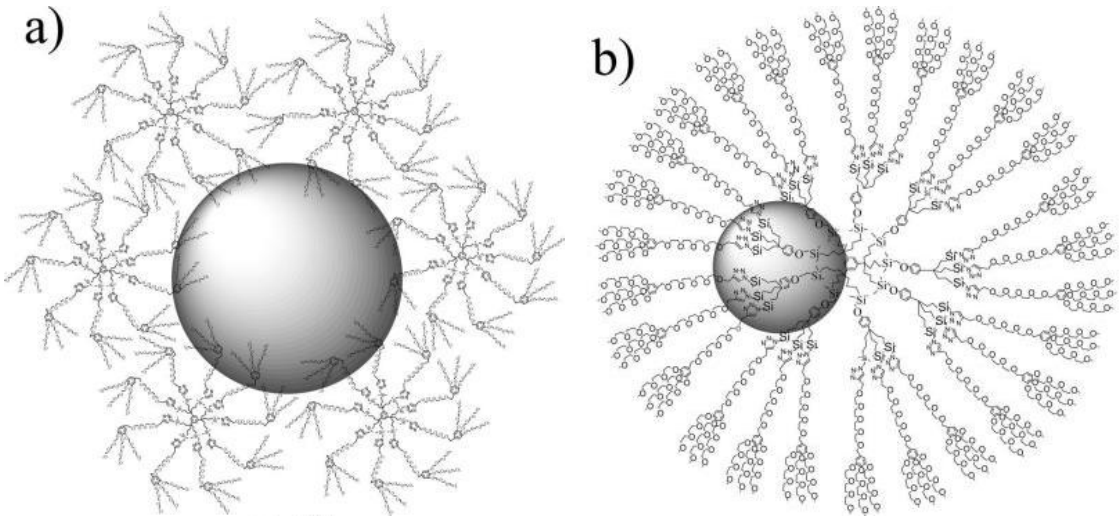

Figure 2. 3. a) gold nanoparticles stabilised by several G0 dendrimers; b) G1 dendrimer encapsulated gold nanoparticles.[145]

In contrast to the systems discussed above, the attachment of anisometric mesogenic ligands to small nanoparticles has resulted in arrays with some degree of anisotropy and a number of such systems displayed long range order on the mesoscale. The elasticity of liquid crystals can be distorted by nanoparticles, causing long-range interparticle interactions, which can be tuned by changing particle size, elastic properties of the liquid crystal solvent, and the interaction between the mesogen molecules and the surface of the

particles. Attempts to order nanoparticles by functionalising them with liquid crystals forming moieties are relatively recent. These include gold nanoparticles with terminally attached cyanobiphenyl,[146, 147] other rod-shaped mesogens,[148, 149] discotic mesogens,[150] bent-core[151] and laterally attached mesogens.[66, 152-154] By end-attaching cyanobiphenyl mesogens to gold nanoparticles via a thioalkyl spacer, a nematic phase in which the particles formed wormlike chains was observed. In the case of bent-core and discotic mesogens attached to gold nanoparticles, the functionalised particles were studied pure as well as dispersed as dopants in host liquid crystals. Only one pure bent-core derivative formed a metastable liquid crystal phase of unknown nature.[151] The discotic capped nanoparticles were thought to cluster at the grain boundaries of the columnar phase. Gold nanoparticles covered by rod-like mesogens attached laterally via a thioalkyl spacer were reported to form a nematic phase, without long-range nanoparticle order. These results on mesogen functionalised nanoparticles highlight the unique character of the materials described here, bearing laterally attached mesogens. Viewed in more general terms, the use of the mesomorphic state is a very powerful tool to organise and induce the organisation of nanoparticles, which opens up the utilisation of techniques employed for fabrication of large panel displays or alternatively if higher order liquid phases are used, for the controlled bottom-up self-organisations in two- or three-dimensional lattices, depending on the great variety type of mesophase morphologies.[147, 155]

Kanie and Ungar synthesised the first highly ordered simple-cubic thermotropic liquid crystal gold hybrids by coupling monodispersed gold nanoparticles with amino substituted organic dendrons and obtained unconventional superlattices,[136] as presented in Figure 2. 4. The effect of dendron generation and surface coverage on self-organisation was investigated.

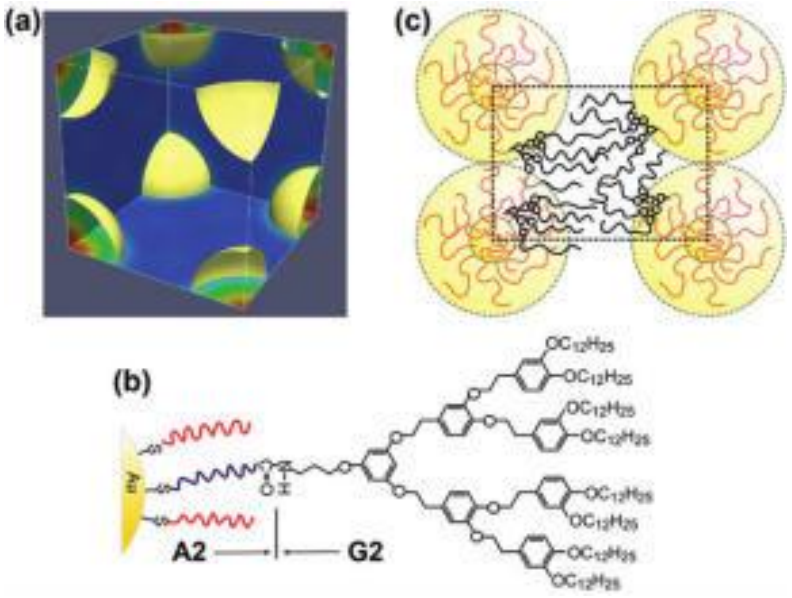

Figure 2. 4. (a) 3D electron density map of a unit cell of the $Pm\bar{3}m$ SC phase reconstructed from the diffraction pattern in Figure 1g (blue, lowest density; red, highest density). The isoelectron surface delimits the spherical region of highest density (i.e., gold); organic matter fills the continuum. (b) Schematic of part of the double corona of a G2/ A2 NP. (c) (110) section through the unit cell.[136]

The first report on liquid crystal gold nanoparticles used the calamitic 10-[(trans-(4-pentylcyclohexyl)phenoxy)] decane-1-thiol as the ligand, which exhibited liquid crystal properties, in a direct synthesis of Brust's two phase method which resulted in 3 nm core size with a homogeneous shell. A similar procedure was applied using cyanobiphenyl with a 12 carbon long hydrocarbon linker and thiolated functional group, in which case, beside the mesophase, a one dimensional arrangement was observed during annealing of the 2.7 nm cores size hybrids. Deschenaux *et al*[156] used a coupling reaction to obtain dendronised gold nanoparticles with liquid crystalline behaviour, but in this case "click chemistry" was applied. Liquid crystalline cyanobiphenyl based dendrons were attached to the gold nanoparticles bearing azide functions resulting in a gold hybrid with exhibits SmA phase. Yu *et al*[66] presented a novel approach for a coupling method where mesogenic groups were grafted to larger gold nanoparticles. Gold nanoparticles were protected by bifunctional capping agents, bearing an amine as the anchoring group. This was further functionalised with a mesogenic group which contained a long spacer and a siloxane group, resulting in a nematic gold hybrid.

Goodby *et al*[147, 155] prepared a range of gold nanoparticles coated with mesogenic thiols and studied the behaviour of doped nematic, smectic and cholesteric phases, such as compound shown below in Figure 2. 5. These nanoparticles are stabilised by mesogenic cyanobiphenyl-terminated thiols, which were designed to match perfectly with the

chemical nature of the liquid-crystal solvent to be used to increase solubility and avoid the possibility of separation as a result of chemical incompatibility of the particle and solvent. The miscibility of other similar gold nanoparticles systems with both nematic and smectic liquid crystal composites were also investigated by Goodby *et al.*[157, 158]

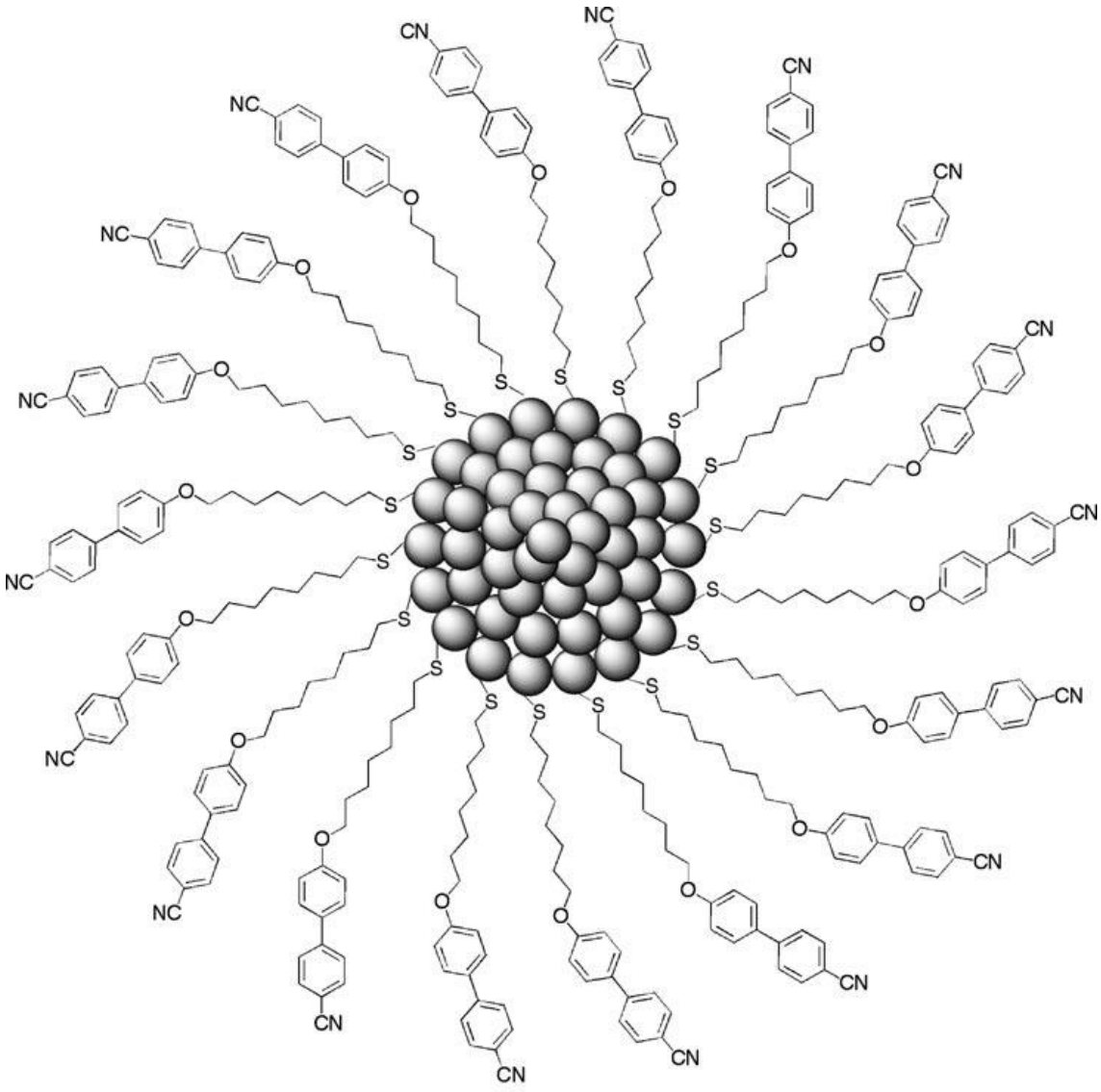

Figure 2. 5. Gold nanoparticles stabilised with mesogenic cyanobiphenyl-erminated thiols

In this thesis, the work presented here follows from earlier studies by Cseh *et al.*[152, 153] The first liquid crystal gold nanoparticles system which exhibits a thermotropic nematic phase in the bulk. Liquid crystals behaviour at room temperature was shown for this type of system design. These nematic gold nanoparticles were obtained in ligand exchange reactions where part of the hydrocarbon, from which the monolayer was built up from around the gold nanoparticles, was replaced with a nematic mesogen (Figure 2. 6).

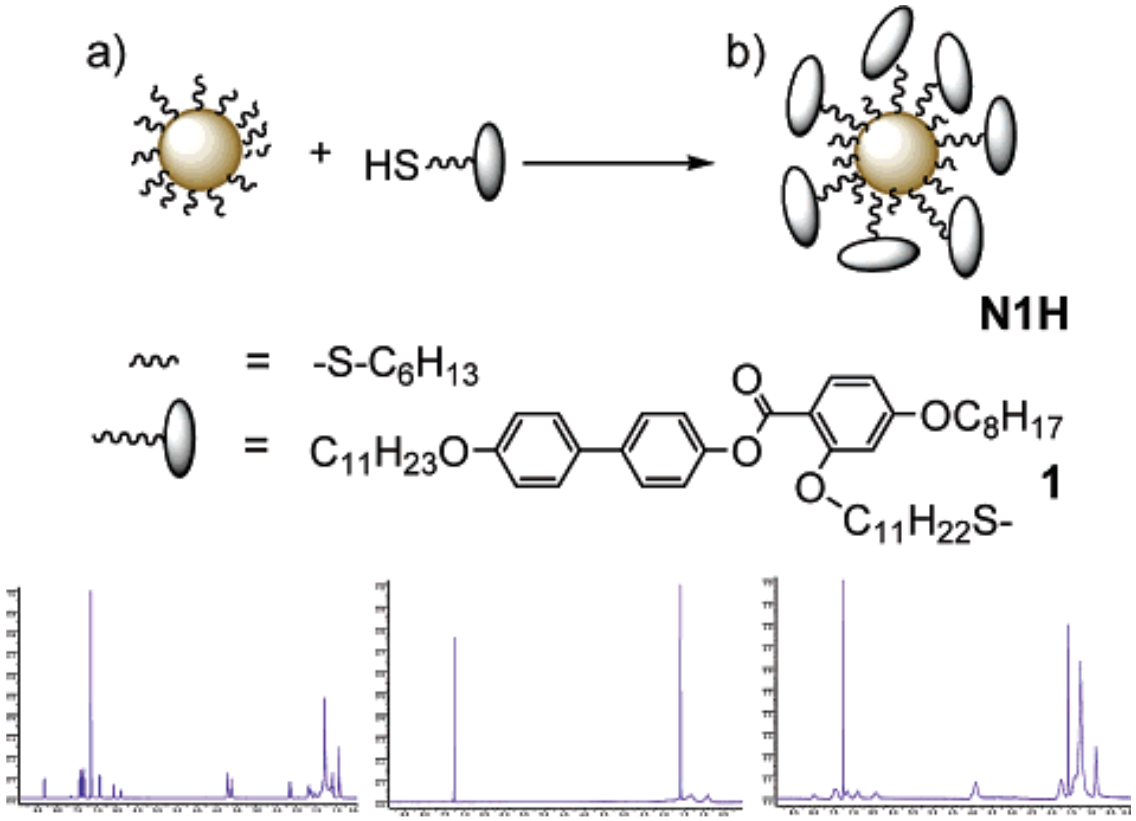

Figure 2. 6. Top: Schematic representations; (a) (left) nanoparticles and (b) (right) exchange reaction yielding N1H. Middle: Chemical structure of the groups covering the particle surface (hexylthiol and mesogen). Bottom: ^{1}H NMR spectrum of mesogen 1 (left), ^{1}H NMR spectrum of hexylthiolfunctionalised nanoparticle (middle); ^{1}H NMR LC nanoparticle N1H (right).[152]

The mesogens are rod-like where the spacer is attached on the side, which is also different from previous reports. The purity was confirmed by ^{1}H NMR. A different hydrocarbon chain length of 1-dodecanethiol was explored. When comparing the two systems, it was observed that the particle size and chain length modify the onset of the liquid crystal phase.[153] Further investigation of some similar materials by Ungar determined that these systems form highly ordered bulk arrays where the gold nanoparticles form strings with rhombohedra or hexagonal columnar lattice, as shown in Figure 2. 7.[154]

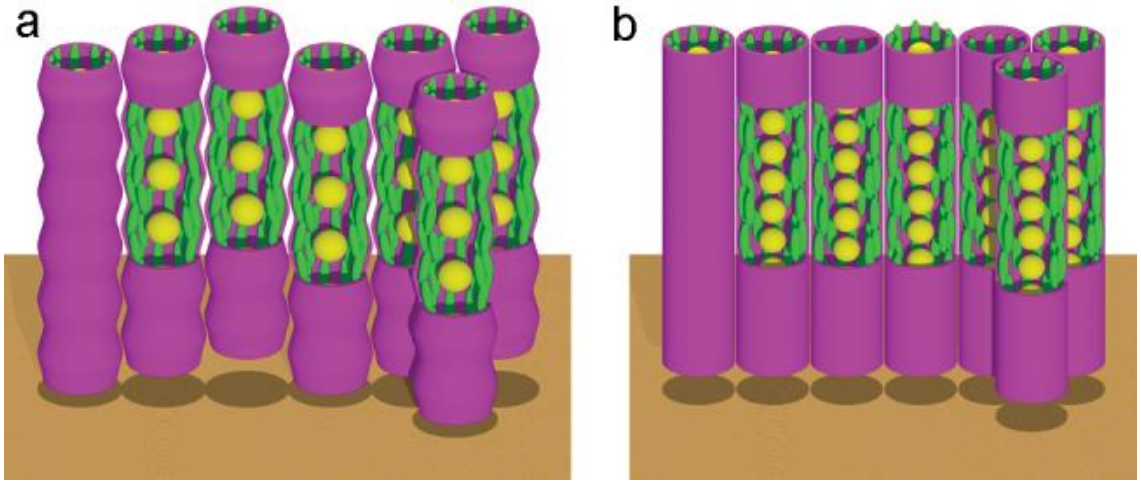

Figure 2. 7. Schematic models of the gold string structures. a) Rhombohedral phase in AuL4C12 and b) hexagonal columnar phase in AuL4C6; yellow: gold nanoparticles, green: mesogens.[154]

Those systems studied were gold nanoparticles covered with hexyl- or dodecylthiol ligands. In the second stage, two fifths of the alkylthiol were replaced by the mesogen ligand in a solvent-mediated exchange reaction, as shown in Figure 2. 8. This work demonstrated that highly ordered superlattices of metal nanoparticles other than those expected from mere packing of spheres can be created by coating the particles with a laterally attached nematogenic ligand. The results give the first rules on which to base on future designs of more complex lattices with a view to build self-assembly metamaterials.

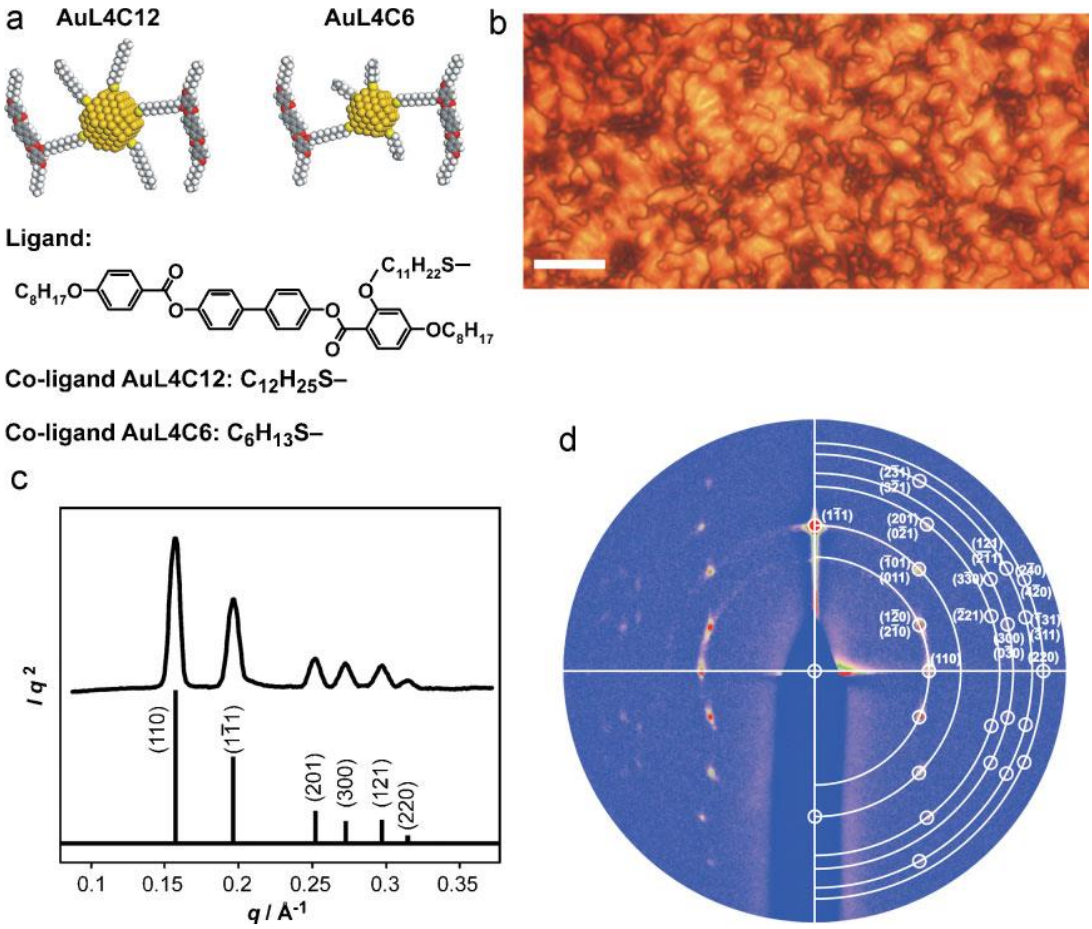

Figure 2. 8. a) Schematic structure of the gold nanoparticles coated with mesogen 4'-(4-octyloxyphenylcarbonyloxy)biphen-4-yl 4-octyloxy-2-(11-mercaptoundecyloxy)benzoate and dodecylthiol (compound AuL_4C_{12}) or hexylthiol chains (compound AuL_4C_6). In the former case, the average numbers of mesogens and alkylthiols per particle are 30 and 45, in the latter case they are 14 and 22, respectively (see below). b) Microscopy image of AuL_4C_{12} between crossed polarizers at room temperature, showing threaded nematic texture. Scale bar: 10 *m*m. c) Experimental (top) and simulated (bottom) powder diffractograms of the LC phase of AuL_4C_{12}. d) GISAXS pattern of a thin layer of AuL_4C_{12}, with the incident beam exactly parallel to the surface of the film. The white circles overlaid on the right-hand half of the diffraction pattern indicate the positions of diffraction peaks as calculated from the best-fit unit-cell parameters. The large semicircles show groups of equivalent diffraction spots.[154]

In conjunction with some new results obtained from similar systems designed with L3 and investigated with mixed and homolithic shell,[65] as presented in Figure 2. 9. While the two ligands with 6 carbons long hydrocarbon co-ligand exhibit a similar hexagonal columnar phase arrangement, using 12 carbons long hydrocarbon long ligands, the AuL4 forms an anisotropic 3D structure of ordered nanoparticle strings in mutual register and with high birefringence. AuL3 has an optically isotropic face-centred cubic structure. The reason for the difference in the lower aspect ratio of the L3 mesogen and the dilution effect of the longer co-ligand was given. Without the co-ligand, AuL3 exhibits a (P_3/mmm) 3D hexagonal, non-birefringent structure. This work demonstrated that the self-assembly mode of nanoparticles and the distance between them in a defined direction can be controlled.

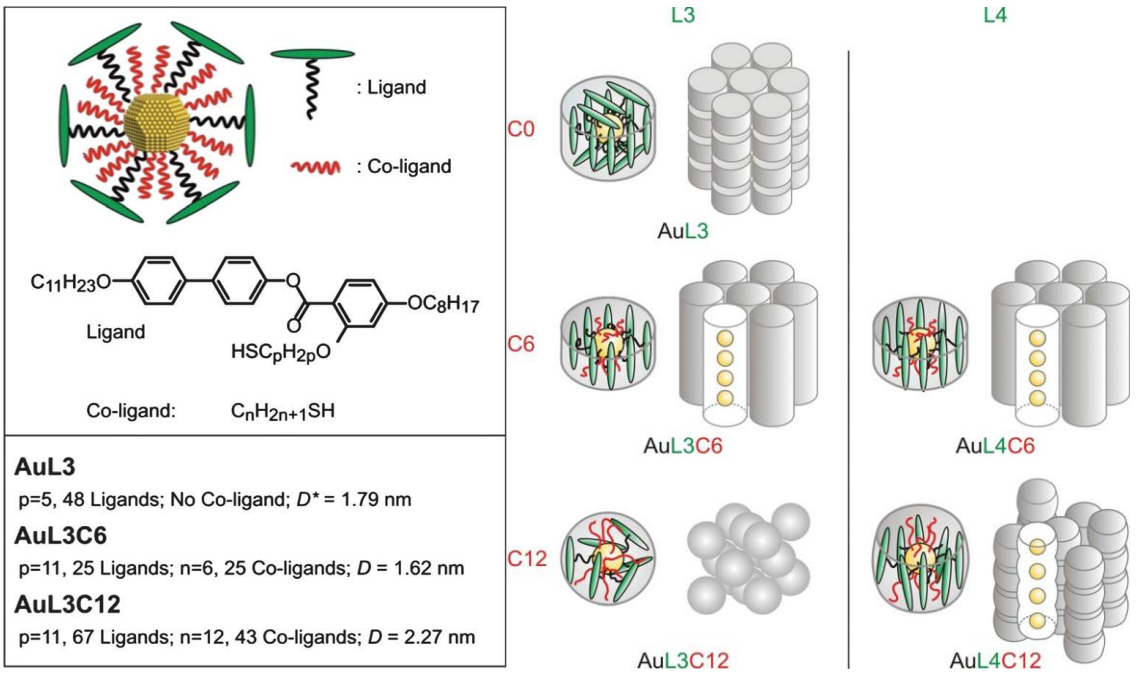

Figure 2. 9. Schematic illustration of the different arrangements of ligands and co-ligands around a nanoparticle depending on the relative amount of co-ligand (red) and the length of the mesogenic ligand (green), and of the different resulting types of ordered self-assembly.[65]

2. 1.4 Gold Nanoparticles Characterisation Techniques

There are three important techniques for the nanoparticle size, monodispersity and content characterisations: transmission electron microscopy (TEM), gel-permeation chromatography (GPC) and thermogravimetric analysis (TGA). Utilisation of one or more of these three methods of identification and characterisation can lead to accurate models of the nanoparticles size, content, number of gold atoms per nanoparticle and co-ligand/ligand ratio.

Transmission electron microscopy (TEM) is the most widely used technique for nanoparticles characterisation. It reveals each nanoparticle with possible self-assembly at very high resolution. However, it is often very difficult to achieve the maximum performance at such resolution, as any slight vibration or drift of sample is significant at this level, and the TEM sample requires much practice to master, as this technique requires a lot of experience. It is hard to identify the monodispersity of sample only by TEM, as only a few tens to hundreds of square nanometre size of area can be viewed as a good quality sample image. Therefore, gel-permeation chromatography (GPC) can be used a good complementary tool to TEM. Since the exact molecular mass of nanoparticles is not required, the GPC could be calibrated to just obtain the size distribution of nanoparticles to determine monodispersity. The nanoparticles content determination can be carried out by thermogravimetric analysis (TGA). Pre-weighted samples are heated to high temperatures in a controlled atmosphere to consume all organic components, leaving only metallic parts, in this case gold.

There are also other techniques used to characterise AuNPs and LC AuNPs, such as elemental analysis (EA). In conjunction with measurements obtained from TEM, GPC and TGA, an accurate model of such AuNPs and LC AuNPs systems could be determined. However, only TEM, GPC and TGA are introduced in more detail, as they are most commonly used in my research project.

2. 1.4.1 Transmission Electron Microscopy (TEM)

The magnifying glass was the very first tool invented by using a simple optics principle. In order to obtain higher resolution, a sophisticated optical microscope was developed later with up to 200 times better resolution than that of the magnifying glass. A specialised instrument consists of a lens or combinations of lenses that enables the human eye to

observe enlarged images of tiny objects. It made visible the fascinating details of a world within the world we live in. In Greek, microscope simply means small (micros) and look at (skopeo). Fortunately, the development did not end here. Ernst Ruska at the University of Berlin, along with Max Knoll combined these characteristics and developed the first transmission electron microscope (TEM) in 1931. Ruska was awarded the Nobel Prize for Physics in 1986 for his invention, which makes it possible to view objects as small as the diameter of an atom.[159-162]

The desire to see further drove the invention of electron microscope which finally reached an insurmountable level of resolution better than 0.05 nm, more than a thousand times better that a typical light microscope and a million times better than the unaided human eye! This level is so high that even individual atoms and how they are arranged in a solid can be pictured with great details.[163] Throughout science history, scientists have always been trying to look at smaller and smaller details of the world around us. Biologists have been trying to investigate the structure of cells, viruses, bacteria and colloidal particles. Materials scientists have always been interested in seeing inhomogeneity and imperfections in metals, crystals and ceramics. In geology, detailed information about rocks, minerals and fossils on a microscopic scale would reveal the origins of our planet and its valuable mineral resources. The smallest objects can see by unaided eye is about 0.1 mm long, such as a grain of salt or even the thickness of a human hair. The light microscope is able to view most biological cells and even bacteria that are 1000 times smaller. The electron microscope can increase magnification another 1000 times on top of that, which has profoundly shaped our understanding of anatomy and cell biology. As shown in Figure 2. 10 below is a log scale of various structures resolved by the human eye, conventional light microscopy and electron microscopy.

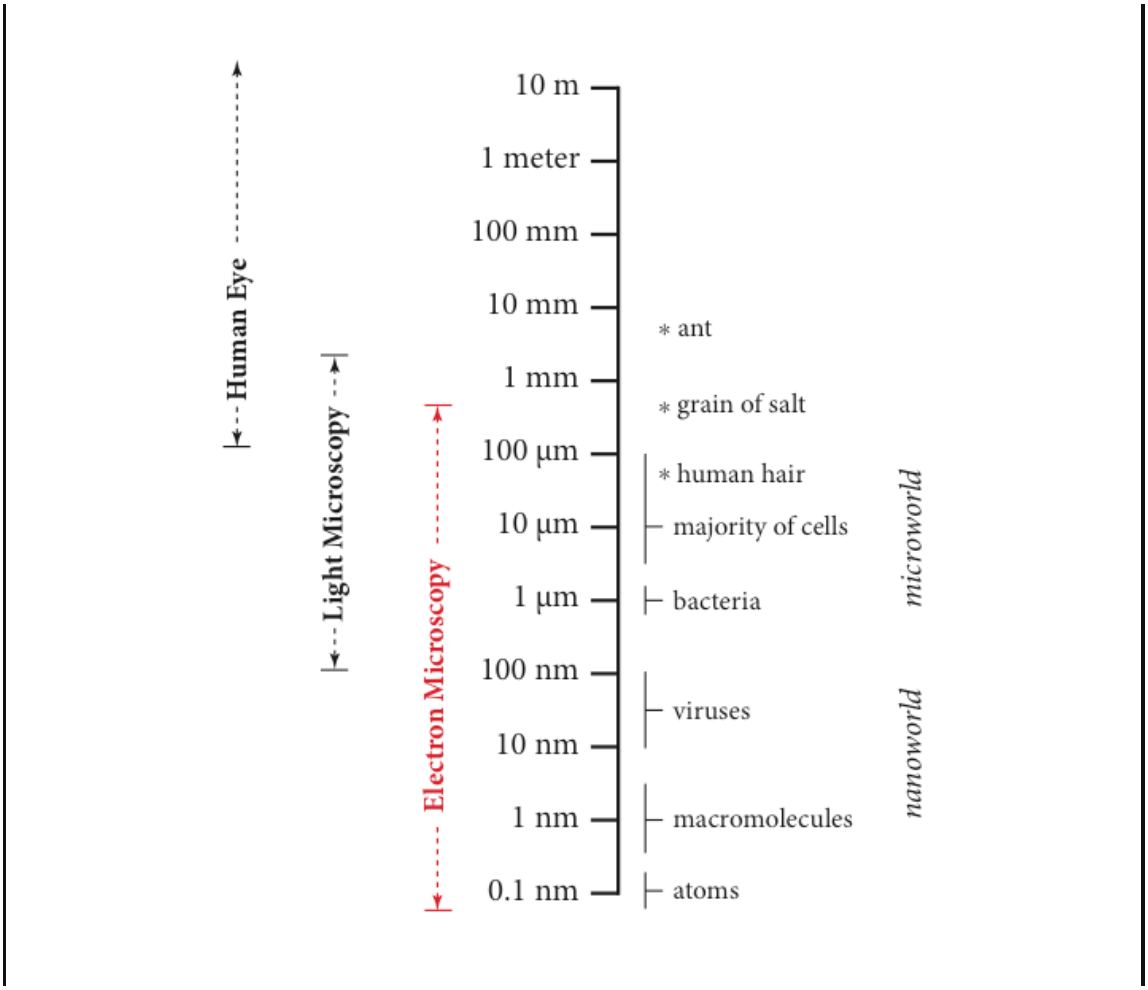

Figure 2. 10. Resolving power of unaided eye versus light and electron microscopy.[164]

In transmission electron microscopy, a beam of electrons instead of light is sent through a very thin slice of the sample. This achieves far better resolution compared to light microscopy due to an electron beam having a far smaller wavelength that light.[162] A transmission electron microscope (TEM) is an ideal technique for a number of different fields such as life sciences, nanotechnology, medical, biological and material research, forensic analysis, gemmology and metallurgy as well as industry and education. Information about the structural, topographical, morphological, compositional, magnetic microstructure, crystalline and defects information can be obtained to characterise the microstructure of materials with very high spatial resolution. This technique allows researchers to view samples on a molecular level or even an atomic level, making it possible to analyse structure and texture at nano-scale. It is being used today in research laboratories around the world to explore the molecular mechanisms of disease, to visualize the 3D architecture of tissues and cells, to unambiguously determine the conformation of flexible protein structures and complexes and to observe individual

viruses and macromolecular complexes in their natural biological context. TEMs can be used in semiconductor analysis, solar, micro-electro-mechanical system labs and data storage devices, electron and ion microscopy provide the high resolution imaging and analysis required to develop and control manufacturing processes. This information is useful in the scientific research and also has many industrial applications. Technology companies use TEMs to identify flaws, fractures and damages to micro-sized objects. This data can help fix problems and/or help to make a more durable, efficient product. Mining companies use automated electron microscopy to analyse millions of micro-scale features in an automated, objective, quantitative and rapid manner. The results compliment bulk chemical assays and together they are used to maximize metal recover and guide decisions in exploration, mining, mineral processing and metal refining. In oil and gas exploration similar analyses provide quantitative lithotype and porosity characteristics of reservoir, seal and source rocks. The results enhance and validate seismic, wireline and mud logs, providing input into geological models and reducing risk in exploration and extraction. They are also being applied successfully in the pursuit of a deeper understanding of the structure-property-function relationships in a wide range of materials and processes such as next generation fuel cell and solar cell technologies, catalyst activity and chemical selectivity, energy-efficient solid-state lighting and lighter, stronger and safer materials. Overall, Transmission Electron Microscopy (TEM) is a very useful cutting edge scientific technique that makes use of the extraordinary wave properties of electrons and has provided many applications in different fields of study. However, the major limitation of transmission electron microscopy is the sample preparation requiring the biological sample to be fixed to preserve its structure before viewing under the microscope, which means live samples cannot be used and it is unable to observe the sample changing in real time.[165] Preparation of thin samples is also vital, in order to obtain this diverse range of structural information at a high resolution. Further detail regarding on some sample preparation techniques will be covered and the basic principle behind transmission electron microscope will be explored within this section.[159, 163, 166, 167]

2. 1.4.1.1 Principle of Transmission Electron Microscopy (TEM)

The basic principle of transmission electron microscopy (TEM) is almost the same as the light microscope, except TEMs use a beam of electrons as a "light source", they have much lower wavelength than light, making it possible to get an optimal resolution

attainable for TEM images, which is a thousand times better than with a light microscope. This means TEMs can reveal objects to the order of a few angstroms (10^{-10} m). For example, finest details of a small cells internal structure can be viewed, or a material can be studied down to the level of individual atoms. Electrons are negatively charged small particles incapable of passing through glass, hence electromagnets are used as lenses of an electron microscope to focus electrons into a very thin beam transmitted through a very thin sample, and the magnification of image formed by varying the power of these electromagnets lenses. During transmission, the speed of electrons directly correlates to the electron wavelength; the faster electrons move, the shorter the wavelength and the greater the quality and detail of image. Magnifications of 350,000 times can be routinely obtained for many materials, whilst magnifications of atoms greater than 15 million times can be imaged in special circumstances. A "light source" at the top of the microscope emits the electrons, and because they are charged particles they will be absorbed and deflected due to the collision with charged molecules of air resulting in a distortion of the beam. Therefore electrons must travel through a microscope column which is under vacuum. The electron source is produced by heating a tungsten filament or lanthanum hexaboride (LaB_6) source at a high voltage source. TEMs usually produce high resolution, black and white images which are recorded on film or digital camera. Because electron beams are invisible to eyes, these images are initially revealed on a fluorescent screen first. The lighter areas of the image show where greater number of electrons was able to pass through the sample with thin area, whereas the darker areas reflect the dense areas of the object with fewer electrons passing through. TEMs produced electrons are accelerated at few hundred kV (typical 200 kV) with wavelengths much smaller that light (0.0025 nm). However the resolution of the electron microscope is limited by aberrations inherent in electromagnetic lenses to about 0.1 – 0.2 nm, hence the value of the electron microscope depends on how great the resolving powers are.[166, 168-170]

In comparison, the light microscope, even one with perfect lenses and perfect illumination which has a highest resolution of approximately 0.2 µm, cannot be used to distinguish objects that are smaller than half the wavelength of light. Whereas the Transmission Electron Microscopes of today have magnification 4000 times better, and are capable of resolving objects 0.05 nanometres apart that is a millionth of a millimetre, which is just the length of a hydrogen atom diameter. A typical TEM usually contains four major sections and consists of many components as shown in Figure 2. 11 below.

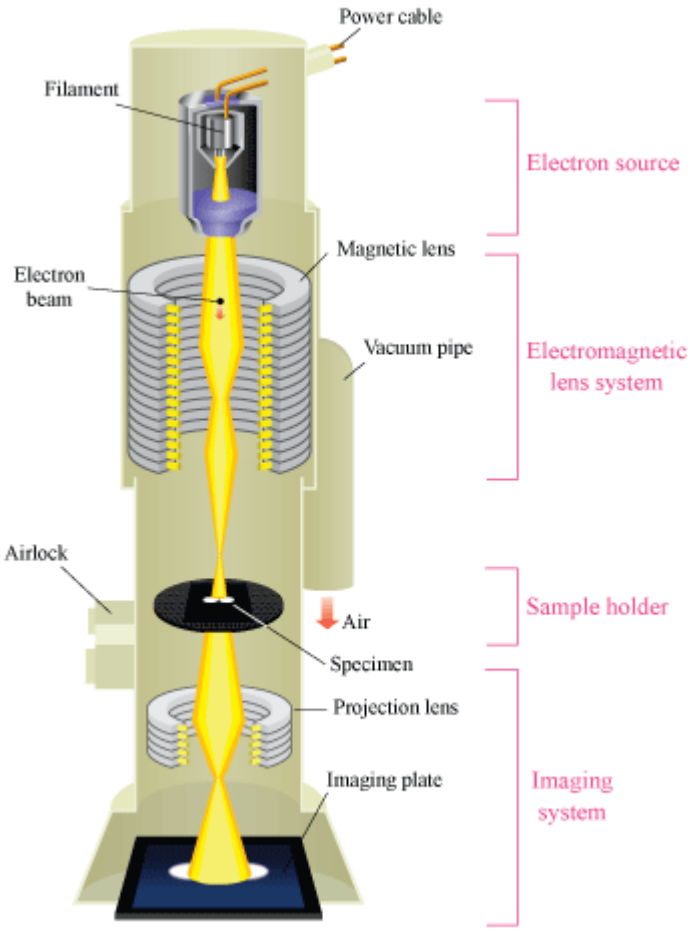

Figure 2. 11. A schematic outline of TEM.[163]

An electron source consists of a cathode and an anode. The cathode is a tungsten filament which emits electrons when being heated. A negative cap confines the electrons into a loosely focused beam (Figure 2. 12). The electron beam is then accelerated towards the specimen by the positive anode. Electrons at the rim of the beam will fall onto the anode while the others at the centre will pass through the small hole of the anode. The electron source works like a cathode ray tube.

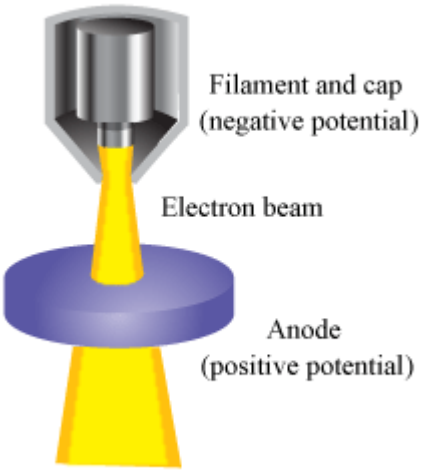

Figure 2. 12. Electron source of TEM.[163]

Electron Gun: the electron gun produces a beam of electrons whose kinetic energy is high enough to enable them to pass through thin areas of the TEM sample. The gun consists of an electron source, also known as the cathode because it is at a high negative potential and an electron-accelerating chamber. There are several types of electron source, operating on different physical principles.[159, 163, 171]

1. Thermionic emission: the electron source is a hairpin filament made of tungsten (W) wire, spot-welded to straight-wire leads that are mounted in a ceramic or glass socket, allowing the filament assembly to be exchanged easily when the filament eventually "burns out". A direct current heats the filament to about 2700 ºC, at which temperature tungsten emits electrons into the surrounding vacuum by the process known as **thermionic emission**. LaB_6 guns operates in a very similar way to tungsten, except that they provide up to 10 times more brightness than tungsten and have significantly longer lifetime, but require higher vacuum levels which increases the microscope's cost. The emitting area of LaB_6 is smaller than tungsten, increasing brightness but reducing total beam current capability.
2. Field emission: if the electrostatic field at a tip of a cathode is increased sufficiently, the width of the potential barrier becomes small enough to allow electrons to escape through the surface potential barrier by quantum-mechanical tunnelling, a process known as **field emission** and these guns are the most expensive type of source. Field emission sources come in two types, cold field emission and Schottky (thermally assisted) field emission. Cold field emission

offers very high brightness but varying beam currents. It also requires frequent flashing to clean contaminants from the tip. Schottky field emission offers high brightness and high, stable current with no flashing. The latest generation of Schottky field emitters retains its current stability while attaining brightness levels close to cold field emission.

Electromagnetic lenses: after leaving the electron source, the electron beam is tightly focused using electromagnetic lens and metal apertures. In TEM the function of the lenses is to transform a point in an object to a point in an image and to focus parallel rays to a point in the focal plane of the lens. Electrons can be focused either by electrostatic or magnetic field. The system only allows electrons with well-defined energy within a small energy range to pass through. Regardless of their nature electrostatic, magnetic or electromagnetic electron lenses are notoriously poor lenses compared to visible light lenses, because aberrations cannot be corrected whereas visible light lenses can be corrected.[159, 163, 171]

1. Magnetic Lens: Circular electro-magnets capable of generating a precise circular magnetic field. The field acts like an optical lens to focus the electrons.
2. Aperture: A thin disk with a small (2-100 micrometres) circular through-hole. It is used to restrict the electron beam and filter out unwanted electrons before hitting the specimen.

Vacuum chamber: the penetration of electrons through air is typically no more than 1 meter. Most of the beam would be lost to collisions of the electrons with the air molecules. It is also not possible to generate the high charge difference between the anode and cathode in the gun because air is not a perfect insulator. The beam on the sample while in air would trap all types of hydrocarbon molecules on the sample, resulting in a thick carbon contamination layer on the sample after removing the hydrogen and oxygen. Therefore a vacuum chamber is required. Electrons behave like light only when they are manipulated in a vacuum. The whole column from source to fluorescent screen is evacuated. Different vacuum pumps are used to obtain and maintain these levels. A number of airlocks and separation valves are built in to avoid having to evacuate the whole column every time a sample or photographic material or a filament is exchanged. In modern TEMs the vacuum system is completely automated and the vacuum level is continuously monitored and fully protected against faulty operation.[159, 163, 171]

Sample stage: the sample holder is a platform equipped with a mechanical arm for holding the specimen and controlling its position. The sample stage is designed to hold the specimen as stationary as possible, as any drift or vibration would be magnified in the final image, impairing its spatial resolution, especially if the image is recorded by a camera over a period of several seconds. But in order to view all possible regions of the sample, it is also necessary to move the specimen horizontally over a distance of up to 3 mm if necessary. The design of the stage must also allow the sample to be inserted into the vacuum of the TEM column without introducing air. This is achieved by inserting the sample through an airlock, a small chamber into which the sample is placed initially and which can be evacuated before the sample enters the TEM column. The sample stage and airlock are one of the most mechanically complex and precision-machined parts of the TEM.[159, 163, 171]

Phosphor or fluorescent screen: the imaging system consists of another electromagnetic lens system and a screen. The electromagnetic lens system contains two lens systems, one for refocusing the electrons after they pass through the specimen, and the other for enlarging the image and projecting it onto the screen. The screen has a phosphorescent plate which glows when being hit by electrons enabling it to convert the electron image to a visible form. The image forms in a way similar to photography. It consists of a metal plate coated with a thin layer of powder that fluoresces (emits visible light) under electron bombardment. The phosphor is chosen so that light is emitted in the middle of the spectrum (yellow-green region), to which the human eye is most sensitive. The TEM screen is used mainly for focusing a TEM image or diffraction pattern. For this purpose, light-optical binoculars are often mounted just outside the viewing window, to provide some additional magnification. The viewing window is made of special high lead content glass and is of sufficient thickness to absorb the x-rays that are produced when the electrons deposit their energy at the screen (Figure 2. 13).[159, 163, 171]

Figure 2. 13. The imaging system of TEM.[163]

The electronics: modern electron microscopes employ a fast, powerful computer to control, monitor and record the operating conditions of the microscope. This results in a dramatic reduction in the number of control knobs, compared with earlier models and a microscope that is easier to use, especially when multiple accessories require simultaneous optimisation. Furthermore, it allows special techniques and experiments to be embedded in the instrument so that the operator can carry them out using the same controls. The computer can be attached to a network to allow automatic backups and data sharing.[159, 163, 171]

TEM works a lot like a slide projector. The light beam only passes through the slide area where patterns are not painted, the pattern is replicated by the transmitted light beam falling on the screen to form an enlarged image of the slide. TEMs work the same way except they have a "light source" equipped at the top of microscope, it emits a beam of electrons (like the light in a slide projector) that travel through vacuum in the column of the microscope, then the specimen (like the slide). In comparison with the light microscope, the TEM uses electromagnetic lenses to focus the electrons into a very thin beam instead of aglass lenses focusing the light in the light microscope. The electron beam then travels through the specimen and whatever part is transmitted is projected onto a phosphor screen. However, the transmission of electron beam in TEM is highly

dependent on the properties, composition and density of material being examined. Some of the electrons are scattered, reflected and disappear from the beam before hitting a fluorescent screen at the bottom of the microscope. The unscattered electrons give rise to a "shadow image" of the specimen with its different parts displayed in varied darkness according to their density. As a result, a specimen with a non-uniform density can be examined by this technique. For example, porous material will allow more electrons to pass through while dense material will allow less. The image can be studied directly by the operator or photographed with a camera. Basically in a TEM, electrons replace photons, electromagnetic lenses replace glass lenses and images are viewed on a screen rather than through an eyepiece. A simple image and sketch are shown below in Figure 2. 14.[163]

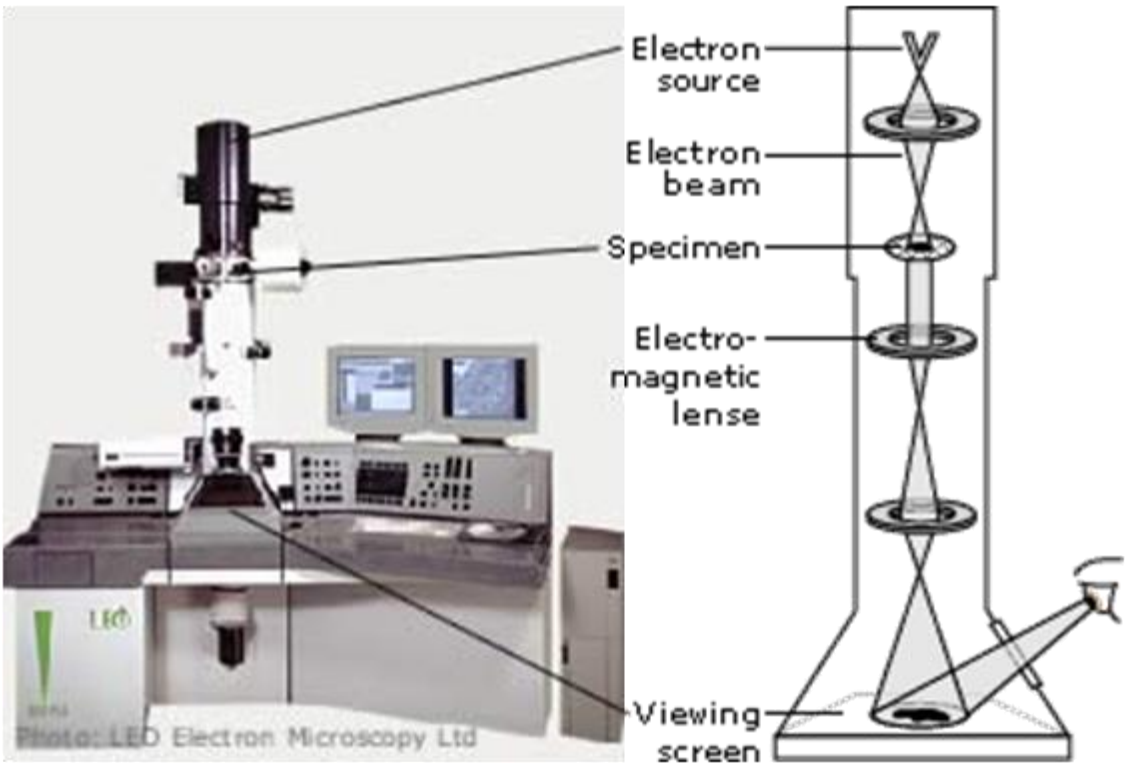

Figure 2. 14. A typical TEM instrument.[168]

A TEM can be used in any branch of science and technology where it is desired to study the internal structure of a sample down to the atomic level. However, the requirement for thin samples containing no volatile components limits the range of possible materials to be studied with TEM. Another issue of sample preparation for TEM is that modifications and alteration of sample may take place during sample preparation process. Materials for TEM must be specially prepared with suitable concentration or thicknesses which allow

electrons to transmit through the sample, much like light is transmitted through materials in conventional optical microscopy. It must be stable and small enough to permit its introduction into the evacuated microscope column and thin enough to permit the transmission of electrons. There are numerous ways to prepare samples for TEM examination for different purpose and different thicknesses are required for different applications. For the ultimate high-resolution materials studies, the sample cannot be thicker than 20 nm; for bio-research, the film can be 300 – 500 nm thick. In general, samples are required to be at a low density that allows electrons to travel through. Samples can be thin sliced or one can study an isolated sample in a solution. In biology, since TEM works in vacuum there may be first a chemical treatment to remove water and preserve the tissue as much as possible in its original state, the water within a biological sample must be removed to avoid disruption when under vacuum. Therefore such samples have to be preserved with different fixatives and trapped as stable structures before being dehydrated in alcohol or acetone. The sample is then embedded in a hardening resin or plastic that polymerise into a solid hard plastic block, which is cut into thin sections by diamond knife in an ultramicrotome instrument producing sections 50 – 100 nm thick. Thin sections of the sample is placed on a copper grid and stained with heavy metals before being analysed by TEM. Heavy metals like uranium and lead can sometimes be used as markers to locate specific biological samples, because they scatters electrons well and improve the contrast in the microscope. A suitable electron dense material salt solution does not bind to the material but forms a "shadow" around the sample and so can be used as a negative staining agent. The sample will appear as a negative image under TEM which provides high contrast and good preservation to determine the sample structure detail. To ensure samples are fully preserved without damaging bonds it is possible to rapidly freeze a given sample in such manner that prevents the water molecules from rearranging themselves. By slamming a specimen into a polished copper block cooled with helium, the water is super-cooled into a vitreous ice without forming crystals. These samples can then be sliced with an ultramicrotome In the case of nanoparticles samples, drop casting of nanoparticles suspension on carbon coated cooper TEM grids, and the grids are left to dry at room temperature. Depending on the sample and sample preparation, few nanoparticles up to 2000 could be captured per image.[161, 172-174]

TEMs can reveal the finest details of internal structure - in some cases as small as individual atoms. The optimal resolution attainable for TEM images is much better magnitude than that from a light microscope due to the wavelength of electrons being much smaller than that of light. Magnifications of 350,000 times can be routinely obtained for many materials, and magnifications for atoms greater than 15 million times can also be achieved in special circumstances. Specialised preparative techniques are required for biological samples to determine the cell structure, morphology and position of those specific components within cells. Phase determination as well as defect and precipitate orientation are also typical outcomes of conventional TEM experiments for non-biological materials. Microstructural characterisation of non-biological materials, including unit cell periodicities, can be readily determined using various combinations of imaging and electron diffraction techniques. Images obtained from a TEM are two-dimensional sections of the material under study, but applications which require three-dimensional reconstructions can be accommodated by these techniques. The energy of the electrons in the TEM determines the relative degree of penetration of electrons in a specific sample, or alternatively, influence the thickness of material from which useful information may be obtained. A typical high power TEM with 400 kV, when compared with the more conventional 100 kV or 200 kV instruments, not only provides the highest resolution but also allows for the thick samples to be observed (eg. less than 0.2 micrometres). TEMs are often employed to determine the detailed crystallography of fine-grained, or rare, materials due to the high spatial resolution obtained. Thus, TEM is a complementary tool to conventional crystallographic methods such as X-ray diffraction for the physical and biological sciences.[170]

2. 1.4.1.2 Advantages and Disadvantages of Transmission Electron Microscopy (TEM)

A Transmission Electron Microscope is a powerful instrument with a number of advantages such as:

- Most powerful magnification, potentially over one million times or more;
- A wide-range of applications and can be utilized in a variety of different scientific, educational and industrial fields;
- Provide information on element and compound structure;
- Images are high-quality and detailed;

- Capable of yield information of surface features, shape, size and structure;
- They are easy to operate with proper training;

Some disadvantages of electron microscopes include:

- Large and very expensive;
- Laborious sample preparation;
- Potential artifacts from sample preparation;
- Operation and analysis requires special training;
- Samples are limited to those that are electron transparent, able to tolerate the vacuum chamber and small enough to fit in the chamber;
- Require special housing and maintenance;
- Images are black and white;

Overall, TEMs are costly, large, cumbersome instruments that require special location to avoid possible exposure to vibration and electromagnetic fields, due to their sensitivity. A TEM also requires a constant high level of maintenance attention to maintaining voltage, currents to the electromagnetic coils and cooling water. Nevertheless, it is one of the most powerful microscopic tools available to-date, capable of producing high-resolution, detailed images one nanometre in size.[167]

2. 1.4.2 Gel-Permeation Chromatography (GPC)

Gel-Permeation Chromatography (GPC) is the chromatographic technique which separates dissolved molecules based on the molecular size of the components, and is used primarily for analytical assays. It is also known as Size Exclusion Chromatography (SEC) or Gel Filtration Chromatography (GFC). It is one of the most powerful and versatile analytical techniques available for the characterisation of a wide variety of polymers or other macromolecules in a mixture. It is the most convenient technique for characterizing the complete molecular weight distribution of a polymer, it is also used to characterise biopolymers, proteins or nanoparticles. It has a little modification in that the column is filled or packed with a stationary phase. The size and shape of the molecule dictates its ability to interact with a bed of porous particles on the stationary phase. Separation is achieved by the differential exclusion from the microporous stationary phase of the packing material with a rigid structure, controlled-porosity column packing and is carried by solvent (mobile phase) through the column. The diameters of pore are in the order few

angstroms similar to that of molecules. The pore size of the packing particles determines the molecular size range within which separation occurs.[175]

The principle involved of this technique is that molecules move through the column under the influence of liquid mobile phase based on their relative physical size or mass (as show in Figure 2. 15). The large molecules cannot interact or move into the pore spaces available in the stationary phase due to their size and elute relatively quickly as they travel shorter path. Those with smaller size or mass typically move through all possible pores without any difficulty, hence travel a longer path and take longer to elute from the column due to their small size. In this manner, a whole range of molecular weights can be characterised when compared to the retention time of standard molecular weights, typically polystyrene reference standards.[175]

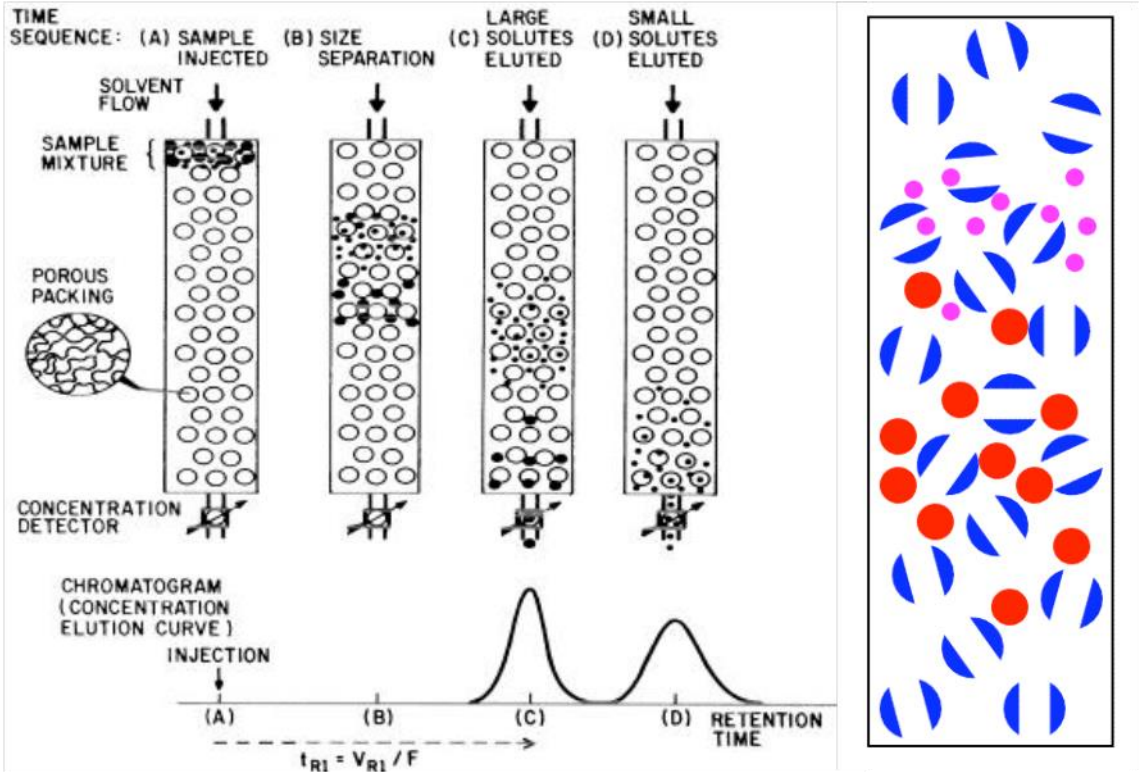

Figure 2. 15. A sketch of how GPC column works.[176]

The gel permeation chromatograph contains a number of different components that work together to provide optimum system performance with minimum effort. In designing instrumentation for GPC, a variety of requirements must be satisfied. Sample solution is introduced into the flowing system by Injectors which should not disturb the continuous mobile phase flow. Pumps deliver the sample and solvents through the columns and system at the same flow rates independent of viscosity differences. Detectors monitor and

record the separation; it must be non-destructive to eluting components and sensitive with a wide linear range in order to respond to both trace amounts. Data acquisition accessories control the test automatically, record the results and calculate the molecular weight averages, it can also provide complete control of GPC systems, hence large numbers of samples can be run unattended and raw data can be automatically processed. A schematic of a basic gel permeation chromatograph is shown in the Figure 2. 16 below.[175]

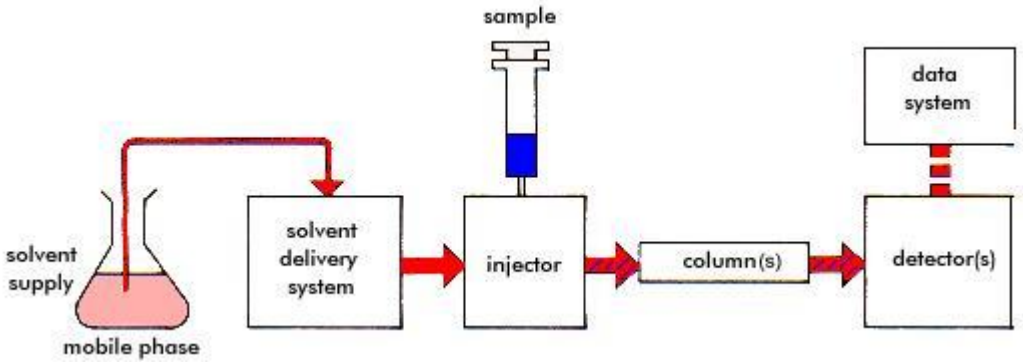

Figure 2. 16. A simple sketch of how GPC system works.[177]

As the sample is separated and eluted from the column, it can be characterised by a single concentration detector (Conventional Calibration) or series of detectors (Universal Calibration and Triple Detection). GPC can determine several important parameters. These include number average molecular weight, weight average molecular weight, Z weight average molecular weight and the most fundamental characteristic of a polymers molecular weight distribution.[175]

As a separation technique GPC has many advantages and disadvantages.[178]

Advantages of GPC:

- well-defined separation time due to the fact that there is a final elution volume for all unretained analytes;
- provide narrow bands, although this aspect of GPC is more difficult for polymer samples that have broad ranges of molecular weights present;
- there is a lower chance for analyte loss to occur, since the analytes do not interact chemically or physically with the column;
- provides a more convenient method of investigating the properties of polymer samples in particular;

Disadvantages of GPC:

- limited number of peaks that can be resolved within the short time scale of the GPC run;
- requires around at least a 10% difference in molecular weight for a reasonable resolution of peaks to occur;
- polymer molecular masses of most of the chains will be too close for the GPC separation to show anything more than broad peaks;
- filtrations must be performed before using the instrument to prevent dust and other particulates from ruining the columns and interfering with the detectors;

2. 1.4.3 Thermogravimetric Analysis (TGA)

Thermogravimetric Analysis (TGA) uses heat to force reactions and physical changes in materials. The amount and rate of change in the weight of a material associated with transition and thermal degradation are measured as a function of temperature or time in a controlled atmosphere. Measurements are used primarily to determine the composition of materials and to predict their thermal stability at temperatures up to 1000 °C. The sample is usually a solid, or more rarely a liquid. The changes in the mass of samples can be caused by a variety of processes such as decomposition, degradation, sublimation, vaporisation, adsorption, desorption, oxidation and reduction. This technique can be used to characterise materials that exhibit weight loss or gain due to decomposition, oxidation, or dehydration. In the above definition, a controlled temperature program means heating or cooling the sample at some predetermined and defined rate. Although it is common to have just one constant heating or cooling rate, it is also advantageous in some cases to have different rates over different temperature ranges and in some cases even a varying rate over a specific temperature range.[179, 180]

A thermobalance is used to determine sample mass change caused by a reaction during a temperature range and these unique characteristics could be used to relate to the molecular structure of the sample as well. It is also used to obtain a thermogravimetric curve for specific materials and chemical compounds, due to unique sequence from physicochemical reactions occurring over specific temperature ranges and heating rates. TGA can also be used in combination with FTIR, which is capable of detailed FTIR analysis of evolved gases produced from the TGA.[181]

Thermogravimetric analysis (TGA) data can be presented in two ways. The TGA curve is a plot of the mass against time or temperature, with the mass loss on the ordinate plotted downward and mass gains plotted upward relative to a baseline. Alternatively, data can be presented as a derivative thermogravimetric analysis (DTGA) curve, which is a plot of the rate of change of mass (m) with respect to time (t) or temperature (T) against time or temperature. The DTG mass losses should also be plotted downward and the gains upward.

Conventionally, thermal analysis experiments are carried out at a constant heating rate, and a property change is measured as a function of time. An alternative approach is to keep the change in property constant by varying the heating rate. For TGA, the rate of mass loss is kept constant by variation in the heating rate. To achieve this, the mass change is monitored and the heating rate decreased as the mass loss increases, and vice versa. At the maximum rate of mass loss, the heating rate is a minimum. This gives mass losses over very narrow temperature ranges and sometimes enables two close reactions to be resolved. This method has the advantage of using fast heating rates when no thermal event is taking place and then slowing down the heating rate when a mass change is in progress.[182, 183]

Thermogravimetry analysis does not give information about reactions that do not involve mass change, such as polymorphic transformations and double-decomposition reactions. Also, it is not useful for identification of a substance or mixture of substances unless the temperature range of the reaction has already been established and there are no interfering reactions. However, when a positive identification has been made, TGA by its very nature is a quantitative technique and can frequently be used to estimate the amount of a particular substance present in a mixture or the purity of a single substance.

As a thermal analysis technique TGA has many advantages and disadvantages.

Advantages of TGA

- Sample held isothermal until transition completed - thus excellent resolution of overlapping transitions;
- Permits careful control of reaction environment;
- Available on all TA Instruments TGA's;

Disadvantages of TGA

- Difficult method development. May require several scans to optimize run conditions;
- Inappropriate parameter choices may produce artifacts;
- Long run time;

TGA is widely used as a QA/QC tool in the manufacture of nanomaterials, such as Carbon Nano Tubes (CNT) and metallic Nanoparticles (NP). TGA is used in CNT manufacturing process to characterise the amount of metallic catalytic residue that remains on the CNT. This is done because CNT are classified by percent purity. TGA is also used to characterise end products that contain nanoparticles (NP) or CNTs as in their usual end product characterisations. Both NP manufacturers and manufacturers of end products that contain NPs and CNTs use these techniques to determine the NPs or CNT contents.[182, 183] TGA is used extensively in my project to characterise gold nanoparticles.

Overall, thermogravimetric (TGA) analysis is an essential laboratory tool used for material characterisation that provides determination of endotherms, exotherms and weight loss on heating and cooling. TGA analysis is widely used to characterise, verify materials and is applicable to most industries. TGA is used as a technique to characterise materials used in various environmental, food science, pharmaceutical, and petrochemical applications. Materials can be analysed by TGA include polymers, plastics, composites, laminates, adhesives, food, coatings, pharmaceuticals, organic materials, rubber, petroleum, chemicals, explosives and biological samples.[182-184]

2. 2 Aims and Objectives of Chapter Two

The objectives of this thesis presented in this Chapter Two, involve the synthesis of 1-dodecanethiol capped gold nanoparticles, which were synthesised following the methodology developed by Brust.[116] In a further step, following the nanoparticle preparation, part of this monolayer was replaced by the pre-synthesised mesogenic ligands following an exchange reaction, as shown in Scheme 2. 8 below.

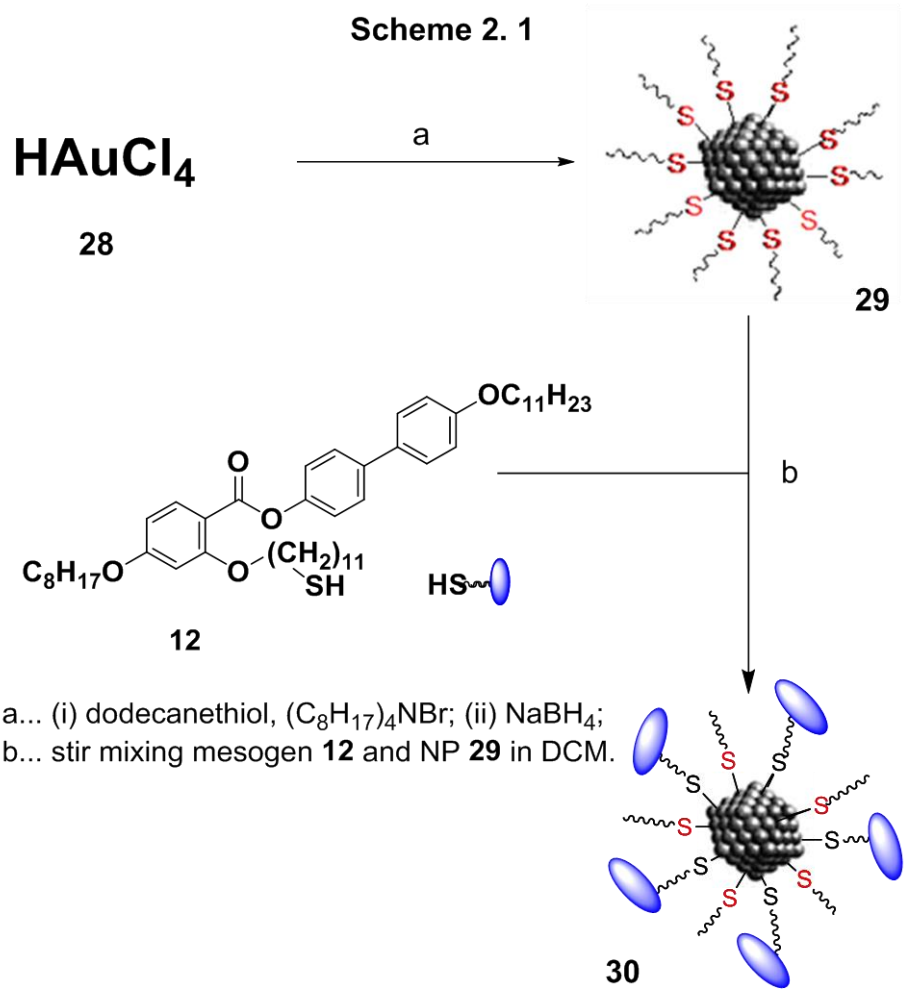

Scheme 2. 1. Synthetic Scheme for the preparation of LC AuNPs

The aims of monolayer protected AuNPs synthesis are:

- Obtaining samples of monodisperse gold nanoparticles in large quantities has been found to be a significant obstacle in this research field, and it has been found generally that it is difficult to produce the same quality of such gold nanoparticles, even if the same preparation procedures were followed; put simply there is a tendency that from batch to batch, particle sizes and polydispersities differ.

However full standard characterisations require sufficient amounts of materials both for this research project and collaborative research. Therefore, the goal was firstly to prepare monodisperse gold nanoparticles by exploiting methods that can produce large amounts of gold nanoparticles with good reproducibility.

- The purification of monolayer protected AuNPs is a problem in this area of research, especially as the scale of reaction increases. Therefore, a much simpler purification technique is required for larger amounts.
- Furthermore, there has been little work carried out with the focus on increasing the size of gold nanoparticles in order to obtain surface plasmonic resonance properties. Therefore, a further reaction conditions optimisation was required to investigate any possible way to prepare larger particles.
- Sample preparation and transferring techniques development for AuNPs characterisations by TEM, GPC, ICP, EA and TGA;

The aims of liquid crystal gold nanoparticles synthesis are:

- First of all: synthesis of liquid crystal gold nanoparticles (LC AuNPs) by using ligand-exchange reactions;
- Investigation of the mesogenic properties of LC AuNPs by OPM and DSC, include sample preparation techniques development;
- Optimisations of the purification procedures to obtain monodisperse LC AuNPs in larger quantities;
- Sample preparation and transferring techniques development for LC AuNPs investigation by TEM, GPC, ICP, EA and TGA;
- Other GISAX and Synchrotron investigation of LC AuNPs physical properties by collaborators from the University of Sheffield;
- Investigation the impact of the ligand-exchange reaction time on the size and content of LC AuNPs investigation;
- Studies of the influence of purification methods on the size and content of LC AuNPs;
- Preparation of larger size LC AuNPs (~ 3.4 nm) Surface Plasmonic Resonance (SPR) and optical properties investigation by collaborators from Switzerland;

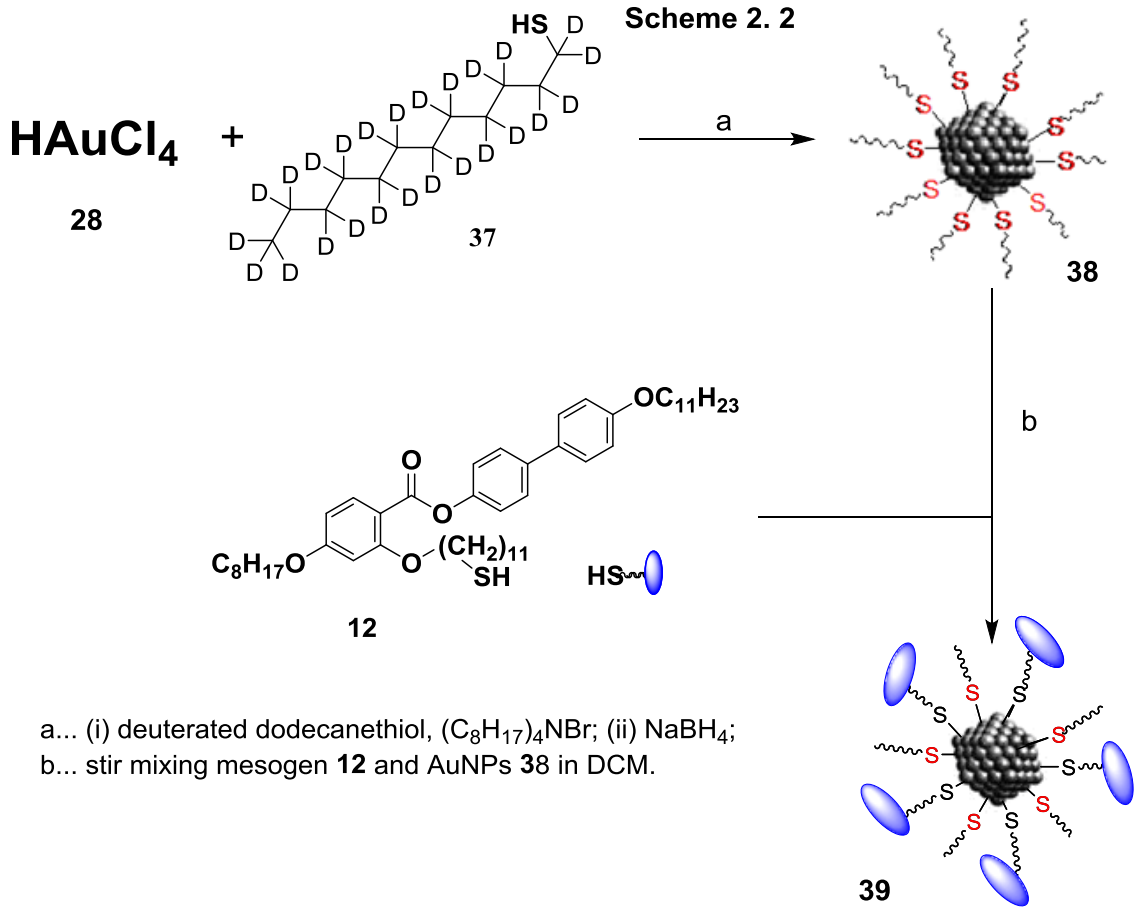

Scheme 2. 2. Synthetic Scheme leading to deuterated LC AuNPs.

This programme of research also aimed to investigate properties of such liquid crystal gold nanoparticles capped with deuterated 1-dodecanethiol (as shown in the scheme 2. 2 above). In order to understand the interaction of capping agents on the surface of gold nanoparticles and how those capping agents behave. Therefore, the aims of both deuterated AuNPs and LC AuNPs synthesis were:

- Preparation of deuterated 1-dodecanethiol from pre-deuterated 1-dodecanol.
- Synthesis of 1-dodecanethiol monolayer protected gold nanoparticles (AuNPs) by using a modified Brust's two phases method;
- Synthesis of larger size of 1-dodecanethiol monolayer protected AuNPs;
- Synthesis and characterisation of deuterated 1-dodecanthiol and intermediates;
- Synthesis of deuterated 1-dodecanethiol monolayer protected gold nanoparticles (deuterated AuNPs) by using a modified Brust's two phases method;

- Synthesis and characterisation of deuterated liquid crystals gold nanoparticles (deuterated LC AuNPs);

2. 3 Results and Discussion

2. 3.1 Synthesis and Characterisation of Gold Nanoparticles

Scheme 8

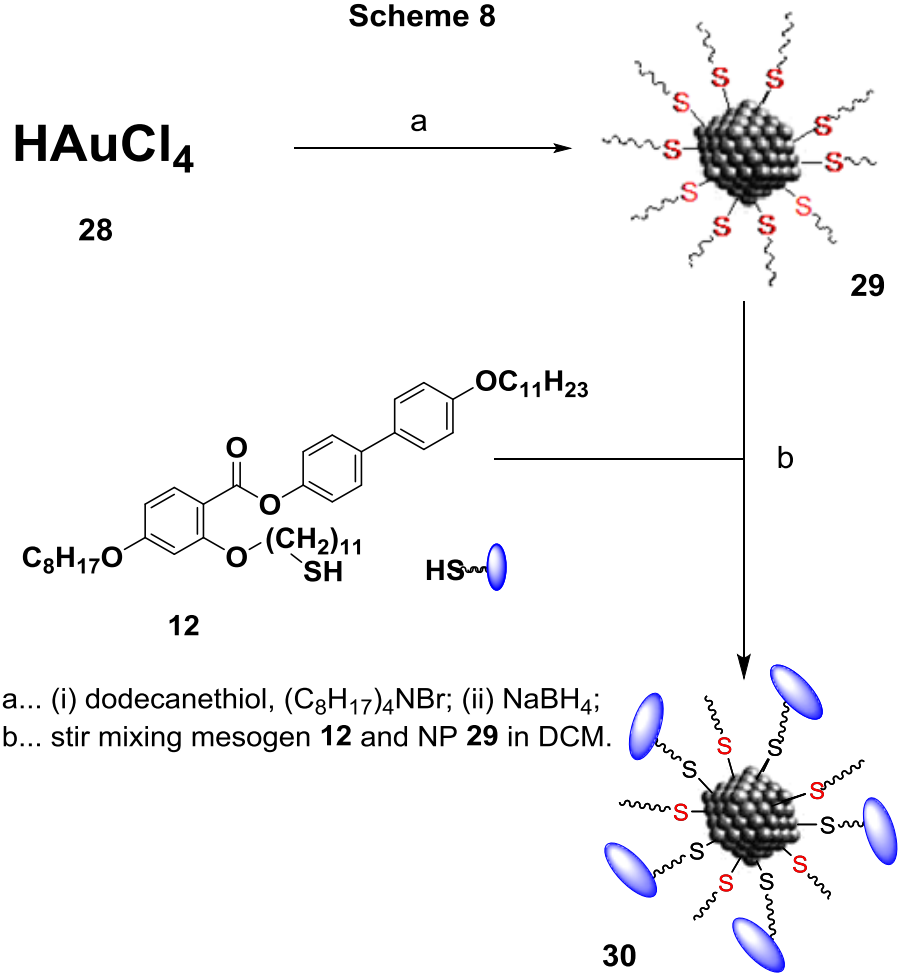

a... (i) dodecanethiol, $(C_8H_{17})_4NBr$; (ii) $NaBH_4$;
b... stir mixing mesogen **12** and NP **29** in DCM.

In this section, the synthesis and properties of AuNPs will be reported. Many different techniques have been developed to synthesize gold nanoparticles (AuNPs) as mentioned in the Introduction section. Followed the previous research done by Cseh *et al*,[152, 153] a modified Brust' biphasic procedure,[116] was used to synthesize desired AuNPs (experimental details are described in the experimental part) with particle sizes ~ 2 nm, which can be used as a source for further reactions. The synthesis followed the standard procedure where a gold salt is dissolved in water and added to a vigorously stirred solution of tetraoctylammonium bromide (TOAB) in toluene. These conditions transfer the gold to the organic phase as evidenced by the change of the colour from yellow to orange. This

is then followed by adding 1-dodecanethiol to the solution, resulting in the lightening of the colour. This colour change reflects the Au (III) is being stabilised in the presence of 1-dodecanethiol and phase transfer agent. This step is followed by the chemical reduction of Au (I)-SR by introducing freshly prepared sodium borohydride ($NaBH_4$). As a result, Au (I)-SR polymers are formed from Au (III) ions and thiol RSH. The organic phase changes colour from orange to dark red under continuous stirring resulting in few seconds. This indicates the formation of AuNPs (Figure 2. 17) and the overall reaction is summarised by equations shown in Introduction section 2. 1.2. The reaction mixture was then concentrated and mixed with excess of ethanol repeatedly at – 18 ^{o}C over night to remove excess 1-dodecanthiol. Finally the product was collected by funnels fitted with frit and washed with plenty of ice-cold acetone and ethanol.

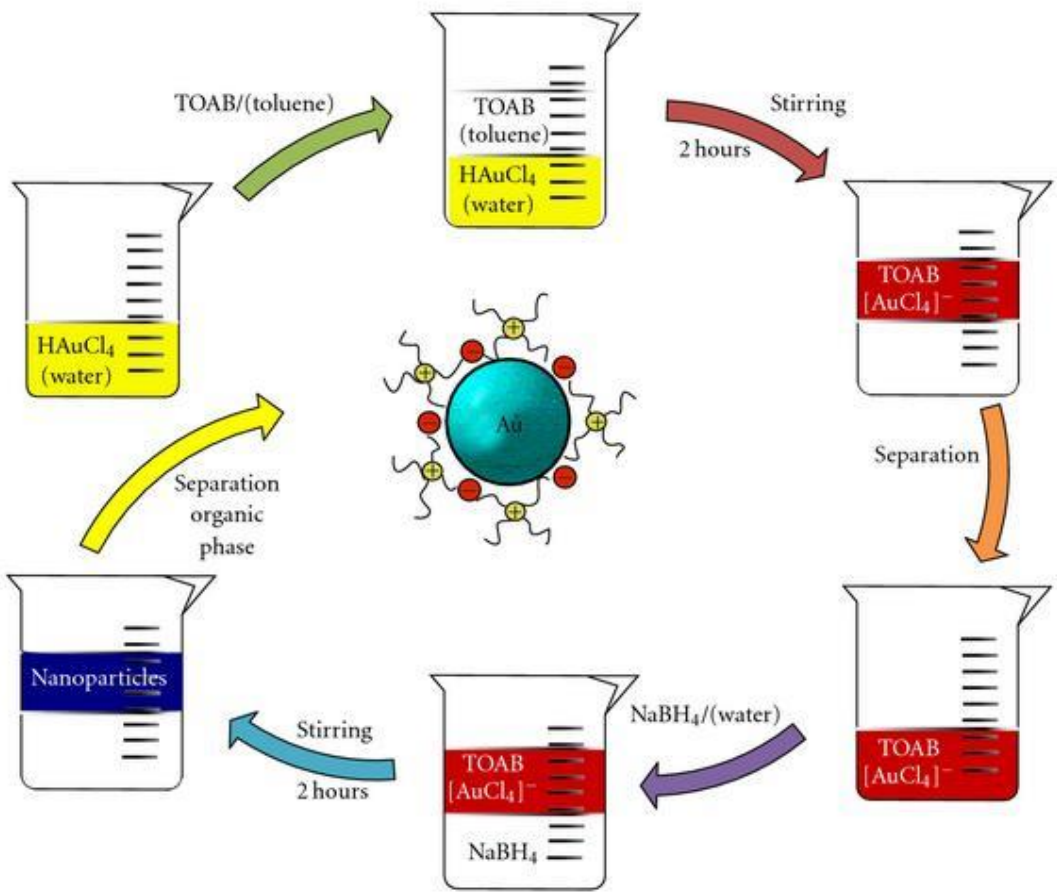

Figure 2. 17. Sketch showing the synthetic steps involved in the Brust synthesis of gold nanoparticles and reaction scheme.[185]

Using the method described above, only a small amount of AuNPs were initially obtained, which were only sufficient for ^{1}H NMR and TEM investigation. A typical example of a

^{1}H NMR spectrum of 1-dodecanethiol and 1-dodecanethiol functionalised gold nanoparticles are shown in Figure 2. 18 below. The sample NMR spectra were used to confirm the chemical attachment of the thiol group of 1-dodecanethiol to the gold cores. The broaden signals peaks of spectra is believed to be caused by a similar effect to that seen in ^{1}H NMR analysis of polymers, where the mobility of alkyl chains is reduced when bonded to the surface of much larger and heavier nanoparticles. When compared to the NMR spectra of the 1-dodecanethiols and AuNPs, the signal peaks at δ 1.10 (ppm) (-SH) and 2.16 ppm (-CH_2-SH) are present in the ligand NMR spectra, but not in the AuNPs NMR spectra. This demonstrates that all 1-dodecanethiol molecules are covalently linked to the AuNPs surface, *i.e.* there are not any free 1-dodecanethiol molecules remaining in the system.[186-188] Under normal circumstances, only 2-3 mg of samples in ~ 1 ml of D-chloroform is sufficient for ^{1}H NMR analysis. However, a large excess amount of AuNPs (20-30 mg) in D-chloroform was used to enhance the signals of the ligands attached to the AuNPs, as only the organic part of sample AuNPs can be analysed by the H^{1} NMR.

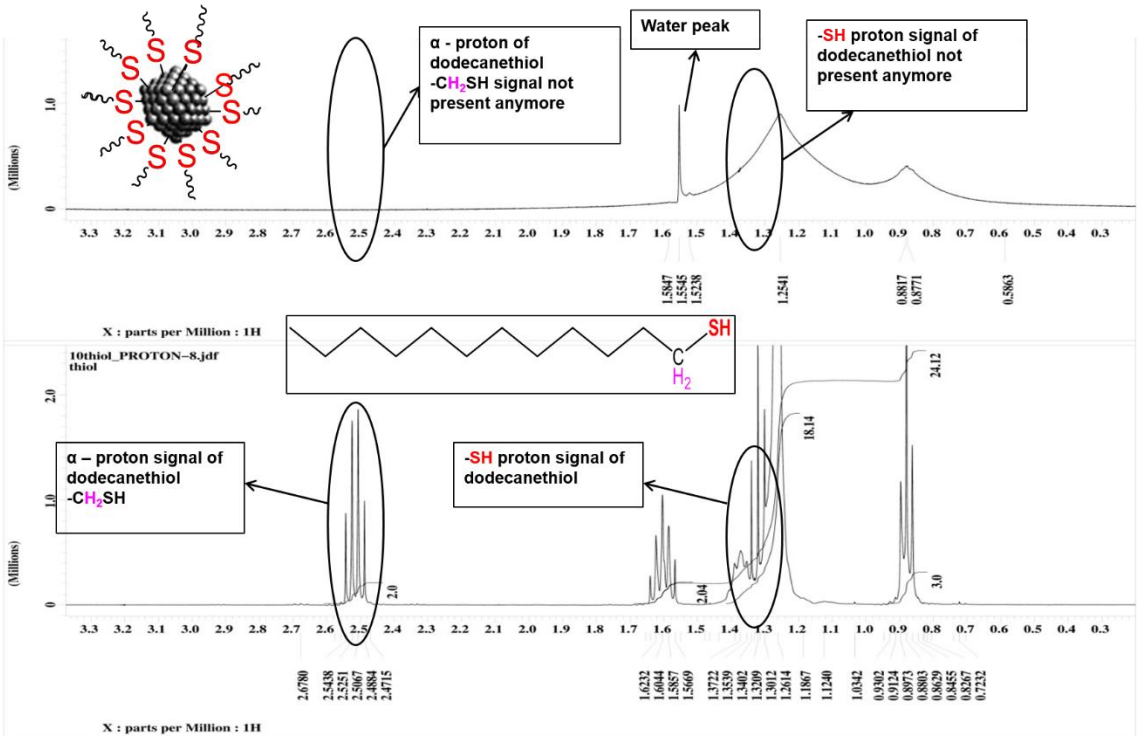

Figure 2. 18. ^{1}H NMR spectrum comparison of AuNPs (top) and 1-dodecanethiol (bottom).

The information about particle size, dispersity of the particles and self-assembly on surface properties were obtained by high resolution transmission electron microscopy (HRTEM). The specimens were prepared by placing a drop of a dilute solution (initial AuNPs in DCM solution was 1 mg / ml and it can be adjusted according to TEM data,

mainly by visual check of the dilution) onto carbon coated copper grids. The TEM sample was air-dried before analysing by HRTEM. Phase contrast images of AuNPs were obtained by using top-entry JEOL 2010EX Transmission Electron Microscope running at 200KV. Images were acquired using a Gatan UltraScan 4000 digital camera.

As shown in Figure 2. 19, the diameters of the AuNPs are approximately ~ 2 nm. It was believed the low concentration of AuNPs TEM sample solution was the reason for the low count number of AuNPs in this initial TEM analysis. As it is important to prepare the TEM sample solution correctly, in order to achieve the optimal TEM analysis condition. Therefore, a suitable TEM sample preparation procedure was required for TEM investigation, and detailed sample preparation investigation will be described in this section.

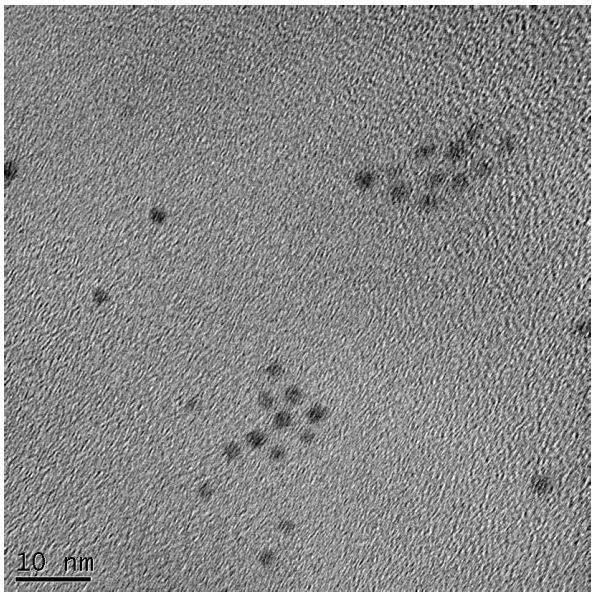

Figure 2. 19. TEM image of the first batch of AuNPs at resolution of 10 nm.

In order to further investigate other properties of AuNPs, a larger reaction scale was necessary to produce sufficient amount of materials. Nevertheless, the major issue was the purification. As the scale of reaction was increased, the nanoparticles purification became rather time-consuming and problematic. Following normal experimental procedures, AuNPs were purified by precipitating twice in ethanol at – 18 ^{o}C overnight for a minimum of 14 hours. As represented in the Figure 2. 24a in precipitation section 2. 3.2.2, the sample polydispersity was poor with a wide particle size distribution. It was suggested that perhaps the concentration of AuNPs was not suitable. Further centrifugation purified AuNPs were analysed by HRTEM and improvement was

minimum (Figure 2. 24b). It was also observed that the particle size of this batch of sample varies between the range of 1 – 5 nm in diameter and possible AuNPs aggregates formed. This indicates undesirable AuNPs with different sizes have to be removed to improve the dispersity. Although the ^{1}H NMR spectra suggested those samples were pure, it was suspected that excess of 1-dodecanethiol might be acting as capping agents for AuNPs and causing aggregation. Additionally, it was noted that the previous batches of AuNPs synthesised were much smaller in quantity and they were precipitated more than twice in ethanol at – 18 ^{o}C overnight for minimum of 14 hours. This implies that further purification might be required to solve the problem. Many tests were carried out to try to purify AuNPs, and three main methods were carried out and compared, they are described and discussed in the sections 2. 3.2.

2. 3.1.1 Larger Gold Nanoparticles Synthesis

During the research project, several parameters were changed to achieve optimal control of this method with their effect investigated systematically on the size, monodispersity and reproducibility of the AuNPs. Parameters varied were the amount of reagents used, reaction stirring speed, purification procedures, speed of reagent introduction and reaction carried out in a presence of nitrogen. As seen in Figure 2. 20, the AuNPs prepared with 1-dodecanethiol and gold salt (thiol : $HAuCl_4$) ratio 1.67:1 on the right has a nanoparticle size of ~ 3 nm, compared to AuNPs on the left prepared from thiol : $HAuCl_4$ ratio 2:1 with nanoparticle diameter ~ 2 nm. It was observed that larger AuNPs could be realised by a decrease of the ratio of thiol : $HAuCl_4$ from 2:1 to 1.67:1. Nevertheless the monodispersity is worse for the size increased nanoparticles. As shown in Figure 2. 20, monodispersity of AuNPs could be improved by further purification procedures, such as repeated precipitation in ethanol at – 18 ^{o}C. All the rest of parameter variations did not improve the monodispersity or had little or no effect on the size. A systematic investigation would be required to fully understand those parameters' impact on AuNPs properties. However, this was not undertaken, as the aim of project was to synthesze sufficient amount of pure sample for further investigation.

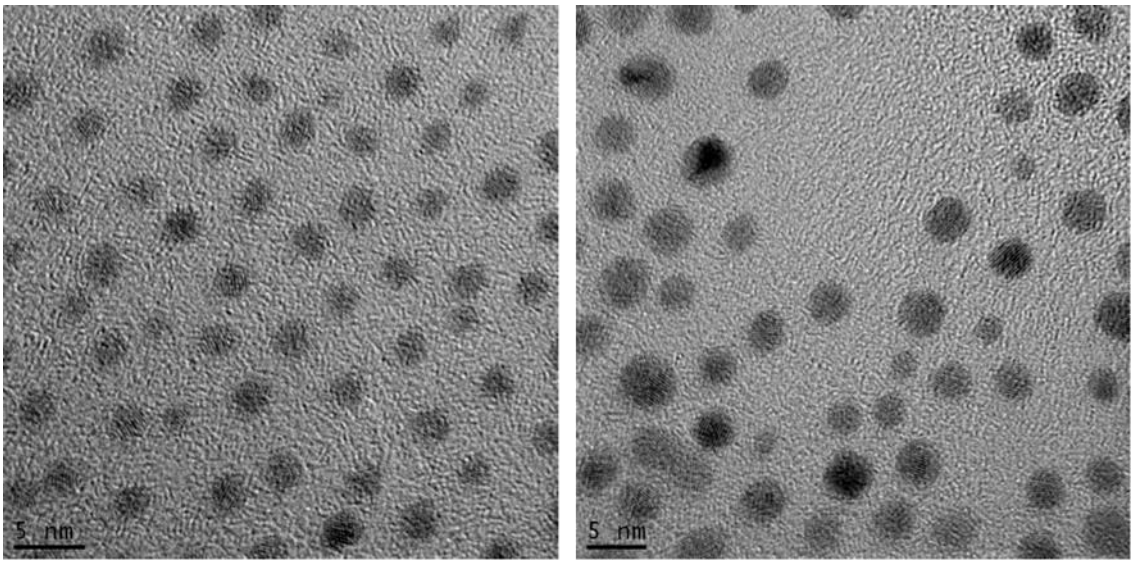

Figure 2. 20. Left: ~ 2 nm AuNPs with thiol: $HAuCl_4$ ratio 1.67:1; Right: ~ 3 nm AuNPs with thiol: $HAuCl_4$ ratio 2:1.

2. 3.1.2 TEM Sample Preparation Investigation

The factors that affect the quality of HRTEM images were investigated thoroughly and is discussed in this section.

It was found that the key to obtain a good image is to have a suitable amount of AuNPs on the TEM grids. Thus the preparation of a suitable concentration of AuNPs suspension in DCM is important. As demonstrated in Figure 2. 21a and b, if the concentration is too high, this results in AuNPs overlapping; too much dilution results in sparsely populated grids and insufficient amount of information obtained. Another considerable factor is that contamination, such as dust or fibres could also influence the TEM analysis (as shown in Figure 2. 21c).

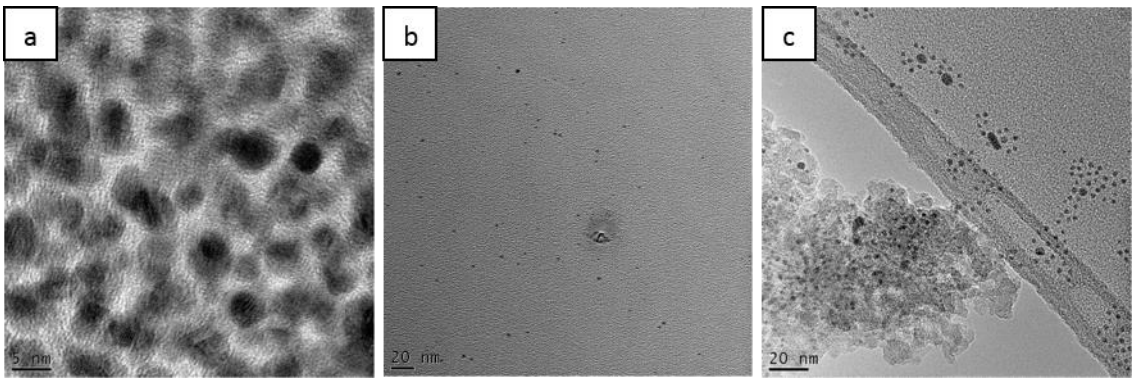

Figure 2. 21. TEM images of AuNPs, a) high sample concentration; b) low sample concentration; c) contaminated.

The first two problems can be resolved easily by optimising the process in trying out different concentrations of sample solution systematically. The last issue of sample contamination is slightly more complicated to solve, as those contaminations could be fibres introduced at any stage. A general good standard of handling samples could help avoiding and minimising contamination. Reaction mixtures should be filtered before evaporation; all samples were stored in a sealed vessel to avoid further contamination, and always filtered through a membrane filter before any analysis, such as GPC, EA and TGA.

2. 3.1.3 Monodispersity Analysis

The monodispersity of final purified AuNPs was determined by Gel Permeation Chromatography (GPC) studies. A solution of approximately 1 mg/ml AuNPs (1-2 ml) in tetrahydrofuran (THF) was firstly prepared. Subsequently, this solution was passed through a membrane filter just before injecting into GPC system. As reported in Figure 2. 22 top section, an analysis of a polydisperse AuNPs results in multiple peaks in the spectra. This study suggested different sizes of AuNPs present. This was confirmed by HRTEM investigations. Thus further purification was required. As shown in Figure 2. 22 bottom section, almost monodisperse AuNPs GPC analysis showed only one major peak and a shoulder in the spectra. This was confirmed by HRTEM analysis. It was calculated that the shoulder represents about ~ 5% of overall AuNPs size distribution.

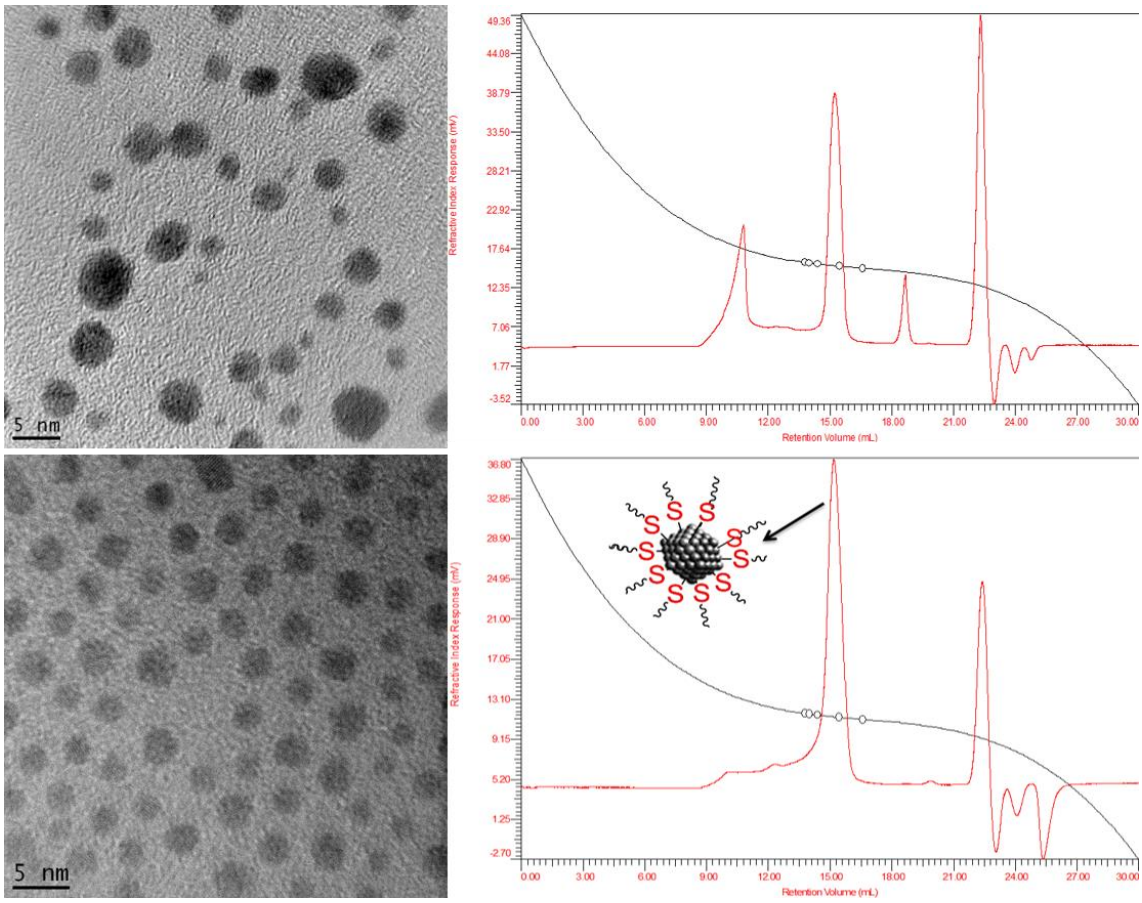

Figure 2. 22. Top section: polydisperse AuNPs TEM and GPC spectrum; bottom section: monodisperse AuNPs TEM and GPC.

2. 3.1.4 Gold Nanoparticles Content Investigation

Having determined the purity and monodispersity of AuNPs, the content of such a material was investigated by Thermo Gravimetric Analysis (TGA), Elemental Analysis (EA) and Inductively Coupled Plasma (ICP) analysis. The product obtained in the AuNPs formation reaction is generally a deep red sticky and waxy solid. One issue in all of these experiments was the stickiness of the materials. This resulted in large loss of materials when transferring to different vessels, simply sticking to surfaces. Thus a method was developed transferring the sample in solution and removing the solvent. This 1-dodecanethiol functionalised AuNPs are soluble in most of non-polar solvents such as toluene, hexane and chloroform. Therefore, a wet method was developed for all analyses required sampler transferring. A solution of AuNPs in DCM was initially prepared and filtered through a membrane filter. It was transferred into a pre-weighed analysis container drop by drop. The solvent of each portion introduced was evaporated before any further additional samples were loaded. It was then placed in an oven at ~ 35 ^{o}C for a slow gentle evaporation. It was finally dried under vacuum at room temperature to

remove any potential moisture. The final mass of sample was determined by an analytical balance and stored in a nitrogen filled dry vessels for further measurement. Although this wet method used was time-consuming, it minimised sample loss during transferring and provided an effective method to maximise the usage of limited amount of sample more efficiently.

This TGA technique was used to determine the weight fraction of the organic part of the hybrids. In this technique, any organic residue is burned off in an inert environment at high temperature and remaining residue is gold, in this case. This instrument measures the weight changes as the temperature increases over the time. The sample was transferred to a pre-weight suitable container via this wet method, approximately 1 – 5 mg of sample were used. Samples were dried according to the method described in the last paragraph. They were then analysed by TGA, heated from room temperature to 950 ^{o}C in the presence of air first, and air cooled to room temperature, followed by heating up again to 950 ^{o}C, but in the presence of nitrogen to avoid any potential oxidisation occurred during the first thermal process. As shown in Figure 2. 23 top chart, it shows AuNPs weight percentage decreases as the temperature rises corresponding over time, and the bottom chart describes the rate of weight loss corresponding to temperature and time. This experiments indicate that 1-dodecanethiol is more readily decomposed when it is linked to the AuNPs surface. The complete thermal decomposition temperature of the 1-dodecanethiol is at 350 ^{o}C, but the 1-dodecanethiol started decomposing from ~ 230 ^{o}C when it is attached to the AuNPs. In most of cases, the complete decomposition of the organic part was complete at ~ 900 ^{o}C. The TGA data indicates that the remaining weight of the sample correspond to the weight of the gold. As a result, such AuNPs sample contains approximately 76% of gold according to TGA measurement. This is close to figures estimated as 75% gold and 25% 1-dodecanethiol according to Brust *et al*[116]. This observation was further proved by Elemental Analysis (EA) discussed in the next section.

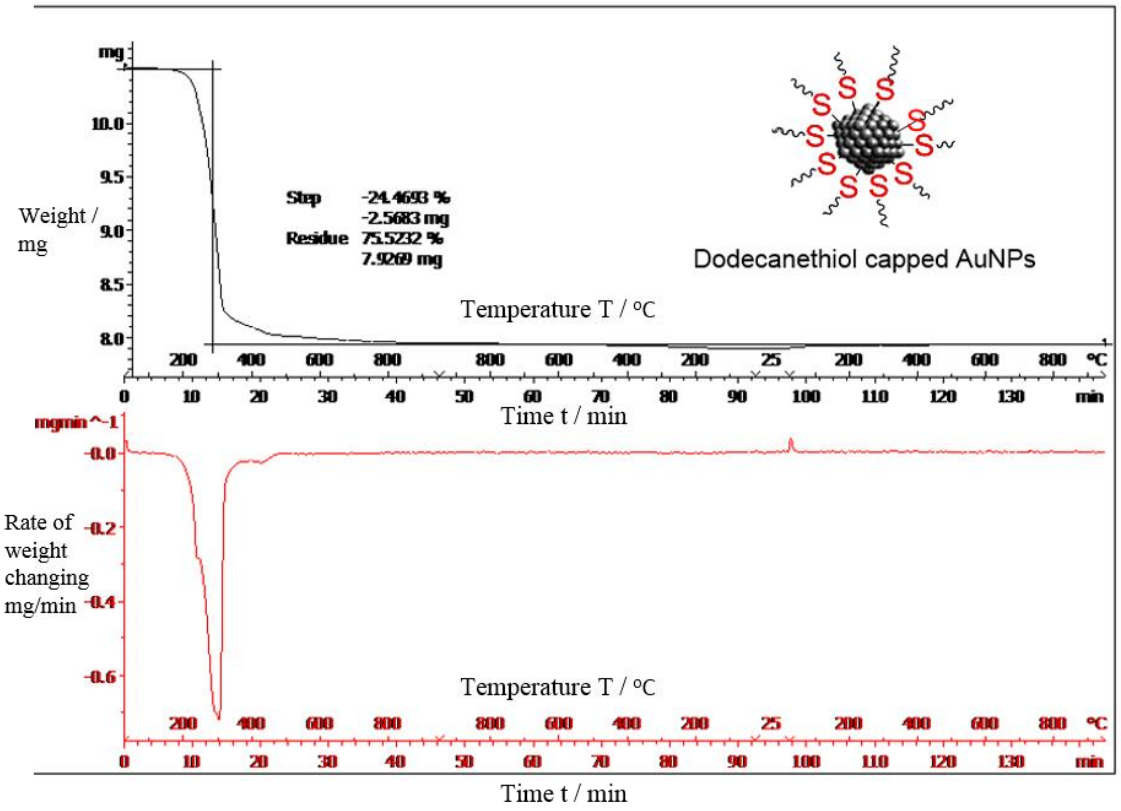

Figure 2. 23. TGA spectrum of 1-dodecanethiol capped gold nanoparticles (AuNPs), top chart: sample loss over time, 76% of residue remain after a full combustion; bottom chart: speed of sample loss mg/ min.

Elemental analysis was taken to determine the mass fractions of carbon, hydrogen and sulphur of AuNPs. This is accomplished by combustion analysis, where the sample is burned in an excess of oxygen, and various traps collect the combustion products – carbon dioxide, water and sulphur oxide. This information is important to help determine the structure of the organic capping agents of AuNPs, as well as to help ascertain the structure and purity of AuNPs. This technique is a process where a sample is analysed for its **C**, **H** and **S** elemental composition. The sample preparation was achieved via the same wet and drying method described in the first paragraph of this section, approximately ~ 1 mg of sample was transferred into a pre-weighted EA sample container before passing to the technician for further analysis. As demonstrated in Table 2. 1, the total percentage of **C**, **H** and **S** present in AuNPs was approximately 22% in average. In general, the **C** : **H** : **S** ratio of pure AuNPs covered only with 1-dodecanethiol is expected to be the same as in pure 1-dodecanethiol, as 1-dodecanethiol is the only organic substance present in such AuNPs system. In comparison with the theoretical results expected for 1-dodecanethiol where the calculated **C** : **H** : **S** ratio (5.5 : 1 : 1.3), the average EA measurement determined by EA is slightly different. This is possibly because of contaminations at any stage of transferring, and possibly due to the trace of solvent dichloromethane (DCM)

vapour trapped in this sticky sample or moisture formed from air when DCM evaporates. This could also be caused by incomplete combustion. Extensive studies of the AuNPs content was also carried out by Inductively Coupled Plasma (ICP) as described in the next section.

Exp.	**C%**	**H%**	**S%**	**Total**	**Experiments** **C : H : S**	**Theoretical** **C : H : S**
Exp. 1	13.97	2.51	3.49	19.97	5.6 : 1 : 1.4	5.5 : 1 : 1.3
Exp. 2	16.24	2.72	3.60	22.56	6.0 : 1 : 1.3	
Exp. 3	16.20	2.79	3.40	22.39	5.8 : 1 : 1.2	
Average	15.47	2.67	3.50	21.64	5.8 : 1 : 1.3	

Table 2. 1. Theoretical and experimental C, H and S percentages of gold nanoparticles (AuNPs) capped with 1-dodecanethiol determined by EA.

Inductively coupled plasma (ICP) is a type of plasma source. The energy is supplied by electric currents which are produced by electromagnetic induction that is by time-varying magnetic fields. The sample was transferred to a Teflon container via the same wet and drying method as discussed in the first paragraphs of this section. Approximately 10 mg of sample was required. It was then dissolved in aqua regia before passing to the technician for analysis. The gold and sulphur proportions of the AuNPs were determined to be 66.524% and 2.755% respectively. This preliminary evidence from ICP was rather disappointing when compared to TGA and EA analyses. There are a number of possible reasons for this discrepancy. Beyond instrumentation related systematic reasons, the difference could be associated with contamination during the process of sample preparation. Inaccurate sample weight recording could also be a reason, as the Teflon sample container is much heavier when compared to the amount of sample added (100x heavier). Additionally, sulphur is not typically considered to be an ideal analyte for ICP, because of a combination of relatively low ionisation and high background levels. Sulphur has three isotopes at masses 32, 33 and 34. Each isotope is subject to polyatomic interference in the presence of oxygen, such as $^{16}O^{17}O$, $^{16}O_2^+$ and so on. One reason for this low sulphur percentage measurement could be the insufficient plasma conditions with not enough carrier gas flow and long sample depth to promote the formation of the stable

SO^* molecular ion.[189] In comparison with TGA and EA, this technique requires a much larger amount of samples, more than what could be afforded for continuous and extensive studies. Therefore, optimal analysis conditions could not be developed due to the lack of sample available, and this analysis technique was abandoned for any future samples analysis.

2. 3.2 Gold Nanoparticles Purifications Techniques

2. 3.2.1 Centrifugation

Centrifugation is a common purification technique in preparation of metal nanoparticles research.[49, 68, 123] Thus, a centrifugation technique was introduced to remove any unwanted excess of capping agents and any AuNPs with undesired size. Samples were transferred to a centrifuge tube with minimum amount of DCM, followed by adding ethanol to two third of the tube before centrifugation. The centrifugation was carried out at a speed of 6000 rpm for 5 minutes and repeated with fresh ethanol. The same procedures were followed with ethanol replaced by acetone. As shown in Figure 2. 24b, there was not any obvious improvement of the AuNPs dispersity after centrifugation. This might be due to the negligible weight difference between small and large particles, as they are both already heavy enough to be separated by centrifugation, or perhaps a slower centrifuge speed may work better. Furthermore, according to literature, centrifugation is generally used to separate metallic nanoparticles from excess stabiliser agents, usually small organic molecules, which are much lighter in weight when compared to metal, and thus, much easier to be separated by centrifugation.

This technique for the gold nanoparticles purification in this project may be improved by trying out different washing solvents, centrifugation time and speed. However this was judged to be time-consuming and ultimately out of the scientific focus of the project. Therefore, this technique was abandoned.

2. 3.2.2 Precipitation

After evaluating the literature and previous synthesis, it was suspected that further precipitation in ethanol may be required. As this is at a much larger synthetic scale when compared to the literature and previous synthesis. Therefore this batch of sample was divided into few small portions, roughly the size according to the literature.[116] Each portion of sample was dissolved into minimum amount of toluene (< 10 ml). They were then introduced drop-wise slowly to 400 ml of ethanol pre-cooled at – 18 ^{o}C, in order to reduce any sample loss. This mixture was kept at – 18 ^{o}C overnight for minimum 14 hours before filter through a frit funnel pro 3, followed by washing the residue with cold ethanol and acetone. The residue was air dried before collecting from the funnel by washing with

DCM. The same procedures were carried out again after evaporating DCM. This procedure could be repeated further if needed.

As seen in Figure 2. 24c, there are some significant changes after precipitation in ethanol at – 18 ^{o}C overnight repeatedly for few more times. The shapes of AuNPs are more uniform and particle monodispersity was improved when compared with samples before further purification (Figure 2. 24a and b). However, the particles dispersity is still not as good as the previous work, this is possibly due to the large reaction scale and possibly due to the pre-cooled ethanol used for precipitation. Pre-cooled ethanol prevented sample loss, but kept all gold nanoparticles with different sizes. Overall, this precipitation purification method was used extensively in the future synthesis and produce results permitted further characterisations.

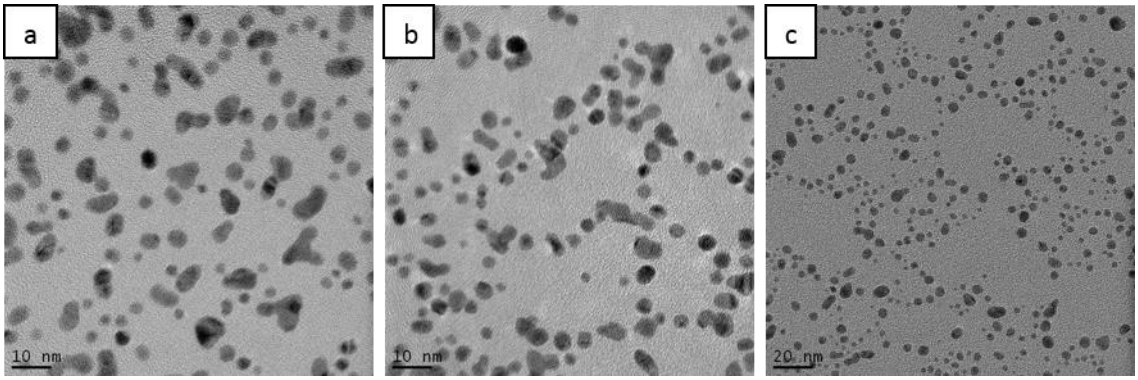

Figure 2. 24. TEM images of AuNPs, a) precipitated twice, resolution at 10 nm; b) same sample with further centrifugation purified TEM analysis, resolution at 10 nm; c) precipitation 3-5 times, resolution at 20 nm.

2. 3.2.3 Ultra-Sonication

Followed by previous research work carried out by Cseh *et al*,[152, 153] sonication can also be used to purify gold nanoparticles.

Gold nanoparticles were collected after all solvent were removed and the residue mixture was collected on the bottom of flask by using minimum amount of DCM, then either air-dried or slowly evaporated in a low heat water bath. Sufficient amount of ethanol was then added to cover this dried residue mixture, before being placed in a sonication bath for 2 – 5 minutes with gentle heat or at room temperature. The solvent was carefully poured away and a filter paper could be used to prevent any loss of sample. The same process was repeated again with ethanol, followed by sonication in acetone twice. The final solid was further dried under vacuum. It was considered that gentle "shake" produced by sonication may be able to loosen any excess of capping agents and other

impurities trapped the residue mixture. This may also be able to "shake" apart any aggregated gold nanoparticles. The final sample was not pure according to ^{1}H NMR analysis, this was possibly due to the insufficient sonication input. However the main concern was that the gold nanoparticles structures conformation may be destroyed if a longer time of sonication was applied, as ultrasound is a very powerful technique that can easily break aluminium foil.[190]

Although this was not a suitable method to purify gold nanoparticles on its own, it was used extensively in combination with precipitation purification method. Gold nanoparticles were further purified by sonication in ethanol and acetone after collection from precipitation. It was sufficient to remove small amount of impurities that are still present in sample after precipitation.

Overall, the best way to purify AuNPs is to precipitate in ethanol at – 18 ^{o}C repeatedly between 3 – 5 times, followed by ultra-sonication if there still small amount of impurities remain, or further precipitation in cold ethanol until all of the impurities are removed.

2. 3.3 Synthesis of Liquid Crystal Gold Nanoparticles

Synthesis of liquid crystal gold nanoparticles (LC AuNPs) were carried out in a solvent-mediated ligand-exchange reaction according to Cseh *et al*,[152, 153] using dodecanethiol functionalised AuNPs and the thiolated mesogens (**11** and **12**) as building blocks and mixing in DCM at room temperature (Scheme 8).

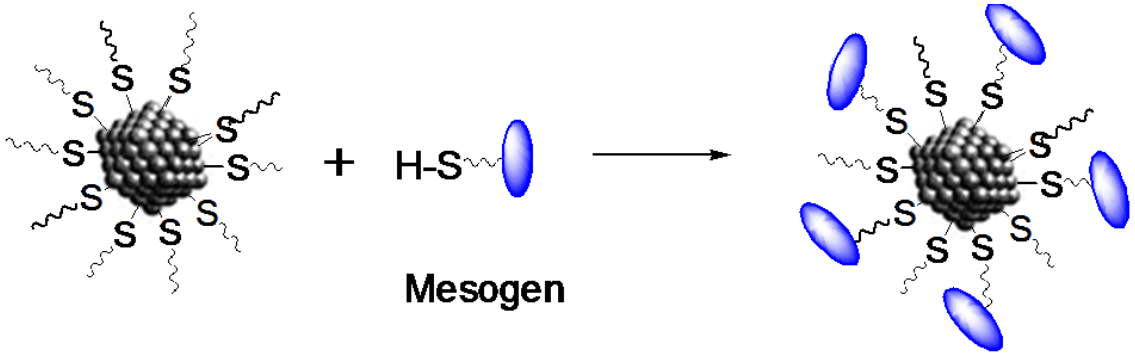

In the thiol-to-thiol exchange reaction, the amount of thiolate mesogens used was 1.5 fold molar excess compared to the ligand of 1-dodecanethiol capped on AuNPs surface. The mixture was stirred at room temperature for several days. This allowed a sufficient amount of mesogen ligands exchange-reaction to take place. The duration of exchange reaction time allows, within limits, a control of the number of mesogens attached to the nanoparticles. Similar research on time progress of exchange reactions of ligands on gold nanoparticles has also been done according to Lennox *et al*.[71] In order to investigate the mesomorphic behaviour, chemical and optical characterisation of LC AuNPs, it is crucial to remove all the excess free 1-dodecanthiol and thiolated mesogens. This assures that the measured properties are not from those free ligands. A full discussion regarding on purification techniques used in this part of experiment will be discussed in the next section 2. 3.4.

Similar to its precursor, the LC AuNPs are also deep red sticky and waxy solids. Additionally, they are air-stable for months and soluble in chloroform, toluene, dichloromethane, hexane and other non-polar solvents. Thus this wet deposition method described in the previous section 2. 3.1 was also deployed here for other sample transferring.

The purity of LC AuNPs were confirmed by ^{1}H NMR spectroscopy (Figure 2. 25) before being characterised by EA, GPC, TEM and TGA. As described in the ^{1}H NMR

spectroscopy below, the broadened signal is also due to the large AuNPs effect. Similarly to 1-dodecanethiol functionalised AuNPs ^{1}H NMR spectra, the final LC AuNPs ^{1}H NMR spectra were compared with the NMR spectra of the mesogen, the signal peak of this α-proton (-CH_2-SH next to the thiol functional group) at δ 2.48 ppm presents in the mesogen NMR spectra, but not in the NMR spectra of LC AuNPs. This undetected signal indicates all ligands are covalently linked to the AuNPs.[186-188]

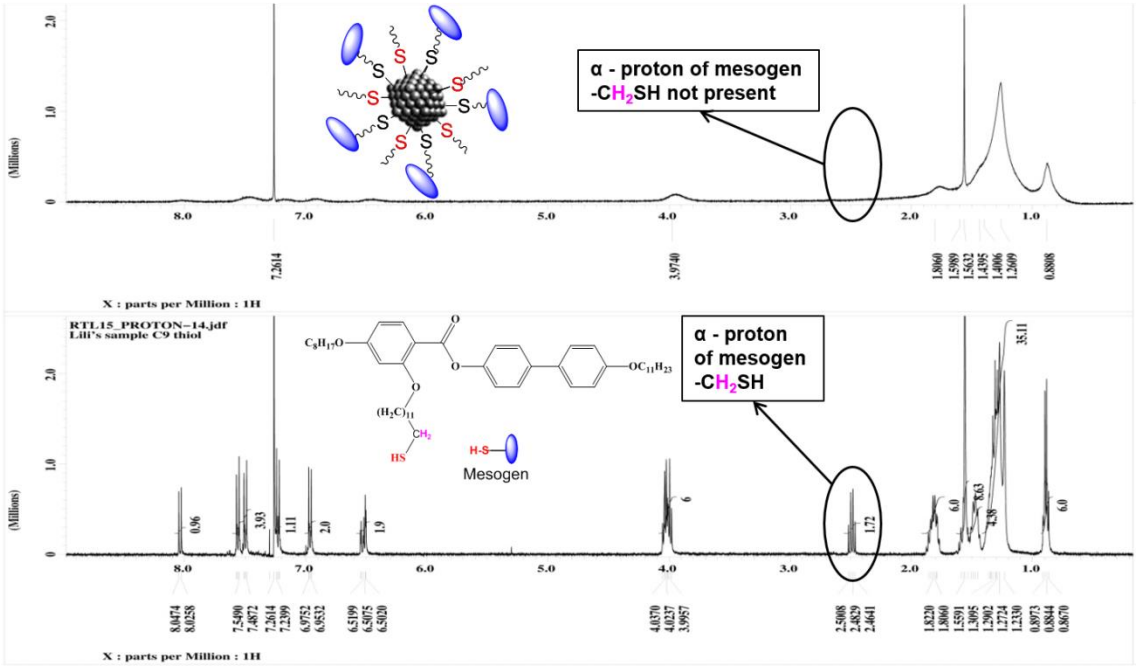

Figure 2. 25. NMR spectrum comparison of LC AuNPs (top) and thiolated mesogen (bottom).

The ultimate goal of this project is to synthesise AuNPs with liquid crystals properties. Hence before any other analyses were carried out, the mesogenic properties of the final LC AuNPs was investigated immediately after purity check by ^{1}H NMR.

2. 3.3.1 Optical Polarising Microscope Studies

Optical Polarising Microscopy (OPM) analysis was attempted to determine birefringence of LC AuNPs. Usual mesogen OPM analysis technique procedures were initially followed. As demonstrated in the Figure 2. 26a and b below, OPM images were taken under crossed polarisers at room temperature and 70 ^{o}C. The LC AuNPs OPM sample was prepared either by a spatula transferring onto a glass slide, or place a drop of sample with solvents that can be easily evaporated, such as DCM. In both cases, the glass slide surface was wiped with clean paper, washed thoroughly by ethanol and acetone. However, it was observed that light could not pass through the sample, even at 70 ^{o}C which is above the transition temperature of mesogen used to functionalise the AuNPs. As discussed in

previous section, this type of samples are very dark coloured and waxy sticky solids due to the content of gold. Therefore it was not possible to visualise any birefringence under the microscope.

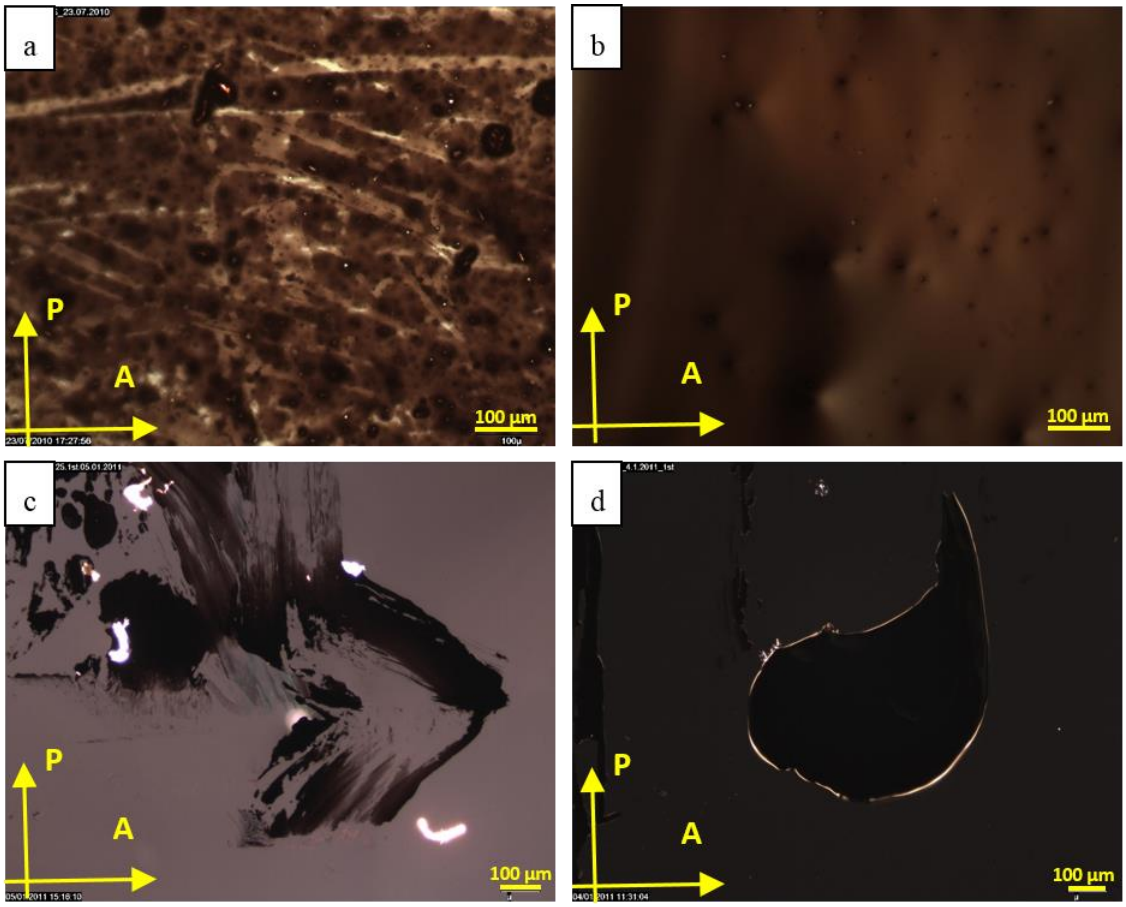

Figure 2. 26. OPM images of LC AuNPs, a) room temperature; b) at 70 ºC; c) contaminated sample; d) sheared sample showing birefringence at the edge of sample.

In order to overcome this issue, the sample was monitored under polarised microscope as the temperature was rising and decreasing. It was also left on a hot-stage annealing overnight and at different temperatures, both above and below mesogen isotropisation temperatures were tested. The aim of annealing was to provide sufficient thermal energy and time to re-align. It was observed that the sample texture become soft gradually from 100 – 200 ºC, however this is an irreversible process and that sample decomposition occurred at high temperature possibly close to 200 ºC. Nevertheless, none of those usual liquid crystal microscopy techniques could produce any evidence of liquid crystal properties present from this final sample. It is worth mentioning that all procedures needed to be carried out in a clean standard way, strictly to avoid contamination, or samples could be ruined by dust as shown in Figure 2. 26c. Therefore, all samples that

used to be transferred by this wet method should be filtered and kept in a clean and inert environment.

During the OPM sample preparation optimising process, it was discovered that birefringence could be obtained with a very thin sample film. As represented in Figure 2. 26d, samples were sheared onto glass slide by a spatula in one direction, and birefringence could be noticed at the edge of sample, where the sample thickness is very thin when compared with the middle area. Thus, a suitable thickness layer was the key to allow enough light passing through the sample. As gold is one of the known noble metal that reflects visible light and with close to 100% infrared reflectance for wavelengths greater than 700 nm. The use of gold as a reflective coating can be achieved at minimum cost by employing films just "thick" enough to develop full reflective properties to achieve zero transmission. This thickness has been measured using thin gold films on glass and found to be about 100 nm, which only require two grams of gold to cover one square metre with a film of such thickness. It is so robust, it is even used as a reflective coating on the visors of astronaut's space helmets, which protects astronaut avoiding heat generated by radiation from the Sun and any other light sources in space. In this application, the reflective film has thickness of ~ 50 nm, which serves a dual purpose as it is in addition an optical coating to reduce glare from sunlight while admitting sufficient light for good vision.[191] Therefore, it is important to prepare an OPM sample with a thickness less than 100 nm to have enough light transmitted through sample and observe birefringence. One of the OPM sample thickness was measured with atomic force microscopy (AFM) by collaborators from Switzerland to be less than 100 nm, which will be further discussed in section 2. 3.3.8.[192] A full description of thin layer of OPM sample preparation is described in the following section.

2. 3.3.1.1 OPM Sample Preparations

Various techniques were attempted to fabricate a thin layer, such as drop casting with solvent evaporates either fast or slow, using different substrates, shearing samples with different tools (capillary glass rods, metal spatulas, edges of glass slides, metal pieces and even sample vials) at different temperatures and so on.

Drop casting

The most common solvents used were DCM and toluene to give a fast and slow evaporation, as this might lead to the samples arrange themselves into large, visible light sized domains. However, it was found that samples tended to move to the edge of droplets regardless fast or slow solvent evaporation, creating a ring like mark on glass slide as shown in Figure 2. 27. This was attempted with different solvents and similar results were obtained.

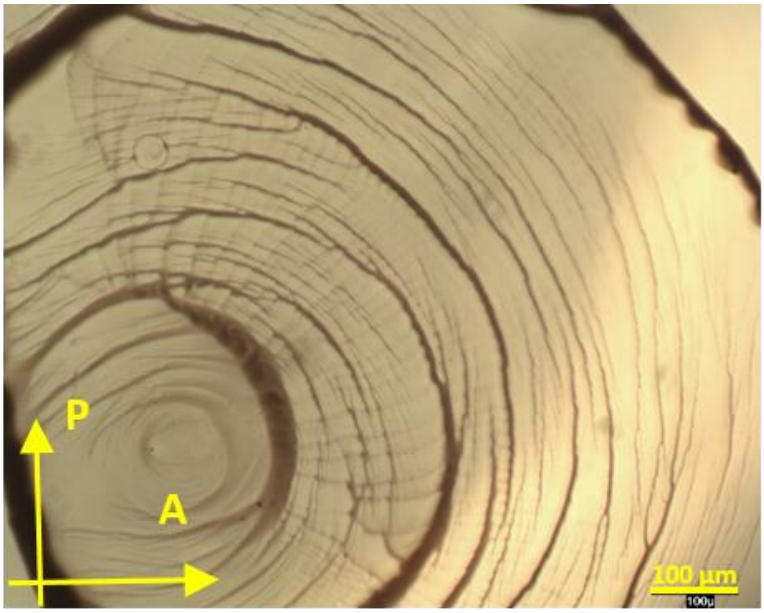

Figure 2. 27. OPM image of LC AuNPs drop casting deposited on glass slide after solvent evaporated at room temperature.

Wet brushing

The outer surface of a capillary glass rod was used as a brush, which was firstly dipped into a LC sample solution in DCM or toluene, followed by a quick brush onto a glass slide before it dried on the capillary glass rod. Nevertheless, most solvents dry quickly and when DCM was used, the result was loss of samples on the capillary glass rods. Even when toluene was used, it was still difficult to place a capillary glass rod evenly on a glass slide and applying an even force gently without any breakage. Sample vials were also used, but no significant improvement was observed.

Shearing

The initial test was carried out with glass slides and small metal plates with large flat sharp edges. The idea was to place the edges of objects on one side of a sample lump and shearing towards one direction with an even force applied, a process somewhat like a pancake preparation. Unfortunately, the result was not as good as expected in the beginning. As can be seen in the Figure 2. 28 below, the sharp edge of metal and glass slide would damage the sample glass slide surface and introduced small glass chips. On top of that, an even thickness of thin layer could not be fabricated. A large number of tools were tested, different temperature and even shearing in combined with drop casting at the same time, the problem with introducing glass chips still remained. However, it was noticed that using slightly higher temperature could make the sample softer and improve the shearing process.

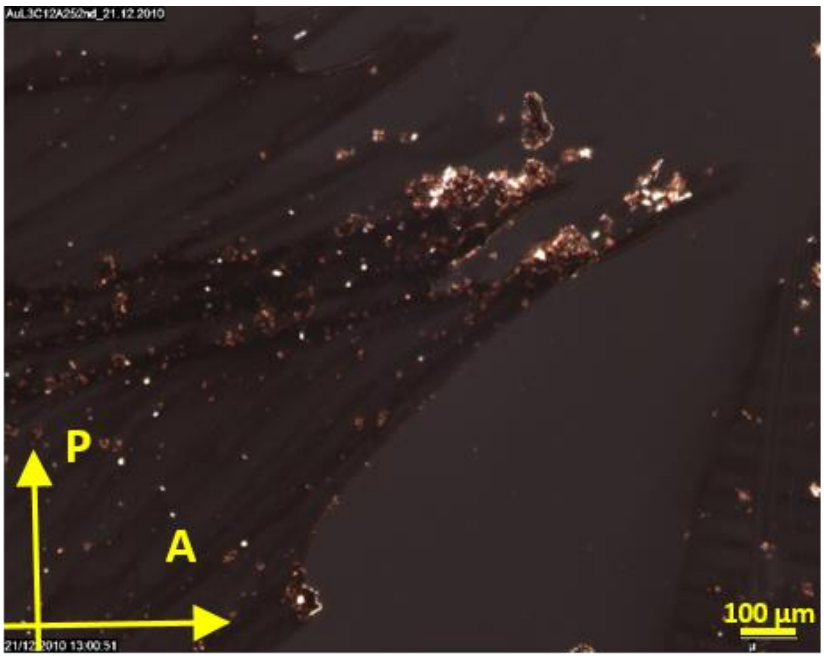

Figure 2. 28. OPM image of samples mixed with glass chips introduced by shearing with sharp objects.

Eventually, it was found that thin films could be fabricated by pressing and moving samples in between cover slide and glass slide together after annealing. As shown in Figure 2. 29, the birefringence is much more obvious with thin film of samples, as sufficient amount of light could be passed through. Although an even thickness layer could not be fabricated, it has constructed thin layers in many regions at a much smaller scale, hence the birefringence.

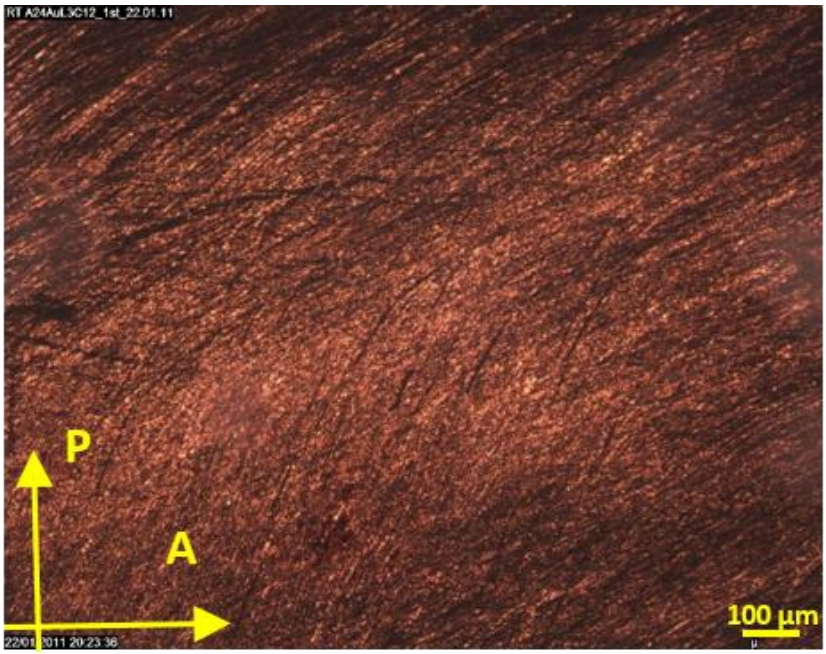

Figure 2. 29. OPM image showing birefringence of sample at room temperature after shearing by pressing and moving samples in between cover slide and glass slide.

Shearing by a small spatula could also produce thin layers in multiple regions at a slightly bigger scale. This spatula must have flat even edge and has to be strong, but flexible at the same time to be able to absorb excess force applied without breaking the glass slide surface. Shearing should be applied in one direction or circling around while moving in one direction, with applied force as even as possible. Heat treatment could also be introduced by annealing the sample on a hot-stage for half an hour or overnight to make the shearing process easier. As illustrated in Figure 2. 30 below, the thin layer area produced is much larger when compared to the formal method. Thus they were used to illustrate the birefringence of this sample. The image on the left is showing light reflections of the middle area. After 90 degree rotation at the same position, the light reflections of this middle area changed when compared with image on the left. This is a clear indication of birefringence. It was possibly due to mesogen molecules alignment caused by the physical shearing of the sample in one direction, which resulted the observation of liquid crystal birefringence property.

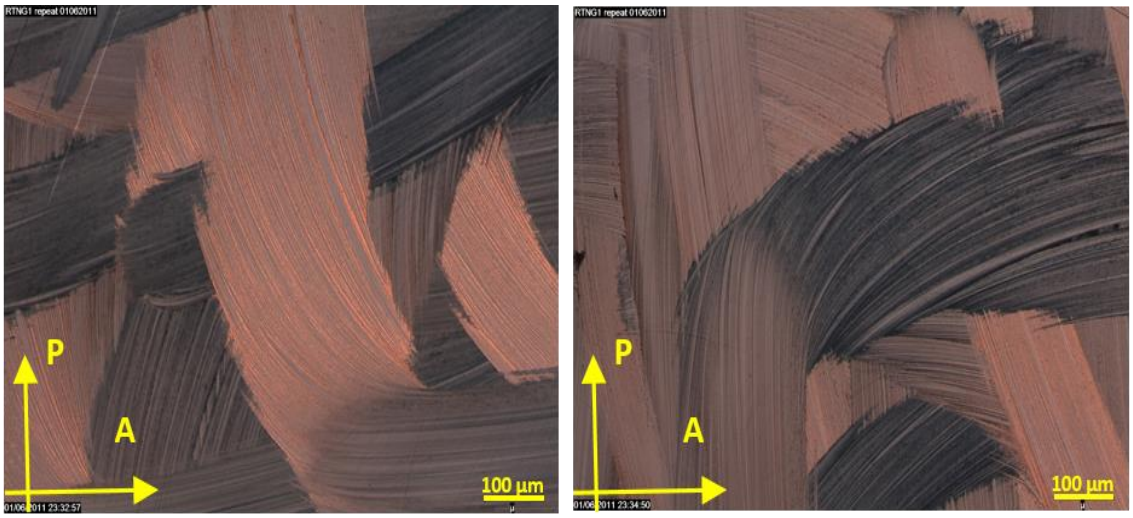

Figure 2. 30. OPM images of sample after shearing by a spatula showing birefringence at room temperature, sample at 0 degree (left) and same position with sample rotating 90 degree (right).

It was pointed out that waxy texture and lack of typical liquid crystals defect textures of the final LC AuNPs, were probably owing to AuNPs metal core, as all mesogen molecules were restricted in this motion to self-assembly easily due to the attachment on a large mass metal core.

2. 3.3.2 TEM Analysis

HRTEM was applied to study the particle size, monodispersity and self-assembly properties of LC AuNPs. The resolution of HRTEM is significantly higher than light microscopy, allows observing objects of a few angstroms. The contrast depends on the electron density of the material, which enables us to observe the gold core, due to its high density. However to characterise nanoparticles with diameter smaller than 2 nm is not easy, as the metal core diameter below this range cannot be distinguished easily from the carbon coated background of the copper grids. The same TEM sample preparation procedures were followed as described in previous section 2. 3.1.2. As represented in Figure 2. 31 below, the nanoparticles were characterised by HRTEM images and size distribution graphs.

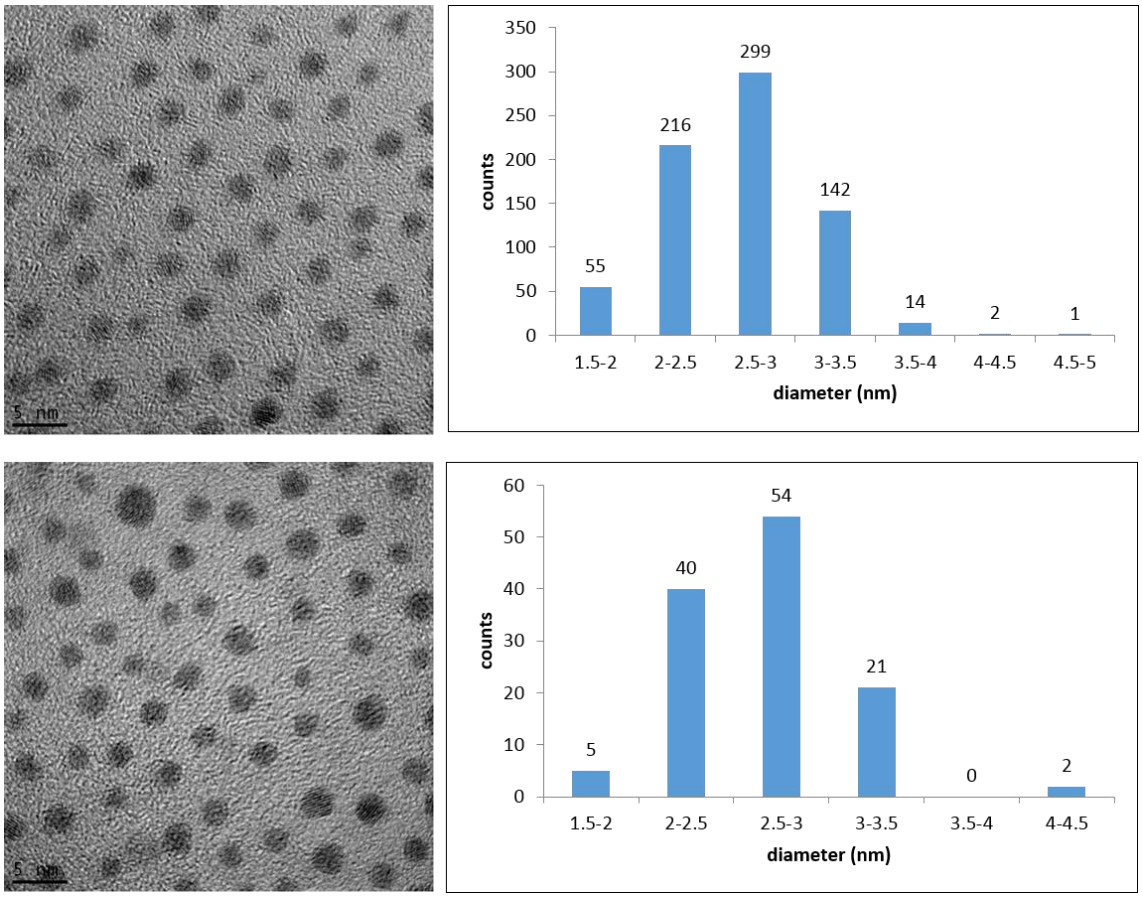

Figure 2. 31. TEM images and size distribution graph, sample NG1 (top) and NG2 (bottom).

The size of nanoparticles was determined by ImagePro Plus 6.0 version of software. The software ImagePro Plus 6.0 was used to measure several hundreds of NPs. The auto-count mode of creating a binary full image to count and size measurements were unfortunately not useful in this case. This was due to the fuzzy background created from the carbon atoms of the grid observed under high resolution. Therefore each nanoparticle had to be counted visually with the software ImagePro Plus 6.0. The diameter of nanoparticle was measured a few times by drawing a line cross the centre of the nanoparticle. The software automatically recorded the length into a spreadsheet and each nanoparticle was measured 4 times to provide much more accurate information. The number of nanoparticles measured were as many as possible, depending on how many TEM images were available. Eventually, the mean diameter of LC AuNPs was calculated along with standard deviation. The number of gold atoms per particle was determined based on the LC AuNPs diameter by the formula[193, 194] as displayed below. Some results calculated by this equation are shown in the next section.

$$N_{\mathrm{Au}} = \frac{4 \times \pi \times R^3}{3 \times v_{\mathrm{g}}} = \frac{4 \times \pi \times D^3}{8 \times 51}$$

Equation 2. 1. *R* – radius of nanoparticle (Å); *D* – diameter of nanoparticle (Å); v_g – volume of gold atom (v_g = 17 Å^3)[145, 152, 153]

2. 3.3.3 Mesogenic Gold Nanoparticles Content Investigations

The proportion of the co-ligands and mesogen ligands to the AuNPs surface area was estimated by evaluation of ^{1}H NMR, EA and TGA spectra. Due to the possible ligands ratio calculation errors from the ^{1}H NMR spectra broadened peak and possible insufficient combustion efficiency from all thermal analysis techniques, the final calculated results by those three techniques analysis has to be corroborated by each other, they can only provide some close estimation of this final sample content.

The TGA sample was prepared via this wet method and dried with the same method as mentioned in the previous sections. The TGA was programmed to thermally heat the sample from room temperature to 950 ^{o}C in the presence of nitrogen. The result showed the degradation temperature of the 1-dodecanethiol occurs at ~ 230 ^{o}C as expected (also found in the previous section 2. 3.1.4). The weight percentage was taken at the temperature when all 1-dodecanethiol was decomposed at ~ 350 ^{o}C. In most cases the complete decomposition of the organic part was complete between 550 ^{o}C to 600 ^{o}C. The TGA data indicates that the remaining weight of the sample correspond to the weight of the gold. The thermal decomposition of the organic part appears to occur in more than one stage: the first stage is the result of the more rapid degradation rate of the 1-dodecanethiol, and the further stage is the decomposition of the mesogen ligands. One example of LC AuNPs (**NG1**) TGA spectra is shown below. The TGA analysis for sample **NG2** determined the gold content to be 55% as shown in Figure 2. 32 below. However, the EA of **NG2** could not be measured due to insufficient amount of sample.

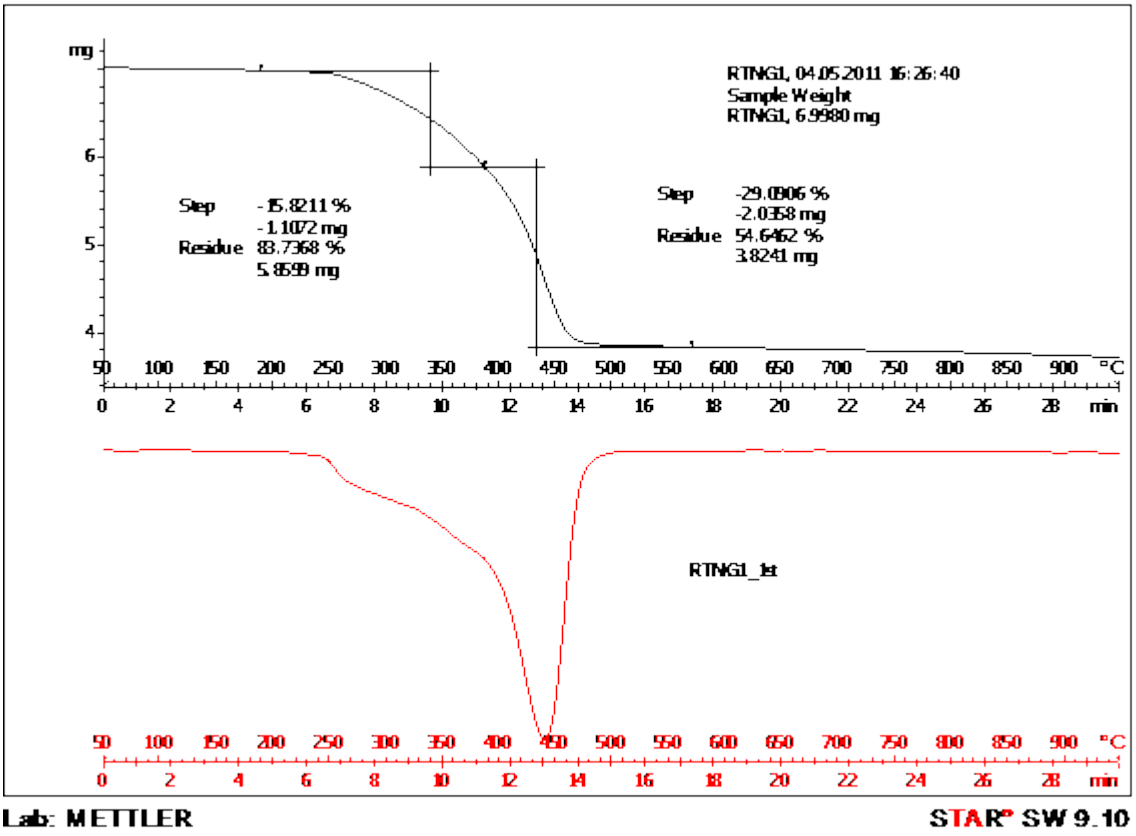

Figure 2. 32. TGA spectrum of sample NG1 showing gold content of 55%.

The percentage of **C**, **H** and **S** for the rest of organic part of sample **NG1** were investigated by EA. The same wet method was used to prepare the sample, which was passed to a technician for EA analysis. The obtained results are presented in the Table 2. 2 below.

Sample	**C**%	**H**%	**S**%	**Total**	**Au**% by TGA
NG1	34.53	4.65	1.85	41.03	54.25

Table 2. 2. Elements C, H and S analysis of sample NG1

Unlike its precursor 1-dodecanethiol functionalised AuNPs, there are mixed ligands of 1-dodecanethiol and mesogen in LC AuNPs. Thus, it is more difficult to estimate an exact fixed **C** : **H** : **S** theoretical ratio for comparison with experimental data, as the ratio of co-ligands and mesogen ligands varies. Nevertheless, EA provided additional information about the total amount of **C**, **H** and **S** presented in the sample, which is 41.03% in this case. The other 5% was suggested to be the content of **O**, which could not be detected by the instrument, as it was given off in a form of gas and water vapour. Overall, this allows for an estimation on the sample content, which is also supported by the TGA results. The results achieved by EA and TGA were also used to calculate the number of co-ligands

and mesogen ligands in conjunction with ^{1}H NMR spectra by signal integration ratios.[152, 153, 195] These calculations allow us to determine the ratio (co-ligand: mesogen ligands) and number of co-ligands and mesogen ligands. All values are presented in the Table 2. 3 below.

Sample	Diameter Mean / nm	Standard Dev.	Au Atoms Number / per particle	D. thiol / Mesogens Ratio	Exchange reaction time
NG1	2.64	0.447	568	0.64 : 1	3 days

Table 2. 3. Sample NG1 content estimation with particle size, total number of Au atoms and ligands ratio.

As presented in the Figure 2. 33 below, the ^{1}H NMR spectra of LC AuNPs, mesogen and 1-dodecanethiol were compared. The particular signal integration was compared to determine the ligand ratio (1-dodecanethiol : mesogen ligand) on LC AuNPs surface. The signal at δ ~ 3.8 ppm could only be originated from the three methylene *α* carbon proton (-CH_2-O-Ph-). This is owing to the electronegativity of the oxygen group of the ether group (-O-). Thus it definitely is not from the 1-dodecanthiol. The signal at δ ~ 0.8 ppm of LC AuNPs is from all methyl group protons (-CH_3) of both mesogen and 1-dodecanethiol. Therefore the ratio of ligands could be estimated, if the signal at δ ~ 3.8 ppm was used as an indicator to integrate the signal peaks at δ ~ 0.8 ppm. Nevethless, these can only be used as estimations as the broadened peak of the ^{1}H NMR spectra does not permit a precise calculation.

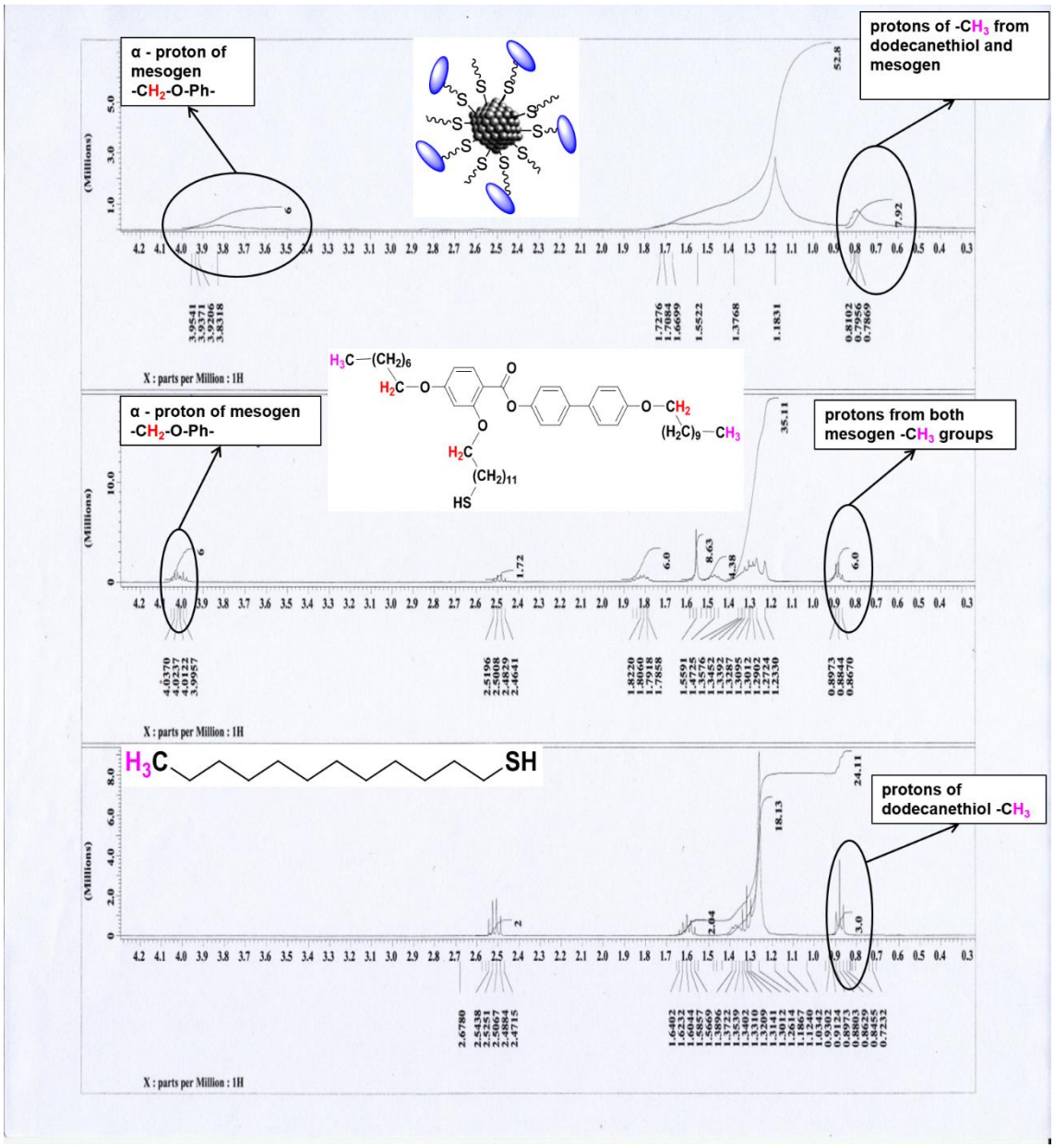

Figure 2. 33. ^{1}H NMR spectrum comparison of LC AuNPs NG1 (top), mesogen (middle) and 1-dodecanethiol (bottom) for ligand ratio calculations.

Considering all the data obtained, an estimation of how many co-ligands and mesogen ligands on the surface of LC AuNPs could be made. As the atomic mass of the single gold atom is 197 g/mol and the percentage of Au percentage was determined to be 54.64% by TGA. Additionally, there are average 568 Au atoms in each AuNPs calculated according to the Equation 2. 1 showed earlier. The step by step of the composition calculation is shown below.

TGA measurement of **NG1** estimated Au: 54.25%, organic: 45.75%. Hence the total mass of one single **NG1** nanoparticle is:

$$mass\ of\ one\ single\ AuNP = \frac{568 * 197 g/mol}{54.25\%} = \mathbf{206259.9}\ g/mol$$

Therefore

$$mass\ of\ organic\ part = \mathbf{206259.9} * 45.75\% = \mathbf{94363.9}\ g/mol$$

The ratio of co-ligand and mesogen is (co-ligand : mesogen = 0.64 : 1) obtained from the ^{1}H NMR spectrum. Therefore, each one unit of thiolated mesogen is equal to 0.64 numbers of co-ligand. Hence:

$$The\ total\ number\ of\ such\ units = \frac{total\ mass\ of\ organic\ part}{0.64 * coligand\ RMM + 1 * mesogen\ RMM}$$

$$total\ number\ of\ units = \frac{94363.9\ g/mol}{0.64 * 202\ g/mol + 1 * 775\ g/mol} = \mathbf{104}$$

Hence

$$\text{the total number of co} - \text{ligand} = 104 * 0.64 = \mathbf{66}$$

$$\text{the total number of mesogen} = 104 * 1 = \mathbf{104}$$

Hence, the total number of ligands attached to this LC AuNPs is approximately **170**, based on the particle size (2.64 nm) calculated from TEM images by using the software ImagePro Plus 6.0.

However, the particle size diameter estimated by using SAXS from collaborators at the University of Sheffield is estimated to be 2.27 nm. Therefore, the number of Au atoms per particle is approximately 360 based on Equation 2. 1. The number of co-ligands and ligands can also be determined by using the same calculation procedures with the same TGA and NMR analysis as shown below:

$$mass\ of\ one\ single\ AuNP = \frac{360 * 197 g/mol}{54.25\%} = \mathbf{130728.1}\ g/mol$$

Therefore

$$mass\ of\ organic\ part = \mathbf{130728.1} * 45.75\% = \mathbf{59808.1}\ g/mol$$

The ratio of co-ligand and mesogen is (co-ligand : mesogen = 0.64 : 1) obtained from the NMR spectrum. Therefore, each one unit of thiolated mesogen is equal to 0.64 numbers of co-ligand. Hence:

$$The\ total\ number\ of\ such\ units = \frac{total\ mass\ of\ organic\ part}{0.64 * coligand\ RMM + 1 * mesogen\ RMM}$$

$$total\ number\ of\ units = \frac{59808.1\ g/mol}{0.64 * 202\ g/mol + 1 * 775\ g/mol} = \mathbf{67}$$

Hence

$$\text{the total number of co} - \text{ligand } = 67 * 0.64 = \mathbf{43}$$

$$\text{the total number of mesogen} = 67 * 1 = \mathbf{67}$$

Hence, the total number of ligands attached to this LC AuNPs is approximately **109**, based on particle size (2.27 nm) estimated from collaborators.

As estimated above, the number of ligands estimation can vary depends on which NP size diameter estimation technique used. Unfortunately, there are none direct size and nanoparticles surface information determination techniques available to use at present for such small size and scale (~ 2 nm). Therefore those nanoparticles size and content information require multiple techniques to obtain each data separately, which can then be combined to make a final nanoparticle size and content estimation.

2. 3.3.4 Monodispersity Investigation

The monodispersity of final purified sample NG1 was determined by Gel Permeation Chromatography (GPC) studies. The same sample solution was prepared following the method mentioned for 1-dodecanethiol functionalised AuNPs GPC measurement. As reported in Figure 2. 34 below, a monodisperse AuNPs GPC analysis shows only one major peak and a shoulder in the spectra. This was confirmed by HRTEM analysis. It was calculated shortly after, the shoulder represents less than 5% of overall **NG1** size distribution.

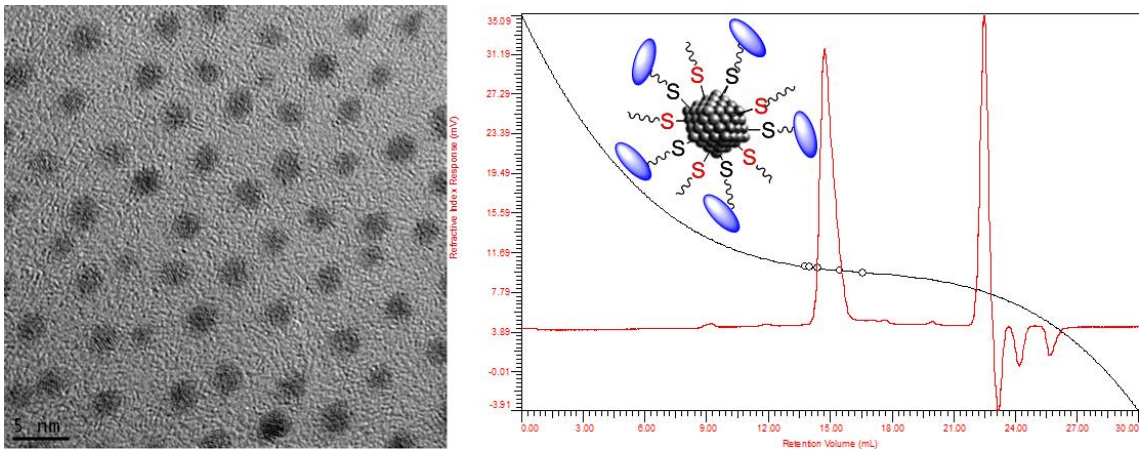

Figure 2. 34. TEM and GPC analysis of LC AuNPs sample NG1 showing > 97% of similar size NPs.

2. 3.3.5 Other Collaborative Investigations

An extensive study of LC AuNPs system (**NG1**) was conducted by collaborators at the University of Sheffield. The sample internal structure was investigated by grazing-incidence small-angle X-ray scattering (GISAXS) and powder small-angle X-ray scattering (SAXS). It is a small-angle scattering technique where the elastic scattering of X – rays by a sample which has inhomogeneities in the nm-range, is recorded at very low angles (typically 0.1 – 10 degrees). A full description regarding sample analysis by this technique and results obtained are detailed in published work.[65] This angular range contains information about the shape and size of macromolecules, characteristic distances of partially ordered materials, pore sizes and other data.[196, 197] As shown in Figure 2. 35 below, the powder SAXS spectrum showed two broad peaks around 4.12 and 2.40 nm with ratio ~ 3 at temperature above 45 ºC. An electron density map was also predicted as shown in the Figure 2. 35 along with calculated *d*-spacing in Table 2. 4, and full description is shown in the published article.[65]

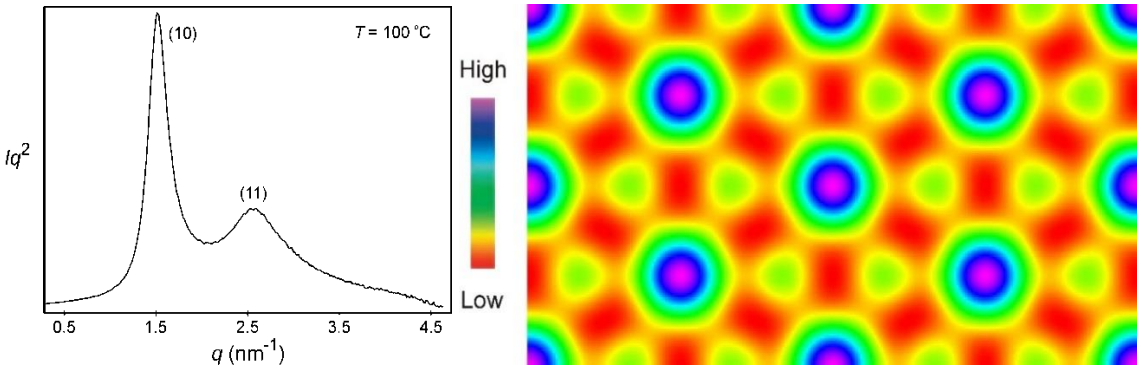

Figure 2. 35. Powder SAXS spectrum of NG1 recorded at 100 ºC and simulated electron density map.

(*hk*)	$d_{obs.}$ –spacing (nm)	$d_{cal.}$ –spacing (nm)	*intensity*	*phase*
(10)	4.12	4.12	100.0	0
(11)	2.40	2.38	36.0*	0
a_{hex} = 4.76 nm				

Table 2. 4. Experimental and calculated *d*-spacings of the observed SAXS reflections of the hexagonal phase at *T* = 100 ºC. All intensities values are Lorentz corrected with correction for multiplicity.

There was not any improvement in the ordering after annealing at up to 170 ºC. However, thin films on silicon prepared by drop casting from chloroform and subsequently annealed in chloroform vapour for 24 hours did develop further order. The GISAXS pattern of the film thus treated is shown in Figure 2. 36. In addition to the diffuse scattering rings at the same *q*-values as in the powder SAXS, sharp Bragg diffraction peaks are prominent (spots superposed on Debye rings). The q^2 ratios of the GISAXS Bragg peaks are very close to 3:4:8:11:12, which is indicative of a face–centred cubic (FCC) lattice. The positions of the diffraction spots in the GISAXS pattern confirm the FCC lattice and reveal two types of fibre-like orientation patterns: in the first it is the [111], and in the second the [110] axis that is normal to the substrate. The best-fit FCC lattice parameter is a = 7.64 nm. From the diffraction intensities the electron density map of the FCC phase was reconstructed, and is shown in Figure 2. 36. As expected, the AuNPs occupy corners and face centres of the unit cell. This was another piece of evidence addressing the lack of birefringence in this material consistent of lack of long-range orientational order of the mesogens. As demonstrated in Figure 2. 36, this sample displays an optically isotropic cubic structure, which is thought to be primarily the lower aspect ratio of this three rings mesogen. It is also suggested that the lack of anisotropy in **NG1** is thought to be the dilution effect of the longer 1-dodecanethiol aliphatic co-ligands on the loss of nematic ordering of the mesogens. Both dilution and the reduction in aspect ratio are known to have a similar effect of disfavouring the nematic phase. As a result of the loss of nematic order, the encapsulated nanoparticle becomes an isotropic sphere with ligands oriented randomly, resulting in a face-centred cubic assembly, a typical mode of close packing of spheres[198, 199].

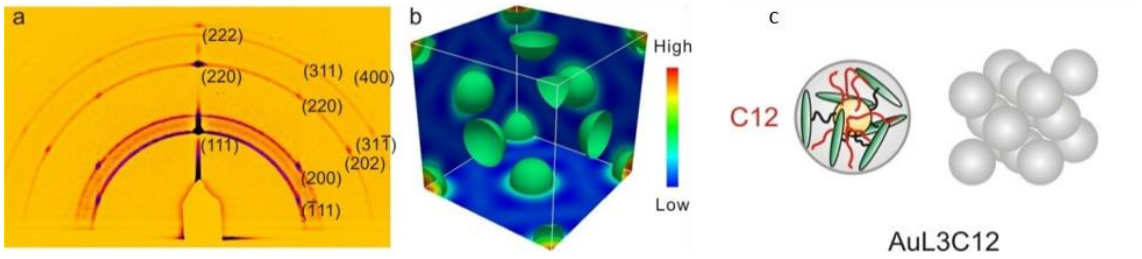

Figure 2. 36. a) GISAXS diffraction pattern of a solvent vapour-annealed thin film of NG1 recorded at 120 °C. Sharp Bragg diffraction maxima can be indexed to a FCC lattice; b) Reconstructed electron density map of the FCC phase, with the iso-electron surfaces enclosing the high electron density region of the gold nanoparticles; c) Schematic illustration of co-ligands (red) and mesogenic ligands (green) around a nanoparticle with the resulting ordered self-assembly.

In the simulation of the diffraction pattern of LC AuNPs (**NG1**), the gold nanoparticles diameter was fixed at 2.27 nm as calculated above. The resulting best-fit RMS displacement of the $\sqrt{(u^2)}$ is 0.44 nm, i.e. 8% of the nearest interparticle distance. This is the highest degree of order of any phases in the AuNPs with lateral mesogens. All detail of results were used to compare with other type of LC AuNPs prepared by Cseh *et al* in the published journal.[65]

The volume of each nanoparticle, including the surrounding ligands and co-ligands, can be calculated as 112 nm^3. From TGA experiments, the weight fraction of nanoparticles in **NG1** is obtained as 55.0%, the volume fraction being 5.52%. Thus the volume of each nanoparticle is 6.15 nm^3, equivalent to 362 Au atoms, and an average nanoparticle diameter of 2.27 nm. This, combined with the results from elemental analysis and NMR experiments, indicates that a **NG1** carries with it an average of 67 mesogenic ligands and 43 dodecylthiol co-ligands.

2. 3.3.6 Ligand-exchange Studies

As suggested by Kassam *et al*,[71] increasing the incoming: outgoing thiol ratio results in a higher coverage of incoming thiol. Hereby it was interesting to study how exchange reaction time would have any impact on the concentration of incoming thiol on AuNPs surface after exchange. Therefore, a few thiol-to-thiol exchange reactions were carried out lasting over 2, 3 and 4 days. Pure samples were prepared and analysed following the same purification procedures described earlier. The TEM images and size distribution graphs are reported in Figure 2. 37 below. The average size of LC AuNPs is larger, as larger precursor 1-dodecanethiol functionalised AuNPs were used to prepare LC AuNPs.

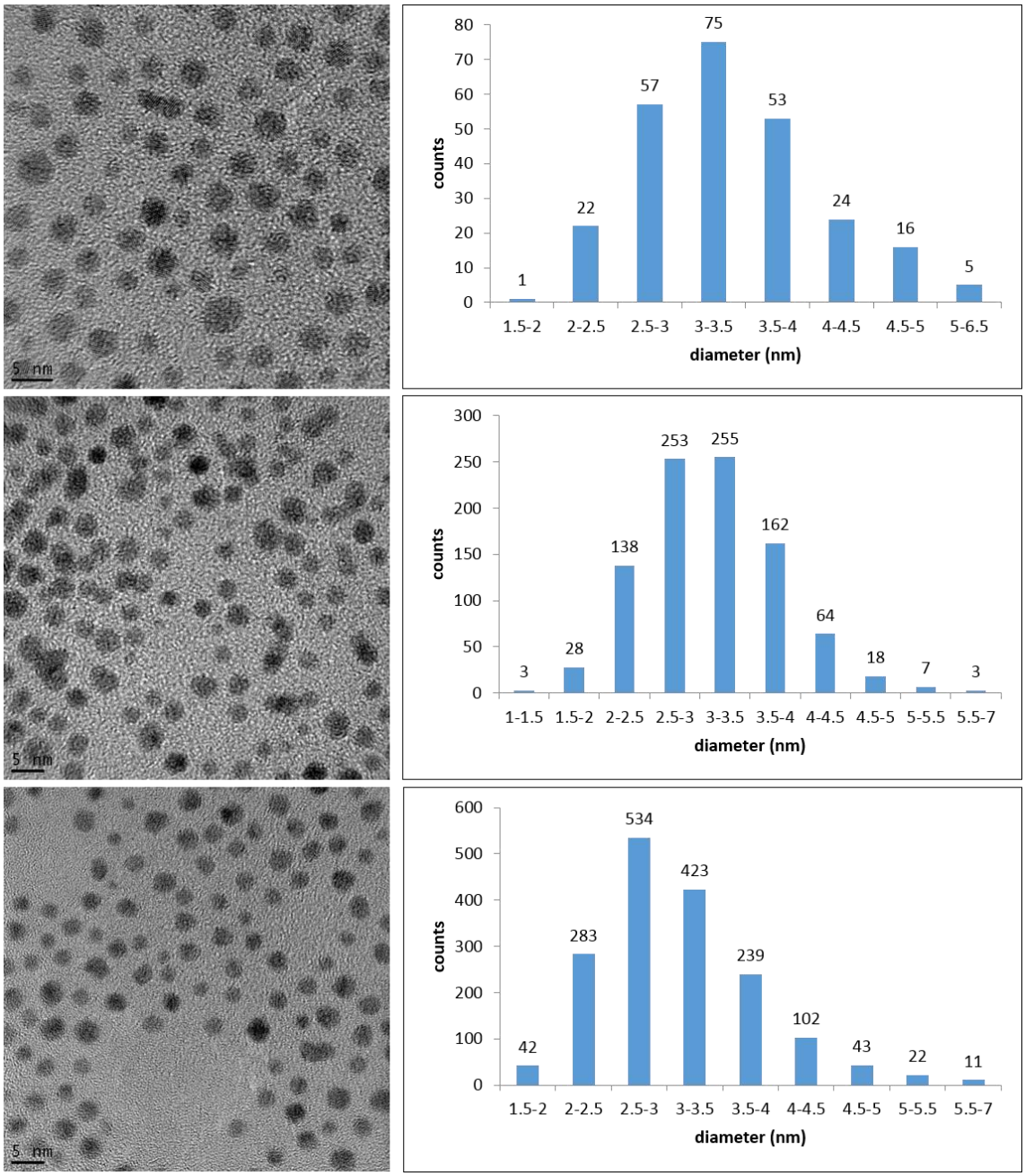

Figure 2. 37. TEM images and particle size distribution of LC AuNPs sample obtained from ligand-exchange time 30a 4 days (top), 30b 3 days (middle) and 30c 2 days (bottom).

The information about nanoparticle size, number of atoms per particle, ligand ratio (co-ligand: mesogen ligand) were determined and are described in the Table 2. 5 below. According to the results, the diameter of NPs increase as the length of exchange time increases, the amount of 1-dodecanethiol co-ligands decreased as the exchange reaction time increased, the number of atoms per particle increased and the size of LC AuNPs became larger. This is possibly because the number of mesogens attached to the NPs increases with the ligand-exchange time increases. Therefore, the total number of all ligands decreased, as mesogen ligand is much larger than 1-dodecanthiol ligand which

requires more space on the surface of LC AuNPs, and few more outgoing thiol ligands were exchanged by each incoming mesogen ligands. This results in a smaller total number of ligands on the surface of LC AuNPs after long exchange reaction time, thus a larger particle size.

Sample	Diameter Mean / nm	Standard Dev.	Au Atoms Number / per particle	D. thiol / Mesogens Ratio	Exchange reaction time
30a	3.38	0.726	1193	2.147 : 1	4 days
30b	3.12	0.690	939	2.877 :1	3 days
30c	3.10	0.713	919	3.243 :1	2 days

Table 2. 5. Particle size, total number of Au atoms and ligands ratio information for LC AuNPs obtained from ligand-exchange reaction with different times.

2. 3.3.7 Influence of Purification on Particle Size

From previous section, it was discovered that the monodispersity of 1-dodecanethiol capped AuNPs could be improved by repeated purification. This was also proposed for sample **30a**, as the AuNPs size distribution is wide according to its TEM images observation in Figure 2. 38 (top). A description of purification techniques are discussed in the section 2. 3.4.

This sample **30b** was further purified by sonication in ethanol and acetone first for 1 – 2 minutes each as standard. The solvent was decanted by carefully pouring out carefully to avoid any sample loss. Finally the sample was dried before using Bio-beads SX1 gel permeation chromatography. As reported in Figure 2. 38 (bottom) below, the monodispersity of sample **30b** has improved when compared with TEM image of sample before purification. According to the size distribution graph, the majority of larger particles presented in the sample were separated after further purification. This was mainly due to the fact that Bio-beads SX1 gel permeation chromatography is a size exclusion technique, hence the main particle size range was able to be modified by isolation of those larger particles.

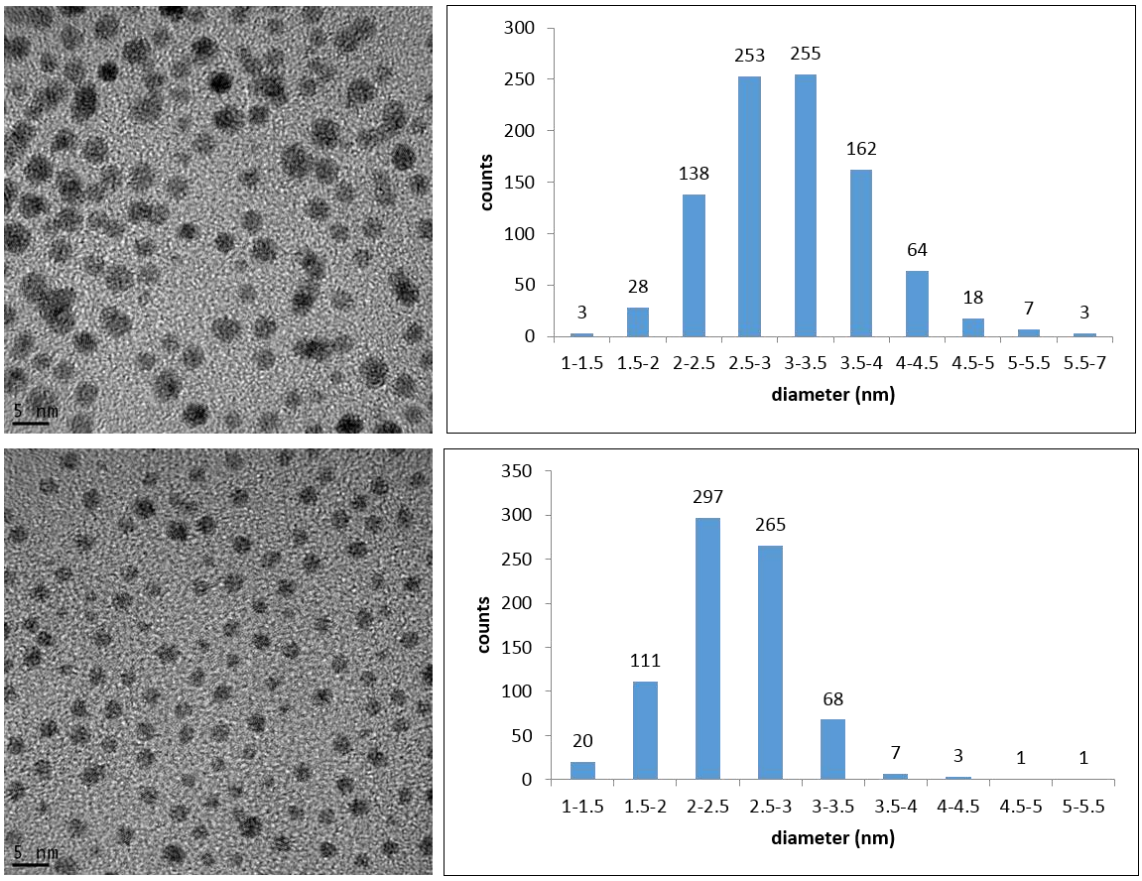

Figure 2. 38. TEM images and particle size distribution graph of LC AuNPs sample 30a before (top) and after (bottom) further purification.

As presented in Table 2. 6 below, the nanoparticle size, number of atoms per particle, ligand ratio (co-ligand: mesogen ligand) were determined by using the same procedures as described in previous sections. The NPs diameter of sample **30b** is decreased after further purification by Bio-beads gel permeation chromatography. The same was found for the number of Au atoms per particle and ligands ratio (co-ligand: mesogen ligand). This was probably owing to the reduction of these larger NPs by further purification.

Sample	**Diameter Mean / nm**	**Standard Dev.**	**Au Atoms Number / per particle**	**D. thiol / Mesogens Ratio**
30b	3.12	0.690	939	2.877 :1
30b re-purified	2.45	0.490	451	0.19 :1

Table 2. 6. Particle size, total number of Au atoms and ligands ratio information of sample 30a before and after further purification.

2. 3.3.8 Properties Investigations of Larger Mesogenic Gold Nanoparticles

According to previous research carried out by colleague Cseh,[152, 153] the first stable monodispersed liquid crystal gold nanoparticles (LC AuNPs) with self-assembly property that exhibits a thermotropic nematic phase at room temperature in the bulk was obtained. However surface plasmonic resonance (SPR) property was not shown, as the particle size reported was too small (~ 1.6 nm). Therefore, larger size of LC AuNPs was required for further SPR investigation.

During this research, a larger size of LC AuNPs (~ 3 nm) sample **NG3** was prepared from a larger precursor of 1-dodecanethiol stabilised AuNPs obtained by using a modified Brust method. A TEM image with the particle size distribution and TGA spectrum of sample **NG3** are presented in Figure 2. 39.

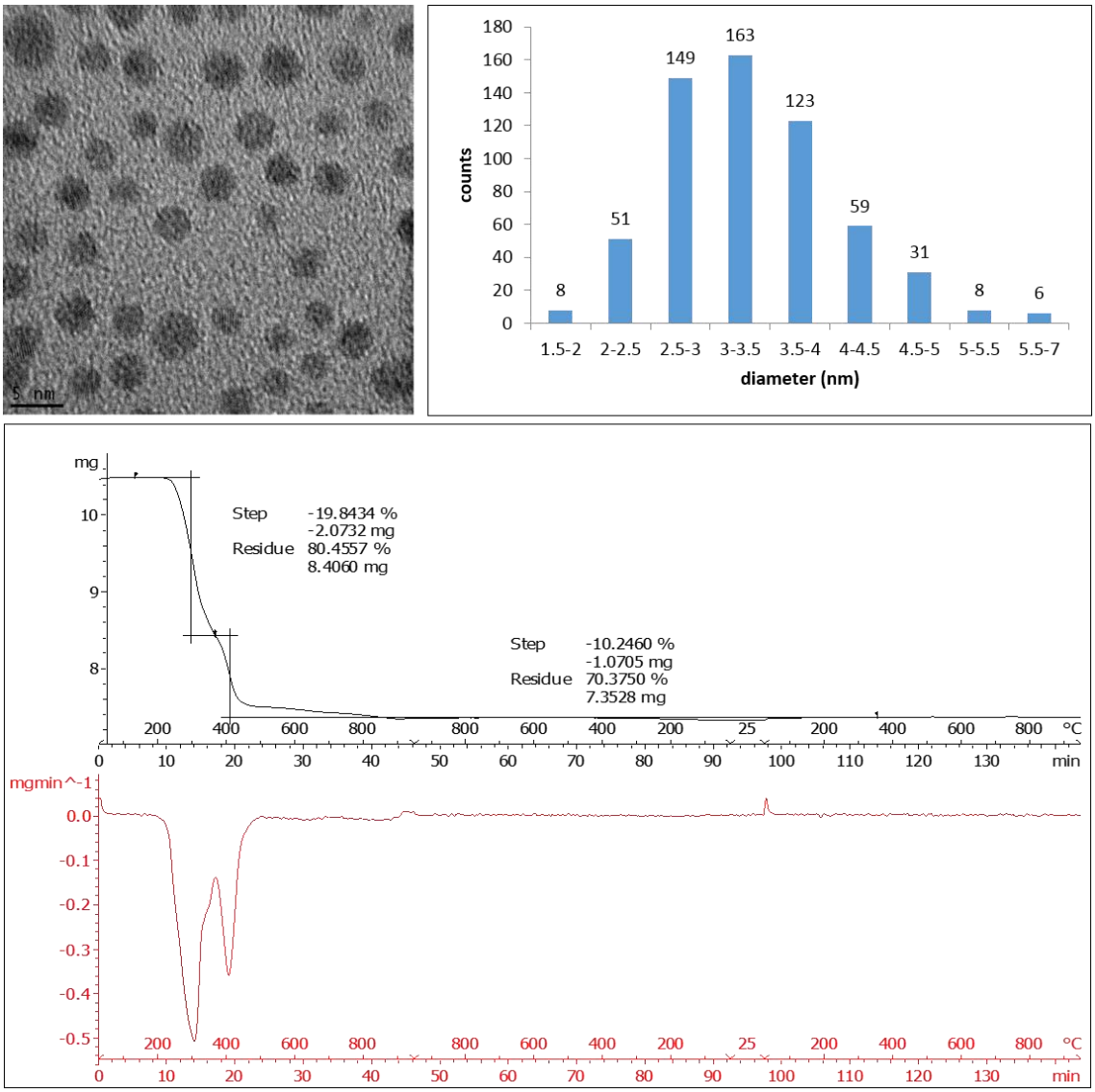

Figure 2. 39. TEM image with particle size distribution and TGA spectrum of sample NG3

Followed the same analysis steps, all information regarding to particles size, number of gold atoms per particle, ligands ratio and the content of sample **NG3** were determined as discussed before, the results are listed in Table 2. 7 below.

Sample	Diameter Mean / nm	Standard Dev.	Au Atoms Number per particle	D. thiol / Mesogens Ratio	Exchange reaction time
NG3	3.36	0.727	1167	2.23 :1	3 days

C%	H%	S%	Total	Au% by TGA	Au/S by ICP
22.49	3.41	3.32	29.22	70.72	73.68 / 2.85

Table 2. 7. Standard LC AuNPs characterisations of particle size, content, number of Au atoms and ligand ratio information for sample NG3.

This particular LC AuNPs sample **NG3** with larger NPs size was further characterised by collaborators at EPFL from Switzerland. The samples surface plasmonic resonance (SPR) and dichroic properties were further investigated.

Here the average size of the NPs is around 3.36 nm as determined by TEM. In comparison with previous reports similar LC AuNPs, which had smaller diameters between 1.5 and 2 nm.[65, 154] As presented in the Figure 2. 39 below, the DSC scan of the LC AuNPs shows a transition at 73.6 °C which is attributed to the isotropisation transition of the attached nematogens (Figure 2. 40). The mesomorphism of such a material is complicated and the isotropisation temperature is difficult to detect with a conventional DSC programme. This is attributed to the lack of mobility of mesogens, as a long time is needed for mesogens to relax or self-organise at a transition temperature when attached to gold nanoparticles. Hence, a specially designed DSC programme was required for such systems with mesogens attached to gold nanoparticles. A series of empty pan DSC references for different temperature rate were prepared, which was then used to be subtracted by the experimental data. As the transition of mesogenic gold nanoparticles was extremely small, which could be easily ignored when mixed with instrumentation noise. The highest temperature for each experiment circle is 100 °C, this was used to avoid any disassociation that may occur during this thermal activity at high temperature. The sample was heated up from room temperature to 100 °C, then annealed at this temperature for 30 minutes before being cooled to – 50 °C at 10 °C per minute. It was thought this may freeze the internal organisation of mesogens that are attached to gold nanoparticles then

rearranged themselves during transitions. This was followed by several cycles of thermal treatment between – 50 °C and 100 °C at the same scanning rate.

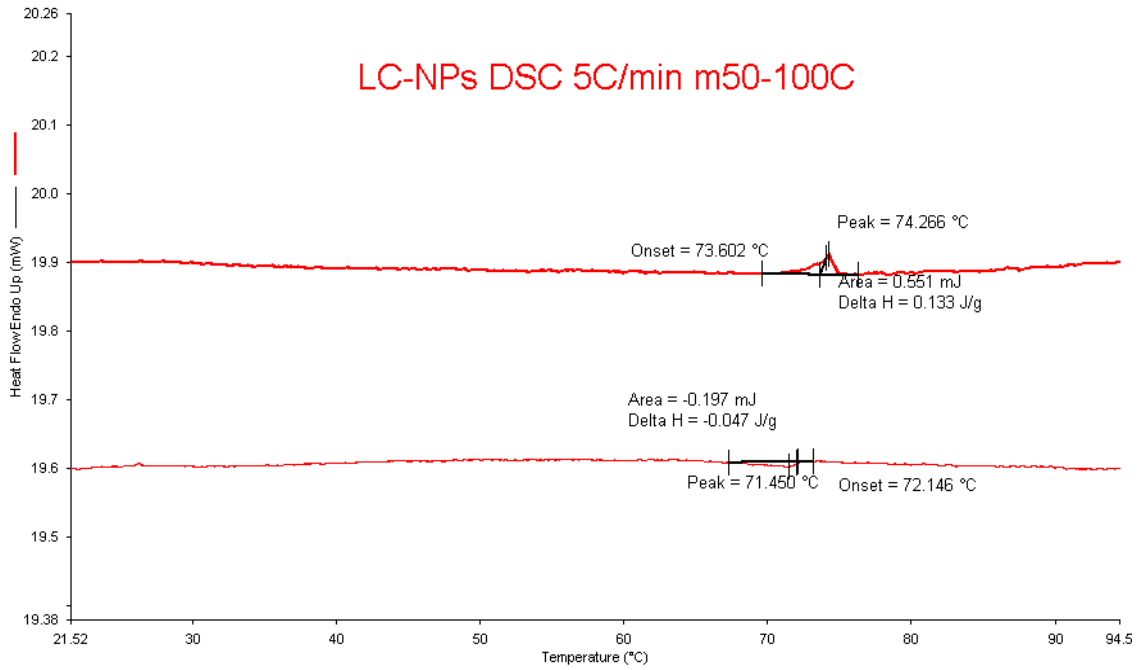

Figure 2. 40. DSC spectrum of sample NG3 showing transition temperature at 73.6°C.

As mentioned in the previous sections, the materials were found to be highly viscous, standard techniques of LC alignment could not be employed, such as the use of electric field or rubbed surface. The sample was sheared onto a glass substrate according to the same method described before. The alignment was confirmed by birefringent textures observed from OPM as shown in the Figure 2. 41 below. A “dark” state is observed when the shearing direction is parallel to one of the polariser axis while a “bright” state is seen when it is rotated by 45°, clearly indicating the presence of an anisotropic axis along the shear direction. The thickness of the resulting thin films was of the order of 50 – 100 nm, as measured by atomic force microscopy; this corresponds to 10 – 20 gold nanoparticles layers, due to the volume of LC AuNPs (NP diameter and length of ligands roughly 5 nm).

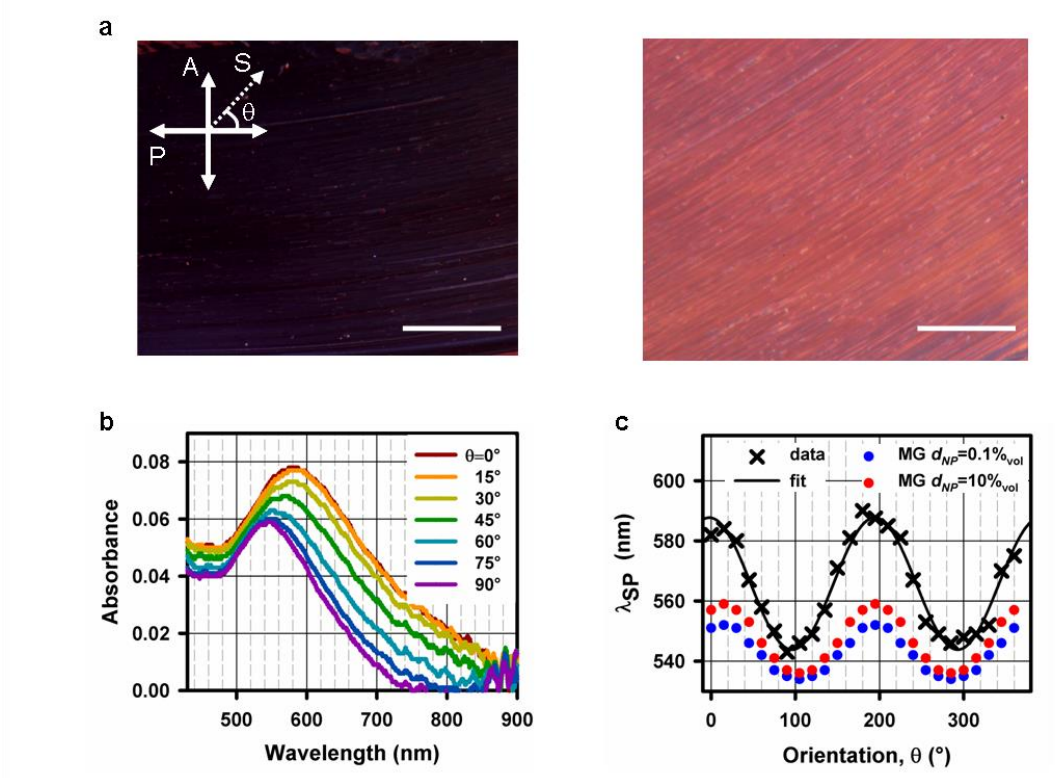

Figure 2. 41. Optical characterisation of thin oriented films of LC AuNPs sample NG3. a) Optical microscopy images of thin oriented films of sample NG3 between crossed polariser (P) and analyser (A) for different orientations of the sample, given by the angle θ between the shearing direction and P: (left) $\theta \approx 0°$ (right) $\theta \approx 45°$ (scale bar is 50 µm). Extinction spectra of the film for different values of θ. c) Evolution of the plasmon peak position as a function of θ: comparison between experimental results (black) and estimations based on the Maxwell-Garnett (MG) formula for nanoparticle volume fractions f_{NP} of 0.1% (blue) and 10% (red).

The impact of the alignment on the plasmonic resonance was investigated, and the polarisation dependant absorption measurements were performed by coupling a fibre optic spectrometer to the polarised microscope. Extinction spectra were recorded with a fixed incoming polarisation by placing a polariser in the illumination path while the sample was rotated in order to monitor the optical response as a function of the angle θ between the polariser (P) and the shearing (S) direction. The results are shown in Figure 2. 41b above. A clear absorption peak associated with the nanoparticles plasmonic resonance is observed in the visible spectra. The peak position appears to be dependent strongly on θ and a red shift from 540 to 590 nm is observed as the sample is rotated from $\theta = 90°$ (S normal to P) to $\theta = 0°$ (S parallel to P). This behaviour is consistent with the anisotropic nature of the medium surrounding the spherical nanoparticles, i.e. the mesogenic ligands with long molecular axis are assumed to be aligned preferentially along the shear direction, as indicated by the OPM images. The dichroic response observed originates from the splitting of the isotropic nanoparticles plasmonic resonance into two orthogonal eigenmodes polarised along the two principal axis of the birefringent

surrounding. Therefore, in an initial rough approximation, the absorption spectra can be modelled in three steps. At first, according to collaborators from University of Jena, the Mie scattering theory is used to calculate the polarisability of the two modes for an individual sphere, assuming an isotropic surrounding medium characterised either by the ordinary (n_o=1.5) or the extraordinary index (n_e=1.7) to match the measured bulk birefringence of the free ligand. The optical constants of gold were taken from literature[200] and corrected for size confinement effects. Maxwell-Garnett relations are then used to calculate the complex effective permittivity for a medium made from such spheres, according to their filling fraction.[152, 153] In a final step, a thin-film transfer matrix algorithm is used to calculate the transmission through the medium characterised by the material properties given by the Maxwell-Garnett effective medium theory. From that transmission, the peak positions of the resonances can be extracted. They are reported in Figure 2. 41c, first for the hypothetical case of a dilute composite with a low NP density (d_{NP} of 0.1%$_{vol}$) in which case no NP-NP interactions are expected and secondly, for a NP density d_{NP} of 10%$_{vol}$, corresponding to the actual volume fraction in our sample, as deduced from the thermogravimetric measurements. Although the sinusoidal variation is well reproduced, the magnitude of the experimental peak shift (~50 nm) is surprisingly high, more than twice the predicted values, even when considering NP-NP coupling. This could not be reproduced in such a simplified model. This discrepancy is indeed remarkable considering that such calculations generally overestimate the splitting, as they assume perfect planar alignment of the liquid crystal director which is difficult to maintain close to the curved surface of the spherical NPs; accordingly, the splitting of the plasmonic resonance observed in previous reports involving liquid crystal doped with nanoparticles of similar birefringence (Δn ~0.2) was generally less than 20 nm. A potential explanation of such discrepancies could be that in addition to the birefringence of the surrounding mesogenic ligands, the plasmonic response is influenced by anisotropic NP-NP interactions due to a specific type of positional order in the sheared self-assembled film which is naturally not considered in the Maxwell-Garnett model.

To test this hypothesis and to understand the effect of shearing on the nanoscale organisation of the gold NPs, small-angle X-ray scattering (SAXS) patterns of the bulk material, as well as grazing-incidence SAXS (GISAXS) experiments on the sheared sample, were carried out (as reported in Figure 2. 42 below). Although the diffuse scattering ring observed in the X-ray diffraction pattern indicates principally a

positionally disordered phase, the three intensity maxima around the diffraction ring in the sheared film attest to the presence of small oriented hexagonal domains with an average domain size of ~13.5 nm as estimated from the FWHM of the scattering peaks.

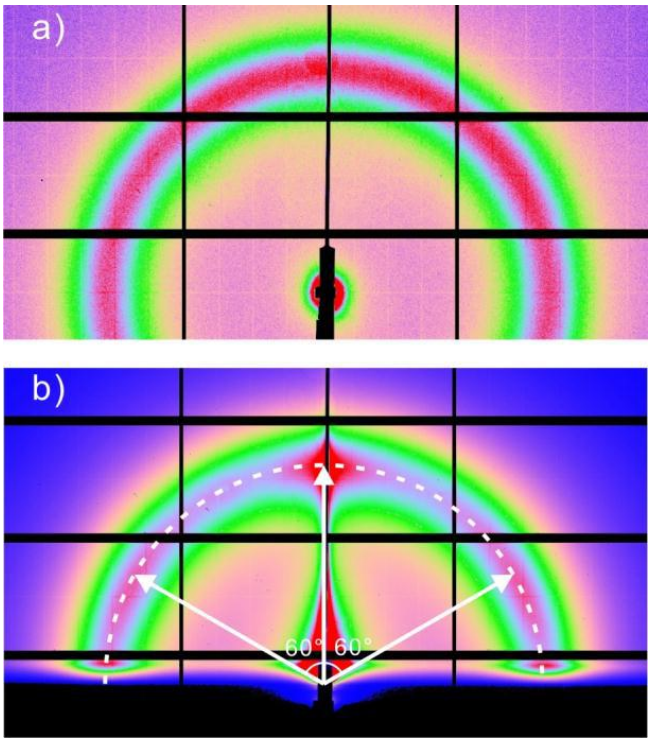

Figure 2. 42. a) Powder Small-Angle X-ray Scattering pattern of the compound. b) Grazing Incidence SAXS pattern of a sheared thin film, with the shearing direction parallel to the incident beam.

To improve the order of the nanoparticles in the film and allow for a more precise determination of the structure, the film sample was subjected to a 48 hour annealing in chloroform vapour. Vapour annealing reduces the glass transition temperature of the system, so that the mobility of the gold nanoparticles is improved, to allow the system to reach its thermodynamic equilibrium more easily. The annealing resulted in the emergence of sharp Bragg spots superimposed on the diffuse scattering crescent (Figure 2. 43 below).

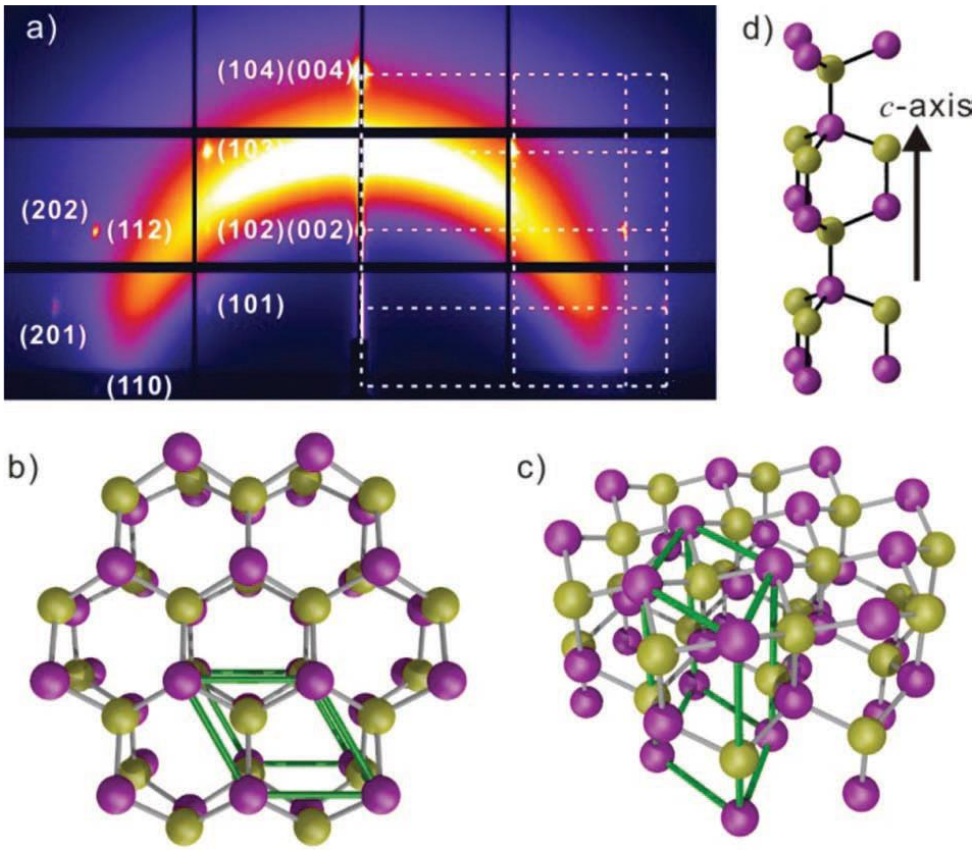

Figure 2. 43. Nanoscale organisation of the LC AuNPs (sample NG3) in thin oriented films. a) GISAXS pattern of a vapour annealed sheared film. The hexagonal (c) axis is normal to the substrate, *i.e.* vertical. Note that due to the relatively high incidence angle, the reflections below the 1st layer line (*i.e. hk*1 and *hk*0) are severely attenuated or extinct, being shaded by the substrate; this also accounts for the curtailment of the lower part of the diffuse semicircle. b-d) Structural model of the phase: b) view along the helical axis, c) oblique view, d) side view of a "column" of nanoparticles. The nanoparticles (not to scale) are coloured yellow and purple to show the local tetrahedral coordination; each yellow nanoparticle is surrounded by four purple nanoparticles and vice versa. The inter-particle distance is 4.2 nm.

The corresponding 3D hexagonal lattice, with the *c*-axis standing perpendicular to the film, has comparatively large cell parameters a = 6.77 nm and c = 11.45 nm. As reflections (001), (003), (111) and (113) are absent, the extinction rule *hhl*: $l = 2n$ applies, indicating the space group $P6_3/mmc$. From the measured Bragg intensities we have been able to reconstruct the electron density map, as presented in the Figure 2. 44 below. The resulting arrangement of nanoparticles is shown in Figure 2. 43 above. There are four nanoparticles in the unit cell. Unusually, each nanoparticles has only four approximately tetrahedrally coordinated nearest neighbours, with a local spatial arrangement almost identical to that of atoms on a diamond lattice. The distance between the nanoparticles (centre-to-centre) is only 4.2 nm. The nanoparticles arrangement can be viewed as crankshaft chains formed by spaced nanoparticles dimers, with their axis oriented along the *c* direction. In fact the structure resembles that of Bernal-Fowler I*h* ice, if one neglects the hydrogens.[201]

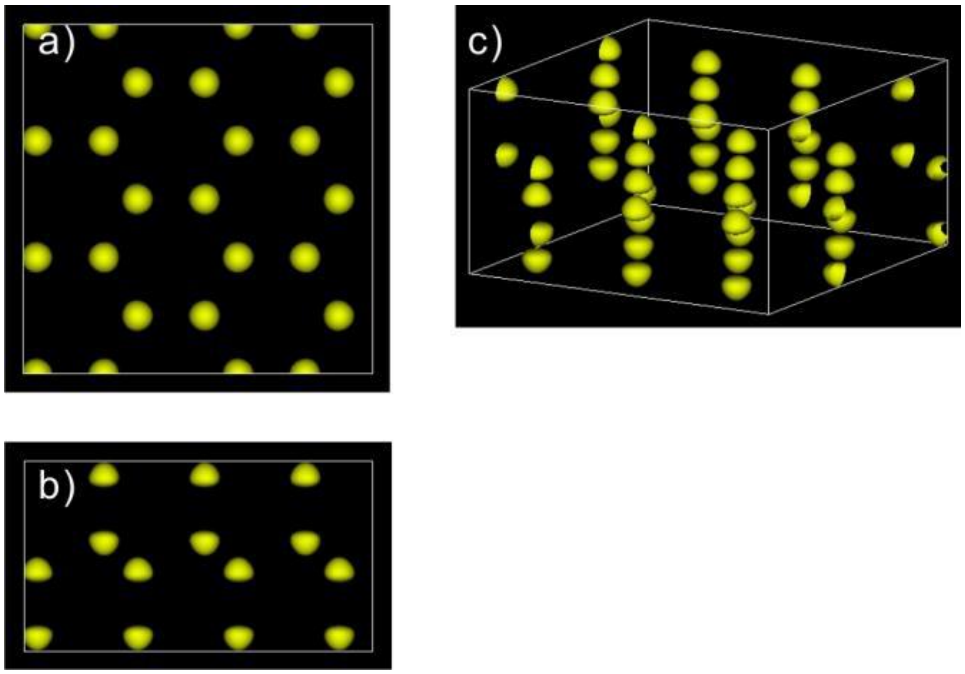

Figure 2. 44. Reconstructed electron density map of the *P*6$_3$/*mmc* phase. Yellow iso-electron surfaces enclose the high density region of the structure (*i.e.* the nanoparticles). a) top view shows the hexagonal symmetry; b) side view the lattice; c) 3D view of the structure.

It is intriguing to note that for a micrometre-size colloidal sphere covered with tangential rods, Nelson *et al.* predicted a director flow on the spherical surface following stitches on a tennis ball with four tetrahedrally directed +1/2 disclinations.[202] While continuum models may not be directly applicable to nanoparticles as small as the one considered in the present work, it may be that a similar arrangement of mesogens surrounds the present gold nanoparticles, leaving the least favoured *loci*, the disclination points, devoid of ligands. This may allow a particularly close approach of the nanoparticles along the four tetrahedrally directed "valences". Further studies are required to test this hypothesis, especially for the small particles used in this study.

It is notable that in a previous study of LC AuNPs with smaller 2 nm nanoparticles but with the same mesogen ligand and alkyl co-ligand, a FCC ordered phase was found. There, each nanoparticle was surrounded by 12 nearest neighbours spaced at 5.4 nm, a distance by almost 1/3 larger than in the present tetrahedral structure. Although in the present system the long range *P*6$_3$/*mmc* order could only be obtained after solvent annealing, it can be safely assumed that the *local* spatial arrangement in the sheared sample is very similar. In fact, the structure in Figure 2. 43, with the large voids in the otherwise closely knit nanoparticles network, explains the surprisingly large *q*-value of the diffuse halo. The diffuse scattering ring has a maximum at q_{max} = 1.81 nm $^{-1}$ (here *q* is the diffraction wave vector equal to $4\pi\sin(\theta)/\lambda$, where 2θ is the diffraction angle and λ the x-ray

wavelength). This is unusually large and should be compared with the much smaller value of q_{max} = 1.52 nm $^{-1}$ for the diffuse scattering maximum observed in the previous study of LC AuNPs.[65] Bearing in mind that the inter-particle distance is proportional to 1/ q_{max}, in the current sheared sample it is 19% larger (1.81/1.52) compared to that in the disordered LC AuNPs described in previous reports,[65] where the nanoparticles were a third smaller (~ 2 nm). This apparent paradox is, however, entirely consistent with the unique tetrahedral local nanoparticles arrangement similar to that in the ordered $P6_3/mmc$ structure. Further evidence supporting the similarity is given in Figure 2. 44b above and in the earlier description.[192]

It has to be stressed that the unusually small inter-particle distance (4.0 – 4.2 nm) suggests, for nanoparticles with a diameter around 3 nm, an extremely strong coupling regime from a plasmonic point of view. The particles affect each other due to their spatial proximity which modifies the plasmonic properties considerably. The anisotropy in the arrangement moreover suggests different coupling conditions in different direction which will reinforce the anisotropic response of the molecular system. Moreover, upon revealing the structural arrangement of the nanoparticles in the unit cell with GISAXS, their collective response can be also simulated to support the experimental optical characterisation.

In order to understand the impact of such geometry on the plasmonic response, theoretical calculations were performed using the generalised Mie theory[203] by collaborators that explicitly takes into account the geometrical positions of all nanospheres forming the clusters as directly extracted from the GISAXS experiments. The simulated geometry consists of a single unit cell with the NP arrangement described above illuminated by a plane wave incident perpendicularly to the plane formed by the four nanoparticles, as depicted in Figure 2. 45a below. As shown previously, the nanoparticles ligands are treated as a homogenous medium with an extraordinary index n_e of 1.7 and an ordinary index n_0 of 1.5, assuming the mesogen director, i.e. the slow axis, is aligned along the long (c) axis of the nanoparticles aggregates. It must be noted that these calculations do not take into account the disordered nanoparticles present in the sample nor the inhomogeneous orientation of the mesogens surrounding the nanoparticles aggregates. Both these effects are expected to weaken the degree of anisotropy of the system. Nevertheless, the magnitude of the red shift of the plasmonic band and its dependence on the polarisation angle θ are well reproduced by the simulations, indicating the essential

role of the anisotropic nanoparticle organisation as presented in Figure 2. 45b and c. Moreover, it is worth mentioning that the larger line width of the measured resonance when compared to the simulations is very likely due to disorder in the NP arrangement. The latter causes local variations in the coupling coefficient, resulting in increasing measured line width. A better insight into the physical origin of the red shift can be gained by inspecting the map of the scattered field intensity for the two orthogonal resonances, e.g. (θ = 90° and θ = 0°), as shown in Figure 2. 45d, the high local field intensities confined in the inter-particle gaps which are oriented along the incident polarisation indicates a directional coupling between the near fields of adjacent NPs, in an analogous way as for NP dimers or chains. Hence, the observed red shift appears to be connected not only to the anisotropic refractive index of the surrounding medium but also to the selective excitation between these two orthogonal plasmonic modes. It is indeed important to note that a good match between experiments and simulations could be found only when both the liquid crystals birefringence and the anisotropic geometrical NP arrangement were taken into account. This confirms the essential role of the NP organisation in explaining the huge shifts of the plasmonic resonances observed in the experiments. It is also worth mentioning that additional simulations were performed by repeating the unit cell along the different lattice directions but the best agreement was found to be the case of a single unit cell, in accordance with the low correlation length found in the GISAXS pattern as presented in Figure 2. 43a.

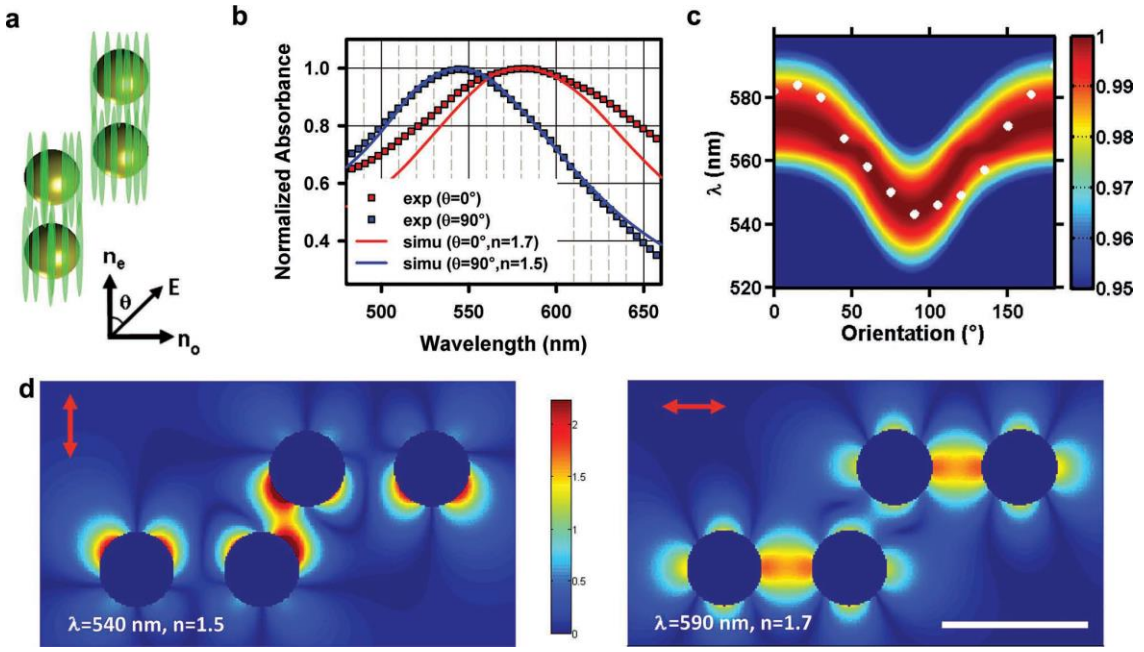

Figure 2. 45. Mie calculations of the optical properties of organised LC AuNPs. a) Sketch of the simulated nanopaticles arrangement; b) Experimental and simulated extinction for θ = 0° and 90°, c) Experimental polarisation dependence of the plasmon peak position (white dots) as compared to the simulated normalised absorption. Please note that the colour bar has a lower limit to provide a better view of the values of interest, d) Map of the intensity of the scattered field for the two orthogonal resonances (red arrows indicate the polarisation of the incident light, scale bar: 5nm).

This single-component material formed hybrid liquid crystals plasmonic composite was prepared by functionalisation of gold nanoparticles with mesogenic ligands, and the optical properties this hybrid were investigated by collaborators. Under shear alignment, this metamaterial exhibits a strong dichroism due to the splitting of its plasmonic resonance. This effect was shown to result from the combined effect of the mesogen birefringence and of anisotropic NP-NP coupling due to short range order in the NP arrangement induced by the mesogenic ligands. These results show that liquid crystals functionalisation enables the realisation of anisotropic metamaterials with enhanced responses. Such properties are of particular interest since they can result in unconventional optical effects like negative refraction[204] or hyperlensing.[205, 206] Furthermore, resorting to mesogen molecules may allow one to benefit from the switching properties of LC, paving the way to the realisation of tuneable self-assembled metamaterials. Those prospects are only indicated in the present material, in which switching behaviour is not observed and plasmonic resonances are still relatively weak due to the small nanoparticle size. However, current efforts are devoted to the design of more flexible mesogenic ligands, so as to mitigate the high viscosity and enable the use of larger NPs with stronger plasmonic resonances.

2. 3.4 Mesogenic Gold Nanoparticles Purification

2. 3.4.1 Ultra-Sonication

The mixture residue was obtained by removing solvent after the ligand-exchange reaction. It was then purified by sonication in ethanol (enough to cover samples) twice for 1 – 2 minutes. The solvent could be carefully poured away without any sample loss, or the solution could be filtered through a filter paper. The same procedures were followed with sonication in acetone before being checked by H^1 NMR for purity. This method should be repeated if impurities were still present. However, large amount of the samples could be lost during repetition of this purification process and the outcome was always difficult to control. There was also some uncertainty as to where the LC AuNPs could be destroyed with too much sonication power input. Therefore, this method was mainly used in combine with Bio-Beads SX1 beads gel permeation chromatography as the scale of reaction increased. The final residue was always purified by sonication first before using Bio-beads gel permeation chromatography. Sonication could be used again after Bio-beads gel permeation chromatography if there was still a small amount of impurities present.

2. 3.4.2 Bio-beads SX1 gel permeation chromatography

The Bio-beads stationary phase was prepared by immersing the dry Bio-beads into a suitable solvent, in this case non-stabilised THF was used. Bio-beads were left to absorb solvent for 3 days to allow sufficient time to fully expand the beads. The resulting slurry was transferred into a suitable column with excess solvent, and the column was only packed by gravitational force. The sample was filtered and dissolved into a minimum amount of non-stabilised THF. It was then deposited on the top bed of the column and samples were collected in amounts of 1 ml per fraction. Due to gravity, the sample will start to elute once it was transferred, hence this process was carried out in as short amount of time as possible. TLC was used to monitor the separation process, to check any trace of free ligands.[187, 188] It is noted that the Bio-beads should not be dried during the whole process to achieve the maximum affect and use gravitational force only to elute the sample inside the column. The rate of eluting could be controlled by adjusting the column solvent exit tap and should always keep the rate of elute slow to provide better separation. A lump of glass wool could be used on the top side of column instead of sands in a

conventional silica gel chromatography. This could prevent the Bio-beads drying out during sample transfer. Non-stabilised DCM could also be used instead of THF, but cautions needed to be taken to avoid the top side of bio-beads column drying out, as DCM has higher density than Bio-beads. The principle of Bio-beads is the same as for a GPC column, where small gaps and tunnels are within each Bio-bead, which enabled small particles or small molecules to pass through and keep them inside the column for a much longer period of time than other larger particles. Some principles of GPC column are described in the Introduction section 2. 1.5.2.

Overall, the best way to purify LC AuNPs is to remove most of impurities by using ultra-sonication first. This is followed by using Bio-beads SX1 gel permeation chromatography in non-stabilised THF. In some cases, only ultra-sonication purification was sufficient when dealing with smaller amount of sample.

2. 3.5 Some Results on Deuterated Gold Nanoparticle

2. 3.5.1 Deuterated 1-dodecanethiol Synthesis

2. 3.5.1.1 Methodology development

In order to synthesis deuterated monolayer gold nanoparticles, deuterium 1-dodecanethiol is required to be synthesised first. Based on the cost and product availability, it was decided to begin this process from deuterium 1-dodecanol by bromination with phosphorus tribromide, followed by preparing this thioester intermediate with potassium thioacetate before a mild hydrolysis process to obtain final thiol compound. However, due to the availability and cost of deuterium compounds, the synthetic method was initially developed by using non-deuterium 1-dodecanol as shown in the scheme below.

Scheme 9

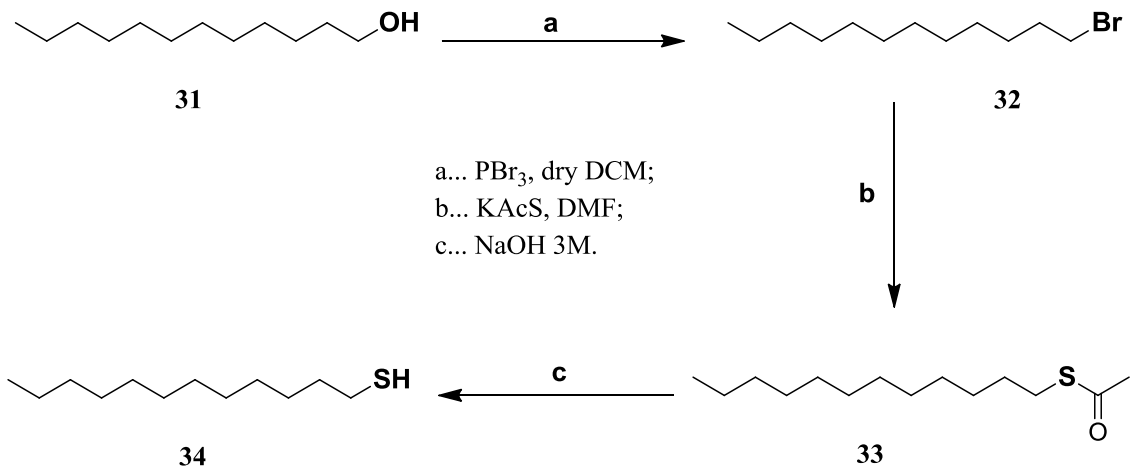

Due to the moisture sensitiveness of PBr_3, a standard bromination procedures was followed. PBr_3 in dry DCM was initially cooled to 0 °C before being introduced drop-wise to a stirred mixture of 1-dodecanol in dry DCM at 0 °C. The mixture was then brought up to room temperature and stirred further for 30 minutes before removing the solvent. The residue was then partitioned between ethyl acetate and water, then the organic layer was separated and dried over $MgSO_4$. An oily residue was obtained after evaporating solvent. It was finally purified by a short silica column flush chromatography in hexane to obtain light brown oil with yield 17.7%. The low yield was suspected to be the quality of PBr_3, as it was possibly not stored properly in a reused container. Another reason could be the product loss during chromatography, as both low molecular mass

starting material and product were sensitivity towards UV radiation. The completion of purification had to be verified with each fraction collected by ^{1}H NMR after removing the solvent. It was very inconvenient and inaccurate. Hence a significant amount of product could still be present in the column.

Despite the low yield production of sample **32** 1-bromododecane, this scheme was carried on for the purpose of the next step to prepare the thioester compound **33**. It was found a high yield over 98% of compound **33** could be achieved by using a microwave reactor. This method was initially tested under a conventional condition by mixing compound **32** and potassium thioacetate in DMF for 5 days. The mixture was then partitioned between water and DCM. The final compound **33** (59.2%) was obtained by evaporating the organic solvent after dried over $MgSO_4$. The same procedures were followed, except less starting materials were used and the mixture was stirred in a microwave reactor under high pressure (240 psi) and high temperature (153 ^{o}C). The whole process lasted less than 30 minutes and product was extracted with DCM. A light orange compound **33** with yield of 98% was obtained after removing solvent. However, it was considered that the low yield of first step in preparing 1-bromododecane would be the drawback of this route. Although these are not problems for non-deuterium starting materials, it would not be viable financially for deuterium containing compound production. Additionally, there is a limitation of the scale of reaction that could be carried out in a microwave reactor. Therefore, another scheme (as shown below) was considered to bypass this bromination step to synthesise thioester directly from the starting material alcohol.

Scheme 10

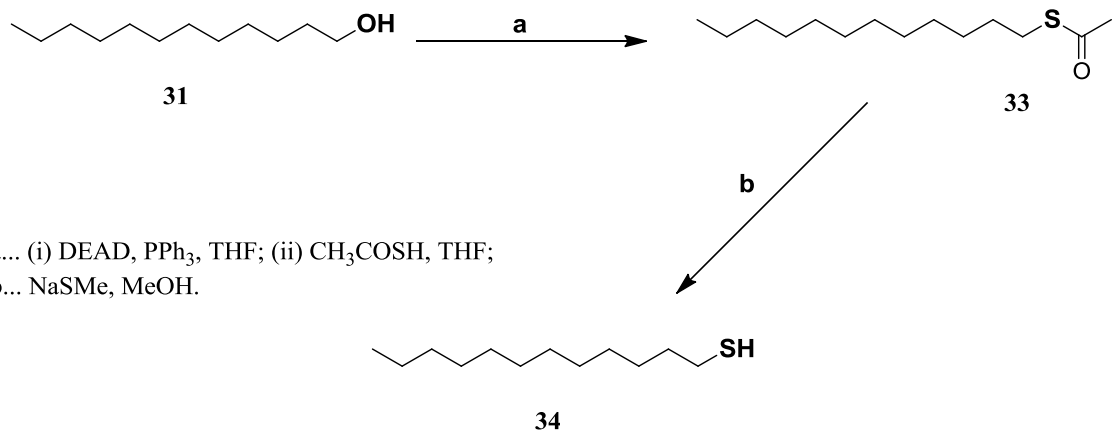

a... (i) DEAD, PPh_3, THF; (ii) CH_3COSH, THF;
b... NaSMe, MeOH.

It was decided to use the Mitsunobu reaction to convert alcohol compound **31** into thioester compound **33**, in the presence of either Diethyl azodicarboxylate (DEAD) or Diisopropyl azodicarboxylate (DIAD) and triphenylphosphine (PPh_3), to generate a phosphonium intermediate that binds to the alcohol oxygen and activating it as a leaving group. Substitution by the thioacetic acid nucleophile completes the process to synthesis thioester compound **33**. This reaction with both DEAD and DIAD reagents were attempted and compared. It is worth mentioning that DEAD is quite dangerous and explodes upon heating, hence all experiments were strictly carried out at a low temperature at 0 ^oC with DEAD added drop-wise slowly. It is also light sensitive and toxic upon long time exposure.

Standard procedures were followed and optimised to achieve high yield, detailed description are shown in the Experimental section. DEAD in dry THF was added drop-wise slowly to a pre-cooled stirring mixture of PPh_3, 1-dodecanol and thioacetic acid in dry THF at 0 ^oC in the presence of nitrogen. It was then brought up to room temperature and left stirring overnight for 18 hours. A few washing and triturate methods were attempted before purification, full detail of those methods are described in the Experimental section. Overall, it was found the yield could be boosted by using excess of DEAD, dry glassware and freshly recrystallised PPh_3 (obtained from ether mixing with minimum amount of hexane). It is also found that trituration with suitable solvents could reduce the amount of triphenylphosphine oxide before silica chromatography, which reduced the loss of product. As the triphenylphosphine oxide usually solidifies on the side surface of the glass column, and forming lumps that traps other compounds on the silica column bed. These resulted in product being trapped and required large amount of solvent to wash off, which induced further dilution of crude sample and a large mixture band during column isolation, causing a bad separation process and losing product. This type of reaction was also attempted with DIAD reagent, which was not successful with the Mitsunobu reaction initial attempt. However, it was able to be improved by introducing excess of DIAD reagent, drier reagents, dry glassware and recrystallised PPh_3. In the end, DEAD reagent was chosen to be the main reagent for this type of reaction, due to its reliability and less complicated experimental procedures.

The final thiol compound **34** was obtained by hydrolysis. Both conventional acid and base hydrolysis were performed initially without any product. Therefore, the mild hydrolysis

with NaSMe was introduced, which was previously used for thiolated mesogen preparation.

2. 3.5.1.2 Deuterium 1-dodecanthiol

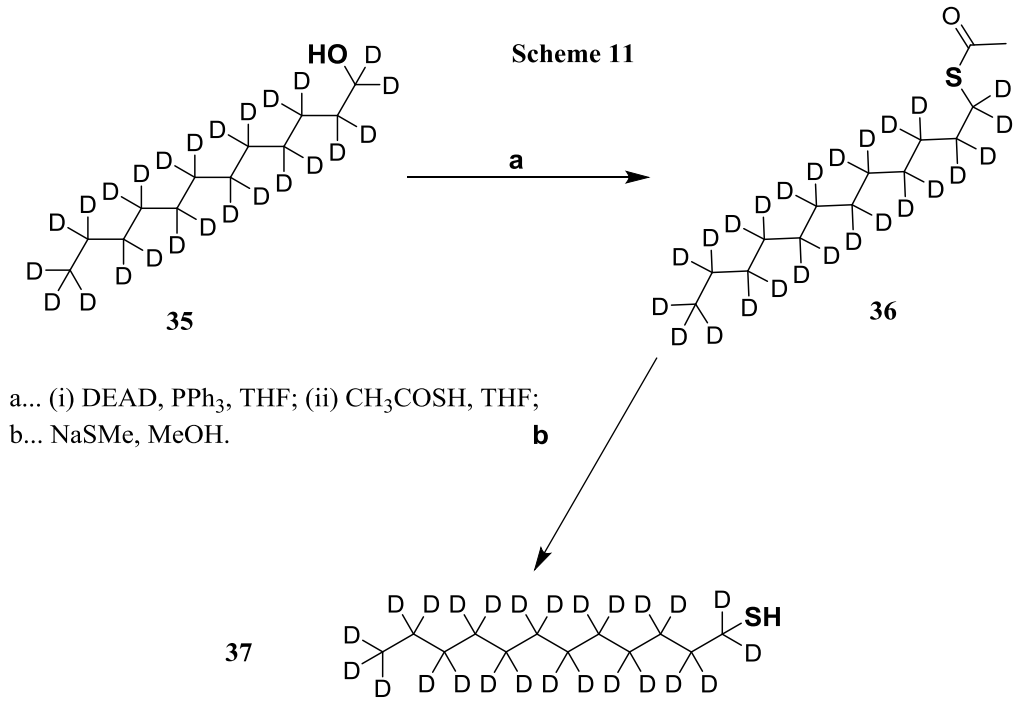

Followed the synthetic route developed with non-deuterium 1-dodecanol. DEAD in dry THF was added to a stirred mixture of compound **35** and thioacetic acid in dry THF at 0 ^{o}C in the presence of nitrogen. It was stirred at this temperature for 1 hour, then brought up to room temperature and further stirred for another 12 hours. The whole process was monitored by TLC for an optimal yield. The final residue was obtained by evaporating the solvent, followed by triturate in hexane before being washed by H_2O_2 (30% w/v, 10 ml), DCM, saturated sodium sulphite and water, finally dried over $MgSO_4$. The deuterium S-Dodecyl ethanethioate was obtained as a light pale brown oil after silica column chromatography. Similar to the thiolate mesogen hydrolysis, the final deuterium 1-dodecanethiol was prepared via a mild hydrolysis with NaSMe.

Due to the nature of those deuterium compound, the conventional purity verifying by conventional ^{1}H NMR could not be carried out. Nevertheless, GC/MS investigation was carried out for purity confirmation of all deuterium compounds with purity up to 98%, which is the same as the purity of starting material deuterium alcohol is also 98%.

2. 3.5.2 Deuterated Monolayer Gold Nanoparticles

In this section, only characterisations of deuterated monolayer gold nanoparticles by TEM, GPC, EA and TGA are reported. Further investigations are required to fully characterise this sample and determine the monodispersity, content and accurate size information.

GPC studies were carried out to determine the monodispersity of this deuterated monolayer gold nanoparticles. The same sample preparation and analysis procedures were followed as explained in previous sections. A GPC spectrum of this sample is shown in Figure 2. 46, which shows the polydispersity by a single major peak present. This study suggested a monodisperse sample which was also confirmed by TEM investigations. It was calculated that main peak represents about ~ 98% of overall AuNPs size distribution.

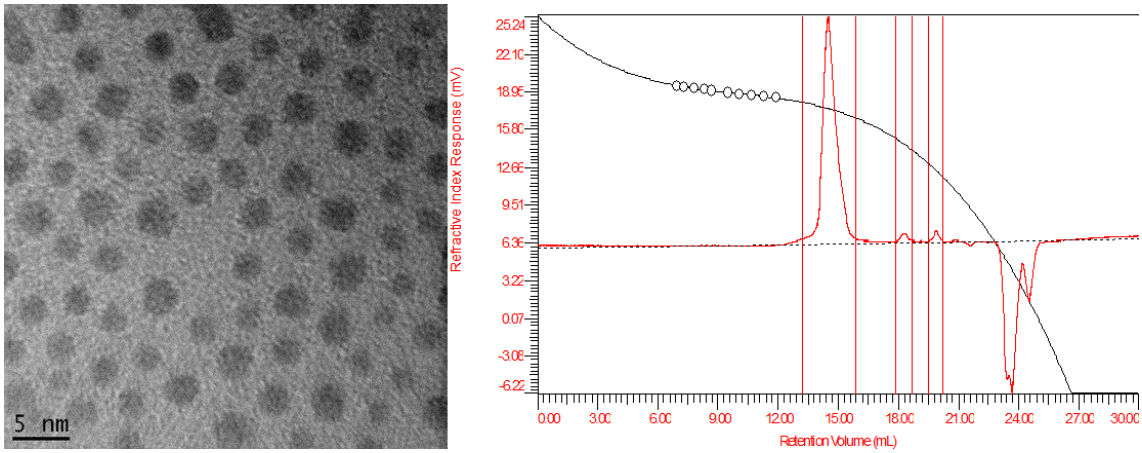

Figure 2. 46. GPC spectrum of deuterium monolayer AuNPs showing a sample distribution about 98 %.

The sample was first analysed by TEM after synthesis and purification followed the same procedures described previously. This preliminary TEM investigation provided some information regarding the monodispersity and size distribution of this deuterated monolayer gold nanoparticles. As presented in Figure 2. 46, a rough estimation of the size of particles from TEM image appears to be in a range of 2 – 3 nm. This was followed by TGA investigation to determine the gold content to be 76% as shown in Figure 2. 47. A further organic content of characterisation by EA provided the ratio of **C** : **H** : **S** to be 14.5 : 2.59 : 2.94 with a total 20.03%. Nevertheless, all results are in parallel with literature results produced according to Brust and previous investigation of non-deuterium monolayer protected gold nanoparticles.[116] However, the application of further purity confirmation techniques are still required, as the ^{1}H NMR is not suitable for deuterium.

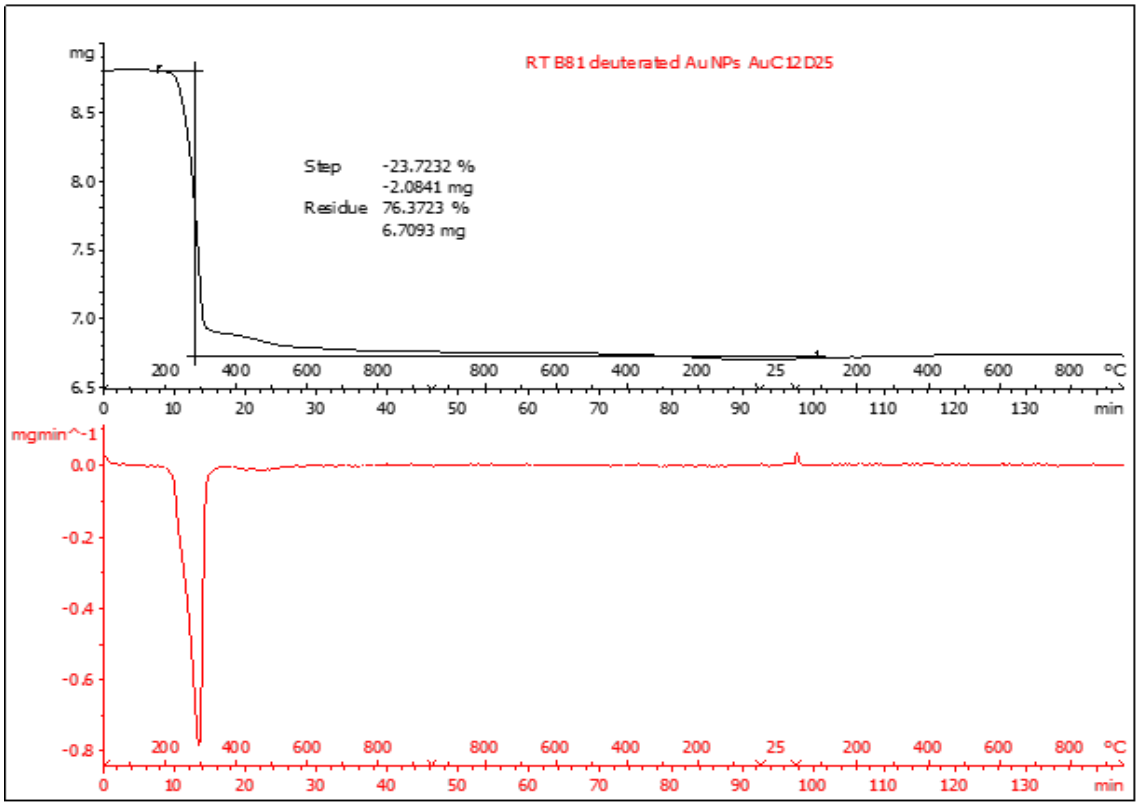

Figure 2. 47. TGA of deuterated monolayer gold nanoparticles showing 76% of Au content.

2. 3.5.3 Deuterated Mesogenic Gold Nanoparticles

In this section, some characterisations of deuterated mesogenic gold nanoparticles were carried out by TEM, GPC, TGA, EA, OPM and DSC are reported. However further investigations are still required at this stage to fully understand the ligand arrangement on the surface of gold nanoparticles. Some brief interpretation of the properties of deuterated mesogenic gold nanoparticles is provided by using these preliminary results.

The purity determination of this deuterated sample by ^{1}H NMR is much more complicated in comparison with previous mesogenic gold nanoparticles without deuterium co-ligands. As there is a completely different signal splitting mechanism when deuterium sample is involved and this has not yet been understood properly. However, an initial study of this sample by GPC was carried out to investigate the monodispersity and also some purity verification. As presented in Figure 2. 48, showing the polydispersity of sample with a major signal peak consist of 95 % of distribution.

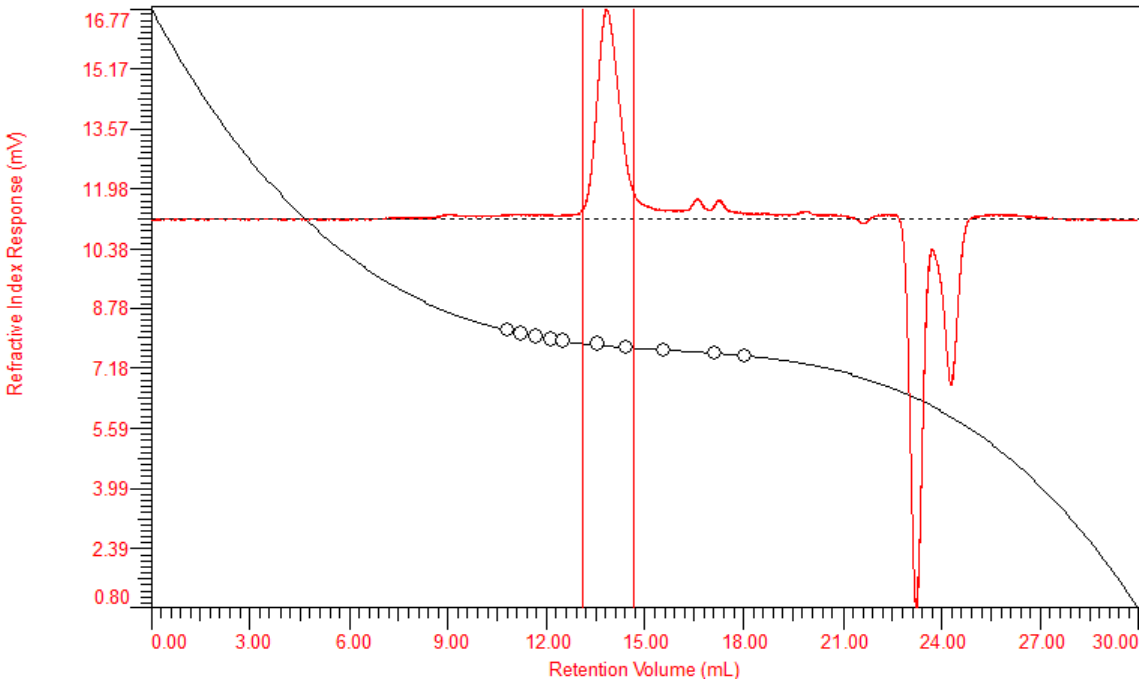

Figure 2. 48. GPC spectrum of deuterated LC AuNPs showing a major peak with sample distribution over 95 %.

TEM observations were also carried out followed by the same sample preparation procedures. The 1D hexagonal particle arrangement was observed from TEM images as shown in Figure 2. 49.

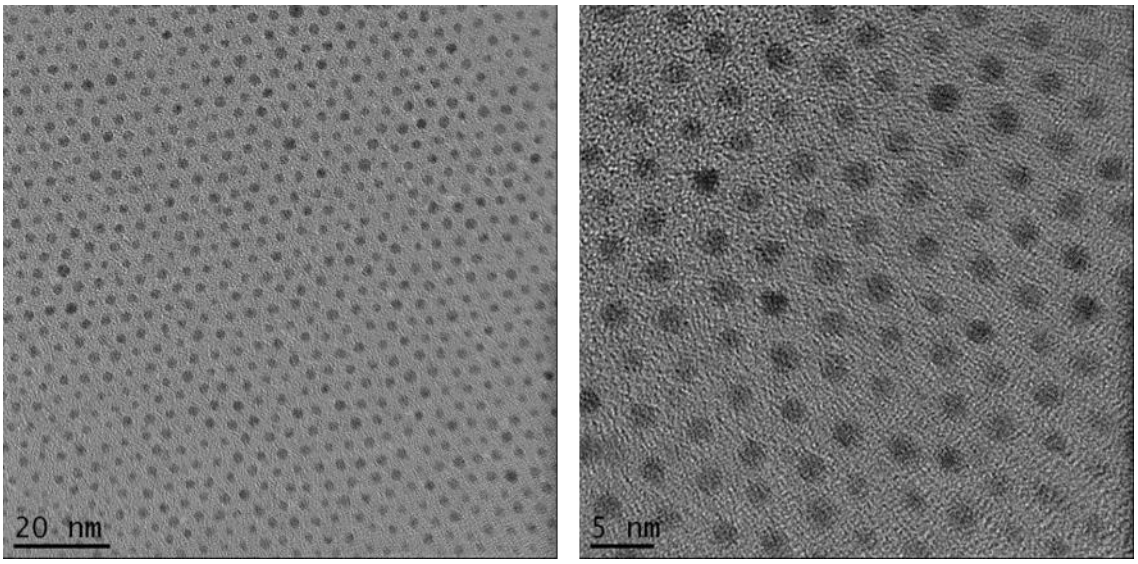

Figure 2. 49. TEM images of deuterated LC AuNPs.

This was followed by OPM and DSC investigations. As presented in Figure 2. 50a and b, a sheared deuterated sample on glass slides showing birefringence when rotated under crossed polariser. The DSC measurement indicates a thermal transition at around 73 °C as shown in Figure 2. 50c, which is slightly higher than the transition temperature of the attached mesogen.

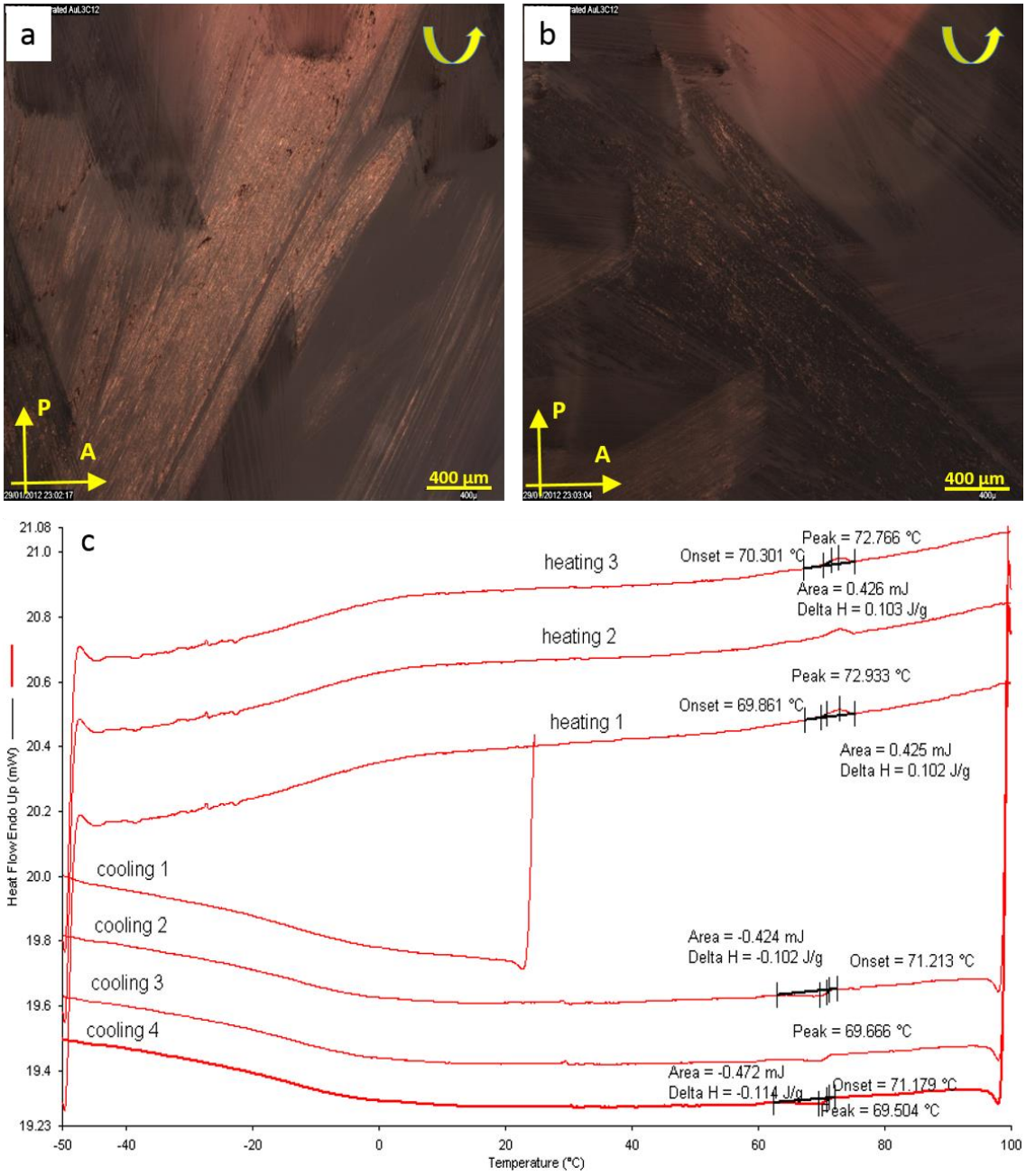

Figure 2. 50. OPM images of deuterated LC AuNPs showing birefringence, a) sample at 0 degree; b) same position with sample rotating 90 degree anti-clockwise; c) DSC of sample investigated at the rate of 5 °C/ min.

The TGA sample was prepared via this wet method and dried with the same method as mentioned in previous sections. The same TGA programme described previously was used to thermally heat the sample from room temperature to 950 ºC, in the presence of nitrogen, followed by thermal heat in air after it was cooled to room temperature in nitrogen. A two stage decomposition of organic part also presented here (Figure 2. 51) with rapid degradation of co-ligands, followed by mesogen ligand decomposition. This was followed with a similar degradation temperatures of this deuterated LC AuNPs. The TGA data indicates that the remaining weight of the sample correspond to the weight of

the gold as 58.6%. A further investigation by EA provided the **C** : **H** : **S** to be 30.61 : 4.15 : 2.31 with total 37.07%. All content measurements are in accordance to previous non-deuterated LC AuNPs samples.

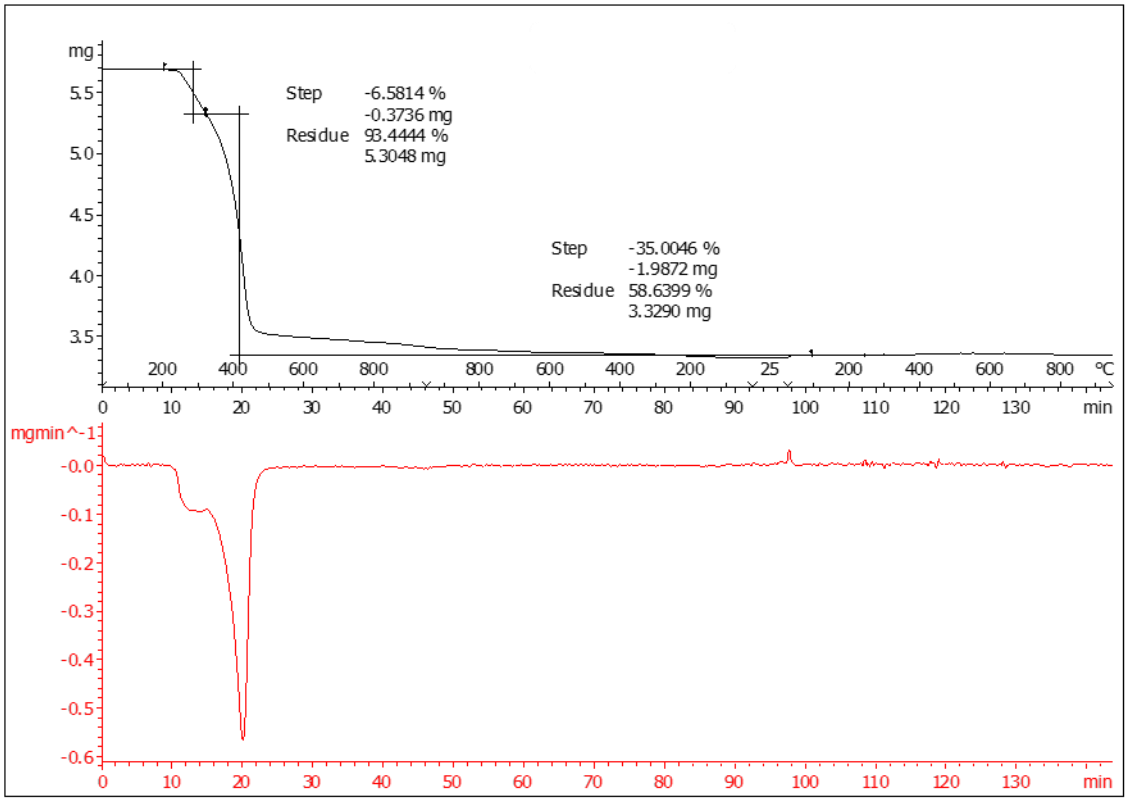

Figure 2. 51. TGA spectrum of deuterated sample showing gold content of 58.6%.

Further studies to seek for alternative purity verification techniques other than ^{1}H NMR is required. The accurate size determination of particles, number of gold atoms per particle and ligands ratios information determination are still in progress with further TEM images analysis. The complete study of the self-assembly and mesomorphic behaviour of the deuterated LC AuNPs by GISAX and Synchrotron will allow the internal organisation to be determined. Further investigation by neutron scattering will help to understand the self-assembly, internal organisation and how ligands are attached to the surface of gold nanoparticles.

2. 4 Conclusions

The aims discussed in this part of the work were to synthesise 1-dodecanethiol capped gold nanoparticles and thiolated mesogen functionalised gold nanoparticles and to investigate their self-assembly, having in view 2D or 3D assemblies.

Overall, the conclusions of this Chapter Two are:

- Monodisperse 1-dodecanethiol monolayer protected AuNPs were prepared by using a modified Brust's two phase method to produce NPs both larger quantity and with larger particle size. A long hydrocarbon chain ligand 1-dodecanethiol was used as spacer to cap gold, due to its strong binding energy with gold.
- Three different purification methods were tested, and the best way to obtain large amounts of monodisperse AuNPs was to precipitate freshly synthesised materials 3 – 5 times in cold ethanol, in combination with sonication if required;
- A TEM sample preparation technique was developed to obtain suitable TEM data;
- Highly monodisperse LC AuNPs were prepared via ligand-exchange reactions with the mesogenic ligands that were described in Chapter One;
- The purity of successfully synthesised hybrids were verified by ^{1}H NMR and transmission electron microscopy (TEM);
- Methods were developed for OPM and DSC sample preparation and the investigation of the liquid crystal properties;
- Mesogenic properties of LC AuNPs were investigated by OPM. Sample layers thicknesses between 50 – 100 nm were required for OPM analysis, and this was achieved by careful shearing with a small spatula;
- DSC investigations of LC AuNPs mesogenic property required a specific sample preparation, analysis method and initial blank data set up;
- A wet method was developed for TEM, GPC, ICP, EA and TGA characterisations with sample transferring;
- Structural properties investigations of LC AuNPs (~ 2.3) nm size were carried out by collaborators from the University of Sheffield, powder SAXS and GISAXS study showing a FCC lattice;
- It was found that the ligand-exchange reaction time can affect the size, content of LC AuNPs and the ratios of capping ligands. In general, longer exchange times

resulted in larger particles size with more mesogen ligands attached, hence resulting in systems with larger number of Au atoms per particle;

- A detailed study showing that purification can improve monodispersity and reduces the size and content of LC AuNPs was carried out. The majority of larger size particles and excess capping ligands can be removed by further purification, hence a reduction the average size of particles is observed;
- The optical properties investigation of larger size LC AuNPs (~ 3.4 nm) were carried out by collaborators from EPFL Switzerland, polarised absorption spectroscopy showing a strong dichroism with a large splitting of the plasmonic band, as large as 50 nm;
- Further purification by both ultra-sonication and Bio-beads resulted in more monodisperse LC AuNPs and allowing for much more reliable purification procedures;
- A synthetic methodology for deuterated 1-dodecanethiol was developed;
- Following the modified Brust's two phase procedures, deuterated 1-dodecanethiol monolayer protected gold nanoparticles (deuterated AuNPs) were synthesised and characterised by TEM, GPC, EA and TGA;
- Using ligand-exchange procedures, deuterated 1-dodecanethiol monolayer protected gold nanoparticles (deuterated LC AuNPs) was synthesised and characterised by TEM, GPC, DSC, EA and TGA, although further properties investigations are still required to fully understand this topic;

In conclusion, the results presented in this thesis demonstrate that the self-assembly mode of nanoparticles and the distance between them in defined directions, can be controlled by selecting appropriately sized mesogens, the length and number of aliphatic co-ligands. A high volume concentration of co-ligands destabilise the alignment of nematogens and a face centred cubic (fcc) phase or a hexagonal phase with the space group $P6_3/mmc$ is formed by the liquid crystal gold nanoparticles. This superstructure formation depends on the size of the NPs and the numbers and the structure of the attached ligands.

It was found that the larger size of LC AuNPs exhibit a strong dichroism due to the splitting of its plasmonic resonance under shear alignment. This effect was shown to result from the combined effect of the mesogen birefringence and of anisotropic NP-NP coupling, due to short range order in the NP arrangement induced by the mesogenic

ligands. These results show that LC functionalisation enables the realisation of anisotropic metamaterials with enhanced responses.

2. 5 Experimental

2. 5.1 Monolayer Gold Nanoparticles (29)

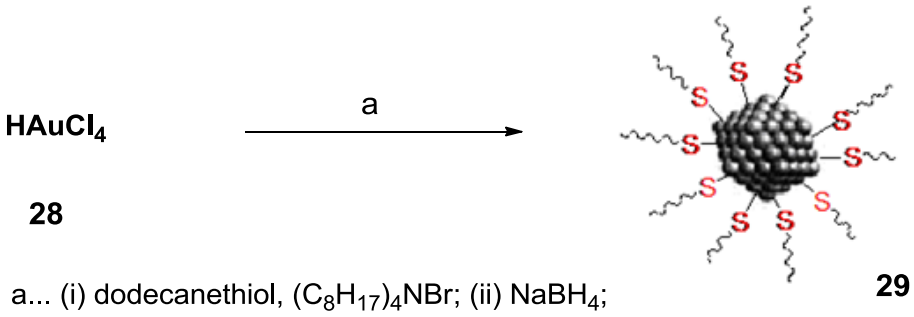

An aqueous solution of hydrogen tetrachloroaurate (788 mg, 67 ml, and 30 mmol dm^{-3}) was mixed with a solution of tetraoctylammonium bromide in toluene (4.852 g, 8.888 mmol, 180 ml, and 50 mmol dm^{-3}). The two-phase mixture was vigorously stirred until all the tetrachloroaurate was transferred into the organic layer and 1-dodecanethiol (675 mg, 3.3345 mmol, 3.334 mmol) was then added to the organic phase. A freshly prepared aqueous solution of sodium borohydride (840 mg, 22.2 mmol, 56 ml, and 0.4 mol dm^{-3}) was slowly added with vigorous stirring. After further stirring for 3 h, the organic phase was separated, evaporated to 10 ml in a rotary evaporator and mixed with ethanol (400 ml) to remove excess thiol. The mixture was kept for 14 h at -18 ^{o}C and the dark brown precipitate was filtered off and washed with ethanol to yield a dark red waxy solid (435.8 mg). Elemental analysis: Found 15.47 % C, 2.67 % H, 3.5 % S. TGA Found 76.89 % Au. ICP found 66.52 % Au, 2.76 % S. Purity (GPC): > 90 %.[116]

2. 5.2 Mesogenic Gold Nanoparticles (30)

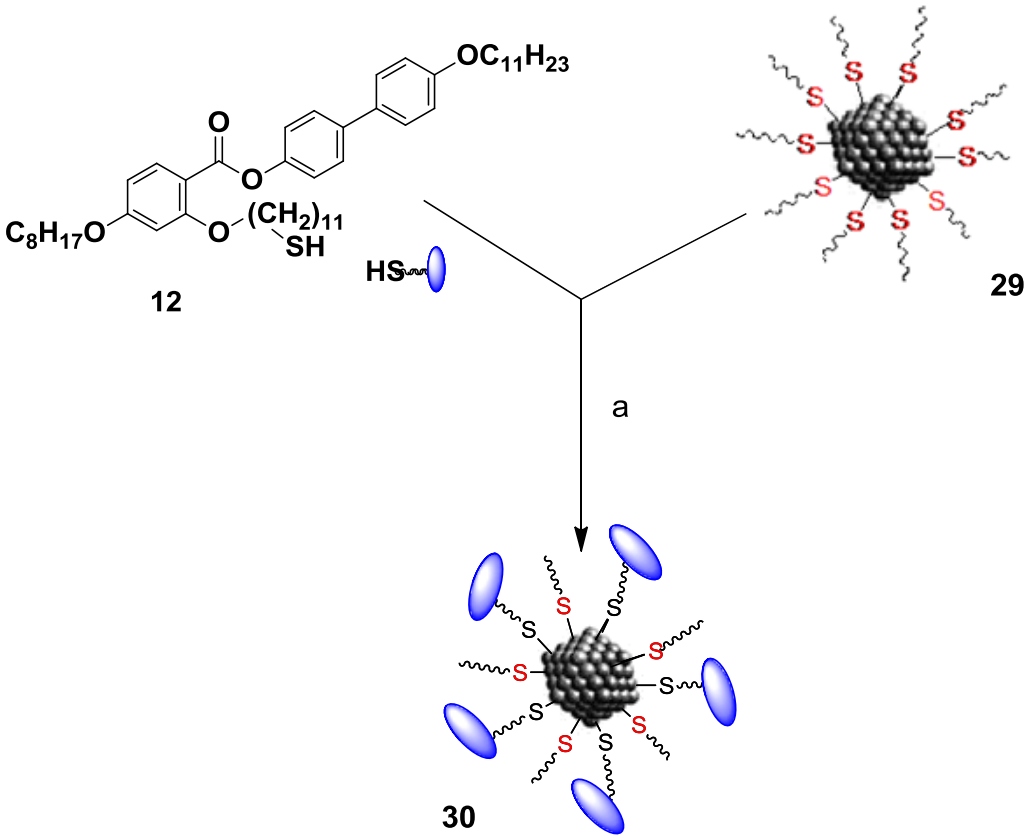

a... stir mixing mesogen **12** and NP **30** in DCM.

Compound **29** (93 mg) and compound **12** (135.8 mg, 0.1752 mmol) were dissolved in DCM (75 ml) and stirred in a closed environment under nitrogen for 4 days. Solvent was removed under reduced pressure at low temperature before bio-beads size exclusion column chromatography in THF, and yielded a deep dark red waxy solid (139.5 mg). Elemental analysis: Found 24.53 % C, 3.39 % H, 3.34 % S. Purity (GPC): > 91 %.

During experiment **30a** – **f**, all main procedures of repeated LC AuNPs experiments were followed as experiment **30** for characterisation. Analysis data of all synthesized LC AuNPs are shown in Table 2.8 below.[152, 153]

Sample	Reaction time	EA	GPC	TGA (Au %)
30a	4 days	24.53 % **C**, 3.39 % **H,** 3.34 % **S**	> 95 %	N/ A
30b	3 days	32.49 % **C**, 4.19 % **H**, 0.86 % **S**		N/ A
30c	5 days	25.05 % **C**, 3.75 % **H**, 2.89 % **S**		N/ A
30d	3 days	22.49 % **C**, 3.41 % **H**, 3.32 % **S**		70.72 %
30e	3 days	24.63 % **C**, 3.58 % **H**, 2.9 % **S**		65.03 %
30f	3 days	25.07 % **C**, 3.83 % **H**, 2.61 % **S**		69.21 %

Table 2. 8. EA and TGA of synthesized LC AuNPs

The purity of synthesized LC AuNPs have confirmed by ^{1}H NMR spectra and compared with ^{1}H NMR spectra of thiol mesogen **12**. Due to lack of product **30a**, **30b** and **30c**, TGA was not carried out. Compound **30d** was analysed by ICP and found 73.68 % Au, 2.85 % S. Further purified compound showed **30b** transition temperature (^{o}C): N 61.43 ^{o}C Iso.

2. 5.3 Deuterated Compounds Synthesis

2. 5.3.1 Synthetic Method Development

2. 5.3.1.1 Bromododecane (32)

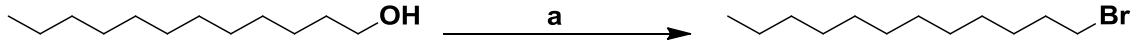

31 a... PBr_3, dry DCM; **32**

To the stirred solution of 1-dodecanol (compound **31**, 0.4658 g, 25 mmol) in dry DCM (2.5 ml), PBr_3 (0.8121 g, 3 mmol) in dry DCM (5 ml) was added dropwise at 0 ^oC. The reaction mixture was stirred at room temperature for 30 minutes. Thereafter the solution was evaporated to obtain a residue which was partitioned between ethyl acetate (15 ml) and water (13 ml), the organic layer was separated and dried over $MgSO_4$ and evaporated to obtain an oily residue. It was quickly purified by a flush chromatography in hexane with short silica column to yield a light brown oil compound **32** (0.22 g, 17.7%). ^{1}H-NMR 400 MHz ($CDCl_3$): δ [ppm] = 0.86 (t, 3 H, CH_3), 1.18-1.45 (s, 18 H, CH_2), 1.78-1.88 (quint, 2 H, CH_2CH_2Br), 3.37 (t, 2 H, CH_2Br).[207]

2. 5.3.1.2 S-Dodecyl ethanethioate (33)

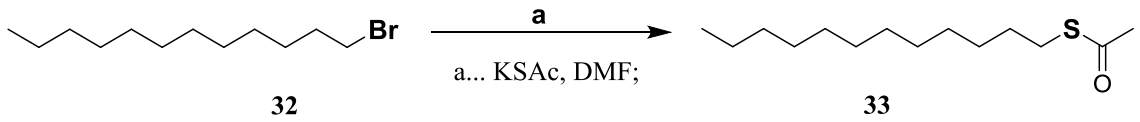

32 **33**

Method 1

Compound **32** (2.0 mmol, 0.498 g) was added to a stirred solution of potassium thioacetate (2.0 mmol, 0.228 g) in DMF (40 ml) and mixture was left stirring at room temperature for approximately 5 days. The solution was then partitioned between water and DCM, and then the combined organic layer was dried over $MgSO_4$ and evaporated in *vacco*. Product was obtained without further purification yield a light yellow oil compound **33** (0.29 g, 59.2%). ^{1}H-NMR 400 MHz ($CDCl_3$): δ [ppm] = 0.87 (t, 3 H, CH_3), 1.20-1.38 (m, 18 H, CH_2), 1.55 (quint, 2 H, CH_2CH_2SCO), 2.31 (s, 3 H, $SCOCH_3$), 2.85 (t, 2 H, SCH_2).[208-211]

Method 2

The same reagents were used as in *method 1*, except a microwave reactor was used instead of a conventional mechanic stirring at room temperature. The setting of this microwave reactor was 200 watts, temperature 153 ^{o}C, pressure 240 psi, high stirring speed (800 rmp) with holding time 2 x 30 seconds for 10 minutes. The targeted temperature was reached in 2 minutes at pressure approximately 55 psi. After cooling the reaction vessel with nitrogen, the reaction mixture was extracted by DCM. The organic solvent was evaporated and yielded light orange compound **33** (0.24 g, 98%). ^{1}H-NMR 400 MHz ($CDCl_3$): δ [ppm] = 0.87 (t, 3 H, CH_3), 1.20-1.38 (m, 18 H, CH_2), 1.55 (quint, 2 H, CH_2CH_2SCO), 2.31 (s, 3 H, $SCOCH_3$), 2.85 (t, 2 H, SCH_2).

Method 3

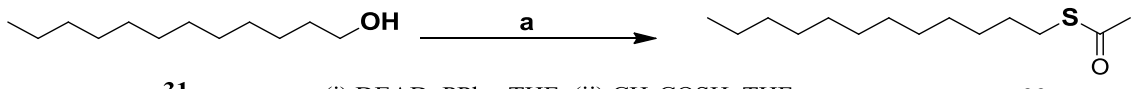

31 a... (i) DEAD, PPh_3, THF; (ii) CH_3COSH, THF; **33**

Diethyl azodicarboxylate (DEAD, 0.5 g, 2.4 mmol) was added to an efficiently stirred solution of triphenyl phosphine (0.63 g, 2.4 mmol) in THF (6 ml) at 0 ^{o}C for 30 minutes

under nitrogen. A solution of 1-dodecanol (**31**, 0.223 g, 1.2 mmol) and thioacetic acid (0.1824 g, 2.4 mmol, 0.41 ml) in THF (3 ml) was added dropwise over 2 minutes and the mixture was stirred for 1 hour at ambient temperature. A clear yellow solution was obtained. The solution was concentrated and the residue was purified by flash chromatography over silica gel (hexane / DCM = 5 / 2) to give desired orange oily thioacetate compound **33** (0.10 g, 34%). ^{1}H-NMR 400 MHz ($CDCl_3$): δ [ppm] = 0.87 (t, 3 H, CH_3), 1.20-1.38 (m, 18 H, CH_2), 1.55 (quint, 2 H, CH_2CH_2SCO), 2.31 (s, 3 H, $SCOCH_3$), 2.85 (t, 2 H, SCH_2).

Method 4

Excess of DEAD (1.0 g, 0.93 ml) in dry THF (3 ml) was added to triphenylphosphine (0.7 g), 1-dodecanol (**31**, 0.28 g, 1.2 mmol) and thioacetic acid (0.5 ml) in dry THF (6 ml) at 0 ^{o}C in an ice bath dropwise slowly under nitrogen, the mixture was stirred for another hour at 0 ^{o}C before bringing up to room temperature and left overnight for 18 hours. The final mixture was quenched with aqueous NH_4Cl and extracted with ethyl acetate. The combined organic phase were washed with brine, dried over $MgSO_4$ and filtered. After evaporation of the solvent, the organic residue was triturated with hexane and the precipitate of triphenylphosphine oxide was filtered off. The filtrate was evaporated and purified by column chromatography to afford compound **33** (0.17 g, 58%). ^{1}H-NMR 400 MHz ($CDCl_3$): δ [ppm] = 0.87 (t, 3 H, CH_3), 1.20-1.38 (m, 18 H, CH_2), 1.55 (quint, 2 H, CH_2CH_2SCO), 2.31 (s, 3 H, $SCOCH_3$), 2.85 (t, 2 H, SCH_2).

Method 5

Most of the experimental procedures were followed as *method 3*, except PPh_3 recrystallised by ether/hexane was used, then NaOH (0.5 M, 2 x 15 ml), water (2 x 15 ml), brine (15 ml), then dried over $MgSO_4$. Organic was evaporated under *vacco*, then dissolved in DCM (20 ml), followed by washing with H_2O_2 (30% w/v, 10 ml) in water (10 ml), and saturated Na_2SO_3 solution (20 ml) was added after. The final aqueous layer was extracted by DCM (20 ml), and then combined DCM solution dried over $MgSO_4$, then column chromatography to yield light orange oil (0.23 g, 78%). ^{1}H-NMR 400 MHz ($CDCl_3$): δ [ppm] = 0.87 (t, 3 H, CH_3), 1.20-1.38 (m, 18 H, CH_2), 1.55 (quint, 2 H, CH_2CH_2SCO), 2.31 (s, 3 H, $SCOCH_3$), 2.85 (t, 2 H, SCH_2).

Several other reaction conditions were explored as shown in the Table 2. 9 below:

Exp.	Reaction conditions	Yield %
33 a	Excess of PPh_3, DEAD; 0 ^oC	0.18 g, 61%
33 b	Dry reagents and glassware; recystallised PPh_3;	0.21 g, 71%
33 c	Pentane / Ether (10 / 1 volume ratio) was used to triturate	0.17 g, 58% and simplified procedures

Table 2. 9. optimised reaction condition for compound 33 synthesis.

Method 6

Diisopropyl azodicarboxylate (DIAD, 0.75 ml, 3.875 mmol) was added to a stirred solution of triphenyl phosphine (1g, 3.8 mmol) in THF (10 ml) at 0 ^oC under nitrogen, and the mixture was stirred at this temperature for 30 minutes. A solution of 1-dodecanol (**31**, 1.925 mmol) and thioacetic acid (0.275 ml, 3.8 mmol) in THF (5 ml) then was added dropwise over 2 minutes. Then mixture was stirred for 1 hour at 0 ^oC and for an additional hour at ambient temperature. The mixture was concentrated and purified by flash chromatography on silica gel (hexane / EtOAc = 95/5). However no product was obtained.

Method 7

Most of the experimental procedures were followed as in *method 2*, except excess of DIAD, dry reagents, dry glassware and recrystallised PPh_3 were used. The reaction mixture was washed with NaOH (0.5 M, 2 x 15 ml), water (2 x 15 ml), brine (15 ml), then dried over $MgSO_4$. After evaporating the organic solvent, a silica column chromatography was used to obtain light orange oil compound **33** (0.23 g, 78%). ^{1}H-NMR 400 MHz ($CDCl_3$): δ [ppm] = 0.87 (t, 3 H, CH_3), 1.20-1.38 (m, 18 H, CH_2), 1.55 (quint, 2 H, CH_2CH_2SCO), 2.31 (s, 3 H, $SCOCH_3$), 2.85 (t, 2 H, SCH_2).

2. 5.3.1.3 Dodecane-1-thiol (34)

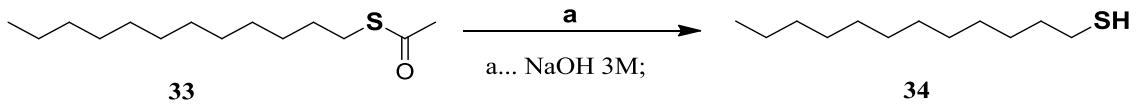

33 34

Method 1

Compound **33** (0.29 g, 1.186 mmol) in acetone (12 ml) was treated with 3M aqueous NaOH (10 ml) for 1 – 2 hours. The solution was then neutralized with 1M HCl to pH7, followed by extraction with DCM (3 x 10 ml). The organic layer was dried over $MgSO_4$. No product was obtained.

Method 2

Compound **33** (0.23 g, 0.941 mmol) in ethanol (2 ml) and NaOH (8.3 M, 0.5 ml) were refluxed for 2 hours, and then cooled to room temperature. The mixture was neutralised with 2 M HCl and transferred to a separating funnel, extracted with ether (2 x 4 ml) and the organic phase washed with brine (2 x 2ml), water (2 x 2 ml), and then dried over with $MgSO_4$. Solvent evaporated under *vacco*. However the desired product was unable to obtain.

Method 3

Compound **33** (0.17 g, 0.6955 mmol) dissolved in solvent mixture of dry MeOH (3 ml) and dry chloroform (4 ml) at room temperature, then NaSMe (73.1 mg, 1.044 mmol) in dry MeOH (1.1 ml) was added into the reaction mixture dropwise, this mixture was stirred at room temperature for 30 min. The solution is then added to aqueous HCl (14 ml / 0. M). The aqueous solution is extracted with DCM. The combined organic layers were washed with brine, water and dried over $MgSO_4$. Filtered and concentrated before column chromatography to yield light brown oil compound **34** (0.12 g, 85%). ^{1}H-NMR 400 MHz ($CDCl_3$): δ [ppm] = 0.87 (t, 3 H, CH_3), 1.19-1.42 (m, 19 H, CH_2 and SH), 1.59 (quint, 2 H, CH_2CH_2SH), 2.49 (quart, 2 H, CH_2SH).[207, 210]

2. 5.3.2 Deuterated Compounds Synthesis

2. 5.3.2.1 Deuterated S-Dodecyl ethanethioate (36)

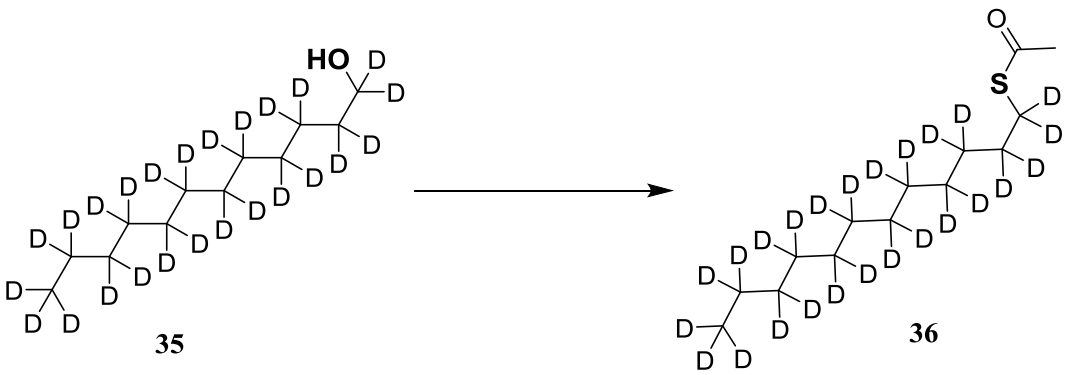

35 **36**

DEAD (95%, 0.5 g, 0.464 ml, 2.4 mmol) in dry THF (6 ml) were added to the mixture of PPh_3 (0.63 g, 2.4 mmol), compound **35** (0.2538 g, 1.2 mmol) and thioacetic acid (97%, 0.1824 g, 2.4 mmol, 1.69 ml) in dry THF (6 ml) was added dropwise very slowly at 0 ºC. The reaction was then stirred at this temperature for 1 hour, followed by stirring at room temperature for 12 h with monitoring by TLC. Reaction progress was monitored by GC and TLC. Solvents were evaporated by *vacco* and the residue was triturated in hexane and washed by H_2O_2 (30% w/v, 10 ml) and DCM, then washed by saturated sodium sulphite and water, finally dried over $MgSO_4$. The oily product was purified by column chromatography to yield light pale brown oil (0.18 g, 56%). The purity of compound **36** was confirmed by GC/MS and TLC.[210]

2. 5.3.2.2 Deuterated 1 – dodecanethiol (37)

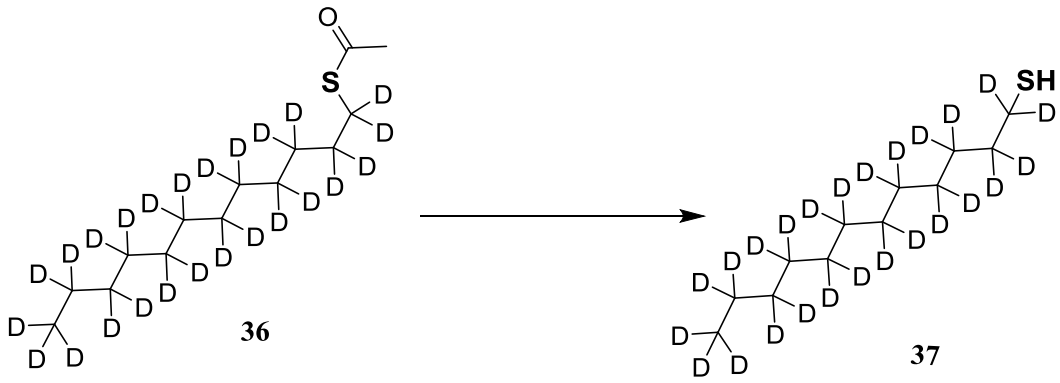

Compound **36** (0.18 g, 0.668 mmol) was dissolved in solvent mixture of dry MeOH (3 ml) and dry chloroform (4 ml) at room temperature, then NaSMe (70.1 mg, 1.0015 mmol) in dry MeOH (1.1 ml) was added into the reaction mixture dropwise. The mixture was stirred for 30 min at room temperature before adding to aqueous HCl (14 ml, 0.1 M). The aqueous solution was extracted with DCM. The combined organic layers were washed with brine, water and dried over $MgSO_4$ before evaporated solvent. The compound **37** (0.12 g, 79%) was obtained by column chromatography. The purity of compound **37** was analysed by GC/MS and confirmed by TLC.[212]

2. 5.3.3 Deuterated Gold Nanoparticles

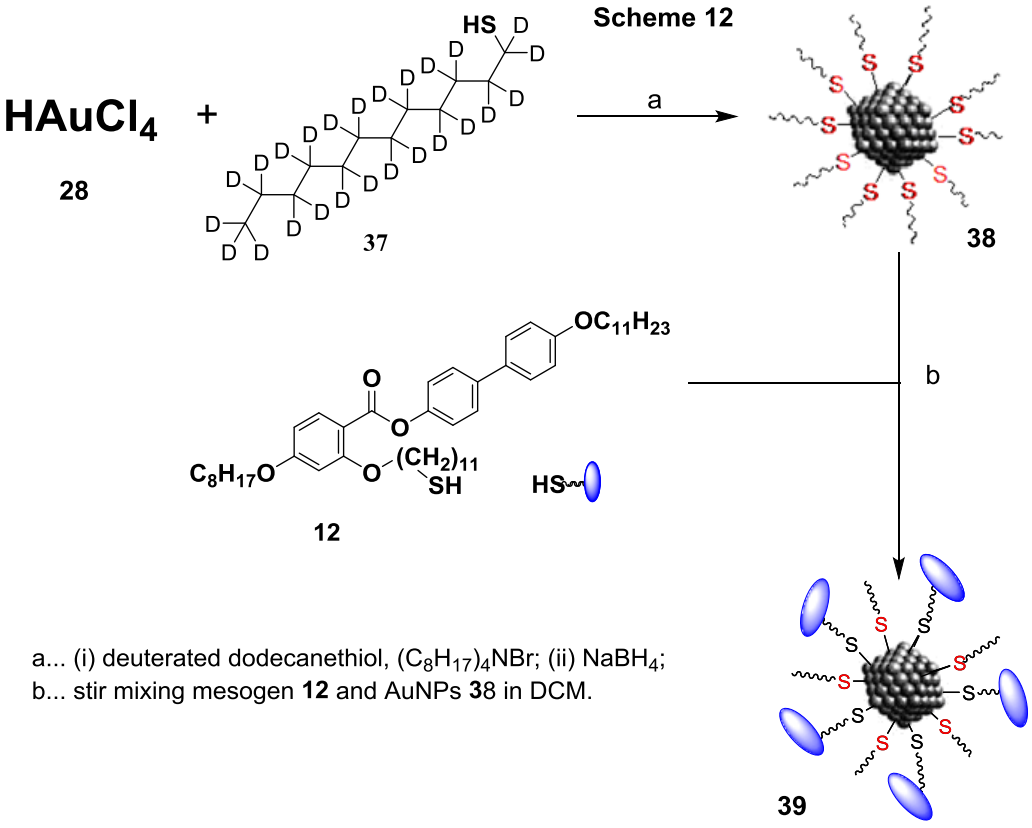

a... (i) deuterated dodecanethiol, $(C_8H_{17})_4NBr$; (ii) $NaBH_4$;
b... stir mixing mesogen **12** and AuNPs **38** in DCM.

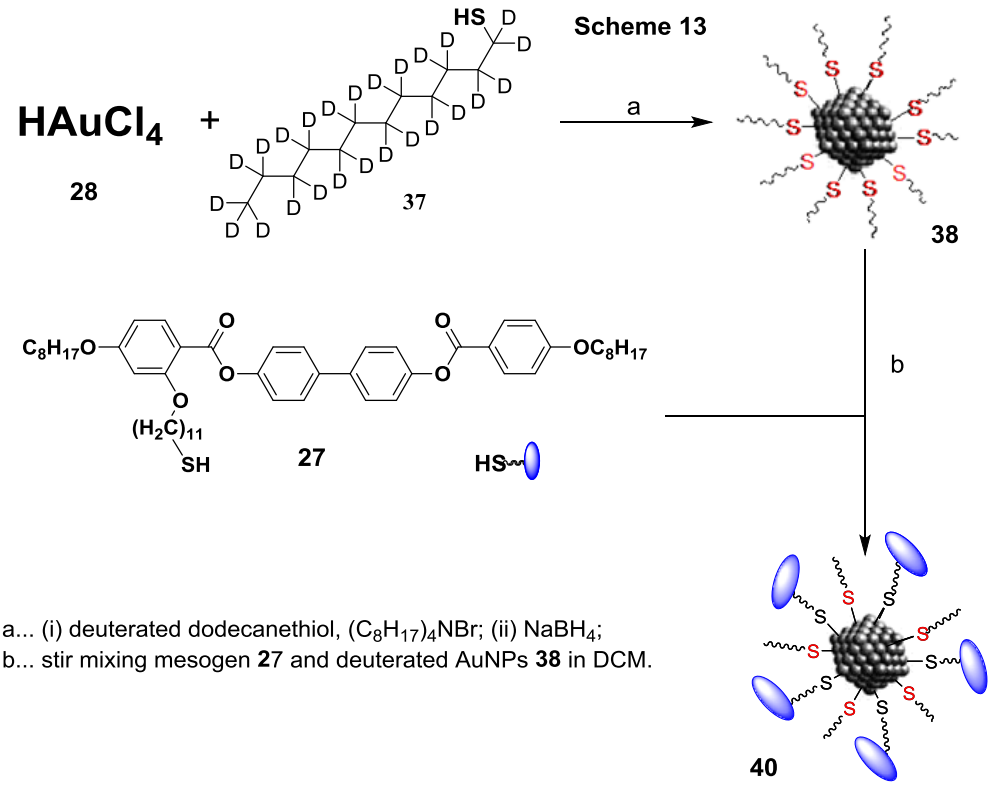

a... (i) deuterated dodecanethiol, $(C_8H_{17})_4NBr$; (ii) $NaBH_4$;
b... stir mixing mesogen **27** and deuterated AuNPs **38** in DCM.

2. 5.3.3.1 Deuterated Monolayer Gold Nanoparticles (38)[116]

All experimental procedures were followed as for compound **29**, except that deuterated 1-dodecanethiol was used as capping agent. Elemental analysis: Found C 14.5 %, H 2.59 % and S 2.94 %. TGA Found Au 76 %. Purity (GPC): > 95 %. Characterisation in progress.

2. 5.3.3.2 Deuterated Mesogenic Gold Nanoparticles (39)[152, 153]

All experimental procedures were followed as for compound **30**, except that deuterated 1-dodecanethiol capped AuNPs **38** was used as the exchange reaction core. Elemental analysis: Found C 30.61 %, H 4.15 % and S 2.31 %. Purity (GPC): > 95 %. Purity (GPC): > 95 %. Thermal transition at around 73 °C. TGA Found Au 58.6 %. Characterisation in progress.

2. 5.3.3.3 Deuterated Mesogenic Gold Nanoparticles (40)[152, 153]

All experimental procedures were followed as for compound **30**, except that deuterated 1-dodecanethiol capped AuNPs **38** and four rings thiol mesogen **27** were used as the exchange reaction reagents. Characterisation in progress.

2. 6 Instrumentations and Techniques

All compounds synthesised were purified and subjected to a range of analytical techniques by using the following instruments, as required, in order to assess both structure and purity. Intermediate compounds were subjected to ^{1}H Nuclear Magnetic Resonance (NMR) spectroscopy in most cases.

2. 6.1 Transmission Electron Microscopy (TEM)

Transmission electron microscopy was used to determine the size of prepared gold nanoparticles. One or two drops of a toluene solution of the nanoparticles is added to carbon coated copper grids and allowed to air dry. The grids are viewed by using a Jeol 2010 Transmission Electron Microscope at an accelerating voltage of 200kV. Images were acquired using a Gatan UltraScan 4000 digital camera.

2. 6.2 Thermo Gravimetric Analysis (TGA)

TGA analysis was used to determine the gold percentage by burning off all organic parts in an inert environment at high temperature, it was carried out by a Metler Toledo TGA/DSC1 with STAR^{e} system software, which controlled gas delivery flow rate system, burning 2 – 15 mg of sample in alumina crucibles in nitrogen first, and then followed with burning in air, at a flow rate of 100 ml/min. The temperature was ramped from room temperature to 950 ^{o}C at 20 ^{o}C/min, and the weight of sample is recorded against both temperature and time.

2. 6.3 Inductively Coupled Plasma (ICP)

ICP analysis of gold and sulphur (Au/S) ratio of some of the AuNPs and final LC AuNPs was carried out by a Perkin-Elmer Optima 5300 dual view ICP-OES with WinLab 32 ICP system software, which controlled gas flow automatically within the range of 0-20 L/min, in 1 L/min increments for plasma argon and 0 to 2.0 L/min in 0.1 L/min increments for auxiliary argon a mass flow controller is supplied with all systems for the nebulizer argon flow and is variable between 0 and 2.0 L/min in 0.01 L/min increments. Samples were prepared by dissolving 5 – 15 mg of AuNPs in agua regia (1 ml HNO_3 and 2.5 ml HCl) at r.t. overnight, and then diluted with water to achieve 10 ppm as in sample weight. The system controlled pump has speeds variable from 0.2 to 5 ml/min in 0.1 ml/min increments using 0.76 mm i.e. tubing.

2. 6.4 Sonication Bath

Sonication bath was used for gold nanoparticles purification. The model used is VWR Ultrasonic Cleaner type USC100TH. The bath is stainless steel and rust-proof with a tank 1L capacity (tank dimensions WxDxH of 190×85×60 mm). It has a heavy duty ultrasonic generator with a maximum output power 60W, heating at 65 °C, not adjustable and fill level.

2. 6.5 Thin Layer Chromatography (TLC)

TLC was used to monitor the progress of some reactions utilising either 100% dichloromethane or 4 : 6 hexane / dichloromethane, where appropriate. TLC was also used in conjunction with column chromatography and to assist in the determination of the purity of materials. The TLC plates used consisted of fluorescent silica gel 60 F_{254} (Merck) on PET aluminium foil and all plates were inspected in conjunction with an ultra violet light at a wavelength of both λ = 254 and 365 nm.

2. 6.6 Preparative Thin Layer Chromatography (Prep – TLC)

Preparative Thin Layer Chromatography was used to isolate product from some of small scale reactions utilising either 100% dichloromethane or 4 : 6 hexane / dichloromethane, where appropriate. The Analtech Inc. Prep-TLC plates (cat. 02012) used consisted of silica gel GF with preparative layer 500 µm and 20 x 20 cm dimensions or either Whatman Prep-TLC plates (4861-840) used consisted of fluorescent silica gel and fluorescent indicator PK6F 60Å preparative layer 1000 µm on glass plates 20 x 20 cm and both types of plates were inspected in conjunction with an ultra violet light at a wavelength of both λ = 254 and 365 nm.

2. 6.7 Column Chromatography

Column chromatography was used to purify many materials and separations carried out using BDH silica gel, 33-70 µm, and eluted using the solvents stated in the appropriate preparation, under the influence of gravity. Final products were also filtered through Schleicher & Schuell filter papers or Porosity Sintered No. 4 funnel to remove particulates.

2. 6.8 Ultraviolet Sources

Two types of UV sources were used to generate radicals for some experiments, and they are:

- A very strong white light bulb (200 – 400 Watt) was used as the first UV source. It was placed 1 cm away from the reaction flask, and it was used in conjunction with foil wrapped in a sealed environment to achieve maximum irradiation.
- A UVGL-Handheld UV Lamp (254/ 365 nm UV, 16 Watt, 230 V, ~ 50Hz and 0.12 Amps) made by UVP used for checking TLC was also used as a UV source, and the lamp was placed 1 cm away from the reaction flask, also the long wavelength 365 nm was selected in conjunction with foil wrapped in a sealed environment to achieve maximum irradiation.

2. 7 References

1. T. K. Sau and A. L. Rogach, *Adv. Mater.*, 2010, **22**, 1781-1804.
2. B. J. Wiley, S. H. Im, Z. Y. Li, J. McLellan, A. Siekkinen and Y. A. Xia, *J. Phys. Chem. B*, 2006, **110**, 15666-15675.
3. I. O. Sosa, C. Noguez and R. G. Barrera, *J. Phys. Chem. B*, 2003, **107**, 6269-6275.
4. C. T. Campbell, S. C. Parker and D. E. Starr, *Science*, 2002, **298**, 811-814.
5. M. Valden, X. Lai and D. W. Goodman, *Science*, 1998, **281**, 1647-1650.
6. K. M. Fergusson, PhD thesis "The Synthesis and Properties of Achiral and Chiral Bent-core Liquid Crystals", Hull, 2008.
7. W. Y. Liang, *Physics Education*, 1970, **5**, 226 - 228.
8. I. Dierking, *Textures of Liquid Crystals*, Wiley-VCH Verlag GmbH & Co. KGaA, 2003.
9. G. Schmid and B. Corain, *Eur. J. Inorg. Chem.*, 2003, 3081-3098.
10. G. Hodes, *Adv. Mater.*, 2007, **19**, 639-655.
11. M. C. Daniel and D. Astruc, *Chem. Rev.*, 2004, **104**, 293-346.
12. P. Alitalo, C. Simovski, A. Viitanen and S. Tretyakov, *Physical Review B*, 2006, **74**.
13. C. Rockstuhl, F. Lederer, C. Etrich, T. Pertsch and T. Scharf, *Phys. Rev. Lett.*, 2007, **99**.
14. C. Rockstuhl and T. Scharf, *Journal of Microscopy-Oxford*, 2008, **229**, 281-286.
15. K. D. Sattler, *Handbook of Nanophysics: Nanoparticles and Quantum Dots*, CRC Press, 2010.
16. S. Muhlig, M. Farhat, C. Rockstuhl and F. Lederer, *Physical Review B*, 2011, **83**.
17. J. B. Pendry, A. J. Holden, D. J. Robbins and W. J. Stewart, *Ieee Transactions on Microwave Theory and Techniques*, 1999, **47**, 2075-2084.
18. V. M. Shalaev, W. S. Cai, U. K. Chettiar, H. K. Yuan, A. K. Sarychev, V. P. Drachev and A. V. Kildishev, *Optics Letters*, 2005, **30**, 3356-3358.
19. J. Valentine, S. Zhang, T. Zentgraf, E. Ulin-Avila, D. A. Genov, G. Bartal and X. Zhang, *Nature*, 2008, **455**, 376-U332.
20. I. Freestone, N. Meeks, M. Sax and C. Higgitt, *Gold Bull.*, 2007, **40**, 270-277.
21. D. G. Richards, D. L. McMillin, E. A. Mein and C. D. Nelson, *Int. J. Neurosci.*, 2002, **112**, 31-53.
22. M. Faraday, *Philosophical Transactions of Royal Society*, 1857, **147**, 145 - 181.
23. M. Matsumoto, H. Yoshimura, V. S. Kulkarni and K. Nagayama, *Colloid Polym. Sci.*, 1990, **268**, 1174-1178.
24. G. Mie, *Ann. Phys*, 1908, **25**.
25. J. Boudon, University fo Neuchatel, 2009.
26. K. Kim, H. B. Lee, J. W. Lee, H. K. Park and K. S. Shin, *Langmuir*, 2008, **24**, 7178-7183.
27. V. Maheshwari, J. Kane and R. F. Saraf, *Adv. Mater.*, 2008, **20**, 284-287.
28. O. P. Khatri, K. Murase and H. Sugimura, *Langmuir*, 2008, **24**, 3787-3793.
29. Y. Bae, N. H. Kim, M. Kim, K. Y. Lee and S. W. Han, *J. Am. Chem. Soc.*, 2008, **130**, 5432-5433.
30. G. Schmid, V. Maihack, F. Lantermann and S. Peschel, *J. Chem. Soc.-Dalton Trans.*, 1996, 589-595.
31. N. Toshima, *Macromol. Symp.*, 2003, **204**, 219-226.
32. S. K. Ghosh and T. Pal, *Chem. Rev.*, 2007, **107**, 4797-4862.
33. M. Brust and C. J. Kiely, *Colloid Surf. A-Physicochem. Eng. Asp.*, 2002, **202**, 175-186.

34. J. C. Love, L. A. Estroff, J. K. Kriebel, R. G. Nuzzo and G. M. Whitesides, *Chem. Rev.*, 2005, **105**, 1103-1169.
35. G. Schmid, *Nanoparticles: From Theory to Application*, Wiley-VCH Verlag GmbH & Co. KGaA, Essen, Germany., 2005.
36. M. C. Bowman, T. E. Ballard, C. J. Ackerson, D. L. Feldheim, D. M. Margolis and C. Melander, *J. Am. Chem. Soc.*, 2008, **130**, 6896-6897.
37. C. J. Murphy, A. M. Gole, J. W. Stone, P. N. Sisco, A. M. Alkilany, E. C. Goldsmith and S. C. Baxter, *Accounts Chem. Res.*, 2008, **41**, 1721-1730.
38. T. W. Odom and C. L. Nehl, *ACS Nano*, 2008, **2**, 612-616.
39. R. A. Sperling, P. Rivera gil, F. Zhang, M. Zanella and W. J. Parak, *Chem. Soc. Rev.*, 2008, **37**, 1896-1908.
40. L. Duchesne, D. Gentili, M. Comes-Franchini and D. G. Fernig, *Langmuir*, 2008, **24**, 13572-13580.
41. J. Zhao, A. O. Pinchuk, J. M. McMahon, S. Z. Li, L. K. Ausman, A. L. Atkinson and G. C. Schatz, *Accounts Chem. Res.*, 2008, **41**, 1710-1720.
42. E. Boisselier and D. Astruc, *Chem. Soc. Rev.*, 2009, **38**, 1759-1782.
43. O. Tzhayik, P. Sawant, S. Efrima, E. Kovalev and J. T. Klug, *Langmuir*, 2002, **18**, 3364-3369.
44. L. A. Porter, D. Ji, S. L. Westcott, M. Graupe, R. S. Czernuszewicz, N. J. Halas and T. R. Lee, *Langmuir*, 1998, **14**, 7378-7386.
45. T. Yonezawa, K. Yasui and N. Kimizuka, *Langmuir*, 2001, **17**, 271-273.
46. A. Manna, P. L. Chen, H. Akiyama, T. X. Wei, K. Tamada and W. Knoll, *Chem. Mat.*, 2003, **15**, 20-28.
47. R. Resch, C. Baur, A. Bugacov, B. E. Koel, P. M. Echternach, A. Madhukar, N. Montoya, A. A. G. Requicha and P. Will, *J. Phys. Chem. B*, 1999, **103**, 3647-3650.
48. N. Felidj, J. Aubard, G. Levi, J. R. Krenn, A. Hohenau, G. Schider, A. Leitner and F. R. Aussenegg, *Appl. Phys. Lett.*, 2003, **82**, 3095-3097.
49. R. Balasubramanian, B. Kim, S. L. Tripp, X. J. Wang, M. Lieberman and A. Wei, *Langmuir*, 2002, **18**, 3676-3681.
50. A. Wei, *Chem. Commun.*, 2006, 1581-1591.
51. R. Balasubramanian, Y. G. Kwon and A. Wei, *J. Mater. Chem.*, 2007, **17**, 105-112.
52. E. J. Shelley, D. Ryan, S. R. Johnson, M. Couillard, D. Fitzmaurice, P. D. Nellist, Y. Chen, R. E. Palmer and J. A. Preece, *Langmuir*, 2002, **18**, 1791-1795.
53. W. W. Weare, S. M. Reed, M. G. Warner and J. E. Hutchison, *J. Am. Chem. Soc.*, 2000, **122**, 12890-12891.
54. M. Green and P. O'Brien, *Chem. Commun.*, 2000, 183-184.
55. D. V. Leff, L. Brandt and J. R. Heath, *Langmuir*, 1996, **12**, 4723-4730.
56. J. Chen, L. C. Calvet, M. A. Reed, D. W. Carr, D. S. Grubisha and D. W. Bennett, *Chem. Phys. Lett.*, 1999, **313**, 741-748.
57. G. T. Li, M. Lauer, A. Schulz, C. Boettcher, F. T. Li and J. H. Fuhrhop, *Langmuir*, 2003, **19**, 6483-6491.
58. W. L. Cheng, S. J. Dong and E. K. Wang, *Angew. Chem.-Int. Edit.*, 2003, **42**, 449-452.
59. F. Tam, G. P. Goodrich, B. R. Johnson and N. J. Halas, *Nano Lett.*, 2007, **7**, 496-501.
60. M. Zayats, R. Baron, I. Popov and I. Willner, *Nano Lett.*, 2005, **5**, 21-25.
61. W. F. Sun, Q. Dai, J. G. Worden and Q. Huo, *J. Phys. Chem. B*, 2005, **109**, 20854-20857.
62. I. H. El-Sayed, X. H. Huang and M. A. El-Sayed, *Nano Lett.*, 2005, **5**, 829-834.

63. J. E. Sipe and R. W. Boyd, *Phys. Rev. A*, 1992, **46**, 1614-1629.
64. W. H. Zhang, X. D. Cui, B. S. Yeo, T. Schmid, C. Hafner and R. Zenobi, *Nano Lett.*, 2007, **7**, 1401-1405.
65. X. B. Mang, X. B. Zeng, B. J. Tang, F. Liu, G. Ungar, R. B. Zhang, L. Cseh and G. H. Mehl, *J. Mater. Chem.*, 2012, **22**, 11101-11106.
66. C. H. Yu, C. P. J. Schubert, C. Welch, B. J. Tang, M. G. Tamba and G. H. Mehl, *J. Am. Chem. Soc.*, 2012, **134**, 5076-5079.
67. Y. Shichibu, Y. Negishi, T. Tsukuda and T. Teranishi, *J. Am. Chem. Soc.*, 2005, **127**, 13464-13465.
68. G. H. Woehrle, L. O. Brown and J. E. Hutchison, *J. Am. Chem. Soc.*, 2005, **127**, 2172-2183.
69. M. J. Hostetler, A. C. Templeton and R. W. Murray, *Langmuir*, 1999, **15**, 3782-3789.
70. R. Hong, J. M. Fernandez, H. Nakade, R. Arvizo, T. Emrick and V. M. Rotello, *Chem. Commun.*, 2006, 2347-2349.
71. A. Kassam, G. Bremner, B. Clark, G. Ulibarri and R. B. Lennox, *J. Am. Chem. Soc.*, 2006, **128**, 3476-3477.
72. S. Si, C. Gautier, J. Boudon, R. Taras, S. Gladiali and T. Buergi, *J. Phys. Chem. C*, 2009, **113**, 12966-12969.
73. M. G. Warner, S. M. Reed and J. E. Hutchison, *Chem. Mat.*, 2000, **12**, 3316-3320.
74. S. Rucareanu, V. J. Gandubert and R. B. Lennox, *Chem. Mat.*, 2006, **18**, 4674-4680.
75. K. A. Flanagan, J. A. Sullivan and H. Mueller-Bunz, *Langmuir*, 2007, **23**, 12508-12520.
76. R. W. Wood, *Proceedings of the Physical Society of London*, 1902, **18**, 269-275.
77. S. Link and M. A. El-Sayed, *J. Phys. Chem. B*, 1999, **103**, 8410-8426.
78. R. H. Ritchie, E. T. Arakawa, J. J. Cowan and R. N. Hamm, *Phys. Rev. Lett*, 1968, **21**, 1530-1533.
79. A. Otto, *Zeitschrift für Physik* 1968, **216**, 398-410.
80. E. Kretschmann and H. Raether, *Z. Naturforsch.*, 1968, **23**, 2315.
81. B. Liedberg, C. Nylander and I. Lunström, *Sensors and Actuators*, 1983, **4**, 299-304.
82. S. Nath, S. Jana, M. Pradhan and T. Pal, *J. Colloid Interface Sci.*, 2010, **341**, 333-352.
83. K. L. Kelly, E. Coronado, L. L. Zhao and G. C. Schatz, *J. Phys. Chem. B*, 2003, **107**, 668-677.
84. K. A. Willets and R. P. Van Duyne, in *Annual Review of Physical Chemistry*, Annual Reviews, Palo Alto, 2007, vol. 58, pp. 267-297.
85. M. M. Miller and A. A. Lazarides, *J. Phys. Chem. B*, 2005, **109**, 21556-21565.
86. S. Underwood and P. Mulvaney, *Langmuir*, 1994, **10**, 3427-3430.
87. P. Mulvaney, *Langmuir*, 1996, **12**, 788-800.
88. A. Henglein, *J. Phys. Chem.*, 1993, **97**, 5457-5471.
89. A. Henglein, *Ber. Bunsen-Ges. Phys. Chem. Chem. Phys.*, 1995, **99**, 903-913.
90. S. Link and M. A. El-Sayed, *Int. Rev. Phys. Chem.*, 2000, **19**, 409-453.
91. A. C. Templeton, J. J. Pietron, R. W. Murray and P. Mulvaney, *J. Phys. Chem. B*, 2000, **104**, 564-570.
92. M. D. Malinsky, K. L. Kelly, G. C. Schatz and R. P. Van Duyne, *J. Am. Chem. Soc.*, 2001, **123**, 1471-1482.
93. S. K. Ghosh, S. Nath, S. Kundu, K. Esumi and T. Pal, *J. Phys. Chem. B*, 2004, **108**, 13963-13971.

94. V. Sharma, K. Park and M. Srinivasarao, *Mater. Sci. Eng. R-Rep.*, 2009, **65**, 1-38.
95. L. M. Liz-Marzan, *Langmuir*, 2006, **22**, 32-41.
96. X. M. Lu, M. Rycenga, S. E. Skrabalak, B. Wiley and Y. N. Xia, in *Annual Review of Physical Chemistry*, Annual Reviews, Palo Alto, 2009, vol. 60, pp. 167-192.
97. E. Petryayeva and U. J. Krull, *Analytica Chimica Acta*, 2011, **706**, 8-24.
98. C. Sonnichsen, B. M. Reinhard, J. Liphardt and A. P. Alivisatos, *Nature Biotechnology*, 2005, **23**, 741-745.
99. C. S. Thaxton and C. A. Mirkin, *Nature Biotechnology*, 2005, **23**, 681-682.
100. Y. Choi, Y. Park, T. Kang and L. P. Lee, *Nat. Nanotechnol.*, 2009, **4**, 742-746.
101. Y. H. Choi, T. Kang and L. P. Lee, *Nano Lett.*, 2009, **9**, 85-90.
102. T. R. Jensen, M. D. Malinsky, C. L. Haynes and R. P. Van Duyne, *J. Phys. Chem. B*, 2000, **104**, 10549-10556.
103. A. V. Gaikwad, P. Verschuren, E. Eiser and G. Rothenberg, *J. Phys. Chem. B*, 2006, **110**, 17437-17443.
104. G. A. Rance, D. H. Marsh and A. N. Khlobystov, *Chem. Phys. Lett.*, 2008, **460**, 230-236.
105. U. Kreibig and M. Volmer, *Optical Properties of Metal Clusters*, Springer-Verlag, Berlin, 1995.
106. S. A. Maier, *Plamonics: Fundamentals and Applications*, Springer, Bath, 2007.
107. B. A. Parviz, D. Ryan and G. M. Whitesides, *IEEE Trans. Adv. Packag.*, 2003, **26**, 233-241.
108. M. P. Pileni, *J. Phys. Chem. B*, 2001, **105**, 3358-3371.
109. S. Lal, S. E. Clare and N. J. Halas, *Accounts Chem. Res.*, 2008, **41**, 1842-1851.
110. H. A. Atwater and A. Polman, *Nat. Mater.*, 2010, **9**, 205-213.
111. H. Yoshikawa, K. Maeda, Y. Shiraishi, J. Xu, H. Shiraki, N. Toshima and S. Kobayashi, *Jpn. J. Appl. Phys. Part 2 - Lett.*, 2002, **41**, L1315-L1317.
112. O. Buchnev, E. Ouskova, Y. Reznikov, V. Reshetnyak, H. Kresse and A. Grabar, *Molecular Crystals and Liquid Crystals*, 2004, **422**, 47-55.
113. H. Qi and T. Hegmann, *J. Mater. Chem.*, 2006, **16**, 4197-4205.
114. H. G. Craighead, *Science*, 2000, **290**, 1532-1535.
115. D. L. Feldheim, K. C. Grabar, M. J. Natan and T. E. Mallouk, *J. Am. Chem. Soc.*, 1996, **118**, 7640-7641.
116. M. Brust, M. Walker, D. Bethell, D. J. Schiffrin and R. Whyman, *J. Chem. Soc.-Chem. Commun.*, 1994, 801-802.
117. J. Turkevich, P. C. Stevenson and J. Hillier, *Discuss. Faraday Soc.*,, 1951, **11**, 55-75.
118. B. V. Enustun and J. Turkevich, *J. Am. Chem. Soc.*,, 1963, **85**, 3317-3328.
119. D. C. Sayle, S. Seal, Z. Wang, B. C. Mangili, D. W. Price, A. S. Karakoti, S. Kuchibhatla, Q. Hao, G. Mobus, X. Xu and T. X. T. Sayle, *ACS Nano*, 2008, **2**, 1237-1251.
120. A. K. Boal, F. Ilhan, J. E. DeRouchey, T. Thurn-Albrecht, T. P. Russell and V. M. Rotello, *Nature*, 2000, **404**, 746-748.
121. R. L. Whetten, J. T. Khoury, M. M. Alvarez, S. Murthy, I. Vezmar, Z. L. Wang, P. W. Stephens, C. L. Cleveland, W. D. Luedtke and U. Landman, *Adv. Mater.*, 1996, **8**, 428-433.
122. S. H. Sun, C. B. Murray, D. Weller, L. Folks and A. Moser, *Science*, 2000, **287**, 1989-1992.
123. S. Srivastava and N. A. Kotov, *Soft Matter*, 2009, **5**, 1146-1156.
124. Z. W. Quan and J. Y. Fang, *Nano Today*, 2010, **5**, 390-411.
125. J. Q. Xu, L. Y. Chen, H. Choi, H. Konish and X. C. Li, *Sci Rep*, 2013, **3**, 5.

126. N. Yamaguchi, VirginiaTech, 1999.
127. Z. T. Nagy, University of Strasbourg, 2012.
128. S. J. Tan, M. J. Campolongo, D. Luo and W. L. Cheng, *Nat. Nanotechnol.*, 2011, **6**, 268-276.
129. S. Y. Park, A. K. R. Lytton-Jean, B. Lee, S. Weigand, G. C. Schatz and C. A. Mirkin, *Nature*, 2008, **451**, 553-556.
130. D. Nykypanchuk, M. M. Maye, D. van der Lelie and O. Gang, *Nature*, 2008, **451**, 549-552.
131. R. Shenhar, T. B. Norsten and V. M. Rotello, *Adv. Mater.*, 2005, **17**, 657-669.
132. B. Donnio, P. Garcia-Vazquez, J. L. Gallani, D. Guillon and E. Terazzi, *Adv. Mater.*, 2007, **19**, 3534-3539.
133. S. Frein, J. Boudon, M. Vonlanthen, T. Scharf, J. Barbera, G. Suss-Fink, T. Burgi and R. Deschenaux, *Helv. Chim. Acta*, 2008, **91**, 2321-2337.
134. H. K. Bisoyi and S. Kumar, *Chem. Soc. Rev.*, 2011, **40**, 306-319.
135. S. I. Lim and C. J. Zhong, *Accounts Chem. Res.*, 2009, **42**, 798-808.
136. K. Kanie, M. Matsubara, X. B. Zeng, F. Liu, G. Ungar, H. Nakamura and A. Muramatsu, *J. Am. Chem. Soc.*, 2012, **134**, 808-811.
137. J. Muller, C. Sonnichsen, H. von Poschinger, G. von Plessen, T. A. Klar and J. Feldmann, *Appl. Phys. Lett.*, 2002, **81**, 171-173.
138. S. Y. Park and D. Stroud, *Phys. Rev. Lett.*, 2005, **94**.
139. G. M. Koenig, B. T. Gettelfinger, J. J. de Pablo and N. L. Abbott, *Nano Lett.*, 2008, **8**, 2362-2368.
140. J. Berthelot, A. Bouhelier, C. J. Huang, J. Margueritat, G. Colas-des-Francs, E. Finot, J. C. Weeber, A. Dereux, S. Kostcheev, H. I. El Ahrach, A. L. Baudrion, J. Plain, R. Bachelot, P. Royer and G. P. Wiederrecht, *Nano Lett.*, 2009, **9**, 3914-3921.
141. C. P. Lapointe, T. G. Mason and Smalyukh, II, *Science*, 2009, **326**, 1083-1086.
142. R. Pratibha, K. Park, I. I. Smalyukh and W. Park, *Optics Express*, 2009, **17**, 19459-19469.
143. C. Huang, A. Bouhelier, J. Berthelot, G. C. des-Francs, E. Finot, J. C. Weeber, A. Dereux, S. Kostcheev, A. L. Baudrion, J. Plain, R. Bachelot, P. Royer and G. P. Wiederrecht, *Appl. Phys. Lett.*, 2010, **96**.
144. E. Boisselier, A. K. Diallo, L. Salmon, J. Ruiz and D. Astruc, *Chem. Commun.*, 2008, 4819-4821.
145. E. Boisselier, A. K. Diallo, L. Salmon, C. Ornelas, J. Ruiz and D. Astruc, *J. Am. Chem. Soc.*, 2010, **132**, 2729-2742.
146. I. In, Y. W. Jun, Y. J. Kim and S. Y. Kim, *Chem. Commun.*, 2005, 800-801.
147. M. Draper, I. M. Saez, S. J. Cowling, P. Gai, B. Heinrich, B. Donnio, D. Guillon and J. W. Goodby, *Adv. Funct. Mater.*, 2011, **21**, 1260-1278.
148. M. Wojcik, W. Lewandowski, J. Matraszek, J. Mieczkowski, J. Borysiuk, D. Pociecha and E. Gorecka, *Angew. Chem.-Int. Edit.*, 2009, **48**, 5167-5169.
149. M. Wojcik, M. Kolpaczynska, D. Pociecha, J. Mieczkowski and E. Gorecka, *Soft Matter*, 2010, **6**, 5397-5400.
150. S. Kumar, S. K. Pal, P. S. Kumar and V. Lakshminarayanan, *Soft Matter*, 2007, **3**, 896-900.
151. V. M. Marx, H. Girgis, P. A. Heiney and T. Hegmann, *J. Mater. Chem.*, 2008, **18**, 2983-2994.
152. L. Cseh and G. H. Mehl, *J. Am. Chem. Soc.*, 2006, **128**, 13376-13377.
153. L. Cseh and G. H. Mehl, *J. Mater. Chem.*, 2007, **17**, 311-315.

154. X. B. Zeng, F. Liu, A. G. Fowler, G. Ungar, L. Cseh, G. H. Mehl and J. E. Macdonald, *Adv. Mater.*, 2009, **21**, 1746-1750.
155. J. W. Goodby, I. M. Saez, S. J. Cowling, V. Gortz, M. Draper, A. W. Hall, S. Sia, G. Cosquer, S. E. Lee and E. P. Raynes, *Angew. Chem.-Int. Edit.*, 2008, **47**, 2754-2787.
156. S. Mischler, S. Guerra and R. Deschenaux, *Chem. Commun.*, 2012, **48**, 2183-2185.
157. J. Milette, S. J. Cowling, V. Toader, C. Lavigne, I. M. Saez, R. B. Lennox, J. W. Goodby and L. Reven, *Soft Matter*, 2012, **8**, 173-179.
158. J. Milette, S. Relaix, C. Lavigne, V. Toader, S. J. Cowling, I. M. Saez, R. B. Lennox, J. W. Goodby and L. Reven, *Soft Matter*, 2012, **8**, 6593-6598.
159. FEI-Company, FEI Company, 2010.
160. M. Bellis, About.com.
161. G. Sosinsky and M. Ellisman, The Electron Microscopy Outreach Program, 2004.
162. D. B. Williams and C. B. Carter, *Transmission Electron Microscopy A Textbook for Materials Science*, 1st edn., Springer, New York, USA, 1996.
163. HongKong-University, Department of Physics, The Chinese University of Hong Kong, 19/10/2000 edn., 2000.
164. BSP, in *Histroy of Science*, The President and Fellows of Harvard College, Basic Science Partnership Harvard Medical School, vol. 2013.
165. BSP, Basic Science Partnership Harvard Medical School, vol. 2013.
166. A. Marshall, Stanford Nanocharacterization Laboratory.
167. H. Anderson, MicroscopeMaster.com 2010.
168. Nobelprize, Nobelprize.org, vol. 2013.
169. Univeristy-of-Aberdeen, University of Aberdeen, 02/10/2000 edn., 2000.
170. Univeristy-of-Queensland, The University of Queensland, 2012 edn., 2012.
171. R. F. Egerton, *Physical Principles of Electron Microscopy - An Introduction to TEM, SEM, and AEM*, Springer Science + Business Media, Inc., Edmonton, Alberta, Canada, 2005.
172. Nobelprize, Nobelprize.org.
173. J. Mayer, L. A. Giannuzzi, T. Kamino and J. Michael, *MRS Bull.*, 2007, **32**, 400-407.
174. B. Voutou, MANSiC, 01/01/2007 edn., 2007.
175. A. M. Striegel, Tau, W. W., Kirkland, J. J., Bly, D. D., *Modern Size-Exclusion Liquid Chromatography*, 2nd edn., John Wiley & Sons, Inc., New Jersey, 2009.
176. B. Prapancham, vol. 2013.
177. in *GPC - Gel Permeation Chromatography*, Waters Limited, vol. 2013.
178. , Wikipedia, the free encyclopedia, Wikipedia, the free encyclopedia, 2013, vol. 2013.
179. J. G. Dunn, *Thermogravimetric Analysis. Characterization of Materials.*, John Wiley & Sons, Inc, 2002.
180. S. Vyazovkin, *Thermogravimetric Analysis. Characterization of Materials. 1–12.*, John Wiley & Sons, Inc, 2012.
181. , Intertek Group plc, vol. 2013.
182. M. P. Sepe, *Thermal Analysis of Polymers* 11, RAPRA technology Ltd, 1997.
183. J. D. Menczel and R. B. Prime, *Thermal Analysis of Polymers - Fundamentals and Applications*, John Wiley & Sons, Inc., Hoboken, New Jersey, 2009.
184. *A Beginner's Guide to Thermogravimetric Analysis (TGA)*, PerkinElmer.
185. P. Calandra, G. Calogero, A. Sinopoli and P. G. Gucciardi, *Int. J. Photoenergy*, 2010, 15.

186. R. H. Terrill, T. A. Postlethwaite, C. H. Chen, C. D. Poon, A. Terzis, A. D. Chen, J. E. Hutchison, M. R. Clark, G. Wignall, J. D. Londono, R. Superfine, M. Falvo, C. S. Johnson, E. T. Samulski and R. W. Murray, *J. Am. Chem. Soc.*, 1995, **117**, 12537-12548.
187. A. C. Templeton, D. E. Cliffel and R. W. Murray, *J. Am. Chem. Soc.*, 1999, **121**, 7081-7089.
188. N. Kanayama, O. Tsutsumi, A. Kanazawa and T. Ikeda, *Chem. Commun.*, 2001, 2640-2641.
189. C. Jones, Agilent Technologies, Inc., Silke Sevemann, University of California, Riverside, CA 92501, USA, 08/02/2007 edn., 2007.
190. H. M. Santos, C. Lodeiro and J. L. Capelo-Martinez, in *Ultrasound in Chemistry: Analytical Applications*, ed. J. L. Capelo-Martinez, Wiley-VCH Verlag GmbH & Co. KGaA, Weinheim, Germany, 2009.
191. R. C. Langley, *Gold Bull.*, 1971, **4**, 62-66.
192. J. Dintinger, B. J. Tang, X. B. Zeng, F. Liu, T. Kienzler, G. H. Mehl, G. Ungar, C. Rockstuhl and T. Scharf, *Adv. Mater.*, 2013, **25**, 1999-2004.
193. M. C. Daniel, J. Ruiz, S. Nlate, J. C. Blais and D. Astruc, *J. Am. Chem. Soc.*, 2003, **125**, 2617-2628.
194. D. V. Leff, P. C. Ohara, J. R. Heath and W. M. Gelbart, *J. Phys. Chem.*, 1995, **99**, 7036-7041.
195. A. Labande, J. Ruiz and D. Astruc, *J. Am. Chem. Soc.*, 2002, **124**, 1782-1789.
196. Wikipedia, Wikipedia, vol. 2011.
197. D. I. Svergun and K. M.H., *Current Opinion in Biomolecular Structure*, 2002, **36**.
198. L. Onsager, *Annals of the New York Academy of Sciences*, 1949, **51**, 627-659.
199. P. J. Flory and G. Ronca, *Molecular Crystals and Liquid Crystals*, 1979, **54**, 289-309.
200. P. B. Johnson and R. W. Christy, *Physical Review B*, 1972, **6**, 4370-4379.
201. J. D. Bernal and R. H. Fowler, *Journal of Chemical Physics*, 1933, **1**, 515.
202. D. R. Nelson, *Nano Lett.*, 2002, **2**, 1125-1129.
203. Y. L. Xu, *Appl. Optics*, 1995, **34**, 4573-4588.
204. A. V. Kildishev, S. Xiao, U. K. Chettiar, H. K. Yuan, W. Cai, V. P. Drachev and V. M. Shalaev, in *Ofc: 2009 Conference on Optical Fiber Communication, Vols 1-5*, Ieee, New York, 2009, pp. 1523-1525.
205. D. R. Smith, P. Kolinko and D. Schurig, *J. Opt. Soc. Am. B-Opt. Phys.*, 2004, **21**, 1032-1043.
206. J. Yao, Z. W. Liu, Y. M. Liu, Y. Wang, C. Sun, G. Bartal, A. M. Stacy and X. Zhang, *Science*, 2008, **321**, 930-930.
207. A. K. Roy, B. Rajaraman and S. Batra, *Tetrahedron*, 2004, **60**, 2301-2310.
208. P. Kumar and K. C. Gupta, *Chem. Lett.*, 1996, 635-636.
209. T. C. Zheng, M. Burkart and D. E. Richardson, *Tetrahedron Lett.*, 1999, **40**, 603-606.
210. X. F. Yang, J. T. Mague and C. J. Li, *J. Org. Chem.*, 2001, **66**, 739-747.
211. P. W. Davies and S. J. C. Albrecht, *Angew. Chem.-Int. Edit.*, 2009, **48**, 8372-8375.
212. O. B. Wallace and D. M. Springer, *Tetrahedron Lett.*, 1998, **39**, 2693-2694.

Summary of Main Conclusions

Overall, it was found possible to synthesise AuNPs in a 1.5 – 3.5 nm regime. The synthetic parameters defining the polydispersity of NPs, such as concentration of reactants, reaction time, critically the purification methods were investigated in detail. Prepared systems were fully characterised, as well as by GPC and TEM. Synthetic parameters for the introduction of nematogen thiolate ligands were explored. A set of systems which show liquid crystal phase behaviours were prepared, polydispersity of such materials were addressed by detailed investigations of purification strategies. The investigation of liquid crystal properties was carried out in detail. Investigation of the liquid crystal properties of the materials, found that the deposition techniques were crucial for the observation of optical birefringence. In collaboration with the researchers at the University of Sheffield and at EPFL Neuchatel Switzerland, the new 3D self-assembly behaviour and surface plasmonic resonance properties were investigated. It was possible to show that some of these materials exhibit complex structures, such as hexagonal lattices and face centred cubic structures. In this collaborative work, it was possible to show the plasmonic properties of AuNPs and the nematic structure of the mesogens are responsible for these novel optical properties. Thus, this thesis spans work going from detailed synthetic investigation through materials and liquid crystals characterisation, towards the investigation of a completely new class of materials via interdisciplinary collaboration. Overall, the bottom-up approach shows clear advantages over the conventional top-down approach in a chemical synthesis and optimised synthetic procedures were developed. The 2D and 3D superstructures make significant contributions to the emerging field of Metamaterials.

Outlook

Based on the current work, it would be extremely interesting to investigate systems with nanoparticle diameter size in the range of 4 – 6 nm, where the surface plasmonic resonance of nanoparticles are stronger and liquid crystals can still be controlled in order to obtain liquid crystal metamaterials. Critical aspects would be the control and understanding of the 3D structure of AuNPs, as well as the liquid crystals behaviour. In order to achieve the optimal properties, the gold content is critical in this project and requires high percentage of gold weight ratio to achieve these properties.

The intention of gold nanoparticles with deuterated capping agent synthesis was to carry out neutron scattering studies of liquid crystal gold nanoparticles. The aim was to investigate whether annealing of liquid crystal gold nanoparticles in a liquid crystal phase results in a change of the scattering signal, which is indicative of rearrangement of the co-ligands and liquid crystal ligands in the liquid crystal phase. The initial portion of gold nanoparticles with deuterated capping agent was prepared, but further characterisations are still required to fully complete this part of research.